Faculty of Engineering and Information Technology

Uncertainty Analysis and Optimization by Using the Orthogonal Polynomials

A thesis submitted for the degree of

Doctor of Philosophy

JINGLAI WU

(2015)

Title of the thesis:

Uncertainty Analysis and Optimization by Using the Orthogonal Polynomials

Ph.D. student:

Jinglai Wu

E-mail: jinglai.wu@student.uts.edu.au

Supervisor:

Dr Zhen Luo

E-mail: zhen.luo@uts.edu.au

Co-Supervisor:

Prof Nong Zhang

E-mail: nong.zhang@uts.edu.au

Address:

School of Electrical, Mechanical and Mechatronic Systems

The University of Technology, Sydney, NSW 2007, Australia

Certificate of Original Authorship

I certify that the work in this thesis has not previously been submitted for a degree nor has it been submitted as part of requirements for a degree except as fully acknowledged within the text.

I also certify that the thesis has been written by me. Any help that I have received in my research work and the preparation of the thesis itself has been acknowledged. In addition, I certify that all information sources and literature used are indicated in the thesis.

Signature of Student:

JINGLAI WU

Date:

Acknowledgments

I would like to take this opportunity to thank many people for their assistance, encouragement and support throughout my candidature.

First and foremost, I extend my deep gratitude to my principal supervisor Dr Zhen Luo. He supported me with outstanding guidance in research direction and academic writing and gave me many encouragements and other help in my study and life. His knowledge, hard-working and research attitude fostered my development in various aspects. I also sincerely thank my co-supervisor, Prof Nong Zhang, for his assistance, guidance and support over past few years. His extensive experience has been much appreciated through my research.

I would like to thank Dr Paul Walker and my colleagues Xingxing Zhou, Yu Wang, Lifu Wang, Sangzhi Zhu, Tianxiao Zhang, Guangzhong Xu, JiagengRuan, Yuhong Fang, Li Sun, Bo Zhu, who supported me in study or life. I also wish to acknowledge gratefully the consistent financial support of the following agents: China Scholarship Council (CSC) and University of Technology, Sydney.

Most especially to my family, words alone cannot express what I own them for their encouragement and whose patient love enabled me to complete this thesis.

Jinglai Wu

Sydney, August, 2015

Publications and Conference Contributions

International scientific journal publications

[1] **Jinglai Wu**, Yunqing Zhang, Liping Chen, Zhen Luo, Interval method with Chebyshev series for dynamic response of nonlinear systems, Applied Mathematical Modelling, 37(4578-4591), 2013.(Chapter 3)

[2] **Jinglai Wu**, Zhen Luo, Yunqing Zhang, Nong Zhang, Interval uncertain analysis for multi-body mechanical systems with Chebyshev inclusion functions, International Journal for Numerical Methods in Engineering, 95(608-630), 2013. (Chapter 3)

[3] **Jinglai Wu**, Zhen Luo, Nong Zhang, Yunqing Zhang, A new uncertain analysis method and its application in vehicle dynamics, Mechanical Systems and Signal Processing, 50-51 (659-675), 2015.(Chapter 4)

[4] **Jinglai Wu**, Zhen Luo, Nong Zhang, Yunqing Zhang, A new interval uncertain optimization method for structures using Chebyshev surrogate models, Computers and Structures, 146(185-196), 2015.(Chapter 5)

[5] **Jinglai Wu**, Zhen Luo, Nong Zhang, Yunqing Zhang, An interval uncertain optimization method for vehicle suspensions using Chebyshev metamodels, Applied Mathematical Modelling, 38(3706-3723), 2014. (Chapter 5)

[6] **Jinglai Wu**, Zhen Luo, Nong Zhang, Yunqing Zhang, A new sampling scheme for developing metamodels with the zeros of Chebyshev polynomials, Engineering

Optimization, 1-25, 2014. (Chapter 5)

[7] **Jinglai Wu**, Zhen Luo, Nong Zhang, Incremental modelling for high-order polynomial surrogate models, Applied Mathematical Modelling, 2015, DOI: 10.1016/j.apm.2015.12.002.

[8] **Jinglai Wu**, Zhen Luo, Nong Zhang, Yunqing Zhang, Robust topology optimization for structures under interval uncertainty, Advances in Engineering Software, under review, 2015. (Chapter 5).

[9] **Jinglai Wu**, Zhen Luo, Nong Zhang, Yunqing Zhang, A new uncertain optimization method for structures using orthogonal series expansions, Computers & Structures, under review, 2015. (Chapter 6)

International scientific conference publications

[10] **Jinglai Wu**, Zhen Luo, Nong Zhang, Yunqing Zhang, Hybrid uncertainties optimization using the orthogonal polynomials expansion, the 8th Australian Congress on Applied Mechanics (ACAM 8), 23-26 November 2014, Melbourne, Australia.

[11] **Jinglai Wu**, Zhen Luo, Nong Zhang, Structural optimization under a description of hybrid uncertainties, the 11th World Congress on Computational Mechanics (WCCM2014), July 20-25, 2014, Barcelona, Spain.

[12] **Jinglai Wu**, Zhen Luo, Nong Zhang, Interval method for solving multi-body dynamics problems with uncertain parameters, Proceedings: the 5th Asia Pacific Congress on Computational Mechanics (APCOM2013) and 4th International

Symposium on Computational Mechanics (ISCM2013), 11-14 Dec 2013, Singapore.

[13] **Jinglai Wu**, Zhen Luo, Nong Zhang, A new method for building high order polynomial regression model, Proceedings: the 1st Australasian Conference on Computational Mechanics (ACCM2013), eds. G.P. Steven, and Q. Li, 3-4 October, 2013, Sydney, Australia.

[14] **Jinglai Wu**, Zhen Luo, Nong Zhang, Interval uncertain optimization of structures using Chebyshev meta-models, Proceedings: the 10th World Congress on Structural and Multidisciplinary Optimization (WCSMO10), May 19-24, 2013, Orlando, USA.

[15] **Jinglai Wu**, Zhen Luo, Yunqing Zhang, Liping Chen, Interval analysis method for dynamics systems with uncertain parameters, Proceedings: 4th International Conference on Computational Methods, Paper ID: 057, 15-28 Nov 2012, Gold Coast, Australia.

[16] **Jinglai Wu**, Zhen Luo, Nong Zhang, Yunqing Zhang, A Chebyshev meta-model for uncertain optimization of vehicle suspensions, Proceedings: 4th International Conference on Computational Methods, Paper ID: 061, 15-28 Nov 2012, Gold Coast, Australia.

List of figures

List of tables

Abbreviations

PC	Polynomial Chaos
SRSM	Stochastic Response Surface Method
ODEs	Ordinary Differential Equations
DAEs	Differential Algebraic Equations
K-L	Karhunen-Loeve
RBDO	Reliability-based Design Optimization
RDO	Robust Design Optimization
LSM	Least Square Method
PCCI	Polynomial-Chaos-Chebyshev-Interval
IM	Interval Mean
IV	Interval Variance
MLB	Mean of Lower Bound
MUB	Mean of Upper Bound
VLB	Variance of Lower Bound
VUB	Variance of Upper Bound
DOF	Degree of Freedom
ASO	Active Set Optimization
MIGA	Multi-Island Genetic Algorithm
SQP	Sequential Quadratic Programming
RTO	Robust Topology Optimization
MMA	Method of Moving Asymptotes
PDF	Probability Density Function
CDF	Cumulative Distribution Function
MCST	Monte Carlo Scanning Test

Abstract

Engineering problems are generally described by mathematic models, and the parameters in mathematic models are usually assumed to be deterministic when solving these models. However, many parameters are hard to obtain accurately in practical application, which leads to the uncertainty of parameters. The uncertain parameters may induce the response of theoretical analysis that is quite different from the actual instance. In order to characterize the response of system more accurately, the uncertainty analysis methods need to be introduced. For the design optimization, considering the uncertainty may help to improve the reliability and robustness of design solution. This thesis investigates both the aleatory (random) uncertainty and epistemic uncertainty (expressed by interval variables in the thesis), by using the Polynomial Chaos (PC) expansion theory and Chebyshev polynomials approximation theory, respectively. Since there are many cases that both types of uncertainty are existed simultaneously, the hybrid uncertainty is also investigated in this thesis. A new hybrid uncertainty analysis method based on the orthogonal series expansion is proposed in this study, which solves the two types of uncertainty in one integral framework. The design optimization under uncertainty is also investigated based on the proposed uncertainty analysis method. The detailed content of this thesis is shown as follows.

The interval uncertainty analysis theory is firstly studied in this thesis. By using the Chebyshev polynomials that have high accuracy in the approximation theory of polynomials, a new Chebyshev inclusion function based on the Chebyshev series expansion is proposed. The Chebyshev inclusion function can compress the wrapping effect of interval arithmetic more efficiently than the traditional Taylor inclusion function, especially for the interval computation of non-monotonic functions. On the other hand,

the Chebyshev inclusion function does not require the derivatives information which has to be given in the computation of Taylor inclusion function. Therefore, the proposed Chebyshev inclusion function is quite easier to implement than the Taylor inclusion function. The Chebyshev inclusion function is applied to solve the ordinary differential equations (ODEs) and differential algebraic equations (DAEs) with interval parameters, which are used to solve the mechanical dynamic systems with interval parameters.

Secondly, the random uncertainty analysis based on the PC expansion is investigated, where the polynomials series are used to approximate the response of a system with respect to the random variables. The hybrid uncertainty analysis method using the orthogonal series expansion is proposed, termed as Polynomial-Chaos-Chebyshev-Interval (PCCI) method, which is the combination of PC expansion method and Chebyshev interval method. Since both the polynomials used in PC expansion and Chebyshev polynomials belong to the orthogonal polynomials, the PCCI method investigates the random uncertainty and interval uncertainty under one integral framework. Two types of evaluation index of hybrid uncertainty are also proposed in the PCCI method, which is then used in the analysis of vehicle dynamics containing hybrid uncertainty.

Thirdly, considering the interval uncertain parameters or variables existed in the optimization problems, the interval optimization design is investigated. To improve the computational efficiency of traditional nested optimization procedure in uncertainty optimization, the interval arithmetic is employed to delete its inner loop optimization. A new Chebyshev polynomials-based surrogate model is proposed to improve the computational efficiency in further. The numerical examples for the vehicle suspension design and truss structure design indicate that the interval optimization method has a good balance between the accuracy and efficiency. The interval optimization method is also

employed to solve the continuous structural topology optimization problem with uncertain load conditions, which gives a more robust solution than the traditional deterministic topology optimization method.

Lastly, the hybrid uncertainty optimization model is proposed by combining the PCCI method and the classical optimization algorithms. To use the traditional mathematical programming method, the sensitivity of objectives and constraints with uncertain parameters are derived. For the application, the proposed hybrid uncertainty optimization method is used in the optimization of a planar truss and a space truss structures. Compared with the deterministic optimization and pure random uncertainty optimization, the hybrid uncertainty optimization provides a more feasible solution.

Key words: interval uncertainty; hybrid uncertainty; Chebyshev polynomials; Polynomial Chaos expansion; orthogonal polynomials.

Contents

Chapter 1 Introduction

1.1 Overview of the project

The parameters in mathematical models of engineering problems are considered as exact values in traditional. However, the parameters in practical situations have some uncertain extent, i.e. the values of parameters are not accurate, which may change around their mean values. In engineering, the uncertainty widely exists, e.g. when we design a mechanical component, there is a tolerance of the geometry size for manufacturing easily; the inhomogeneity of materials may cause more uncertain mechanics parameters, including the mass and mass moment of inertia uncertainty induced by the uncertain density, and the stiffness uncertainty induced by the variation of elastic modulus; the variation of environment changes the performance of a system, such as the automotive will have different response when it drives on different roads. In many complicated systems, especially for the highly nonlinear system, an even very little variation of parameters may lead to a quite different response of the system. At the same time, the uncertain parameters have an obvious influence on the reliability and robustness of the system, so it is quite necessary to investigate the uncertainty in practical engineering problems.

Uncertainty can be classified into two different types [1, 2], namely aleatory and epistemic uncertainty. Aleatory uncertainty, also termed as objective or stochastic uncertainty, describes the inherent variation associated with a physical system or environment. Epistemic uncertainty or subjective uncertainty, on the other hand, derives from some level of ignorance or incomplete information about a physical system or environment. The aleatory uncertainty is commonly described by the probabilistic

variables while the epistemic uncertainty may be described as the interval variables or fuzzy variables and so on. Although the probabilistic methods to solve the stochastic problems have more application in the uncertainty research, there may be some deficiency for the probability methods in solving the epistemic uncertainty problems. Most epistemic uncertainties are hard to be described by a probabilistic model accurately. If we still try to use the probabilistic methods to solve these problems, the uncertain variables have to be assumed to satisfy some probability distribution. However, Ben-Haim and Elishakoff [3] have shown that even small variations deviating from real values may cause relatively large errors to the probability distributions. To overcome the weakness of probabilistic methods, the interval method is quite fit for solving the epistemic uncertainty problems. Nonetheless, the interval methods are the complimentary rather than the replacement of probabilistic methods. If there is plenty of information to describe the uncertain variables, the probabilistic methods will be a good choice since they can provide more useful information, but the interval methods are better for the case that only a little information can be obtained.

The interval arithmetic has been rapidly developed in recent two decades for its high computational efficiency. Therefore, there have been more and more researchers using the interval arithmetic to solve the interval uncertainty problems. The overestimation intrinsically existed in interval arithmetic usually lead to a very conservative result, so most of the investigations about interval arithmetic are focused on the control of overestimation. In the dynamic systems, the overestimation is more difficult to control than the static problems, which is still a hot point in the research of interval arithmetic.

On the other hand, the research of uncertainty is mainly focused on only one type of uncertainty, i.e. the pure probability uncertainty or pure interval uncertainty. As the author's known, there are only a few publications that study the two types of uncertainties

simultaneously, but many practical engineering problems contain both types of uncertainties. For example, in vehicle dynamics, the stiffness and damping ratio of suspension have some aleatory uncertainties that should be expressed by the random variables. At the same time, the mass, mass center position, and mass moment of inertia have some epistemic uncertainties that are induced by the load condition variation. It is hard to obtain the probability distribution information of the load, so they are fit to denote as interval variables. In this case, if we only use the probability methods to solve the problem, some assumptions have to be added, which may lead to a large deviation between the theory analysis and actual results. On the contrary, if only the interval methods are used, some probability information cannot be utilized, which produces less useful information. Therefore, it is necessary to propose a new theory and method of hybrid uncertainty, which provides higher accuracy and more useful information. Some scientific problems should be solved, e.g. the evaluation index of hybrid uncertainty, and the hybrid uncertainty modeling considering both types of uncertainty characteristics.

In the design of optimization, it is necessary to consider the uncertain factors to guarantee the reliability and robust of systems, which impels the rapid development of the reliability-based design optimization (RBDO) and robust design optimization (RDO). Nevertheless, most of the RBDO and RDO focus on the probability uncertainty optimization while the interval uncertainty and hybrid uncertainty optimizations have not been investigated widely. To extend the application of uncertainty design of optimization, both the interval uncertainty and hybrid uncertainty optimization will be researched in this thesis. When the interval uncertainty and hybrid uncertainty optimization are studied, the uncertainty evaluation index and optimization efficiency are two key points need to solve.

In this thesis, the Chebyshev polynomials are firstly used to solve interval uncertainty problems. The proposed Chebyshev interval method can control the overestimation better than the traditional Taylor interval method, especially for the dynamic problems. Secondly, the orthogonal polynomials are used to build the hybrid uncertainty model, which incorporates the Polynomial Chaos (PC) expansion theory with the Chebyshev interval method to propose a new hybrid uncertainty analysis method. Two types of evaluation indexes will be proposed to characterize the hybrid uncertainty. Finally, the design of optimization under the interval uncertainty and hybrid uncertainty will be studied by using the proposed uncertainty analysis theory and some optimization algorithms.

1.2 Research objective and contribution to knowledge

The specific objectives and contributions are given as follows:

(1) Propose a new Chebyshev polynomials based interval analysis method to solve the dynamic problems, including the ordinary differential equations (ODEs) and differential algebraic equations (DAEs) under interval uncertainty. The Chebyshev interval method has better performance to compress the overestimation of interval arithmetic compared with the traditional Taylor inclusion function method, especially for the calculation of non-monotonic functions, which is quite important to the research of interval arithmetics.

(2) The Polynomial-Chaos-Chebyshev-Interval (PCCI) method, a hybrid uncertainty analysis method, based on the orthogonal series expansion will be proposed. The PCCI method handles the random uncertainty and interval uncertainty in the one integral framework, and also investigates the new evaluation indexes of hybrid uncertainty. The hybrid uncertainty analysis is more suitable for the practical

engineering application than the traditional pure probability or pure interval uncertainty method.

(3) The interval uncertainty optimization will be investigated. The interval optimization model considers both the reliability and robustness simultaneously. The interval arithmetic is employed to improve the computational efficiency and feasibility of design solution. The robust topology optimization of continuous structure considering interval uncertainty will also be studied, where the load is considered as interval parameters.

(4) The design optimization under hybrid uncertainty will be investigated. To use the traditional mathematical programming method, the sensitivity of objectives and constraints with uncertain parameters are induced. The design of optimization under hybrid uncertainty is more in line with the practical cases of engineering problems.

1.3 Outline of the thesis

The thesis consists of 7 chapters, shown as follows:

Chapter 1: The main aims and contributions of the thesis are introduced.

Chapter 2: A literature review of the probabilistic uncertainty, interval uncertainty, and the design of optimization under uncertainty are given in this chapter.

Chapter 3: The interval arithmetic is firstly introduced in this chapter. The Chebyshev polynomials approximation theory is then used to derive the Chebyshev inclusion function. The ODEs and DAEs with interval parameters are solved by using the proposed Chebyshev inclusion function, which is applied in mechanical dynamic problems.

Chapter 4: The PC expansion theory is introduced at the beginning of this chapter. A new hybrid uncertain analysis method is proposed, which combines the PC expansion and Chebyshev interval method, termed as PCCI method. Two types of evaluation indexes are defined to describe the hybrid uncertainty information. The application of the PCCI method on vehicle dynamics analysis is provided at the end of this chapter.

Chapter 5: The design of optimization under interval uncertainty is presented. The interval optimization model is used to replace the traditional nested optimization model, which improve the computational efficiency of optimization. The interval uncertainty optimization is applied to the design of a planar structure, a double wishbone vehicle suspension, and a Mitchell-type structure.

Chapter 6: The design of optimization under the hybrid uncertainty is presented. The hybrid uncertainty optimization model is based on the robust design optimization theory and hybrid uncertainty analysis method. The hybrid uncertainty optimization method is applied to optimize a planar truss and a space truss structures.

Chapter 7: Discussion and further development recommendation are given, and the contributions of the thesis are summarized.

Chapter 2 Background and literature review

The mathematical models are widely used to describe the inner principle that causes the much different external phenomenon. This procedure usually introduces a lot of uncertainties, which in transport-transformation models can be classified as natural uncertainty, model uncertainty, and data or parametric uncertainty, depending on their origins and on how they can be addressed [4].

Natural uncertainty exists in some systems, especially in environment and biological systems, which are inherently stochastic due to unavoidable unpredictability. Some quantities random in principle, e.g. in air pollution systems, the turbulent atmosphere and unpredictable emission-related activities contribute to the natural uncertainty. Some quantities are modelled as random quantities due to the unaffordable expensive precise measurement. On the other hand, some quantities vary over time, over space, or across individuals in a population, termed “variability”, which also belongs to the natural uncertainty.

When the mathematical model is used to express the engineering problems, the practical problems usually need to be simplified or increase some corresponding assumptions. The best mathematical model uses the simplest way to describe the problems that we are interested in, and its accuracy can satisfy our requirement. When we choose the model, the trade-off between the accuracy and efficiency has to be considered. Choosing different model will produce a different analysis result, which contributes the model uncertainty.

There are many resources that can produce the parametric uncertainty. Measurement error is the largest resource of parametric uncertainty, including the random errors in the

measurement device, systematic biases that occur due to imprecise calibration or inaccuracies in the assumptions used to infer the actual quantity of interest from the observed readings of a "surrogate" or "proxy" variable. Other potential sources of uncertainties in estimates of parameters include misclassification, estimation of parameters through a small sample, and estimation of parameters through non-representative samples [4].

The parametric uncertainty is mainly researched in this thesis. Parametric uncertainty can be further classified into two different types, namely aleatory uncertainty and epistemic uncertainty [1, 2]. Aleatory uncertainty or objective uncertainty describes the inherent variation associated with a physical system or environment, generally expressed by probabilistic variables. Epistemic uncertainty or subjective uncertainty derives from some level of ignorance or incomplete information about a physical system or environment, which is described as the non-probabilistic variables, e.g. the interval variables or fuzzy variables and so on. Figure 2-1 shows the probabilistic variable, fuzzy variable, and interval variable. It can be found that the probabilistic variable is characterized by the probability distribution function and the fuzzy variable is expressed by its membership function, while the interval variable is only expressed by its bound values.

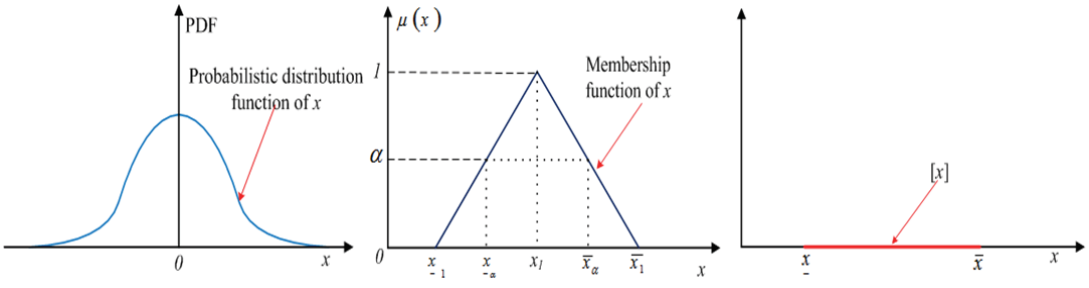

Figure 2- 1(a) probabilistic variable (b) fuzzy variable (c) interval variable

This thesis is focused on the investigation of interval uncertainty, and the hybrid of probability and interval uncertainty, so more detailed reviews about the probability

uncertainty analysis, interval uncertainty analysis, and design of optimization under uncertainty will be provided in the following subsections.

2.1 Probabilistic uncertainty analysis

Probabilistic methods are the most widely used approach in uncertainty research. There have been many pieces of literature studied the theory and application of probabilistic methods, e.g. Papoulis [5] illustrated the probability theory and random variables comprehensively. In the probability methods, uncertain parameters are described by the random variables that satisfy some probability distributions, and the response of the system is also expressed by some probability distributions. There are two steps for probabilistic methods solving the engineering problems, the first of which is the determination of the probability distribution of input parameters (random variables), and the second of which is the uncertainty propagation of computational model. The distribution of parameters may be obtained through the statistics or the experience of experts. The statistics use a large number of samples or some representative samples to estimate the probability distribution, which have been introduced by many publications [6]. When the number of samples is limited, the professional knowledge of experts may be used to determine the probability distribution type. The propagation of uncertainty is the key to probabilistic method, which studies how to obtain the probability characteristics of system response from the probability information of input parameters.

The methods for solving the propagation of probabilistic uncertainty in engineering can be broadly classified into two major categories: methods using a statistical approach and methods using a non-statistical approach. Monte Carlo method [7, 8] is one of the most widely used statistical methods, which can be utilized in any engineering areas because it is easy to implement. The Monte Carlo method takes samples of the random variables

based on the probability distribution of these random variables (input) and then computes the probability distribution of response (output) directly. The accuracy of Monte Carlo method depends on the sampling size, in accordance with the 'weak law of large number' (the convergence ratio is $\frac{1}{\sqrt{N}}$, where *N* denotes the sampling size). Therefore, to get enough high accuracy, the Monte Carlo method usually requires thousands of sampling points. For many complicated engineering models, each running takes a large amount of time, e.g. a finite element simulation for vehicle crash usually takes over tens of hours. In this case, the thousands of running for Monte Carlo method cannot be affordable. As a result, the Monte Carlo method is often used as the reference of other methods. To improve the efficiency of Monte Carlo method, some researchers propose some modified Monte Carlo methods, in which the sampling methods are improved, so less sampling points are required, such as the stratified sampling, Latin hypercube sampling, and so on [9, 10].

For the non-statistical approaches, the differential analysis methods are most popular, including the perturbation method and Neumann expansion method. The perturbation method expands the random field by using the Taylor series around its mean and truncated at certain order. Typically, at most second-order expansion is employed because the system of equations becomes extremely complicated beyond second-order. This approach also termed as the 'second moment analysis', has been used extensively in various fields [11-13]. The weakness of perturbation method is that the uncertainties cannot be too large, i.e. the variance of random field cannot be too large compared with their mean values, e.g. typically less than 10% [11]. At the same time, higher order statistics is not readily available for the second moment method. The Neumann expansion is based on the inverse of the stochastic operator in a Neumann series, but it also requires

the small uncertainty extent of random variables.

Another type of non-statistical method comes from the stochastic finite element spectral method, which relies on the use of representing stochastic processes in terms of a series expansion, specifically the Karhunen-Loeve expansion [5, 14]. This expansion is termed as Polynomial Chaos (PC) expansion, so this method is also called as PC expansion method. The PC expansion allows high-order representation and promises fast convergence; coupled with K-L decomposition for the input and Galerkin projection in random space, it results in computationally tractable algorithms for large engineering systems [15]. More efficient Monte Carlo algorithms can also be designed when combined with the PC expansion technique [15, 16]. More recently, a theoretical framework of discretizing the random field via the finite element approach, i.e., piecewise polynomials, was proposed in [17].

The PC expansion method has been developed fast in recent two decades since it is quite fit for the problems with large uncertainty extent parameters. It has been widely used in various engineering problems, such as in fluid mechanics, multibody dynamics, vehicle dynamics, and so on.

Xiu et al. [11] presented a generalized polynomial chaos algorithm for the solution of stochastic elliptic partial differential equations subject to uncertain inputs. A Galerkin projection in random space was applied to derive the equations in the weak form. The resulting set of deterministic equations for each random mode was solved iteratively by a block Gauss–Seidel iteration technique. Both discrete and continuous random distributions were considered, and convergence was verified in model problems and against Monte Carlo simulations. The authors also used the generalized PC expansion algorithm to model the input uncertainty and its propagation in incompressible flow

simulations [18].

Field Jr et al. [19] explored features and limitations of PC expansion approximations. Metrics was developed to assess the accuracy of the PC expansion approximation. A collection of simple but relevant examples was examined. The examples demonstrated that (1) the accuracy of the PC expansion approximation improved in some metrics as additional terms were retained but did not exhibit this behavior in all metrics considered, (2) PC expansion approximations for strictly stationary, non-Gaussian stochastic processes were initially non-stationary and gradually might approach weak stationarity as the number of terms retained increased, and (3) the development of PC expansion approximations for certain processes might become computationally demanding, or even prohibitive, because of the large number of coefficients that needed to be calculated.

Wan et al. [20] formulated a Multi-Element generalized Polynomial Chaos (ME-gPC) method to deal with long-term integration and discontinuities in stochastic differential equations. The main idea of ME-gPC is to decompose the space of random inputs when the relative error in variance becomes greater than a threshold value, and then a gPC expansion is employed in each subdomain or random element. The authors developed a criterion to perform such decomposition adaptively and demonstrated its effectiveness for ODEs.

Ghanem et al. [21] presented a methodology that permitted the prediction of the evolution of dynamical systems in the presence of stochastic uncertainty. Specifically it has been demonstrated that the random scatter in the model properties can be efficiently and accurately characterized in a PC basis. Encoding the model uncertainty in this fashion led to response predictions that accurately reflected the systems behavior. An alternative to the simulation-based non-intrusive estimation of the response chaos, the propagation of

the model uncertainty can also be performed through the intrusive evaluation of the time history, based on Galerkin projections. The latter approach was particularly efficient if the variability of the systems properties was small, since then a Taylor approximation of the stochastic restoring force was accurate, and the complexity of the computations was drastically reduced.

Williams et al. [22] employed the PC expansion to solve a simple first order stochastic differential equation that was typical of transport problems. Because the equation had an analytical solution, it provided a useful test of the efficacy of PC expansion. The results show that the convergence was very rapid in some cases but that the increased complexity associated with many random variables could lead to very long computational times. The usefulness of white noise approximation was also assessed. Extensive numerical results were given which highlight the weaknesses and strengths of PC expansion. The general conclusion was that the method was promising but required further detailed study by application to a practical problem in transport theory.

Li et al. [23] developed an algorithm to calculate the tractive capacity of an off-road vehicle with stochastic vehicle parameters, operating on soft soil with an uncertain level of moisture, and on a terrain topology that induced rapidly changing external excitations on the vehicle. Both the Monte Carlo method and PC expansion method were used, and the results showed that the two methods provided similar accuracy, but the PC expansion method was much more computationally efficient.

The PC expansion methods in the papers mentioned above are mainly based on the Galerkin projection, which is a kind of intrusive method. For some complicated models, especially for the black box problems, the Galerkin method is difficult to use. To solve this problem, some researchers have proposed the Stochastic Response Surface Method

(SRSM) [24-27], which is still based on the PC expansion theory. Be different from the Galerkin projection, the SRSM uses the regression method to realize the PC expansion. Sandu et al. [28] have proved the equivalence between the Galerkin method and SRSM. The procedure of SRSM is the same with the traditional response surface method; the only difference is that the SRSM employs the orthogonal polynomials as the basis of regression procedure. Therefore, the SRSM is a kind of non-intrusive method, which can be more widely used to the complicated models and black box models. The SRSM has been used in multibody dynamics, structure dynamics, and optimization problems [29-33].

In summary, the Monte Carlo method is usually used as the reference of other methods while the PC expansion methods are very useful to solve the problems with large uncertainty extent but low dimensional problems. Particularly, the SRSM of the PC expansion methods has quite good performance to solve the complicated or black box problems.

2.2 Interval uncertainty analysis

When the probability information of uncertain variables is hard to obtain, the interval numbers can be used to characterize the uncertainty. An interval number is determined by its upper bound and lower bound, and all the possible values of the variable are located in the range of the two bounds. A famous and very old example of an interval enclosure was given by the method due to Archimedes. He considered inscribed polygons and circumscribing polygons of a circle with radius 1 and obtained an increasing sequence of lower bounds and at the same time a decreasing sequence of upper bounds for the area of the corresponding disc. Thus stopping this process with a circumscribing and an inscribed polygon, each of n sides, he obtained an interval containing the number π. By choosing n large enough, an interval of arbitrary small width can be found in this way containing π

[34].

Reference [35] stated the rules for the arithmetic of intervals and applied it to evaluate the rational expression, which is called today interval arithmetic, and it is one of the first references to introduce the interval arithmetic as a tool in numerical computation. According to [36], Dwyer has discussed matrix computations using interval arithmetical ready in his book [37] in 1951. Probably one of the most important papers for the development of interval arithmetic was published by the Japanese scientist Teruo Sunaga [38]. In this publication not only the algebraic rules for the basic operations with intervals could be found but also a systematic investigation of the rules which they fulfilled. However, these results did not find much attention until the first book on interval analysis appeared which was written by Moore [36].

Initially, the interval arithmetic was designed to solve the problem of numerical error occurring on the computer, including the truncated error and round-off error. Because the irrational number cannot be exactly described by the float number of the computer while only the closest float number can be used to denote the actual number, so there may be some accumulative error in the calculation of computer. To solve this problem, Moore et al. changed the expression of an irrational number by two closest float numbers on the computer, and defined a corresponding arithmetic to guarantee the exact result of computation be located in an interval. In recently several decades, the interval arithmetic has not only developed rapidly in numerical computation but also been applied in many engineering, especially for the uncertainty analysis and optimization, e.g. the reliability based design optimization and robust design optimization and so on. In the interval arithmetic, the uncertain input parameter x is expressed by the symbol $[x]=[\underline{x},\overline{x}]$, in which we do not know the exact value of x but only know its two bounds, and then using

the interval arithmetic to compute the interval response of a system $[y]=[\underline{y},\overline{y}]$.

The interval arithmetic can obtain the response range of system in high efficiency, but it has a weakness that is the overestimation induced by the wrapping effect, which means the range obtained by the interval arithmetic is usually enlarged, compared with the actual result. In general, the more times of interval variables occur in the expression of a function, the wider interval result may be obtained. Therefore, even the same function under different expression may produce different interval result by using interval arithmetic. How to reduce or control the overestimation of interval arithmetic is the key of interval arithmetic used in practical engineering problems and is also the main research content of interval arithmetic. In the following subsections, we will review the application of interval arithmetic in static problems and dynamic problems, respectively.

2.2.1 Interval arithmetic solving the static problems

Interval arithmetic to solve the static problems includes the following contents: the interval range estimation of a function, the solving of the linear system and nonlinear system, and the eigenvalue problems. The static problems have been used in engineering, such as the stress and displacement analysis of structure, the frequency of vibration system, the reliability analysis in product design, and global optimization.

When the real float number is extended to real interval number, the traditional real function will also be extended to the interval real function. One of the most important capabilities of interval arithmetic is to compute the interval enclosure of a function, so interval function is also called as inclusion function. Interval arithmetic can compute an interval enclosure of the range of a function, but this interval enclosure may be enlarged much, which is termed as overestimation. As a result, the original interval arithmetic has to be adjusted. There have been three types of interval inclusion function to compute the

interval range of a function, including the natural inclusion function, centred inclusion function, and Taylor inclusion function [39].

The Natural inclusion function is the direct extension of the original real function, in which the interval arithmetic is directly used to compute the interval function value, but the overestimation is usually quite large, especially for a function that the interval variables occur several times in its expression. Reference [40] stated that the natural inclusion function will not be enlarged if the interval variables only occur once in the expression of a function, but most of the functions cannot make each interval variable only occur once.

The centred inclusion function uses the mean value theorem to rewrite the original expression as a new expression with respect to the mid-value and derivative of the function, and then the interval arithmetic is used to calculate the interval range. The Taylor inclusion function, which is an extension of centred inclusion function, expands the original function as high-order Taylor series and then uses the interval arithmetic to calculate the interval range. The Taylor inclusion function requires that the evaluated function has high-order continuity. Reference [41] has compared the three inclusion functions, which shows that the Taylor inclusion function produces the tightest interval in most cases while the centred inclusion function shows better performance than the natural inclusion function only in the case that the interval variables have large uncertain range.

The solving of interval linear system is the inverse problem of the function range estimation. The interval linear system is expressed as following equation

$$\mathbf{Ax} = \mathbf{b}\ , \qquad (2\text{-}1)$$

where the **A** denotes the interval matrix, **b** is an interval vector, and the solution **x** is also an interval vector. The traditional Gaussian elimination method can be combined with the

interval arithmetic to present the interval Gaussian elimination method [42]. However, this method usually produces large overestimation, so its application is restricted. To control the overestimation, some researchers have proposed some interval iteration methods to solve the interval linear system, e.g. the references [43-47].

Be different from the interval arithmetic solving the linear system that contains the interval parameters, the nonlinear system does not contain interval parameters while the interval arithmetic is only used to solve the traditional certain nonlinear equations. Since the nonlinear equation has several solutions generally, the interval arithmetic can be used to seek all the solutions that are located in a given initial interval. The interval methods to solve the nonlinear system include the interval Newton method [36], Krawczyk method [48, 49], and the forward-backward propagation method [39, 50]. Interval Newton method is the interval extension of traditional Newton method. Since the interval Newton method requires solving a linear interval equation in iteration where the Jacobian matrix may be singular and is limited to solve the problem with small interval solution, its application is restricted. The Krawczyk method does not require solving the interval linear equation in the iteration, which improves the solving efficiency and reliability. Although the Krawczyk method still needs to calculate the inverse matrix, the matrix is real matrix rather than the interval matrix. Hensen and Sengupta [51] proposed the Hensen-Sengupta algorithm that combined the Gauss-Seidel procedure and the Krawczyk method. Neumainer [49] stated that the Hensen-Sengupta algorithm produced tighter interval than Krawczyk method. Benhamou and Jaulin proposed the forward-backward propagation method [39, 50] based on the Waltz's propagation theory [52-54].

When the elements of a matrix are interval numbers, the eigenvalues and eigenvectors are also interval numbers and interval vectors, respectively. Rohn et al. [55] investigated the standard eigenvalue of symmetric interval matrix and derivated the formula to solve

eigenvalue when the radius of interval matrix equaled to 1. Hallot et al. [56] found that the characteristic spectrum of interval matrix depended on the characteristic spectrum of its endpoints. Deif et al. [57] proposed the theorem to solve the standard interval eigenvalues problems. Qiu et al. [58-60] extended the Deif's method to generalized interval eigenvalues problems.

The interval methods mentioned above have been used in engineering, especially in the structure dynamics. Chen et al. [61] used the interval arithmetic to the finite element method, computing the static displacement of a structure under interval parameters. The authors also used the interval arithmetic to investigate the robustness of vibration control system [62]. Qiu et al. [63, 64] combined the finite element method and non-probabilistic convex model theory, proposing a convex model method and interval analysis method to compute the static displacement of the structure. Moens et al. [65] proposed an interval sensitivity analysis method that has been used in interval numerical method. More applications of the interval arithmetic solving the static problems can be found in references [66-70].

2.2.2 Interval arithmetic solving the dynamic problems

The governing equations of dynamic problems are usually the differential equations, including the Ordinary Differential Equations (ODEs), Partial Differential Equations (PDEs), and Differential Algebraic Equations (DAEs). Traditional numerical algorithms to solve the differential equations assume that all the parameters in the differential equations are exactly known. When some parameters are considered to be interval numbers, the interval differential equations should be solved. Solving the dynamic problems under interval uncertainty is quite different from the static problem because the numerical methods for solving the differential equations contain a larger number of

iterations. If only the interval set theory is used to solve the interval differential equations, the wrapping effect will increase with the increase of time, and even makes the numerical methods divergent. Therefore, besides the basic interval theory, some special algorithms have to be incorporated to control the overestimation.

There are two types of methods to solve the interval ODEs, interval Taylor series method [34, 71-73] and Taylor model method [74-77]. Interval arithmetic can obtain the upper bound and lower bound of the solution in the time domain, which guarantees the exact result to be located in the interval defined by the two bounds, so this method is also called as validated method.

Each step of interval Taylor series method includes two phases, where the first phase is to compute a step size and a prior enclosure of the solution that contains the exact solution of the time span from the current time step to the next time step (algorithm Ⅰ), while the second phase is to compute a tighter enclosure of the solution (algorithm Ⅱ) [72].

In phase 1, Moore et al. used Banach's fixed point theorem and the Picard Lindelof operator to determine the step size. However, even the high-order Taylor series was used to decrease the overestimation in phase 2, the step size of Moore's method was limited to Euler step size, i.e. the first-order enclosure [71]. To increase the step size, some researchers proposed the polynomials enclosure method [78] and high-order Taylor series method [36, 72, 79], which were called as the high-order enclosure. Phase 2 is the key to controlling the overestimation for interval Taylor series method. Moore et al. [36, 80] proposed a local transformation method to control the wrapping effect. Kruckeberg et al. [81] used the linear transformation of interval vector to enclose the solution of ODEs at each step. Lohner et al. [82] proposed a QR decomposition method that denoted the solution of ODEs by the linear transformed interval vectors. Rihm et al. [83] proposed an

extended mid-value method, which was similar to the QR decomposition method but usually showed better performance. Besides the interval Taylor series method, Nedialkov et al. [84] proposed an interval Hermite-Obreschkoff (IHO) method. IHO method can be thought as a generalized interval Taylor series method, but it had smaller truncated error and higher stability. The IHO method calculates less high-order Taylor coefficients and Jacobian matrix, so it has higher computational efficiency.

Taylor model method, which was proposed by Berz et al. [74, 75, 77, 85-90], combined the two phases of interval Taylor series method to one phase. Taylor model method tries to reduce the dependence among interval variables to control the wrapping effect, so its basic principle is different from the interval Taylor series method. Taylor model expands the ODEs to a high-order Taylor series with respect to the time and the interval initial values, which may reduce the dependence among the interval variables, so as to control the overestimation. Besides the high-order Taylor series are used to express the Taylor model, another interval term should be added to guarantee the exact solution to be located in the interval. The coefficients of Taylor series is calculated based on the float number, which also helps to reduce the overestimation. Berz et al. coded a toolbox COSY IFINTY [91] to solve the dynamic problems under interval uncertainty, which was based on the Taylor model method.

Both the interval Taylor series method and Taylor model method only solve the ODEs with interval initial values, without considering interval parameters. The Taylor model method is easier to extend to solve the ODEs with interval parameters because it can also be expanded as Taylor series with interval parameters. Lin et al. programmed the software toolbox VSPOSE [92], which used the phase 1 of the Taylor series method to control the step size, and then employed the extended Taylor model method in phase 2. At the same time, the additional interval term of Taylor model was computed by QR decomposition

method. Since the VSPODE assemble several interval methods, it usually produced tighter interval result than other single method.

The aforementioned numerical methods for solving the interval ODEs were focused on the characteristic of 'rigorous enclosure', i.e. the interval solution must contain all the exact solution of the interval ODEs firstly, and then reduced the overestimation induced by the interval arithmetic. When the ODEs have a strong nonlinear characteristic, or the range of interval parameters is large, these methods will still produce too large overestimation to be used. To keep the numerical stability, the approximated method is commonly used in engineering. Although the approximated method may not guarantee the solution to be validated, it has more practical usefulness due to the stability.

Qiu et al. [93, 94] combined the perturbation theory and finite element method to analyze the dynamic response of structure considering interval parameters. Wu et al. [95] used the first order Taylor expansion method to calculate the dynamic response of the linear structure with interval parameters. Zhang et al. [96] computed the dynamic response of a close-loop system under interval uncertainty by using the matrix perturbation theory and interval arithmetic. Han et al. [97] employed the linear function to approximate the dynamic response of composite–laminated plates with uncertain load and material properties, but this method was only fit for the case that uncertain range was small enough. Qiu et al. [98] investigated the dynamic response of nonlinear vibration system by using the second order Taylor expansion method. These methods mentioned above are actual a simplified Taylor model method, by using the first or second order Taylor model without considering the additional interval term. Due to the additional interval term is neglected, they are more stable. However, only low-order Taylor series expansion is used, there will be a large numerical error in solving the highly nonlinear problems. More

applications of interval arithmetic in dynamic problems can be found in references [99-101].

To overcome the weakness of Taylor model method, the author proposed the Chebyshev interval method [102]. The Chebyshev interval method firstly expands the evaluation function with respect to the interval variables using the Chebyshev series, and then uses the interval arithmetic to estimate their bounds. In fact, the Chebyshev method can also be considered as a degenerated PC expansion method, since it also expands the original function to an orthogonal series. However, the Chebyshev series expansion only needs the bounds information rather than the probability distribution information of uncertain variables, which is quite different from traditional PC expansion in solving the random uncertainty.

There is only a little research about interval method for solving the PDEs [103-105] and DAEs [106-110]. In mechanical dynamics, especially for multibody dynamics, most of the control equations are DAEs. Compared to the ODEs, even the traditional DAEs only containing certain parameters are hard to solve, so there will be more difficulties to solve the DAEs with interval parameters. The author used the Chebyshev interval method to solve the multibody dynamic problems with interval parameters [111], which showed that the Chebyshev interval method provides tighter result than the Taylor inclusion function based method.

2.3 Uncertainty optimization

Traditional design optimization is based on the assumption that all the values of parameters are exactly known, which may lead the design of a solution to be located in the unfeasible region when the uncertainties exist. Therefore, it is necessary to investigate

the design of optimization under uncertainty since the uncertainty cannot be avoided in practical engineering problems.

There have been many different methods that can be used to model uncertainty optimization, among which the reliability-based design optimization (RBDO) [112] and the robust design optimization (RDO) [113-115] represent two major paradigms. RDO aims at determining a robust design to optimize the deterministic performance about a mean value, while making it insensitivity with respect to uncertain variations by minimizing the performance variance. RBDO focuses on a risk-based solution taking into account the feasibility of design target at expected probabilistic levels, in which the failure probabilities and expected values are used to quantitatively express the effects of uncertainties. In fact, RDO and RBDO can be represented in the uniform theory framework. For instance, Du et al. [116] proposed an integrated framework for the design optimization under uncertainty, which took both the robust of the design objective and the probability of the constraints into account.

The implementation of the design optimization considering uncertain parameters contains two procedures. The first is the optimization algorithm for seeking the optimum solution at the nominal values of the design variables, while the second is the uncertainty quantification that quantifies the uncertainty by using some evaluation indexes, such as the probability of failure or the generalized reliability index [117], the variance of evaluation functions (objective and constraint functions) in optimization model [114] and so on. In most cases, the two procedures are implemented by using the double-loop [112, 118] or the sequential single-loop optimization [119]. To reduce the computational cost of the double-loop optimization, one option is to use the first-order Taylor series expansion to approximate the maximum and minimum values in the inner loop [120], instead of using the optimization algorithm. Chakraborty et al. [121] applied the matrix perturbation

theory via a first order Taylor series expansion to obtain a conservative dynamic response of interval functions. Chen et al. [62] used the first-order Taylor series expansion to analyze robust response of interval vibration control systems. In fact, the linearization model optimization is actually a type of degenerative nested optimization, in which the inner loop of optimization is replaced by the first-order Taylor series expansion. However, the linearization model has a lower numerical accuracy, which may lead to a solution located in unfeasible regions. There also have been some studies that try to combine the two procedures into one single step, e.g. the single-loop optimization in RBDO [122-124], but the uncertain ranges of parameters are required to be small.

Since the first procedure only refers to the conventional optimization algorithms, the second procedure for uncertainty quantification (or uncertainty analysis) will be the key for design of optimization under uncertainty. In the quantification of the uncertainty about probabilistic variables, the optimization method [125], Monte Carlo simulation [7, 126], and PC expansion method [11, 127] are usually employed. The optimization method is mainly used in the first-order reliability method (FORM) to find the most probable point (MPP) [123]. The optimization method has also been combined with the response surface method to quantify the uncertainty [128, 129]. The Monte Carlo simulation can be conveniently implemented and may obtain comprehensive statistic information of evaluation functions, such as mean, variance, failure probability, probability density function (PDF) and cumulative distribution function (CDF). However, the Monte Carlo simulation usually requires a large number of sampling points due to its low convergence ratio, so the computational cost may be expensive for engineering models.

The PC expansion method can be used to estimate the response of a system under random uncertainty, to greatly reduce the computational cost. Hu et al. [130] presented an adaptive-sparse PC expansion method for performing engineering reliability analysis and

design, and the applications demonstrate the efficiency and accuracy of this method. Li et al. [131] proposed a hybrid approach by sampling both the PC expansion surrogate model and the original system to evaluate the failure probability efficiently. Coelho et al. [132] combined the moving least squares and PC expansion to build a surrogate model and then research the reliability based design optimization in truss structure, which showed the method provided accurate solutions at an affordable computational time. To improve the accuracy of PC expansion based surrogate model, Xiong et al. [133] proposed a new weighted SRSM based on PC expansion that considered the sampling probabilistic weights.

In the quantification of interval uncertainty, the evaluation indexes of uncertainty are described by the upper and lower bounds (maximum and minimum values) of the evaluation functions. The bounds of evaluation functions can be calculated using optimization methods [134, 135] or interval arithmetic [61, 98, 136]. The optimization methods may capture the exact bounds of the evaluation functions if the optimization algorithms have the capacity to seek the global optimum. Since the global optimization algorithms are generally time-consuming, the mathematical programming methods are usually employed to find a local optimum solution, which will be effective when there are not multiple local solutions in the uncertainty range. Interval arithmetic is the other effective method to estimate the bounds of the evaluation function, and it may produce an envelope of the evaluation function. The interval arithmetic has higher efficient than the optimization algorithm, but the envelope is usually wider than the actual bounds (overestimation) [36]. There have been some techniques developed to control the overestimation, referred to subsection 2.2. The author studied the interval optimization of vehicle suspension [137] and truss structure [138] under interval uncertainty by using the

Chebyshev interval method, which shows a good trade-off between the accuracy and efficiency.

Most of the aforementioned methods of uncertainty quantification are only focused on one type of uncertainty. However, many engineering problems involve both types of uncertainties simultaneously. Qiu et al. [139] proposed a probabilistic and interval hybrid reliability model to solve the structural design optimization problem, but the expression of limit state functions is required to be simple. Gao et al. [140] studied the hybrid uncertainty analysis for structures, in which both the Taylor expansion and Monte Carlo simulation are combined to determine the bounds of mean and standard deviation of the evaluation functions. Du et al. [141] investigated the reliability analysis under the hybrid uncertainty. The aleatory uncertainty was modeled with probability distributions by the probability theory, while the epistemic uncertainty was modeled with basic probability assignments by the evidence theory. A computational method was developed to compute belief and plausibility measures for black-box performance functions. This method involved the nested probabilistic analysis and interval analysis. To handle black-box functions, the first order reliability method for probabilistic analysis and nonlinear optimization for interval analysis were employed. Jiang et al. [142] employed the nested double-loop optimization to implement the analysis of hybrid uncertainties, in which the outer layer optimization is to find the MPP induced by the random uncertainty and the inner layer optimization is to seek the extreme values under interval uncertainty. The nested optimization is computationally prohibitive for design problems in engineering, and so Du et al. [143] used the sequential single-loop optimization to analysis the hybrid uncertainties. Ge et al. [144] applied the single-loop optimization for the hybrid reliability assessment. Eldred et al. [145] combined the PC expansion and interval optimization to quantify the hybrid uncertainties. However, the above methods are normally implemented

by using the optimization algorithms so that the efficiency will be low. Recently, the author combined the PC expansion method and Chebyshev interval method to develop a new uncertainty analysis method for vehicle dynamics performance under the hybrid uncertainties, which shows good accuracy and efficiency [146]. This hybrid uncertainty analysis method will be used in this thesis.

Chapter 3 Interval uncertainty analysis based on Chebyshev series

3.1 Interval arithmetic

3.1.1 Basic theory of interval arithmetic

The uncertain parameter may be expressed by interval number, i.e. interval number is an enclosure of all the possible values of the uncertain parameter. A real interval number $[x]$ denotes a connected subset on real set, defined as

$$[x]=[\underline{x},\overline{x}] \tag{3-1}$$

where $\underline{x}$ and $\overline{x}$ denotes the lower bound and upper bound of interval number $[x]$, respectively, i.e. the possible minimum and maximum number of $[x]$, which can also be delegated by inf($[x]$) and sup($[x]$), respectively. The mid value and width of interval number are defined as follows:

$$x_c=\mathrm{mid}([x])=\frac{\underline{x}+\overline{x}}{2} \tag{3-2}$$

$$w([x])=\overline{x}-\underline{x} \tag{3-3}$$

The interval number can also be transformed to the following expression

$$[x]=x_c+[\Delta x],\ \ [\Delta x]=\left[-\frac{w([x])}{2},\frac{w([x])}{2}\right] \tag{3-4}$$

where $[\Delta x]$ is the symmetrical interval of $[x]$. The basic interval arithmetic between two interval numbers is defined as

$$[x]+[y]=\left[\underline{x}+\underline{y},\overline{x}+\overline{y}\right] \tag{3-5a}$$

$$[x]-[y]=\left[\underline{x}-\overline{y},\overline{x}-\underline{y}\right] \tag{3-5b}$$

$$[x]\times[y]=\left[\min\left(\underline{x}\underline{y},\underline{x}\overline{y},\overline{x}\underline{y},\overline{x}\overline{y}\right),\max\left(\underline{x}\underline{y},\underline{x}\overline{y},\overline{x}\underline{y},\overline{x}\overline{y}\right)\right] \tag{3-5c}$$

$$[x]/[y]=[x]\times 1/[y],\quad 1/[y]=\begin{cases}\varnothing, & [y]=[0,0]\\ \left[1/\overline{y},1/\underline{y}\right], & 0\notin[y]\\ \left[1/\overline{y},\infty\right], & \underline{y}=0,\overline{y}>0\\ \left[-\infty,1/\underline{y}\right], & \underline{y}<0,\overline{y}=0\\ \left[-\infty,\infty\right], & \underline{y}<0,\overline{y}>0\end{cases} \tag{3-5d}$$

The power function of interval variable can be computed by using the following formula

$$[x]^n=\begin{cases}\left[0,\max\left(\underline{x}^n,\overline{x}^n\right)\right], & n=2k,\ 0\in[x]\\ \left[\min\left(\underline{x}^n,\overline{x}^n\right),\max\left(\underline{x}^n,\overline{x}^n\right)\right], & n=2k,\ 0\notin[x]\\ \left[\underline{x}^n,\overline{x}^n\right], & n=2k+1\end{cases} \tag{3-6}$$

where k denotes non-negative integer. If a function f is defined as a mapping from real set **R** to **R**, the corresponding interval function $[f]$ is defined as the enclosure of function f mapped from the interval domain $[x]$, such that

$$[f]([x])=\left[\left\{f(x)\middle|x\in[x]\right\}\right] \tag{3-7}$$

Most of the continuous interval functions can be computed through the combination of Eqs. (3-5) and (3-6), but some elementary functions have to be computed by some special algorithms. The interval exponential function is computed by the Eq. (3-8).

$$[\exp]([x])=\left[\exp\left(\underline{x}\right),\exp\left(\overline{x}\right)\right] \tag{3-8}$$

The previous formula uses the monotonic of exponential function. For the trigonometric, its periodic characteristic can be used to implement the interval computation. The algorithm of interval Cosine function is given as follows

$$\begin{aligned}
&\text{if}\quad \exists k\in Z\left|2k\pi-\pi\in[x]\right.\\
&\quad\text{then}\quad \inf\left([\cos]([x])\right)=-1;\\
&\text{else}\quad \inf\left([\cos]([x])\right)=\min\left(\cos\underline{x},\cos\bar{x}\right);\\
&\text{if}\quad \exists k\in Z\left|2k\pi\in[x]\right.\\
&\quad\text{then}\quad \sup\left([\cos]([x])\right)=1;\\
&\text{else}\quad \sup\left([\cos]([x])\right)=\max\left(\cos\underline{x},\cos\bar{x}\right).
\end{aligned}\tag{3-9}$$

where Z denotes the integer set. For example [cos]([1, 5.5])=[-1, 0.7087], shown as Fig. 3-1.

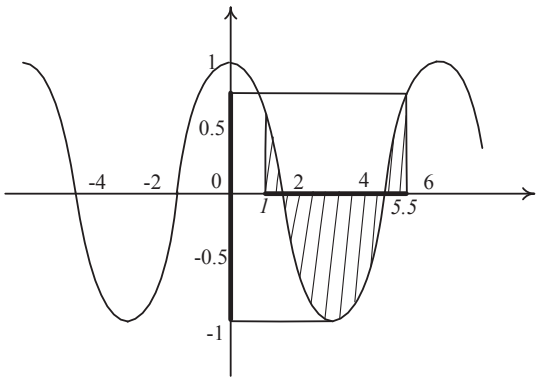

Figure 3-1 The computation of interval Cosine function

3.1.2 Interval inclusion function

Consider a function **f** from $\mathbf{R}^n$ to $\mathbf{R}^m$. The interval function [**f**] from $\mathbf{IR}^n$ to $\mathbf{IR}^m$ is an inclusion function for **f** if

$$\forall[\mathbf{x}]\in\mathbf{IR}^n,\mathbf{f}\left([\mathbf{x}]\right)\subset[\mathbf{f}]\left([\mathbf{x}]\right)\tag{3-10}$$

where **IR** denotes the interval real set. The interval function [**f**]([**x**])=$\mathbf{R}^m$, for all $[\mathbf{x}]\in\mathbf{IR}^n$ is an example of a (not very useful) inclusion function for all functions **f** from $\mathbf{R}^n$ to $\mathbf{R}^m$. One of the purposes of interval analysis is to provide, for a large class of functions **f** that can be evaluated reasonably quickly and such that [**f**]([**x**]) is not too large. The function **f**

may, for instance, be polynomial, or given by an algorithm. It may even be defined as the solution of a set of differential equations.

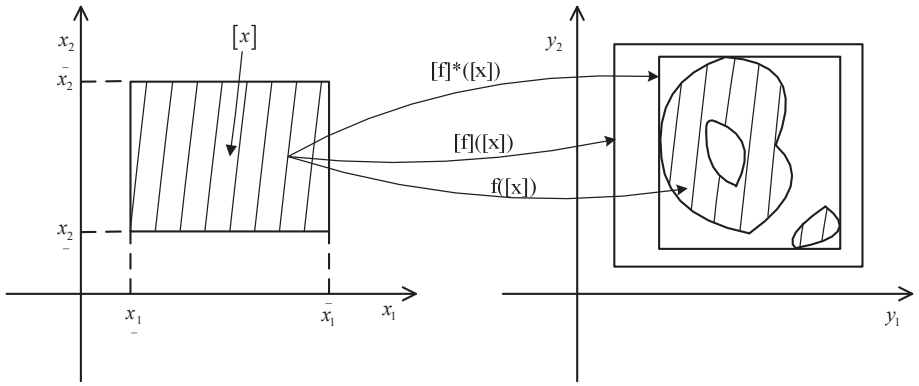

Figure 3-2 The interval inclusion function from $\mathbf{R}^2$ to $\mathbf{R}^2$

To illustrate the notion of inclusion function, consider a function **f** from $\mathbf{R}^2$ to $\mathbf{R}^2$, with variables x_1 and x_2 that vary within $[x_1]$ and $[x_2]$. The image set [**f**]([**x**]) may have any shape, e.g. shown as Fig. 3-2 [39]. It may be non-convex, or even disconnected if **f** is discontinuous. Whatever the shape of [**f**]([**x**]), an inclusion function [**f**] of **f** makes it possible to compute a box [**f**]([**x**]) guaranteed to contain it.

We find that the inclusion function may be quite wider than actual function, which is the unavoidable overestimation in interval arithmetic. How does the overestimation occur in inclusion function? Let us use a simple one-dimensional function to express the reason clearly.

Consider the following one-dimensional quadratic polynomial function

$$f\left(x\right)=x^2-2x+1,\ \left[x\right]=\left[0,2\right] \tag{3-11}$$

If the interval arithmetic is used to calculate this function, the calculation contains three steps: 1) calculate the interval function $[f_1]([x])=[x]^2=[0,4]$, shown as the left plot of Fig.

3-3; 2) calculate the interval function $[f_2]([x])=-2x+1=[-3,1]$, shown as the middle plot; 3) calculate the interval function $[f]([x])=[f_1]([x])+[f_2]([x])=[0,4]+[-3,1]=[-3,5]$, shown as the right plot. Therefore, the final interval result is [-3, 5] by using the interval arithmetic. However, the actual interval should be $[f(x)^*]=[0, 1]$, if we plot the $f(x)$ on the domain of [0, 2].

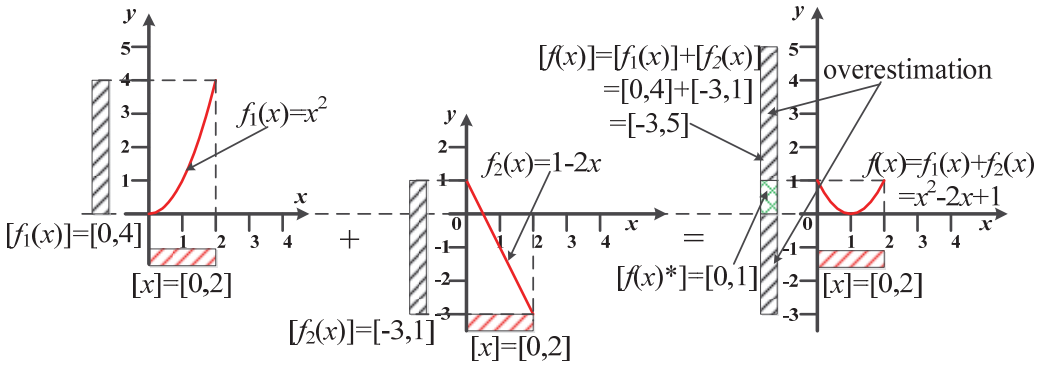

Figure 3-3 Overestimation of interval arithmetic

The overestimation is induced by that the $f_1(x)$ and $f_2(x)$ are considered to be two independent interval numbers, but they are dependent actually, i.e. both of them are the function of x. Most of the overestimation in interval arithmetic is induced by the dependency among several interval variables.

The first idea that comes to mind in order to build an inclusion function for f: $\mathbf{R}^n \rightarrow \mathbf{R}$ is to perform two optimizations to compute the infimum and supremum of f when each x_i is constrained to belong to $[x_i]$. At least in principle, one should thus get the smallest interval containing $f([x_1],\ldots,[x_n])$, denoted by $[f]^*([x_1],\ldots,[x_n])$. However, these optimization problems turn out be far from trivial in general [39], so the interval inclusion function is usually used to estimate the interval range of function. There are mainly three types of inclusion function, i.e. natural, centred, and Taylor inclusion function.

Natural inclusion function

Consider a function

$$f:\mathbf{R}^n \to \mathbf{R}, (x_1,...,x_n) \to f(x_1,...,x_n) \tag{3-11}$$

expressed as a finite composition of the operator +, -, ×, / and elementary functions (e.g. sin, cos, exp, sqr…). An inclusion monotonic and thin inclusion function [39] [f]: $\mathbf{IR}^n \to \mathbf{IR}$ for f is obtained by replacing each real variable x_i by an interval variable $[x_i]$ and each operator or function by its interval counterpart. This function is called the natural inclusion function of f. If f involves only continuous operators and continuous elementary functions, then [f] is convergent. If, moreover, each of the variables (x_1,…,x_n) occurs at most once in the formal expression of f then [f] is minimal.

Natural inclusion functions are not minimal in general, because of the dependency and wrapping effects. The accuracy of the resulting interval strongly depends on the expression of f, as illustrated by the following example [39]

$$f(x) = x(x+1) = x^2 + x = (x+1/2)^2 - 1/4 \tag{3-12}$$

The three formal expressions of f are equivalent for the computation of float numbers. Evaluate their natural inclusion function for $[x]=[-1, 1]$:

$$[f_1]([x]) = [x]([x]+1) = [-2,2], \tag{3-13a}$$

$$[f_2]([x]) = [x]^2 + [x] = [-1,2], \tag{3-13b}$$

$$[f_3]([x]) = ([x]+1/2)^2 - 1/4 = [-1/4,2]. \tag{3-13c}$$

The accuracy of the interval result thus depends on the formal expression of f (Fig. 3-4). Since $[x]$ occurs only once in f_3 and f_3 is continuous, $[f_3]$ is minimal, i.e. equals to the

exact range of $f([x])$. In most cases, it is impossible to find a formal expression that each interval variable occurs only once, so the natural inclusion function is rarely used.

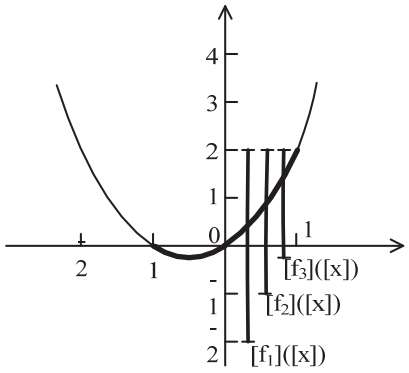

Figure 3-4 Three natural inclusion function for the same function

Centred inclusion function

Let $f:\mathbf{R}^n \to \mathbf{R}$ be as scalar function of a vector $\mathbf{x}=[x_1,...,x_k]^{\mathrm{T}}$. Assume that f is differentiable over the box $[\mathbf{x}]$, and denote mid($[\mathbf{x}]$) by $\mathbf{x}_c$. the mean-value theorem then implies that

$$\forall \mathbf{x} \in [\mathbf{x}], \exists \mathbf{z} \in [\mathbf{x}] \left| f(\mathbf{x}) = f(\mathbf{x}_c) + \mathbf{g}^{\mathrm{T}}(\mathbf{z})(\mathbf{x}-\mathbf{x}_c) \right. \tag{3-14}$$

Where $\mathbf{g}^{\mathrm{T}}$ is the gradient of f, i.e., a column vector with entries $g_i = \partial f / \partial x_i, i = 1,...,k$.

Thus,

$$\forall \mathbf{x} \in [\mathbf{x}], f(\mathbf{x}) \in f(\mathbf{x}_c) + [\mathbf{g}^{\mathrm{T}}]([\mathbf{x}])([\mathbf{x}]-\mathbf{x}_c) \tag{3-15}$$

Where $[g^{\mathrm{T}}]$ is an inclusion function for g^{T}, so

$$f([\mathbf{x}]) \subseteq f(\mathbf{x}_c) + [\mathbf{g}^{\mathrm{T}}]([\mathbf{x}])([\mathbf{x}]-\mathbf{x}_c) \tag{3-16}$$

Therefore, the interval function

$$[f_c]([\mathbf{x}]) = f(\mathbf{x}_c) + [\mathbf{g}^{\mathrm{T}}]([\mathbf{x}])([\mathbf{x}]-\mathbf{x}_c) = f(\mathbf{x}_c) + [\mathbf{g}^{\mathrm{T}}]([\mathbf{x}])[\Delta\mathbf{x}] \tag{3-17}$$

is an inclusion function for f, which we shall call the centred inclusion function. To illustrate the interest of this function in the 1-dimensional case, consider the function $[f_c](x)$ from **R** to **IR** defined by

$$[f_c]([x]) = f(x_c) + [f']([x])[\Delta x] \tag{3-18}$$

for any given [**x**]. This function can be viewed as affine in **x** with an uncertain slope belonging to $[f'](x])$. The smaller w([**x**]) is, the better the centred inclusion function is. When the width of [**x**] tends to 0, there will be the following formula

$$\frac{w([f_c]([x]))}{w(f([x]))} \to 1 \tag{3-19}$$

When the width of [**x**] is small, the effect of the pessimism possibly resulting from the interval evaluation of $[\mathbf{g}^T]([\mathbf{x}])$ is reduced by the scalar product with $[\Delta x]$, which is a small interval centred on zero.

The centred inclusion function for a function f from $\mathbf{R}^n$ to **R** can be noticeably improved by using the mixed centred inclusion functions. The main idea to get a mixed centred inclusion function is to apply the centred inclusion function with each variable in turn. The mixed centred inclusion of the n-dimensional function is expressed by

$$f([\mathbf{x}]) \subseteq f(\mathbf{x}_c) + \sum_{i=1}^{k} [g_i]([x_1],...,[x_i], x_{i+1c},..., x_{kc})([x_i] - x_{ic}) \tag{3-20}$$

The mixed centred inclusion function can get tighter interval than the centred inclusion function for multi-dimensional function.

Taylor inclusion function

Reconsidering the derivation of centred inclusion function, the high-order Taylor series can be used to approximate the function $f : \mathbf{R}^n \to \mathbf{R}$, which leads to the Taylor inclusion

function. Assume that function $f(\mathbf{x})$ has kth-order continuous derivatives with respect to $\mathbf{x}=[x_1...x_n]^{\mathrm{T}}$, so $f(\mathbf{x})$ can be expanded as following kth-order Taylor series.

$$\begin{aligned} f(\mathbf{x}) = f(\mathbf{x}_c) + \sum_{\sum_{i=1}^{n} p_{1,i}=1} \left.\frac{\partial f}{\partial x_1^{p_{1,1}}...\partial x_n^{p_{1,n}}}\right|_{\mathbf{x}_c} (x_1\text{-}x_{1c})^{p_{1,1}}...(x_n\text{-}x_{nc})^{p_{1,n}} + ... \\ + \frac{1}{p_{k,1}!...p_{k,n}!} \sum_{\sum_{i=1}^{n} p_{k,i}=k} \left.\frac{\partial^k f_c}{\partial x_1^{p_{k,1}}...\partial x_n^{p_{k,n}}}\right|_{\mathbf{x}_c} (x_1\text{-}x_{1c})^{p_{k,1}}...(x_n\text{-}x_{nc})^{p_{k,n}} + R_{k+1} \end{aligned} \tag{3-21}$$

where R_{k+1} is the remainder term of Taylor expansion, and $p_{k,i} = 0,1,2...,k$. To simplify the expression, introduce the following operator

$$(\mathbf{G}.\nabla)^h = \sum_{\substack{p_1+...+p_n=h \\ 0\le p_1,...,p_n\le h}} \frac{1}{p_1!...p_n!} G_1^{p_1}...G_n^{p_n} \left.\frac{\partial^h}{\partial x_1^{p_1}...\partial x_n^{p_n}}\right|_{\mathbf{x}_c} \tag{3-22}$$

The Eq. (3-21) can be simplified as

$$f(\mathbf{x}) = \sum_{h=0}^{k} \left((\mathbf{x}\text{-}\mathbf{x}_c)\cdot\nabla\right)^h f + R_{k+1} \tag{3-23}$$

Therefore, the Taylor inclusion function is expressed by

$$[f_T]([\mathbf{x}]) = \sum_{h=0}^{k} \left(([\mathbf{x}]\text{-}\mathbf{x}_c)\cdot\nabla\right)^h f + [R_{k+1}] = \sum_{h=0}^{k} \left([\Delta\mathbf{x}]\cdot\nabla\right)^h f + [R_{k+1}] \tag{3-24}$$

In engineering, the interval remainder term $[R_{k+1}]$ in Eq. (3-24) is usually neglected, because this term has little influence on the result if the k is large enough.

Under mild technical conditions, the natural, centred and Taylor inclusion function are convergent. Roughly speaking, the convergence rate of a convergent inclusion function is the largest α such that [39]

$$\exists\beta \mid w\left([f]([x])\right) - w\left(f([x])\right) \le \beta w\left([x]^{\alpha}\right) \tag{3-25}$$

when w([x]) tends to 0. When an inclusion function is minimal, its convergence rate is infinite. The convergence rate of a natural inclusion function is at least linear, i.e., $\alpha \geq 1$, whereas the convergence rate of centred form is at least quadratic ($\alpha \geq 2$). The convergence rate of a Taylor inclusion function is also at least quadratic for any order $n \geq 2$. Quadratic convergence looks of course more interesting than linear convergence, but it should be remembered that it only means that more accurate results will be obtained in the case of infinitesimal boxes. Noting similar can be said on the behavior of these inclusion functions for boxes of a more realistic size. When the box involved is large, the natural inclusion function is generally more satisfactory than the centred inclusion function, whereas the latter performs better when the box is small, with the mixed version superior to the standard version [39]. No approach to building an inclusion function can claim to be uniformly the best, and a compromise between complexity and efficiency must often be struck. One may also use several inclusion functions and take the intersection of their image sets to get a better approximation of the image set of the original function.

To compare these inclusion functions, the following function is evaluated by the three inclusion functions.

$$f(x) = 1 - x + x^2 + e^x \tag{3-26}$$

Compute the range of the function on two different intervals respectively

$$[x_1] = [0, 2],\ [x_2] = [0.9, 1.1] \tag{3-27}$$

Using the natural, centred, and second order Taylor inclusion function to evaluate the $f(x)$, the corresponding expression is shown as

$$[f]_n([x]) = 1 - [x] + [x]^2 + e^{[x]}. \tag{3-28a}$$

$$[f]_c([x]) = f(1) + [f'][x]([x]-1). \tag{3-28b}$$

$$[f]_T([x]) = f(1) + f'(1)([x]-1) + \frac{1}{2}[f'']([x])([x]-1)^2. \tag{3-28c}$$

where

$$f'(x) = 2x - 1 + e^x,\ f''(x) = 2 + e^x \tag{3-29}$$

Since this function is a monotonically increasing function on the given interval, the exact interval of $f([x])$ can be calculate be the following expression

$$[f]^*([x]) = \left[1 - \underline{x} + \underline{x}^2 + e^{\underline{x}}, 1 - \overline{x} + \overline{x}^2 + e^{\overline{x}}\right] \tag{3-30}$$

The computational results are shown in Table 3-1, where $\Delta = w([f]([x])) - w(f([x]))$.

Table 3-1 Comparing inclusion functions

	$[x_1]=[0, 2]$		$[x_2]=[0.9, 1.1]$	
$[f]$	$[f]([x_1])$	Δ_1	$[f]([x_2])$	Δ_2
$[f]_n$	[0, 12.3891]	2.0	[3.1696, 4.3142]	0.4
$[f]_c$	[-6.6708, 14.1074]	10.3991	[3.2978, 4.1387]	0.0963
$[f]_T$	[0, 12.1311]	1.742	[3.3464, 4.1152]	0.0242
$[f]^*$	[0, 10.3891]	-	[3.3696, 4.1142]	-

The results show that when the width of interval variable is relatively large, the natural inclusion function obtain tighter interval than the centred inclusion function; the centred inclusion function shows better performance than the natural inclusion function when the width of interval variable is small. Nonetheless, the Taylor inclusion function provides the best results for both two cases.

3.2 The Chebyshev inclusion function

The Taylor inclusion function may be the best choice of the three traditional inclusion functions, but it still produces large overestimation for some complicated functions, especially for the non-monotonic functions. Therefore, this section will propose a new inclusion function to reduce the overestimation in further.

3.2.1 Chebyshev polynomial approximation theory

To reduce the computational cost, the complicated functions are usually approximated by some simple functions. The classical Taylor expansion is a kind of polynomials approximation, which uses the Taylor series to approximate the original functions. In mathematical analysis, based on the Weierstrass approximation theory, if any function $f(x)$ is included in $C[a, b]$, i.e., $f(x)$ is continuous over $[a, b]$, there exists a polynomials $p(x)$ which converges to the function $f(x)$ on $[a, b]$ [147], that is

$$\left\| f(x) - p(x) \right\|_{\infty} < \varepsilon, \quad x \in [a,b] \tag{3-31}$$

This expression is validity for any $\varepsilon > 0$. Polynomial is the simplest function and is very convenient to calculate on the computer, so this approximation theorem is very important in numerical analysis.

Let $P_k(x)$ denote the set of polynomials of degree not bigger than k, for every nonnegative integer k, there exists a unique polynomial $p_k^*(x)$ in $P_k(x)$, such that

$$\left\| f(x) - p(x) \right\|_{\infty} \geq \left\| f(x) - p_k^*(x) \right\|_{\infty} = E_k(f), \text{ where } x \in [a,b] \tag{3-32}$$

For all $p(x) \in P_k(x)$ other than $p_k^*(x)$, $E_k(f)$, the infimum of maximum error, is defined as

$$E_k(f)=\inf_{p_k\in P_k}\left\|f(x)-p_k(x)\right\|_\infty, \text{ where } x\in[a,b] \tag{3-33}$$

Here $p_k^*(x)$ is the best uniform approximation of polynomial with degree k to $f(x)$ on [a, b]. However, it's difficult to obtain $p_k^*(x)$ when the degree of polynomials k>2. The truncated Chebyshev series, which are very close to the best uniform approximation polynomials [148, 149], will be employed to approximate the original function.

1-dimensional problem

Firstly, considering the 1-dimensional case, the Chebyshev polynomial for $x\in[-1,1]$ of degree i is denoted by C_i and defined as [150]

$$C_i(x)=\cos i\theta,\ \theta=\arccos(x)\in[0,\pi] \tag{3-34}$$

where i denotes the nonnegative integer. The Chebyshev polynomial can also be defined on interval $x\in[a,b]$, with $\theta=\arccos((2x-b-a)/(b-a))\in[0,\pi]$. The Chebyshev polynomial may also be expressed with respect to $x\in[-1,1]$, and the recursive formula is shown as

$$\begin{aligned}&C_0(x)=1;\\&C_1(x)=x;\\&C_i(x)=2xC_{i-1}(x)-C_{i-2}(x),i\geq 2\end{aligned} \tag{3-35}$$

The Chebyshev polynomial have both the continuous orthogonality relation and discrete orthogonality relation [151], such that

$$\int_{-1}^{1}\frac{C_r(x)C_s(x)}{\sqrt{1-x^2}}dx=\int_0^\pi\cos r\theta\cos s\theta d\theta=\begin{cases}\pi, & r=s=0\\ \pi/2, & r=s\neq 0\\ 0, & r\neq s\end{cases} \tag{3-36}$$

$$\sum_{j=1}^{k}C_r\left(x^{(j)}\right)C_s\left(x^{(j)}\right)=\sum_{j=1}^{k}\cos r\theta^{(j)}\cos s\theta^{(j)}=K_r\delta_{rs},\quad r,s<k \tag{3-37}$$

where $1/\sqrt{1-x^2}$ is the weighting function, $K_0 = k$ and $K_r = k/2$ when $1 \le r < k$, and $x^{(j)}$ and $\theta^{(j)}$ denote the zeros of the *k*-th order Chebyshev polynomial in **x** space and **θ** space, respectively

$$x^{(j)} = \cos\theta^{(j)}, \theta^{(j)} = \frac{2j-1}{k}\frac{\pi}{2}, j = 1, 2, ..., k \tag{3-38}$$

The function $f(x)$ included in $C[a, b]$ can be approximated as the truncated Chebyshev series of degree *k*:

$$f(x) \approx p_k(x) = \frac{1}{2}f_0 + \sum_{i=1}^{k} f_i C_i(x) \tag{3-39}$$

where f_i are the constant coefficients. The error between the truncated Chebyshev series $p_k(x)$ and original function $f(x)$ is shown as follow [153]:

$$e_k(f) = \left|f(x) - p_k(x)\right| \le \frac{2^{-k}}{(k+1)!}\left\|f^{(k+1)}\right\|_\infty \tag{3-40}$$

In the above equation, if *k* is large enough, $e_k(f)$ can be neglected. The truncated Chebyshev series can approximate the original function better than the truncated Taylor series, as shown by Example 3.1 as below.

Constructing the Chebyshev series shown in Eq. (3-39), the key is to compute the coefficients f_i in the expression. If we multiply the Chebyshev polynomial $C_i(x)$ to the two sides of Eq. (3-39) and integrate it in accordance with the weighting function $1/\sqrt{1-x^2}$, the equation will be transformed to

$$\begin{aligned}\int_{-1}^{1}\frac{1}{\sqrt{1-x^2}}f(x)C_i(x)dx &\approx \int_{-1}^{1}\frac{1}{\sqrt{1-x^2}}\left(\frac{1}{2}f_0 + \sum_{j=1}^{k} f_j C_j(x)\right)C_i(x)dx \\ &= \int_{-1}^{1}\frac{1}{\sqrt{1-x^2}}\frac{1}{2}f_0 C_i(x)dx + \sum_{j=1}^{k}\int_{-1}^{1}\frac{1}{\sqrt{1-x^2}}f_j C_j(x)C_i(x)dx\end{aligned} \tag{3-41}$$

By using the continuous orthogonality of Chebyshev polynomials (Eq. (3-36)), the right side of the previous equation will be simplified to $\pi f_i/2$. Therefore, the coefficients of Chebyshev series f_i can be computed by the following formula

$$f_i = \frac{2}{\pi}\int_{-1}^{1} \frac{f(x)C_i(x)}{\sqrt{1-x^2}}dx = \frac{2}{\pi}\int_0^{\pi} f(\cos\theta)\cos i\theta d\theta, i = 0,1,2,...,k \qquad (3\text{-}42)$$

This integral equation has to be computed by numerical integral formula. The Mehler integral, also called Gaussian-Chebyshev integration formula [152] is employed to calculate Eq. (3-42), which is a type of interpolation integral formula expressed as follows:

$$\int_a^b \rho(x) f(x) dx \approx \sum_{j=1}^{p} A_j f\left(x^{(j)}\right) \qquad (3\text{-}43)$$

where A_j are the integral coefficients.

If the interpolation points $x^{(1)}$, $x^{(2)}$...$x^{(p)}$ are the zeros of the orthogonal polynomials of degree p with the weight function $\rho(x)$, the algebraic precision order of this integral formula is 2p-1. For Eq. (3-43), if the weight function is chosen as $\rho(x) = 1/\sqrt{1-x^2}$, the corresponding orthogonal polynomials will be the Chebyshev polynomials. The interpolation points are the zeros of the p-th order Chebyshev polynomials (Eq. (3-38)). In this case, all the integral coefficients $A_j = \pi/p$ [151]. Substitute A_j into Eq. (3-42), we get the Gauss-Chebyshev integral formula as follows:

$$\int_{-1}^{1} \frac{1}{\sqrt{1-x^2}} f(x) dx \approx \frac{\pi}{p}\sum_{j=1}^{p} f\left(x^{(j)}\right) = \frac{\pi}{p}\sum_{j=1}^{p} f\left(\cos\theta^{(j)}\right) \qquad (3\text{-}44)$$

If the function f has 2p-th order derivative on [-1, 1], the numerical error of the Gauss-Chebyshev integral formula is noted as $E_p(f)$, expressed by

$$E_p(f)=\frac{\pi}{(2p)!2^{2p-1}}f^{(2p)}(\xi),-1\le\xi\le1 \tag{3-45}$$

The integral error can be neglected when p is large enough。

Substituting Eq. (3-44) into Eq. (3-42), the coefficients of Chebyshev polynomials are calculated as

$$f_i=\frac{2}{\pi}\int_{-1}^{1}\frac{f(x)C_i(x)}{\sqrt{1-x^2}}dx\approx\frac{2}{\pi}\frac{\pi}{p}\sum_{j=1}^{p}f\left(x^{(j)}\right)C_i\left(x^{(j)}\right)=\frac{2}{p}\sum_{j=1}^{p}f\left(\cos\theta^{(j)}\right)\cos i\theta^{(j)} \tag{3-45}$$

Substituting the coefficients into the Eq. (3-39), the truncated Chebyshev series can be obtained. To minimize the integral error, the order of integral formula should be high enough. In computing the coefficient f_k, the integrand contains the Chebyshev polynomial $C_k(x)$, so the order of integral formula should be larger than k, e.g. p=k+1 in this thesis.

The truncated Chebyshev series has higher approximation accuracy than the truncated Taylor series with same order. To validate the accuracy of Chebyshev approximated polynomials, consider the following mathematical example.

Example 3.1 For function $f(x)=\arctan x$, where $x\in[-1,1]$. Considering use the 5-th order Chebyshev polynomials to approximate this function, the Eqs. (3-38) and (3-45) can be used to compute the coefficients of Chebyshev series. The approximation of 5-th order of truncated Chebyshev polynomials is given by

$$p_5(x)=0.8284\cos\theta-0.0474\cos3\theta+0.0049\cos5\theta \tag{3-46}$$

where $\theta=\arccos x\in[0,\pi]$. The truncated Taylor series approximation of 5-th order is expressed by

$$T_5(x)=x-x^3/3+x^5/5 \tag{3-47}$$

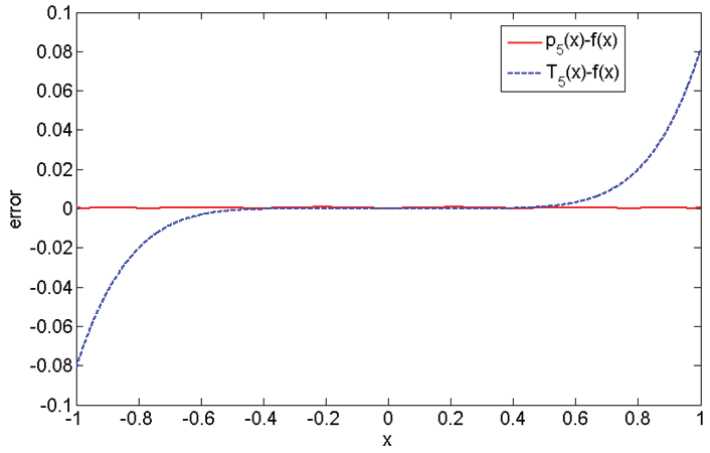

Figure 3-5 Errors of $\arctan x$ **for Chebyshev series and Taylor series**

The errors for Eqs. (3-46) and (3-47) related to the original function are displayed in Fig. 3-5. The results show that the maximum error of the Chebyshev series is much smaller than the conventional Taylor series.

Multi-dimensional problem

For the multi-dimensional problem, the polynomials are the tensor product of each one-dimensional polynomial, e.g. the *n*-dimensional Chebyshev polynomials of $\mathbf{x} \in [-1,1]^n$ is defined as

$$C_{k_1,k_2,\ldots,k_n}(x_1,x_2,\ldots,x_n) = \cos k_1\theta_1 \cos k_2\theta_2 \ldots \cos k_n\theta_n \tag{3-48}$$

where $\theta_i = \arccos(x_i)$. Using the *k*-th order Chebyshev series to approximate the function $f(\mathbf{x}):\mathbf{R}^n \to \mathbf{R}$, the approximation expression can be expressed by extending the Eq. (3-39)

$$f(\mathbf{x}) \approx \sum_{i_1=0}^{k} \ldots \sum_{i_n=0}^{k} \left(\frac{1}{2}\right)^l f_{i_1,\ldots,i_n} C_{i_1,\ldots,i_n}(\mathbf{x}) \tag{3-49}$$

where $f_{i_1,\ldots,i_n}$ denotes the n-dimensional Chebyshev coefficients, and l denotes the total number of zero(s) to be occurred in the subscripts of $C_{i_1,\ldots,i_k}(\mathbf{x})$. For example, l=2 for $C_{0,0}(\mathbf{x})$, while l=0 for $C_{2,1}(\mathbf{x})$. By using the orthogonality of Chebyshev polynomials, the coefficients $f_{i_1,\ldots,i_n}$ can still be obtained by the integration, but the 1-dimensional integration has to be extended to multi-dimensional integration, i.e.

$$\begin{aligned} f_{i_1,i_2,\ldots,i_n} &= \left(\frac{2}{\pi}\right)^n \int_{-1}^{1}\cdots\int_{-1}^{1} \frac{f(\mathbf{x})C_{i_1,\ldots,i_n}(\mathbf{x})}{\sqrt{1-x_1^2}\cdots\sqrt{1-x_n^2}}dx_1\ldots dx_n \\ &= \left(\frac{2}{\pi}\right)^n \int_{0}^{\pi}\cdots\int_{0}^{\pi} f(\cos\theta_1,\ldots,\cos\theta_n)\cos i_1\theta_1\ldots\cos i_n\theta_n d\theta_1\ldots d\theta_n \end{aligned} \tag{3-50}$$

Using the Gaussian-Chebyshev integral formula in each dimension sequentially, the coefficient can be computed by following numerical integral formula

$$\begin{aligned} f_{i_1,\ldots,i_n} &= \left(\frac{2}{\pi}\right)^n \int_{-1}^{1}\cdots\int_{-1}^{1} \frac{f(\mathbf{x})C_{i_1,\ldots,i_n}(\mathbf{x})}{\sqrt{1-x_1^2}\cdots\sqrt{1-x_n^2}}dx_1\ldots dx_n \\ &\approx \left(\frac{2}{k+1}\right)^n \sum_{j_1=1}^{k+1}\cdots\sum_{j_n=1}^{k+1} f\left(\cos\theta_1^{(j_1)},\ldots,\cos\theta_n^{(j_n)}\right)\cos i_1\theta_1^{(j_1)}\ldots\cos i_n\theta_n^{(j_n)} \end{aligned} \tag{3-51}$$

The n-dimensional interpolation points are the tensor product of the 1-dimensional interpolation points, e.g. the second order interpolation points in 1-dimensional case is $\boldsymbol{\theta}=[\pi/4 \quad 3\pi/4]$, then the corresponding interpolation points in 2-dimensional case will be $\boldsymbol{\theta}=[(\pi/4,\pi/4) \quad (\pi/4,3\pi/4) \quad (3\pi/4,\pi/4) \quad (3\pi/4,3\pi/4)]$. Substituting Eq. (3-51) into Eq. (3-49), the multi-dimensional Chebyshev series can be obtained.

3.2.2 Chebyshev inclusion function

The truncated Chebyshev series has high accuracy in approximation; meanwhile it controls the overestimation efficiently when it is used in interval arithmetic, especially for the non-monotonic functions. For the sake of simplicity but without losing any generality,

we consider the 1-dimensional problem. The Taylor inclusion function expands the original function by Taylor series firstly, and then using the interval arithmetic to compute the interval of monomials and polynomial. Similarly, we can expand the original function to a Chebyshev series and then employ the interval arithmetic to compute the interval of Chebyshev series. Replacing the variable x by interval variable $[x]$ in Eq. (3-39), the Chebyshev inclusion function can be obtained as

$$\left[f_{C_k}\right]\left([x]\right)=\frac{1}{2}f_0+\sum_{i=1}^{k}f_i C_i\left([x]\right)=\frac{1}{2}f_0+\sum_{i=1}^{k}f_i\cos i[\theta] \tag{3-52}$$

where $[x]=[-1,1]$, and $[\theta]=\arccos([x])=[0,\pi]$. There are two types of expressions for the Chebyshev polynomial $C_i(x)$, i.e. it can be expressed as a polynomial with respect to x or a trigonometric function with respect to θ. When the interval arithmetic is used, the expression of trigonometric function should be employed, because it controls the overestimation more efficiently than the polynomial expression. For example, compute the $C_3([x])$ by the two expressions respectively,

$$\begin{aligned} &C_3\left([x]\right)=4[x]^3-3[x]=4\times[-1,1]^3-3\times[-1,1]=[-7,7]\\ &C_3\left([x]\right)=[\cos]\left(3[\theta]\right)=[\cos]\left([0,3\pi]\right)=[-1,1] \end{aligned} \tag{3-53}$$

It can be noted that the expression of trigonometric function provides much tighter result than that of polynomial expression. Particularly, since $[\theta]=[0,\pi]$, for any Chebyshev polynomial with $i>0$, such that

$$C_i\left([x]\right)=[\cos]\left(i[\theta]\right)=[\cos]\left([0,i\pi]\right)=[-1,1] \tag{3-54}$$

The plot of Chebyshev polynomials with different order is shown in Fig. 3-6.

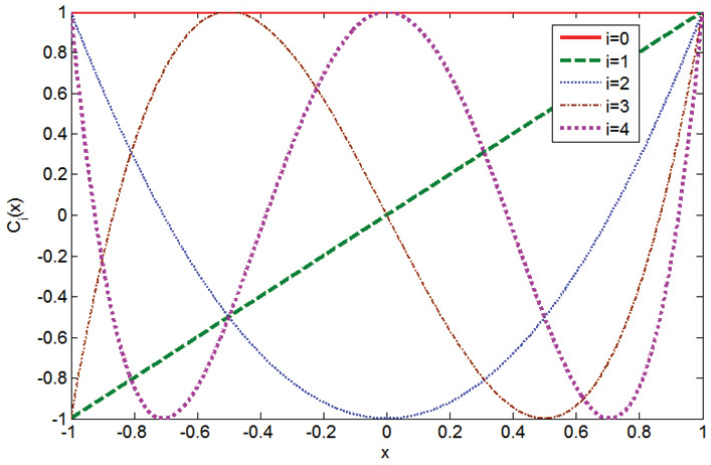

Figure 3-6 The plot of Chebyshev polynomials

Based on this characteristic of Chebyshev polynomials, the Eq. (3-52) can be further simplified as

$$\left[f_{C_k}\right]\left([x]\right)=\frac{1}{2}f_0+\sum_{i=1}^{k}f_i\left[\cos\right]\left(i\left[\theta\right]\right)=\frac{1}{2}f_0+\sum_{i=1}^{k}f_i\left[-1,1\right]=\frac{1}{2}f_0+\left[-1,1\right]\sum_{i=1}^{k}\left|f_i\right| \quad (3\text{-}55)$$

For some highly nonlinear functions, the Chebyshev inclusion function can control the overestimation better than the Taylor inclusion function. Still considering the Example 3.1 in last subsection, use the Chebyshev inclusion function and Taylor inclusion function to compute the bounds of $f([x])=\arctan[x],[x]=[-1,1]$, respectively. The Chebyshev inclusion function is expressed as

$$\begin{aligned}\left[f_{C_5}\right]\left([x]\right)&=0.8284\left[\cos\right]\left(\left[\theta\right]\right)-0.0474\left[\cos\right]\left(3\left[\theta\right]\right)+0.0049\left[\cos\right]\left(5\left[\theta\right]\right)\\&=\left[\text{-}1,1\right]\times\left(\left|0.8284\right|+\left|-0.0474\right|+\left|0.0049\right|\right)=\left[\text{-}0.8807,0.8807\right]\end{aligned} \quad (3\text{-}56)$$

The Taylor inclusion function is

$$\left[f_{T_5}\right]\left([x]\right)=[x]-\frac{[x]^3}{3}+\frac{[x]^5}{5}=\left[\text{-}1.5334,1.5334\right] \quad (3\text{-}57)$$

The exact interval range of $f([x])$ is given by

$$f^*\left([x]\right)=\left[\arctan \underline{x}, \arctan \overline{x}\right]=\left[-0.7854, 0.7854\right] \tag{3-58}$$

Compared the three previous equations, it can be noted that the Chebyshev inclusion function get tighter interval than the Taylor inclusion function. The other advantage of the Chebyshev inclusion function is that it does not need to calculate the derivatives of the original function, so it can be used to solve the black box problems.

Extending the 1-dimensional problem to multi-dimensional problems, the *n*-dimensional Chebyshev inclusion function is expressed by

$$\left[\mathbf{f}_{C_k}\right]\left([\mathbf{x}]\right)=\sum_{i_1=0}^{k}\cdots\sum_{i_n=0}^{k}\left(\frac{1}{2}\right)^l \mathbf{f}_{i_1,\ldots,i_n} C_{i_1,\ldots,i_n}\left([\mathbf{x}]\right)=\frac{1}{2^n}\mathbf{f}_{0,\ldots,0}+[-1,1]\sum_{\substack{0\le i_1,\ldots,i_n\le k\\ i_1+\ldots+i_n\ge 1}}\left(\frac{1}{2}\right)^l\left|\mathbf{f}_{i_1,\ldots,i_n}\right| \tag{3-59}$$

It should be noted that the Chebyshv inclusion function is not a rigorous inclusion function since it neglects the truncated error and numerical error in integration. However, the two parts are usually small compared with the overestimation of interval arithmetic, so they can be neglected.

3.3 The algorithm for solving interval ODEs

In most cases, the dynamic responses of mechanical systems are governed by a set of ODEs, especially by the second-order ODEs. Since the second-order ODEs will be generally transformed to the first-order ODEs in numerical solver, this study is mainly focused on the first-order ODEs. The ODEs of a *m*-dimensional problem can be described as follows:

$$\mathbf{y}'\left(t\right)=\mathbf{f}\left(t,\mathbf{y},\mathbf{x}\right),\ \mathbf{y}\left(t_0\right)=\widehat{\mathbf{y}} \tag{3-60}$$

where t denotes time, $\mathbf{f}=[f_1, f_2, \ldots, f_m]^{\mathrm{T}}$ is a m-dimensional nonlinear function vector, $\mathbf{x}\in R^n$ is a n-dimensional uncertain parameter vector, and $\widehat{\mathbf{y}}$ denotes the m-dimensional

initial vector. As mentioned in Chapter 2, there are many uncertain parameters in engineering. Here we consider some interval parameters existed in the system, i.e. $[\mathbf{x}] \in \mathbf{IR}^n$, and the initial values can also be considered as interval parameters, i.e. $[\hat{\mathbf{y}}] \in \mathbf{IR}^m$.

The solution of Eq. (3-60) subjecting to the interval uncertain condition can be expressed as an interval vector [**y**]

$$[\mathbf{y}] = \left\{ \mathbf{y} : \mathbf{y}'(t) = \mathbf{f}(t, \mathbf{y}, \mathbf{x}), \mathbf{y}(t_0) \in [\hat{\mathbf{y}}], \mathbf{x} \in [\mathbf{x}] \right\} \tag{3-61}$$

The lower bound and upper bound to be solved can be given by

$$\begin{aligned} \underline{\mathbf{y}} &= \min_{\mathbf{x} \in [\mathbf{x}]} \left\{ \mathbf{y} : \mathbf{y}'(t) = \mathbf{f}(t, \mathbf{y}, \mathbf{x}), \mathbf{y}(t_0) \in [\hat{\mathbf{y}}], \mathbf{x} \in [\mathbf{x}] \right\} \\ \overline{\mathbf{y}} &= \max_{\mathbf{x} \in [\mathbf{x}]} \left\{ \mathbf{y} : \mathbf{y}'(t) = \mathbf{f}(t, \mathbf{y}, \mathbf{x}), \mathbf{y}(t_0) \in [\hat{\mathbf{y}}], \mathbf{x} \in [\mathbf{x}] \right\} \end{aligned} \tag{3-62}$$

In general, the precise bounds of the solution cannot be easily obtained through the Eq. (3-62) which has to use the global searching algorithms. To reduce the computational effort, the interval arithmetic is used to estimate the range of the solution.

3.3.1 The interval ODEs solved by Taylor inclusion function

When the interval Taylor series method [72, 154] and Taylor model method [74, 89] solve the interval ODEs, they try to obtain the rigorous enclosure of actual solution. The rigorous interval method methods have two problems. The first problem is low accuracy for strong nonlinear problems. The overestimation in rigorous interval method is larger and larger with the integral range (time domain) increasing, so the divergence of the numerical algorithms cannot be avoided in essential. The other problem is the low efficiency, because a large amount of computational cost has to be spent on handling the interval remainder term, which is actually quite small. In engineering application, the

number of uncertain parameters is usually large, so the computational efficiency should be considered. This subsection propose an approximated Taylor model method to solve ODEs, which only considers the second order Taylor series expansion and neglects the interval remainder term, so the computational efficiency will be improved obviously.

In Eq. (3-60), combining the two interval vectors $[\hat{\mathbf{y}}]$ and $[\mathbf{x}]$ to one interval vector as $[\mathbf{z}]=[[\hat{\mathbf{y}}]^{\mathrm{T}} \quad [\mathbf{x}]^{\mathrm{T}}]^{\mathrm{T}}$. Therefore, $\mathbf{y}$ can be thought as an interval function of $[\mathbf{z}]$, so as the $\mathbf{f}$ is the interval function of $[\mathbf{z}]$. Expanding the $\mathbf{f}$ with respect to $\mathbf{z}$ at the mid-value $\mathbf{z}_c$ by second order series, there will be the following equation.

$$\begin{aligned}\mathbf{f}\left(t,\mathbf{y},\mathbf{z}\right)\approx\mathbf{f}\left(t,\mathbf{y}_c,\mathbf{z}_c\right)+\sum_{j=1}^{m+n}\left(\sum_{i=1}^{m}\frac{\partial\mathbf{f}}{\partial y_i}\frac{\partial y_i}{\partial z_j}+\frac{\partial\mathbf{f}}{\partial z_j}\right)\Bigg|_{(\mathbf{y}_c,\mathbf{z}_c)}\Delta z_j+\\ \frac{1}{2}\sum_{i=1}^{m+n}\sum_{j=1}^{m+n}\left(\sum_{p=1}^{m}\sum_{q=1}^{m}\frac{\partial^2\mathbf{f}}{\partial y_p\partial y_q}\frac{\partial y_p}{\partial z_i}\frac{\partial y_q}{\partial z_j}+2\sum_{p=1}^{m}\frac{\partial^2\mathbf{f}}{\partial y_p\partial z_i}\frac{\partial y_p}{\partial z_j}+\sum_{p=1}^{m}\frac{\partial\mathbf{f}}{\partial y_p}\frac{\partial^2 y_p}{\partial z_i\partial z_j}+\frac{\partial^2\mathbf{f}}{\partial z_i\partial z_j}\right)\Bigg|_{(\mathbf{y}_c,\mathbf{z}_c)}\Delta z_i\Delta z_j\end{aligned} \tag{3-63}$$

Use the second order Taylor series to expand the $\mathbf{y}$ in the left side of Eq. (3-60) at $\mathbf{z}_c$

$$\mathbf{y}\approx\mathbf{y}_c+\sum_{j=1}^{m+n}\frac{\partial\mathbf{y}}{\partial z_j}\Bigg|_{(\mathbf{y}_c,\mathbf{z}_c)}\Delta z_j+\frac{1}{2}\sum_{i=1}^{m+n}\sum_{j=1}^{m+n}\frac{\partial^2\mathbf{y}}{\partial z_i\partial z_j}\Bigg|_{(\mathbf{y}_c,\mathbf{z}_c)}\Delta z_i\Delta z_j \tag{3-64}$$

Since both the two sides of this equation are depend on the time t, we can differentiate them with t

$$\mathbf{y}'\approx\mathbf{y}'_c+\sum_{j=1}^{m+n}\left(\frac{\partial\mathbf{y}}{\partial z_j}\Bigg|_{(\mathbf{y}_c,\mathbf{z}_c)}\right)'\Delta z_j+\frac{1}{2}\sum_{i=1}^{m+n}\sum_{j=1}^{m+n}\left(\frac{\partial^2\mathbf{y}}{\partial z_i\partial z_j}\Bigg|_{(\mathbf{y}_c,\mathbf{z}_c)}\right)'\Delta z_i\Delta z_j \tag{3-65}$$

Substitute the Eq. (3-63) and Eq. (3-65) into the right and left side of Eq. (3-60), respectively

$$\mathbf{y}_c' + \sum_{j=1}^{m+n}\left(\left.\frac{\partial \mathbf{y}}{\partial z_j}\right|_{(\mathbf{y}_c,\mathbf{z}_c)}\right)'\Delta z_j + \frac{1}{2}\sum_{i=1}^{m+n}\sum_{j=1}^{m+n}\left(\left.\frac{\partial^2 \mathbf{y}}{\partial z_i \partial z_j}\right|_{(\mathbf{y}_c,\mathbf{z}_c)}\right)'\Delta z_i \Delta z_j$$
$$= \mathbf{f}\left(t,\mathbf{y}_c,\mathbf{z}_c\right) + \sum_{j=1}^{m+n}\left(\left.\sum_{i=1}^{m}\frac{\partial \mathbf{f}}{\partial y_i}\frac{\partial y_i}{\partial z_j} + \frac{\partial \mathbf{f}}{\partial z_j}\right)\right|_{(\mathbf{y}_c,\mathbf{z}_c)}\Delta z_j + \tag{3-66}$$
$$\frac{1}{2}\sum_{i=1}^{m+n}\sum_{j=1}^{m+n}\left(\left.\sum_{p=1}^{m}\sum_{q=1}^{m}\frac{\partial^2 \mathbf{f}}{\partial y_p \partial y_q}\frac{\partial y_p}{\partial z_i}\frac{\partial y_q}{\partial z_j} + 2\sum_{p=1}^{m}\frac{\partial^2 \mathbf{f}}{\partial y_p \partial z_i}\frac{\partial y_p}{\partial z_j} + \sum_{p=1}^{m}\frac{\partial \mathbf{f}}{\partial y_p}\frac{\partial^2 y_p}{\partial z_i \partial z_j} + \frac{\partial^2 \mathbf{f}}{\partial z_i \partial z_j}\right)\right|_{(\mathbf{y}_c,\mathbf{z}_c)}\Delta z_i \Delta z_j$$

Because the Δz can be any values, Eq. (3-66) can be transformed to the following equations

$$\mathbf{y}_c' = \mathbf{f}\left(t,\mathbf{y}_c,\mathbf{z}_c\right) \tag{3-67a}$$

$$\left(\left.\frac{\partial \mathbf{y}}{\partial z_j}\right|_{(\mathbf{y}_c,\mathbf{z}_c)}\right)' = \left(\left.\sum_{i=1}^{m}\frac{\partial \mathbf{f}}{\partial y_i}\frac{\partial y_i}{\partial z_j} + \frac{\partial \mathbf{f}}{\partial z_j}\right)\right|_{(\mathbf{y}_c,\mathbf{z}_c)} \tag{3-67b}$$

$$\left(\left.\frac{\partial^2 \mathbf{y}}{\partial z_i \partial z_j}\right|_{(\mathbf{y}_c,\mathbf{z}_c)}\right)' = \left(\left.\sum_{p=1}^{m}\sum_{q=1}^{m}\frac{\partial^2 \mathbf{f}}{\partial y_p \partial y_q}\frac{\partial y_p}{\partial z_i}\frac{\partial y_q}{\partial z_j} + \sum_{p=1}^{m}2\frac{\partial^2 \mathbf{f}}{\partial y_p \partial z_i}\frac{\partial y_p}{\partial z_j} + \sum_{p=1}^{m}\frac{\partial \mathbf{f}}{\partial y_p}\frac{\partial^2 y_p}{\partial z_i \partial z_j} + \frac{\partial^2 \mathbf{f}}{\partial z_i \partial z_j}\right)\right|_{(\mathbf{y}_c,\mathbf{z}_c)} \tag{3-67c}$$

Eq. (3-67a) is the ODEs that the interval parameters are set as their mid valued in Eq. (3-60). The second and third equations compute the first derivative and second derivative of **y**. Therefore, the original interval ODEs are transformed to three ODEs with deterministic parameters. Solving the previous deterministic ODEs, and then substituting the solution to the Taylor inclusion function, we can obtain the final interval solution of **y**.

Example 3.2 Solve the following linear ODEs using the rigorous Taylor model method and approximated Taylor model method.

$$\mathbf{y}' = \begin{bmatrix} y_1' \\ y_2' \end{bmatrix} = \mathbf{f} = \begin{bmatrix} x_1 + x_2 y_1 + x_3 y_2 \\ y_1 \end{bmatrix},\ \mathbf{y}_0 = \begin{bmatrix} 0 \\ 0 \end{bmatrix},\ \mathbf{x} \in [\mathbf{x}] = \left[\begin{bmatrix}99,101\end{bmatrix}\ \begin{bmatrix}-1.01,-0.99\end{bmatrix}\ \begin{bmatrix}-10.1,-9.9\end{bmatrix}\right]^{\mathrm{T}} \tag{3-68}$$

The initial values $\mathbf{y}_0$ are deterministic, and there are three interval parameters x_1, x_2 and x_3. The computational results are shown in Fig. 3-7.

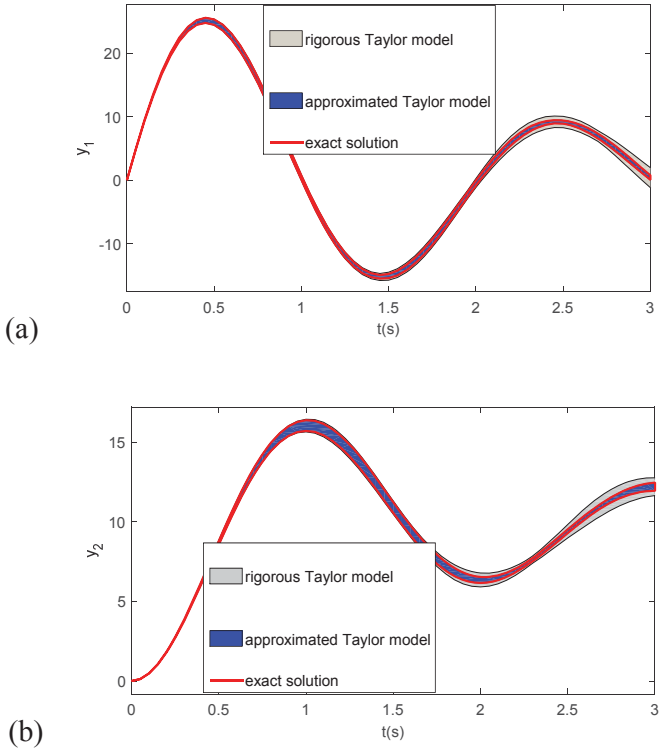

Figure 3-7 (a) The plot of y_1; (b) The plot of y_2

The exact solution is obtained by the scanning method with 10 symmetrical sampling points in each dimensional interval parameter. It can be found that the interval solution of approximated Taylor model method is quite close to the exact solution, so the approximated Taylor model method can control the overestimation better than the rigorous Taylor model method. Although the rigorous Taylor model method encloses all the exact solution, it is enlarged too much after 2 second to be used in practical engineering. For the computational cost, the approximated method takes about 0.2s which is much less than the rigorous method (about 10s). Therefore, the approximated Taylor method is fit for engineering problems, which will be used in below.

3.3.2 The interval ODEs solved by Chebyshev inclusion function

Change the ODEs (3-60) to expression of interval parameters, shown as

$$\mathbf{y}'(t)=\mathbf{f}\left(t,\mathbf{y},[\mathbf{x}]\right),\ \mathbf{y}\left(t_0\right)=[\widehat{\mathbf{y}}] \tag{3-69}$$

Introduce the interval vector $[\mathbf{z}]=[[\widehat{\mathbf{y}}]^{\mathrm{T}}\quad[\mathbf{x}]^{\mathrm{T}}]^{\mathrm{T}}\in\mathbf{IR}^{m+n}$, which can be expressed by the standard interval vector $[\boldsymbol{\eta}]=[-1,1]^{m+n}$, i.e.

$$[\mathbf{z}]=\begin{bmatrix}[\mathbf{y}^0]\\ [\mathbf{x}]\end{bmatrix}=\begin{bmatrix}\dfrac{\underline{y}_1^0+\overline{y}_1^0}{2}+\dfrac{\overline{y}_1^0-\underline{y}_1^0}{2}[\eta_1]\\ \vdots\\ \dfrac{\underline{x}_n+\overline{x}_n}{2}+\dfrac{\overline{x}_n-\underline{x}_n}{2}[\eta_{m+n}]\end{bmatrix} \tag{3-70}$$

When the ODEs are solved by numerical method, the integration domain should be discretized to several sub-integration domains by time nodes, and then compute the solution at each time node. The solution at each time node depends on the solution at previous time node. The solution of first time node is the function of the initial values, expressed as

$$[\mathbf{y}^1]=\mathbf{y}^1\left(t,[\mathbf{y}^0],[\mathbf{x}]\right)=\mathbf{y}^1\left(t,[\boldsymbol{\eta}]\right) \tag{3-71}$$

Here we use superscript to denote the sequential number of time node. The right side of this equation is the function of interval vector $[\boldsymbol{\eta}]$, so we can use the *k*-th order Chebyshev inclusion function to compute it.

$$[\mathbf{y}^1]=\sum_{i_1=0}^{k}\cdots\sum_{i_{m+n}=0}^{k}\left(\frac{1}{2}\right)^l\mathbf{y}^1_{i_1,\ldots,i_{m+n}}C_{i_1,\ldots,i_{m+n}}\left([\boldsymbol{\eta}]\right)=\frac{1}{2^{m+n}}\mathbf{y}^1_{0,\ldots,0}+[-1,1]\sum_{\substack{0\le i_1,\ldots,i_{m+n}\le k\\ i_1+\ldots+i_{m+n}\ge 1}}\left(\frac{1}{2}\right)^l\left|\mathbf{y}^1_{i_1,\ldots,i_{m+n}}\right| \tag{3-72}$$

where $\mathbf{y}^1_{i_1,\ldots,i_{m+n}}$ is the Chebyshev coefficient, computed by the following formula

$$\mathbf{y}^1_{i_1,\ldots,i_{m+n}}=\left(\frac{2}{k+1}\right)^{m+n}\sum_{j_1=1}^{k+1}\cdots\sum_{j_{m+n}=1}^{k+1}\mathbf{y}^1\left(\cos\theta_1^{(j_1)},\ldots,\cos\theta_{m+n}^{(j_{m+n})}\right)\cos i_1\theta_1^{(j_1)}\ldots\cos i_{m+n}\theta_{m+n}^{(j_{m+n})} \quad (3\text{-}73)$$

It should be noted that $\mathbf{y}^1(\cos\theta_1^{(j_1)},\ldots,\cos\theta_{m+n}^{(j_{m+n})})$ denotes the solution of ODEs (3-71) at time node t_1 when the standard interval variables are set to be some float numbers, i.e. $\boldsymbol{\eta}=[\cos\theta_1^{(j_1)},\ldots,\cos\theta_{m+n}^{(j_{m+n})}]^{\mathrm{T}}$. $\cos\theta_i^{(j_i)}$ is the zeros of Chebyshev polynomials. Substituting the coefficients into Eq. (3-72), the interval solution $[\mathbf{y}^1]$ can be obtained.

When we compute the $\mathbf{y}^1(\cos\theta_1^{(j_1)},\ldots,\cos\theta_{m+n}^{(j_{m+n})})$, there is no limitation for numerical methods, which means any traditional numerical methods (e.g. the Runge-Kutta method) for solving ODEs can be used, because the ODEs to be solved have been transformed to the traditional deterministic ODEs.

Since the solution of ODEs at each time node depends on solution at previous time node, and $[\mathbf{y}^1]$ is the function of $[\boldsymbol{\eta}]$, $[\mathbf{y}^j]$ will be the function of $[\boldsymbol{\eta}]$ for any $t_j>t_1$. If the solution at time node t_j has been obtained, the solution at t_{j+1} can be expressed by

$$\left[\mathbf{y}^{j+1}\right]=\mathbf{y}^{j+1}\left(t,\left[\mathbf{y}^j\right],[\mathbf{x}]\right)=\mathbf{y}^{j+1}\left(t,[\boldsymbol{\eta}]\right) \quad (3\text{-}74)$$

Similarly, using the Chebyshev inclusion function to compute the right side, we obtain

$$\left[\mathbf{y}^{j+1}\right]=\left[\mathbf{y}_{C_k}^{j+1}\right]\left(t,[\boldsymbol{\eta}]\right)=\frac{1}{2^{m+n}}\mathbf{y}_{0,\ldots,0}^{j+1}+[-1,1]\sum_{\substack{0\le i_1,\ldots,i_{m+n}\le k\\ i_1+\ldots+i_{m+n}\ge 1}}\left(\frac{1}{2}\right)^l\left|\mathbf{y}_{i_1,\ldots,i_{m+n}}^{j+1}\right| \quad (3\text{-}75)$$

$$\mathbf{y}^{j+1}_{i_1,\ldots,i_{m+n}}=\left(\frac{2}{k+1}\right)^{m+n}\sum_{j_1=1}^{k+1}\cdots\sum_{j_{m+n}=1}^{k+1}\mathbf{y}^{j+1}\left(\cos\theta_1^{(j_1)},\ldots,\cos\theta_{m+n}^{(j_{m+n})}\right)\cos i_1\theta_1^{(j_1)}\ldots\cos i_{m+n}\theta_{m+n}^{(j_{m+n})} \quad (3\text{-}76)$$

Here, $\mathbf{y}^{j+1}(\cos\theta_1^{(j_1)},\ldots,\cos\theta_{m+n}^{(j_{m+n})})$ denotes the solution of ODEs (3-69) at time node t_{j+1} when the interval parameters are set as $\boldsymbol{\eta}=[\cos\theta_1^{(j_1)},\ldots,\cos\theta_{m+n}^{(j_{m+n})}]^{\mathrm{T}}$.

In summary, there are two main steps using the Chebyshev inclusion function solve the interval ODEs: (1) solve the ODEs at the given interpolation points; (2) compute the Chebyshev coefficients and the Chebyshev inclusion function. The first step transforms the original interval ODEs to several deterministic ODEs, and then use traditional numerical methods to solve the ODEs. This process is similar to the Taylor model method, but there are obvious differences between them. Firstly, the Taylor model method transforms the original ODEs into three ODEs. Except the first ODEs, another two ODEs have different expression from original ODEs. However, the Chebyshev method does not change the expression of the ODEs, but only changes the values of initial conditions and interval parameters. Secondly, the Taylor model is hard to extend to higher order expansion, because the derivation of the formulas over second order is extremely complicated. The Chebyshev method is very easy to be extended to higher order, just by increasing more interpolation points. Therefore, the Chebyshev inclusion function based method can be easier implemented and also get higher accuracy.

The flow chart of using Chebyshev inclusion function to solve interval ODEs is shown in Fig. 3-8. From the flow chart, four main steps are involved. The first step is to produce the interpolation points, and the second step is to solve the ODEs at the interpolation points to calculate the value of $\mathbf{y}$. The coefficients of Chebyshev polynomials are calculated in the third step. Finally, the Chebyshev inclusion function will be constructed and the corresponding interval result $[\mathbf{y}]$ will be obtained.

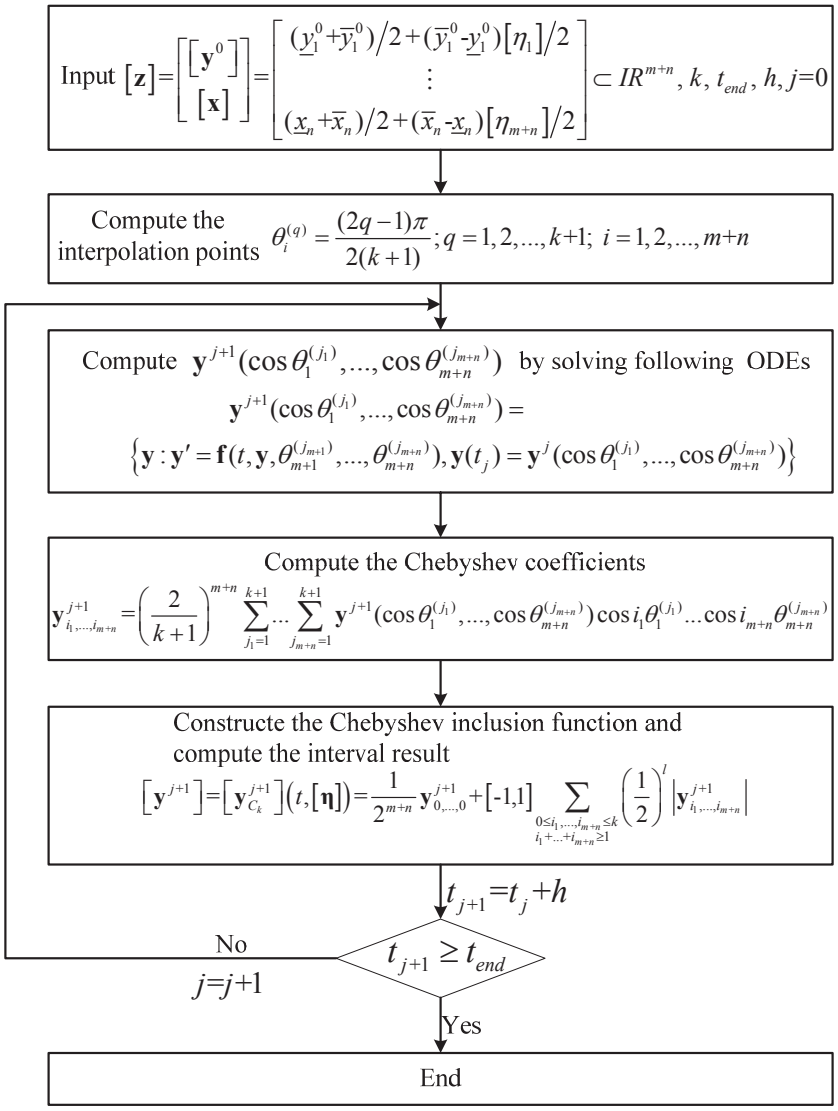

Figure 3-8 The flow chart of Chebyshev inclusion function solving interval ODEs

3.3.3 The numerical example

Consider the double pendulum as the numerical example. The schematic of a double pendulum is shown in Fig. 3-9, where m_1 and m_2 represent the mass of the two pendulums, respectively, and l_1 and l_2 denote the length of the two pendulum rods, respectively.

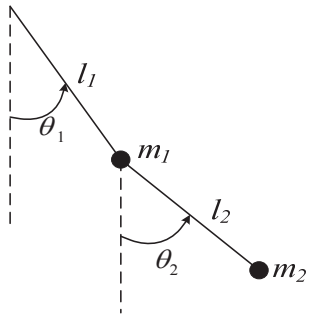

Figure 3-9 Schematic of a double pendulum

The ODEs of this system can be expressed by [92]

$$\begin{cases} \dot{\theta}_1 = \omega_1 \\ \dot{\theta}_2 = \omega_2 \\ \dot{\omega}_1 = \dfrac{-g\left(2m_1+m_2\right)\sin\theta_1 - m_2 g\sin\left(\theta_1-2\theta_2\right) - 2m_2\sin\left(\theta_1-\theta_2\right)\left(\omega_2^2 l_2 - \omega_1^2 l_1\cos\left(\theta_1-\theta_2\right)\right)}{l_1\left(2m_1+m_2-m_2\cos\left(2\theta_1-2\theta_2\right)\right)} \\ \dot{\omega}_2 = \dfrac{2\sin\left(\theta_1-\theta_2\right)\left(\omega_1^2 l_1\left(m_1+m_2\right)+g\left(m_1+m_2\right)\cos\theta_1+\omega_2^2 l_2 m_2\cos\left(\theta_1-\theta_2\right)\right)}{l_2\left(2m_1+m_2-m_2\cos\left(2\theta_1-2\theta_2\right)\right)} \end{cases} \quad (3\text{-}77)$$

Here θ_1 and θ_2 denote the angles of the pendulum rods, ω_1 and ω_2 are the angle velocities of the two rods, and g is the gravity acceleration. It is assumed that two interval parameters are included in the ODEs. The lengths of the two rods are considered as the interval parameters that are expressed as l_1=[0.18, 0.22]m and l_2=[0.36, 0.44]m, and the gravity acceleration is set to the point value with g=9.8m/s^2. The initial conditions are $[\theta_1,\theta_2,\omega_1,\omega_2]=[\pi/3,3\pi/5,0,0]$. The Chebyshev method, Taylor method, and scanning method are applied to solve the ODEs in the period of 0 to 10 second, respectively. For the Chebyshev inclusion function, we choose k=4. With respect to the scanning method, the symmetrical 10 sampling points are used for each uncertain parameter, and the number of calculation is $(k+1)^2$=25 and 20^2=800, respectively. The results of the two pendulum rod angle are shown in Fig. 3-10. It can be found that the Taylor method enlarges the range of results along with the process of the iterations, while Chebyshev

method enclosure the actual results in the entire numerical period with less overestimation. However, it is noted that there are still some overestimation for the Chebyshev method, which cannot be totally avoided when the interval arithmetic is applied to systems with high nonlinearity. Some additional optimization algorithms may be incorporated to eliminate the overestimation ensentially, but it takes much computational effort.

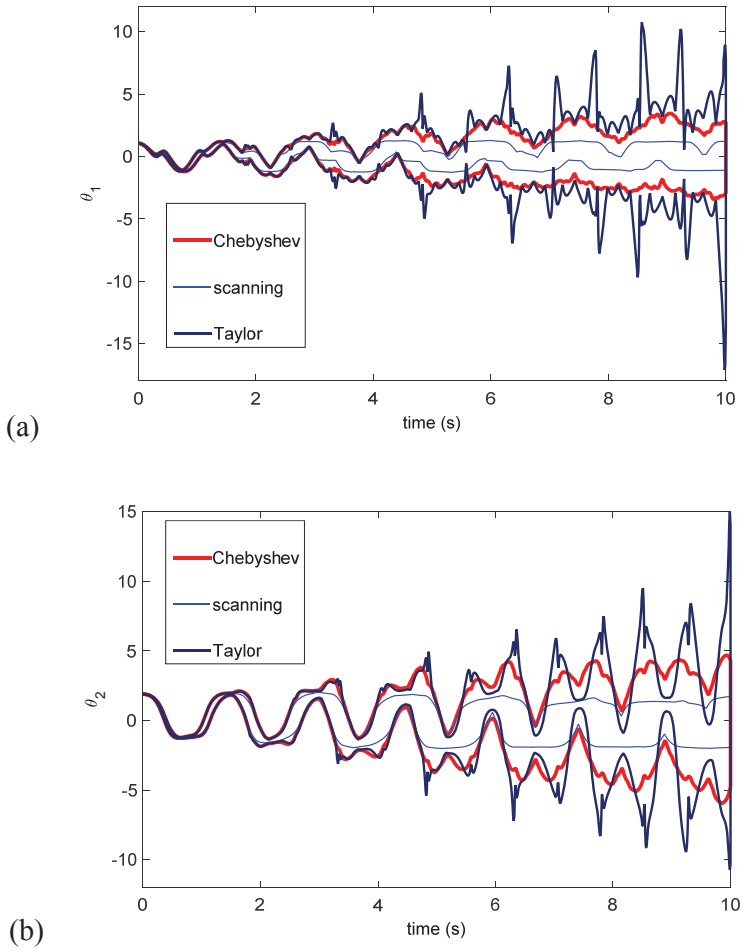

Figure 3-10 The angle of pendulum: (a) top pendulum; (b) bottom pendulum

For the computational cost, the Taylor method takes about 165s, while the Chebyshev method takes only about 5s. Therefore, the Chebyshev method has better performance than the Taylor method in both accuracy and efficiency.

3.4 Chebyshev inclusion function solving multibody system

3.4.1 The Modeling for multibody dynamic system

Multibody dynamics of mechanical systems are widely involved in mechanisms, robotics, vehicles and machines, which consist of many mechanical components interconnected by joints and force elements. Such dynamic systems are often governed by index-3 differential algebraic equations (DAEs) [155], which combine differential equations with algebraic equations to account for the dynamics and holonomic constraints of the system, respectively. Although mathematical modeling methods for multi-body dynamic systems have experienced a rapid growth over the past, most studies assumed that the parameters of the system are deterministic. However, a majority of real-world multi-body systems are too complex to be defined deterministically, due to the lack of complete information. Actually, a variety of uncertainties are inherent in loads, geometry and material parameters, as well as the assembly process and manufacturing tolerances and/or wear, ageing and so on. In these cases, the deterministic assumption may lead to unfeasible designs, as variations associated with the uncertainties might result in significant performance changes of the system. Thus, there is an increasing demand to consider uncertainties in the numerical analysis of multi-body dynamic systems, to ensure the safety of mechanical systems and avoid breakage and even collapse of the mechanism in extreme working conditions.

Multibody systems are characterized by two distinct features: System components undergo finite relative rotations, and the components are connected by mechanical joints that impose restrictions on their relative motions [156] as algebraic constraints. Hence, the constrained equations for multi-body dynamic systems can be typically expressed as [155] a set of DAEs that combine differential and algebraic equations:

$$\begin{cases} \dot{\mathbf{q}} = \mathbf{v} \\ \mathbf{M}(\mathbf{q})\dot{\mathbf{v}} = \mathbf{Q}(t,\mathbf{q},\mathbf{v},\boldsymbol{\lambda},\mathbf{u}(t)) - \boldsymbol{\Phi}_{\mathbf{q}}^{\mathrm{T}}(\mathbf{q},t)\boldsymbol{\lambda} \\ \boldsymbol{\Phi}(\mathbf{q},t) = \mathbf{0} \end{cases} \tag{3-78}$$

where $\mathbf{q} \in R^n$ and $\mathbf{v} \in R^n$ are the generalized coordinates and velocities, respectively. $\boldsymbol{\lambda} \in R^m$ are the Lagrange multipliers, and $\mathbf{u} : R \to R^c$ are time-dependent external dynamics, e.g. control variables. The matrix $\mathbf{M}$ is the generalized mass matrix; $\mathbf{Q}$ is the vector of generalized applied forces, and $\boldsymbol{\Phi}$ is the set of m holonomic constraints.

The classical numerical techniques for DAEs contain two types: state-space methods and direct methods [157]. State-space methods transform DAEs into a set of smaller-dimensional ODEs, and then solve the problem using the conventional ODE solvers. The intrinsic drawback in association with the state-space method is the computational expensive process of transforming DAEs to ODEs, which will be further worsened in the context of implicit integrations [155]. Direct methods discretise constrained equations and transform DAEs to a set of algebraic equations at each integral step. Many direct methods have been proposed to solve the index-3 DAEs, including the Newmark method [158], HHT-I3 [159], and generalized α-method [160]. In this study, HHT-I3 is used as the solver for the DAE systems.

Discretize the Eq. (3-78) with respect to time leads to the following equations [155]:

$$\begin{cases} \mathbf{q}_{n+1} = \mathbf{q}_n + h\dot{\mathbf{q}}_n + \dfrac{h^2}{2}\left[(1\text{-}2\eta)\mathbf{a}_n + 2\eta\mathbf{a}_{n+1}\right] \\ \dot{\mathbf{q}}_{n+1} = \dot{\mathbf{q}}_n + h\left[(1-\gamma)\mathbf{a}_n + \gamma\mathbf{a}_{n+1}\right] \\ \dfrac{1}{1+\alpha}\left(\mathbf{M}(\mathbf{q})\mathbf{a}\right)_{n+1} - \left(\boldsymbol{\Phi}_{\mathbf{q}}^{\mathrm{T}}\boldsymbol{\lambda} - \mathbf{Q}\right)_{n+1} - \dfrac{\alpha}{1+\alpha}\left(\boldsymbol{\Phi}_{\mathbf{q}}^{\mathrm{T}}\boldsymbol{\lambda} - \mathbf{Q}\right)_n = \mathbf{0} \\ \dfrac{1}{\beta h^2}\boldsymbol{\Phi}\left(\mathbf{q}_{n+1}, t_{n+1}\right) = \mathbf{0} \end{cases} \tag{3-79}$$

where h is the integration step size, $\mathbf{a}_{n+1}$ is the approximation of $\ddot{\mathbf{q}}$, and the initial value $\mathbf{a}_0$ can be chosen as $\mathbf{a}_0 = \ddot{\mathbf{q}}_0$, where subscript n denotes the nth integral step, and subscript $\mathbf{q}$ is the derivative of with respect to $\mathbf{q}$. α, β and γ are the parameters in the HHT-I3, which are used to confirm the conditions as:

$$\beta = (1-\alpha^2)/4,\ \alpha \in [-1/3, 0] \text{ and } \gamma = 1/2 - \alpha \tag{3-80}$$

Smaller value of α will result in larger numerical dissipation of HHT-I3, but it will make the solution more stable. The last two equations in Eq. (3-79) are the nonlinear system of $\mathbf{w}_{n+1} = [\mathbf{a}_{n+1} \ \ \boldsymbol{\lambda}_{n+1}]^{\mathrm{T}}$. Using the Newton method to solve the system leads to the following Jacobian matrix:

$$\mathbf{J} = \begin{bmatrix} \dfrac{1}{1+\alpha}(\mathbf{M}+\mathbf{P})_{n+1} & (\boldsymbol{\Phi}_{\mathbf{q}}^{\mathrm{T}})_{n+1} \\ (\boldsymbol{\Phi}_{\mathbf{q}})_{n+1} & \mathbf{0} \end{bmatrix} \tag{3-81}$$

where $$\mathbf{P} = \beta h^2 (\mathbf{M}(\mathbf{q})\ddot{\mathbf{q}} + \boldsymbol{\Phi}_{\mathbf{q}}^{\mathrm{T}}\boldsymbol{\lambda} - \mathbf{Q})_{\mathbf{q}} - \gamma h \mathbf{Q}_{\dot{\mathbf{q}}} \tag{3-82}$$

The initial value $\mathbf{w}_0$ should be firstly determined to enable the Newton iteration. Differentiating the equation of constraints twice with respect to time leads to the following equation:

$$\mathbf{Q}_{\mathbf{d}} = \boldsymbol{\Phi}_{\mathbf{q}}\ddot{\mathbf{q}} = -\boldsymbol{\Phi}_{tt} - 2\boldsymbol{\Phi}_{\mathbf{q}t}\dot{\mathbf{q}} - (\boldsymbol{\Phi}_{\mathbf{q}}\dot{\mathbf{q}})_{\mathbf{q}}\dot{\mathbf{q}} \tag{3-83}$$

The governing equations of multi-body dynamic systems in Eq. (3-78) can be re-written by

$$\begin{bmatrix} \mathbf{M} & \boldsymbol{\Phi}_{\mathbf{q}}^{\mathrm{T}} \\ \boldsymbol{\Phi}_{\mathbf{q}} & \mathbf{0} \end{bmatrix} \begin{bmatrix} \ddot{\mathbf{q}} \\ \boldsymbol{\lambda} \end{bmatrix} = \begin{bmatrix} \mathbf{Q} \\ \mathbf{Q}_{\mathbf{d}} \end{bmatrix} \tag{3-84}$$

As a result, the initial value can be calculated by

$$\mathbf{w}_0 = \begin{bmatrix} \ddot{\mathbf{q}} \\ \boldsymbol{\lambda} \end{bmatrix} = \begin{bmatrix} \mathbf{M} & \boldsymbol{\Phi}_{\mathbf{q}}^{\mathrm{T}} \\ \boldsymbol{\Phi}_{\mathbf{q}} & \mathbf{0} \end{bmatrix}^{-1} \begin{bmatrix} \mathbf{Q} \\ \mathbf{Q}_{\mathbf{d}} \end{bmatrix} \tag{3-85}$$

The major procedures for the HHT-I3 method is outlined as **Algorithm 3.1** in 'A 3.1' [155]. Here, ε denotes the error limitation, the functions $\mathbf{I_1}$ and $\mathbf{I_2}$ are the second and first functions in Eq. (3-79), and Y represents the last two functions in Eq. (3-79). The Algorithm does not explicitly address the uncertain parameters in the equations, and the uncertainties will be discussed in the following sections.

$$\begin{cases} \text{Input: } \mathbf{w}_0 \\ \text{Compute: } \mathrm{t}_{n+1} = t_n + h; \\ \quad w_{n+1}^{(0)} = w_n \\ \quad \begin{cases} \text{Do} \\ \quad \begin{cases} \dot{\mathbf{q}}_{n+1}^{(k)} = \mathbf{I}_1(\mathbf{w}_{n+1}^{(k)}); \\ \mathbf{q}_{n+1}^{(k)} = \mathbf{I}_2(\mathbf{w}_{n+1}^{(k)}); \\ \text{Evaluate } \mathbf{J}; \\ \text{Solve } \mathbf{J}\Delta\mathbf{w}^{(k)} = \mathbf{Y}(\mathbf{w}_{n+1}^{(k)}); \\ \quad \begin{cases} \text{If } \|\Delta\mathbf{w}^{(k)}\| \le \varepsilon \quad \text{break}; \\ \text{else } \mathbf{w}_{n+1}^{(k+1)} = \mathbf{w}_{n+1}^{(k)} - \Delta\mathbf{w}^{(k)}; \end{cases} \\ \text{End do} \end{cases} \\ \quad \mathbf{w}_{n+1} = \mathbf{w}_{n+1}^{(k)}; \\ \text{Output: } \mathbf{w}_{n+1} \end{cases} \tag{A 3.1}$$

3.4.2 The interval DAEs solved by Chebyshev inclusion function

Since the DAEs are usually transformed to algebraic equations and then solved by Newton iteration method, this section firstly research solving the nonlinear algebraic functions with interval parameters based on Chebyshev inclusion function. Consider m-dimensional function group $\mathbf{Y} = [y_1, ..., y_m]^{\mathrm{T}} \subset \mathbf{R}^m \to \mathbf{R}^m$. The algebraic equations can be defined as follows:

$$\mathbf{Y}(\mathbf{X}) = \mathbf{0} \tag{3-86}$$

The Newton method can be used to calculate the value of $\mathbf{Y}$, and the iteration algorithm is described as

$$\mathbf{X}^{i+1} = \mathbf{X}^{i} - \mathbf{J}(\mathbf{X}^{i})^{-1}\mathbf{Y}(\mathbf{X}^{i}) \tag{3-87}$$

where the superscript denotes the iteration step, and $\mathbf{J}(\mathbf{X}^{i})$ is the Jacobin matrix at the *i*th iteration step. The iteration terminal condition is $\left\|\mathbf{J}(\mathbf{X}^{i})^{-1}\mathbf{Y}(\mathbf{X}^{i})\right\|_{\infty} < \varepsilon$, where ε is a small positive real number.

Considering interval parameters contained in the function group, where the uncertain parameters are $\boldsymbol{\eta} \subset [-1,1]^{k}$ (uncertain ranges are transformed to [-1, 1]). The corresponding iterative algorithm be described by

$$\mathbf{X}^{j+1}(\boldsymbol{\eta}) = \mathbf{X}^{j}(\boldsymbol{\eta}) - \mathbf{J}(\mathbf{X}^{j}(\boldsymbol{\eta}), \boldsymbol{\eta})^{-1}\mathbf{Y}(\mathbf{X}^{j}(\boldsymbol{\eta}), \boldsymbol{\eta}) \tag{3-88}$$

The right side of Eq. (3-88) can be regarded as a function of $\boldsymbol{\eta}$. So each iteration step is to calculate the inclusion function with respect to $\boldsymbol{\eta}$. If the interval inclusion functions are directly applied to the iterative algorithm, the results will be easily subject to overestimation. Using the *n*th-order Chebyshev series to approximate the $\mathbf{X}^{i}$

$$\mathbf{X}^{j}(\boldsymbol{\eta}) = \sum_{i_1=0}^{k} \cdots \sum_{i_n=0}^{k} \left(\frac{1}{2}\right)^{l} \mathbf{X}^{j}_{i_1,\ldots,i_n} \cos(i_1\theta_1) \ldots \cos(i_n\theta_n) = \mathbf{X}^{j}(\boldsymbol{\theta}) \tag{3-89}$$

where $\boldsymbol{\theta} = \arccos(\boldsymbol{\eta}) \subset [0,\pi]^{k}$, and $\mathbf{X}^{j}_{i_1,\ldots,i_n}$ is the vector of coefficients. Based on the content in Section 3.2, the coefficients can be computed by

$$\mathbf{X}^{j}_{i_1,\ldots,i_n} = \left(\frac{2}{k+1}\right)^{n} \sum_{j_1=1}^{k+1} \cdots \sum_{j_n=1}^{k+1} \mathbf{X}^{j}\left(\theta_1^{(j_1)},\ldots,\theta_n^{(j_n)}\right) \cos i_1\theta_1^{(j_1)} \ldots \cos i_n\theta_n^{(j_n)} \tag{3-90}$$

where k+1 is number of interpolation points in each dimensional variable，$[\theta_1^{(j_1)},...,\theta_n^{(j_n)}]^{\mathrm{T}}$ are the interpolation points in $\boldsymbol{\theta}$ space， $\mathbf{X}^j(\theta_1^{(j_1)},...,\theta_n^{(j_n)})$ denotes the value of $\mathbf{X}^i$ at the interpolation points。

Substituting Eq. (3-89) into Eq. (3-88), the right side of Eq. (3-88) will be a function of $\boldsymbol{\theta}$ as

$$\mathbf{X}^{j+1}(\boldsymbol{\eta}) = \mathbf{X}^j(\boldsymbol{\theta}) - \mathbf{J}(\mathbf{X}^j(\boldsymbol{\theta}),\cos\boldsymbol{\theta})^{-1}\mathbf{Y}(\mathbf{X}^j(\boldsymbol{\theta}),\cos\boldsymbol{\theta}) =: \mathbf{X}^{j+1}(\boldsymbol{\theta}) \tag{3-91}$$

Similarly, the $\mathbf{X}^{j+1}$ can be expanded by the Chebyshev series

$$\mathbf{X}^{j+1}(\boldsymbol{\eta}) = \sum_{i_1=0}^{k}...\sum_{i_n=0}^{k}\left(\frac{1}{2}\right)^l \mathbf{X}_{i_1,...,i_n}^{j+1}\cos(i_1\theta_1)...\cos(i_n\theta_n) \tag{3-92}$$

The coefficients are computed by

$$\mathbf{X}_{i_1,...,i_n}^{j+1} = \left(\frac{2}{k+1}\right)^n \sum_{j_1=1}^{k+1}...\sum_{j_n=1}^{k+1}\mathbf{X}^{j+1}\left(\theta_1^{(j_1)},...,\theta_n^{(j_n)}\right)\cos i_1\theta_1^{(j_1)}...\cos i_n\theta_n^{(j_n)} \tag{3-93}$$

Considering Eq. (3-89), the value of $\mathbf{X}^{j+1}$ at the interpolation point $\boldsymbol{\eta} = \cos([\theta_1^{(j_1)},...,\theta_1^{(j_n)}]^{\mathrm{T}})$ can be computed by the following equation

$$\begin{aligned}&\mathbf{X}^{j+1}\left(\theta_1^{(j_1)},...,\theta_n^{(j_n)}\right) = \mathbf{X}^j\left(\theta_1^{(j_1)},...,\theta_n^{(j_n)}\right)\\&-\mathbf{J}\left(\mathbf{X}^j\left(\theta_1^{(j_1)},...,\theta_n^{(j_n)}\right),\cos\left(\theta_1^{(j_1)},...,\theta_n^{(j_n)}\right)\right)^{-1}\mathbf{Y}\left(\mathbf{X}^j\left(\theta_1^{(j_1)},...,\theta_n^{(j_n)}\right),\cos\left(\theta_1^{(j_1)},...,\theta_n^{(j_n)}\right)\right)\end{aligned} \tag{3-94}$$

Therefore, if the value of at the interpolation point has known, the value of at the same interpolation point can be calculated by this function. It can be found that Eq. (3-94) is the expression of Eq. (3-91) with the uncertain parameters setting as $\boldsymbol{\eta} = \cos([\theta_1^{(j_1)},...,\theta_n^{(j_n)}]^{\mathrm{T}})$, i.e. the Newton iteration formula for solving the following equation

$$\mathbf{Y}(\mathbf{X},\boldsymbol{\xi})\big|_{\boldsymbol{\eta}=\cos\left(\left[\theta_1^{(j_1)},\ldots,\theta_n^{(j_n)}\right]^{\mathrm{T}}\right)}=\mathbf{0} \tag{3-95}$$

When the iteration is terminated, we can obtain the final value of $\mathbf{X}^*$ at the interpolation point $\mathbf{X}^*(\theta_1^{(j_1)},\ldots,\theta_n^{(j_n)})$. Using Eq. (3-90), we can obtain the final Chebyshev coefficients

$$\mathbf{X}^*_{i_1,\ldots,i_n}=\left(\frac{2}{k+1}\right)^n\sum_{j_1=1}^{k+1}\cdots\sum_{j_n=1}^{k+1}\mathbf{X}^*\left(\theta_1^{(j_1)},\ldots,\theta_n^{(j_n)}\right)\cos i_1\theta_1^{(j_1)}\ldots\cos i_n\theta_n^{(j_n)} \tag{3-96}$$

Substituting the coefficients into the Chebyshev inclusion function，the interval solution of algebraic equations can be obtained

$$\mathbf{X}^*(\boldsymbol{\eta})=\sum_{i_1=0}^{k}\cdots\sum_{i_n=0}^{k}\left(\frac{1}{2}\right)^l\mathbf{X}^*_{i_1,\ldots,i_n}\cos\left(i_1[\theta_1]\right)\ldots\cos\left(i_n[\theta_n]\right) \tag{3-97}$$

The detailed algorithm for using Chebyshev inclusion function to solve algebraic equations is shown as Algorithm 3.2.

Algorithm 3.2

Input: $k,\boldsymbol{\eta}=[\mathbf{a},\mathbf{b}]\subset\mathbf{IR}^n$

Compute: $\theta^{(j)}=(2j-1)\pi/2(k+1);\ j=1,2,\ldots,k+1$

$\eta_i^{(j)}=(a_i+b_i)/2+(b_i-a_i)\cos\theta^{(j)}/2;\ i=1,2,\ldots,n$

$\mathbf{X}^*(\eta_1^{(j_1)},\ldots,\eta_n^{(j_n)})\Leftarrow$ solve $\mathbf{Y}(\mathbf{X},\eta_1^{(j_1)},\ldots,\eta_n^{(j_n)})=0$ (Newton iteration);

$\mathbf{X}^*_{i_1,\ldots,i_n}=\left(\frac{2}{k+1}\right)^n\sum_{j_1=1}^{k+1}\cdots\sum_{j_n=1}^{k+1}\mathbf{X}^*(\eta_1^{(j_1)},\ldots,\eta_n^{(j_n)})\cos i_1\theta_1^{(j_1)}\ldots\cos i_n\theta_n^{(j_n)}$; (A 3.2)

$\mathbf{X}^*_{C_k}=\sum_{i_1=0}^{k}\cdots\sum_{i_n=0}^{k}\left(\frac{1}{2}\right)^l\mathbf{X}^*_{i_1,\ldots,i_n}\cos i_1\theta_1\ldots\cos i_n\theta_n;\ \theta\in[0,\pi]$

$[\mathbf{X}^*_{C_k}]=\sum_{i_1=0}^{k}\cdots\sum_{i_n=0}^{k}\left(\frac{1}{2}\right)^l\mathbf{X}^*_{i_1,\ldots,i_n}\cos i_1[\theta_1]\ldots\cos i_n[\theta_n];$

Output: $[\mathbf{X}^*_{C_k}]$

Section 3.4.1 shows that the numerical method for solving a multi-body dynamic system usually transforms the DAEs into a system of algebraic equations at each integral step, considering the uncertain parameters and uncertain external excitations in the system,

e.g., the manufacturing tolerance of components inducing the mass and center of mass uncertainties, the density uncertainty leading to the mass and moment of inertia uncertainties, as well as the fluctuation of the driving force. If the bounds of uncertain parameters are known, they can be expressed as interval parameters like $\boldsymbol{\eta} \subset [\mathbf{a}, \mathbf{b}]^n$.

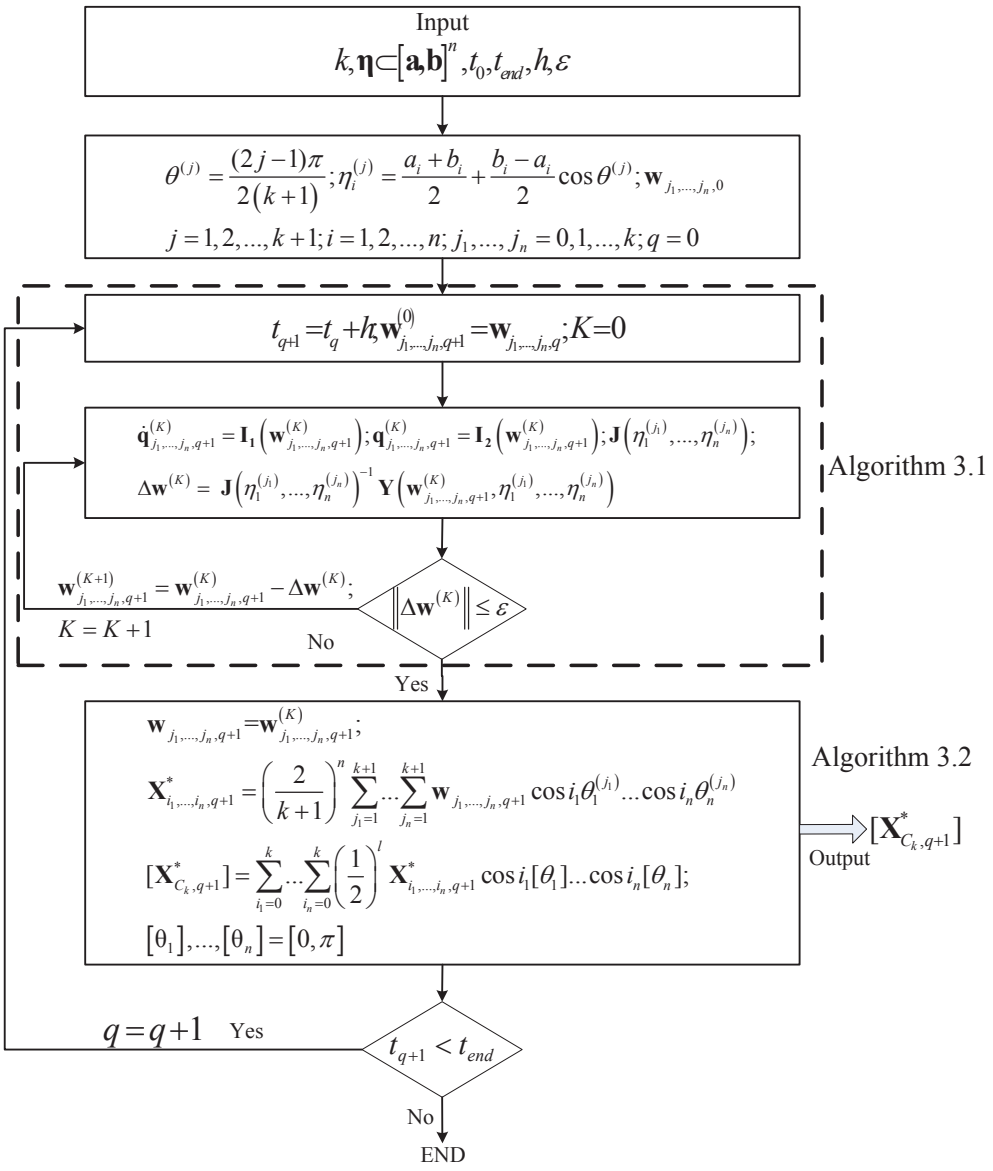

Figure 3-11 The calculation flow for uncertain multi-body system

Combining the Algorithm 3.1 and Algorithm 3.2, the flowchart for solving multibody system with uncertain parameters is given in Fig. 3-11. The input parameters t_0 and t_{end}

are used to denote the initial and terminal time, and $\mathbf{w}_{j_1,\ldots,j_n,q+1}$ is the generalized coordinates, velocities, and accelerations of the $(q+1)$-th step at given interpolation points. It can also be found that the algorithm for solving the uncertain problem includes an inner numerical process (Algorithm 3.1), denoted by the dash block, which can be regarded as a black box module that can be replaced by any other appropriate numerical solvers.

3.4.3 The numerical example

We consider the slider-crank mechanism[102] as the numerical example, in which both the geometry parameter and external force moment are considered as interval parameters. The schematic of the slider crank mechanism is shown in Fig. 3-12, and the parameters are given in Table 3-2.

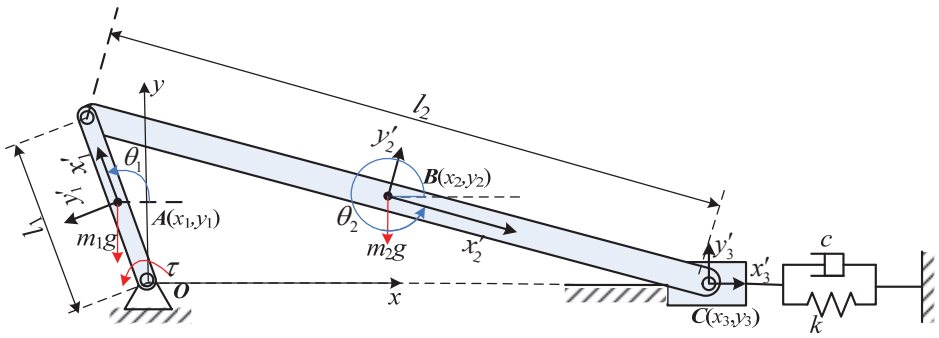

Figure 3-12 Schematic of slider crank

Table 3-2 Parameters of slider crank mechanisms

parameter	l_1(m)	l_2(m)	m_1(kg)	m_2(kg)	m_3(kg)	c(N/(m/s))	k(N/m)	τ (Nm)
value	0.15	0.56	0.37	0.77	0.45	1	5	-0.5

As shown in Fig. 3-12, points *A, B*, and *C* denote the gravity centers of the crank, connecting the rod, and slider, respectively. θ_1 and θ_2 show the angles between the global coordinate and local coordinate of the crank and connecting rod, respectively. The slider is connected with a spring damper, and the spring force is zero when the angle θ_1 and θ_2 equal to zero. l_1 and l_2 are the lengths of the crank and connecting rod. m_1, m_2, and m_3 represent the mass of the crank, connecting rod and slider, respectively. c is the damp coefficient of the spring damper, k is the stiffness of the spring damper, and τ is the external torque applied to the crank.

Choose the generalized coordinate as $\mathbf{q}=[x_1, y_1, \theta_1, x_2, y_2, \theta_2, x_3]^{\mathrm{T}}$, where the subscripts 1, 2, and 3 denote the crank, connecting rod, and slider, respectively. Firstly, supposing the length of the crank l_1 containing uncertainty with 1% of its nominal value, then we have

$$\hat{l}_1 = l_1\left(1+0.01\eta_1\right) \tag{3-98}$$

where $\eta_1 \in [-1,1]$. The mass of the crank is proportional to the length, so the mass and moment of the inertia are given by

$$\hat{m}_1 = m_1\left(1+0.01\eta_1\right), \hat{I}_1 = \frac{1}{12}\hat{m}_1\hat{l}_1^2 = \frac{1}{12}m_1 l_1^2\left(1+0.01\eta_1\right)^3 \tag{3-99}$$

The initial conditions are set as

$$\mathbf{q_0} = \left[\hat{l}_1/2, 0, 0, \hat{l}_1 + l_2/2, 0, 0, \hat{l}_1 + l_2\right]^T, \dot{\mathbf{q}}_\mathbf{0} = \left[0,0,0,0,0,0,0\right]^T \tag{3-100}$$

The system is solved for a period of 2s by using the Chebyshev inclusion function with order 5 and the second order Taylor method, respectively. The scanning method is employed to ensure the precise ranges of the results, with a set of symmetrical 30 sampling points. The results are shown in Fig. 3-13. It can be found that both the intervals of the Taylor method and the Chebyshev method enclose the scanning interval tightly in

the initial stage. However, after the time 1.2s, the overestimation of the Taylor method increases significantly while the results obtained by the Chebyshev method still encloses the range of the scanning method without large overestimation in the whole simulation period.

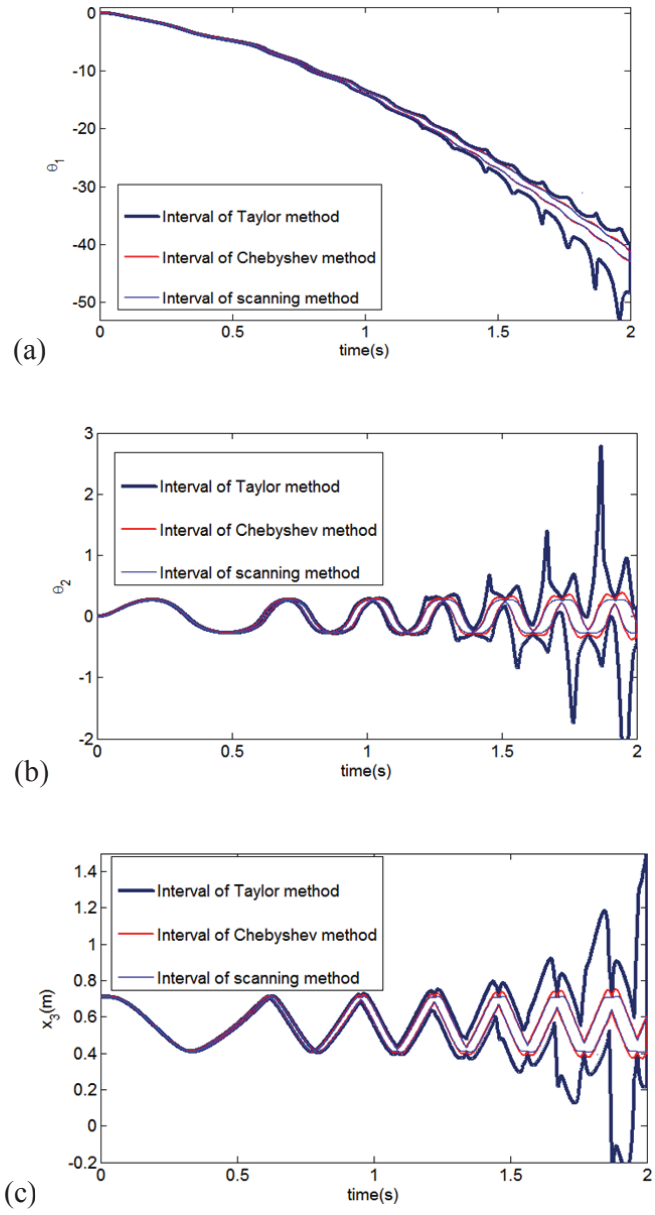

Figure 3-13 (a) Rotation angle of crank with uncertain length of the crank; (b) Rotation angle of connecting rod with uncertain length of the crank; (c) Displacement of piston with uncertain length of the crank

Secondly, we also consider the external torque τ under the interval uncertainty with 1% of its nominal value, and the uncertain external torque is then expressed as

$$\hat{\tau} = \tau\left(1+0.01\eta_2\right), \text{ where } \eta_2 \in [-1,1] \tag{3-101}$$

The initial conditions keep unchanged. Solve the system for a period of 2s using the the fifth-order Chebyhev inclusion function and the second-order Taylor inclusion function. In the scanning method, symmetrical 30 sampling points are employed for each uncertain parameter, and the results are shown from Fig. 3-14. We can find that the number of sampling points (solving the DAEs) for the Chebyshev method is m^2=36 and for the scanning method is 30^2=900, respectively.

The results show that the overestimation induced by the Taylor method is more significant than the case only including one uncertain variable. The Chebyshev method leads to little overestimation, which is much smaller than the Taylor method. The computation time for the three methods is given in Table 3-3. It can be seen that the Chebyshev method requires the least computational time, and then the Taylor method and the scanning method.

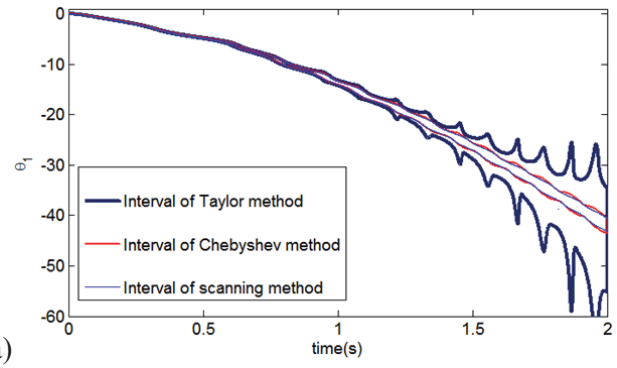

(a)

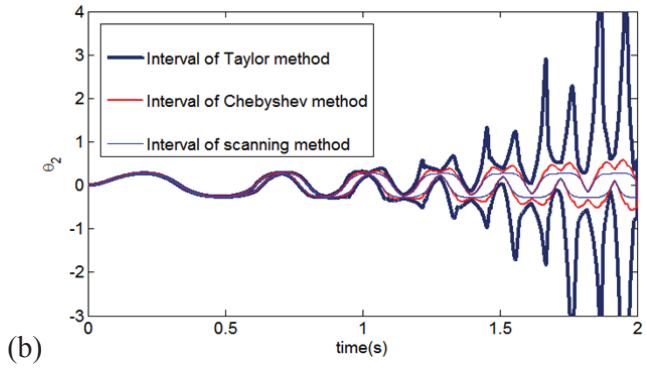

(b)

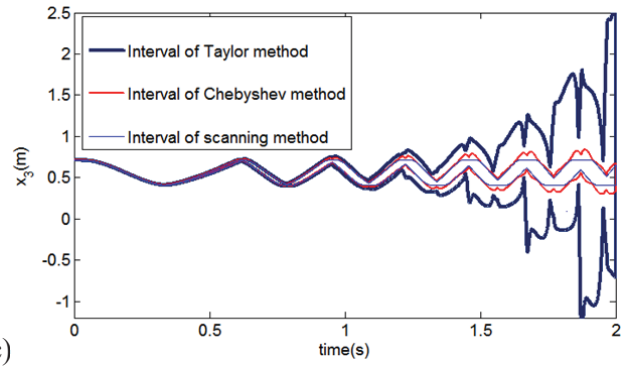

(c)

Figure 3-14 (a) Rotation angle of crank with uncertain torque; (b) Rotation angle of connecting rod with uncertain torque; (c) Displacement of the piston with uncertain torque

Table 3-3 Computational cost

Methods	Chebyshev	Taylor	Scanning
Computation time (s)	422	1392	10584

3.5 Summary

In this chapter, the interval arithmetic is firstly introduced, and then the three types of interval inclusion functions are given. To control the overestimation in further, a new Chebyshev inclusion function is proposed. The Chebyshev inclusion function is based on the Chebyshev series which has high accuracy in approximation theory. The Chebyshev

inclusion function may produce tighter interval than traditional Taylor inclusion function, especially for the non-monotonic functions. At the same time, the proposed Chebyshev inclusion function does not require the derivatives information of the original function, which is easier to realize than the Taylor inclusion function. The Chebyshev inclusion function is employed to solve the ODEs and DAEs with interval parameters. The Chebyshev interval method is a kind of non-intrusive approach so that it can be used for many complicated engineering models and black box models. The numerical examples for solving the mechanical dynamics problems with interval uncertainty indicate that the Chebyshev inclusion function based method control the overestimation better than the Taylor inclusion function based method and is also easier to implement.

Chapter 4 Hybrid uncertainty analysis using orthogonal series expansion

Most works in the uncertainty analysis field were mainly focused on either the aleatory (random) uncertainty or the epistemic (interval) uncertainty, respectively. However, in practical engineering, there are many circumstances that both types of uncertainties existed simultaneously, e.g. vehicle dynamics should comprise both probability uncertainty for random parameters, such as stiffness and damping ratio of components, and non-probabilistic (e.g. interval) uncertainty for uncertain-but-bounded variables, such as loading and geometry size. This chapter will investigate the hybrid uncertainty analysis by using the orthogonal series expansion method, which incorporates the Chebyshev interval method proposed in Chapter 4 and the PC expansion method that is a very popular approach in probability uncertainty analysis.

4.1 The Polynomial Chaos expansion theory

4.1.1 The generalized Polynomial Chaos expansion theory

The fundamental idea of Polynomial Chaos (PC) expansion is that the random process of interest can be approximated by sums of orthogonal polynomials of random independent variables [18]. For a deterministic model with random inputs, if the inputs are represented in terms of the set $\{\xi_i\}_{i=1}^{n}$, the output metrics can also be represented with the same set, as the uncertainty of the outputs is solely because of the uncertainty of the inputs [4] . A random process $Y(\kappa)$, viewed as a function of the random event κ, can be expanded in terms of the orthogonal polynomial chaos as:

$$Y(\kappa)=\sum_{j=0}^{\infty} y_j \phi_j\left(\boldsymbol{\xi}(\kappa)\right) \tag{4-1}$$

Here y_j represents the deterministic coefficients to be estimated, $\phi_j(\boldsymbol{\xi})$ are the generalized Askey-Wiener polynomial chaos of order j, according to the multi-dimensional random variable $\boldsymbol{\xi}=(\xi_1,...,\xi_n)$ [18]. For uniformly distributed random variables the basis are Legendre polynomials, for Gaussian random variables the basis are Hermite polynomials, and more basis for other random variables can be found in [18]. In this chapter, only the uniformly distribution random variables are considered, and other random variables can be dealt with in the same way. In the numerical implementation, we have to employ finite terms to approximate the accuracy value. If we remain s terms, $Y(\kappa)$ can be expressed by

$$Y(\kappa)=\sum_{j=0}^{s-1} y_j \phi_j\left(\boldsymbol{\xi}(\kappa)\right) \tag{4-2}$$

The one dimensional Legendre polynomials satisfy a three-term recurrence relation, which is given by

$$L_0(\xi)=1, L_1(\xi)=\xi, L_{i+1}(\xi)=\frac{2i+1}{i+1}\xi L_i(\xi)-\frac{i}{i+1}L_{i-1}(\xi), (i=1,...,n) \tag{4-3}$$

where $\xi \sim U(-1,1)$. The subscript i denotes the order of Legendre polynomials. For multi-dimensional random variables $\boldsymbol{\xi}=(\xi_1...\xi_n)$, the Legendre polynomials can be expressed as:

$$L_{k_1,k_2...k_n}(\xi_1...\xi_n)=\prod_{j=1}^{n} L_{k_j}(\xi_j),\ \ k_j=0,1,2,... \tag{4-4}$$

For an n-dimensional Legendre polynomials, the order no more than k of the polynomials contain s terms, which are given in Eq. (4-5):

$$s = \frac{(n+k)!}{n!k!} \tag{4-5}$$

The Legendre polynomials $L_{k_1,\ldots,k_n}(\xi_1 \ldots \xi_n)$ in Eq. (4-4) are corresponded with the polynomials ϕ_j in Eq. (4-2). For example, if n=2, the correlation can be shown as follows:

$$\begin{aligned}
&\phi_0 = L_{0,0}(\xi_1,\xi_2) = 1, \\
&\phi_1 = L_{1,0}(\xi_1,\xi_2) = \xi_1, \phi_2 = L_{0,1}(\xi_1,\xi_2) = \xi_2, \\
&\phi_3 = L_{2,0}(\xi_1,\xi_2) = \frac{3}{2}\xi_1^2 - \frac{1}{2}, \phi_4 = L_{1,1}(\xi_1,\xi_2) = \xi_1\xi_2, \phi_5 = L_{0,2}(\xi_1,\xi_2) = \frac{3}{2}\xi_2^2 - \frac{1}{2}, \\
&\ldots
\end{aligned} \tag{4-6}$$

The Legendre polynomial forms a complete orthogonal basis in the L_2 space consisting of the uniformly random variables, i.e.

$$\langle \phi_i, \phi_j \rangle = \langle \phi_i^2 \rangle \delta_{ij} \tag{4-7}$$

where δ_{ij} is the Kronecker delta, and $\langle .,. \rangle$ denotes the ensemble average inner product.

$$\langle f(\xi), g(\xi) \rangle = \int f(\xi) g(\xi) w(\xi) d\xi \tag{4-8}$$

Here $w(\xi) = (1/2)^n$ is the weighting function of Legendre polynomials. With the orthogonality, the coefficient y_i in Eq. (4-2) can be obtained via the following expression

$$y_i = \frac{\langle Y, \phi_i \rangle}{\langle \phi_i^2 \rangle} = \frac{1}{\langle \phi_i^2 \rangle} \int Y \phi_i(\xi) \omega(\xi) d\xi \tag{4-9}$$

Once getting the coefficients, the statistics characteristics can be obtained. The mean of Y is given by the 0th order term in the stochastic expansion, and the variance of Y can be expressed by the sum of square of other terms multiplying with $\langle \phi_i^2 \rangle$

$$\mu = y_0, \ \sigma^2 = \left\langle \left(Y - \bar{Y}\right)^2 \right\rangle = \sum_{i=1}^{s\text{-}1} y_i^2 \langle \phi_i^2 \rangle \tag{4-10}$$

4.1.2 The stochastic response surface method

Although some numerical methods can be applied to calculate the integral in Eq. (4-9), it may be difficult to implement for high dimensional problems. However, the coefficients of the PC expansion can be obtained through the collocation method, by using the model outputs at some selected collocation points to regress the coefficients [4]. The collocation points are selected from the tensor product of the roots of polynomial, which is one order higher than the PC expansion. Eq. (4-5) shows that the *n*-dimensional polynomials with *k*-th order containing $s=(n+k)!/(n!k!)$ terms, while the number of roots combinations is $(k+1)^n$, which is larger than *s*.

For example, to solve the problem with *n*=2 and *k*=1, we can use the roots of the second order Legendre polynomial $-\sqrt{1/3}$ and $\sqrt{1/3}$. The possible collocation points (tensor product of the roots) are $\left(-\sqrt{1/3},-\sqrt{1/3}\right),\left(-\sqrt{1/3},\sqrt{1/3}\right),\left(\sqrt{1/3},-\sqrt{1/3}\right)$ and $\left(\sqrt{1/3},-\sqrt{1/3}\right)$, but the number of coefficients is $s=(2+1)!/2!1!=3$. The collocation method [18] needs to choose at least *s* points from the combinations to run the experiment. If only *s* points are selected, the result may be unstable, because each point in the model space may evidently change the coefficients of the polynomial. Thus, the number of sampling points must be higher than the number of coefficients to be estimated; selecting the number of points equaling twice the number of coefficients is recommended for obtaining robust result [4].

Once the collocation points selected, the least square method can be used to produce the coefficients, i.e.

$$\mathbf{y}=\left(\mathbf{X}(\xi)^T\mathbf{X}(\xi)\right)^{-1}\mathbf{X}(\xi)^{\mathrm{T}}\mathbf{Y},\ \ \mathbf{X}(\xi)=\begin{bmatrix}\phi_0(\xi_1) & \cdots & \phi_{s\text{-}1}(\xi_1)\\ \vdots & \ddots & \vdots\\ \phi_0(\xi_N) & \cdots & \phi_{s\text{-}1}(\xi_N)\end{bmatrix} \tag{4-11}$$

where $\mathbf{Y}=\left[Y\left(\xi_1\right)...Y\left(\xi_N\right)\right]^{\mathrm{T}}$ denotes the model output vector at the collocation points, N denotes the number of collocation points, $\mathbf{y}=\left[y_0,y_1...y_{s-1}\right]^{\mathrm{T}}$ is the coefficients vector of PC expansions, $\mathbf{X}(\xi)$ is the transform matrix, and $\xi_1,...,\xi_N$ denote the collocation points in a n-dimensional space. It can be found that this procedure is quite similar to the response surface method (RSM), except that the basis functions ϕ_i are orthogonal polynomials with respect to the random variables. Therefore, the collocation method for solving the PC expansion is also called stochastic response surface method (SRSM).

4.1.3 Numerical example

Considering the vehicle handling performance, it affects the safety of vehicle directly, especially when the vehicle speed is very high. Simplify the vehicle model to a two-degree-of-freedom (2DOF) bicycle model which does not consider the influence of steering system and suspension system and assumes that the longitudinal velocity of vehicle keep constant to research the vehicle handling characteristic, shown in Fig. 4-1.

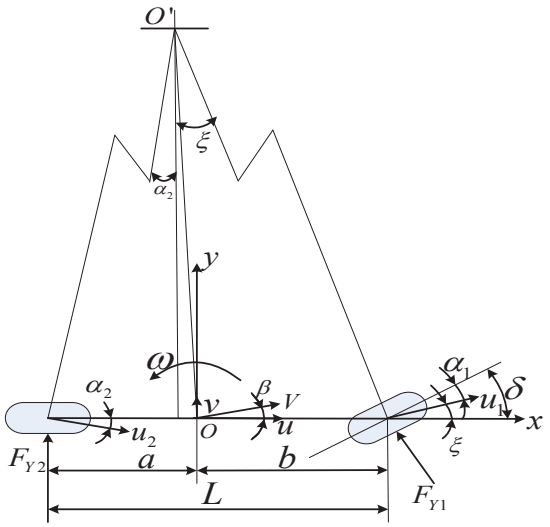

Figure 4-1 The 2 DOF Bicycle model for vehicle

The symbols in the figure are noted as follows:

O: the center of gravity of the vehicle;

O' : the turning center of vehicle;

F_{Y1}, F_{Y2}: lateral force of front wheel and rear wheel;

a, b: the distance from the front and rear axles to the center of gravity;

u, v: the longitudinal velocity and lateral velocity for the center of gravity;

u_1, u_2: the velocity for front wheel and rear wheel;

$\alpha_1, \alpha_2, \beta$: the slip angle for the front wheel, rear wheel and center of gravity;

δ : the steering angle for front wheel;

ξ : the angle between the direction of velocity for front wheel and the x axis;

ω : the yaw velocity of vehicle.

The differential equation of this model is shown in Eq. (4-12).

$$\begin{cases} m\dot{v} = \dfrac{v}{u}\left(k_f + k_r\right) + \dfrac{1}{u}\left(ak_f - bk_r\right)\omega - k_f\delta - mu\omega \\ I_z\dot{\omega} = \dfrac{v}{u}\left(ak_f - bk_r\right) + \dfrac{1}{u}\left(a^2k_f + b^2k_r\right)\omega - ak_f\delta \end{cases} \tag{4-12}$$

where k_f and k_r are the front and rear tire cornering stiffness respectively. The yaw velocity ω and lateral acceleration a_y are mainly researched in this paper. The lateral acceleration can be expressed as

$$a_y = \dot{v} + u\omega \tag{4-13}$$

We consider the dynamic response of the steer angle step input. The step input means that the driver increases the steering angle and then keeps the steer angle unchanged. The step input is that the front tire turns to 2 *degree* in 0.2 second and then keeps the angel constant, as shown in Fig. 4-2.

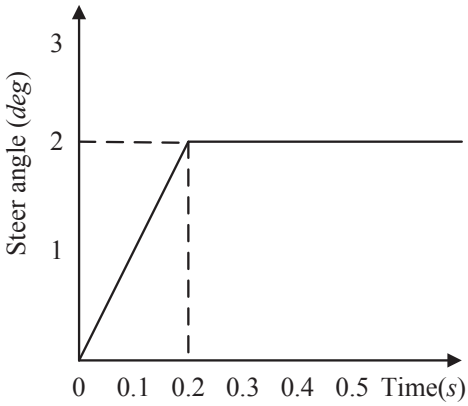

Figure 4-2 Steering angle step input

The step input can be defined as Eq. (4-14).

$$\delta = \begin{cases} \dfrac{10\pi}{180} t & t \le 0.2 \\ \dfrac{2\pi}{180} & t \ge 0.2 \end{cases} \tag{4-14}$$

A group of parameters for a car are shown in Table 4-1. Consider that the parameters *a, b,* k_f, and k_r as random variables. Assume that there is 1% uncertain range for each variable which satisfies independent uniformly distribution. At the same time, the initial conditions are considered as uniformly random variables which are $v_0 \sim U(-0.1, 0.1), \omega_0 \sim U(-0.1, 0.1)$. The indications we researched for vehicle handling are the yaw velocity ω and lateral acceleration a_y, and we use the PC expansion method to solve this problem.

Table 4- 1 Parameters for a car

	$m(kg)$	$I_z(kgm^2)$	$a(m)$	$b(m)$	$k_f(N/rad)$	$k_r(N/rad)$
Mean value	1188	2000	1.117	1.223	-30000	-40000

Use the second order PC expansion method to solve this problem. The Monte Carlo method with 10000 samples is used to validate the PC expansion method. Fig. 4-3 and 4-4 present the mean values of yaw velocity and lateral acceleration for PC expansion method and Monte Carlo method respectively, which show that the mean values for PC expansion method have little error with Monte Carlo simulation.

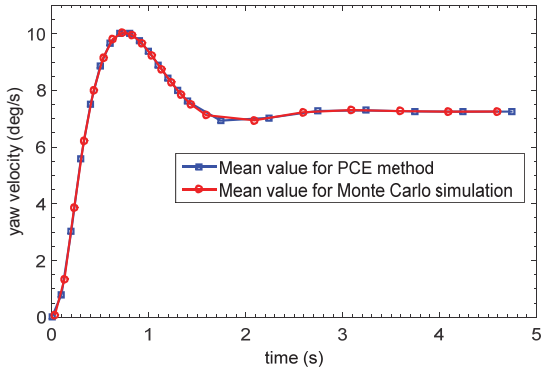

Figure 4-3 Mean value for yaw velocity

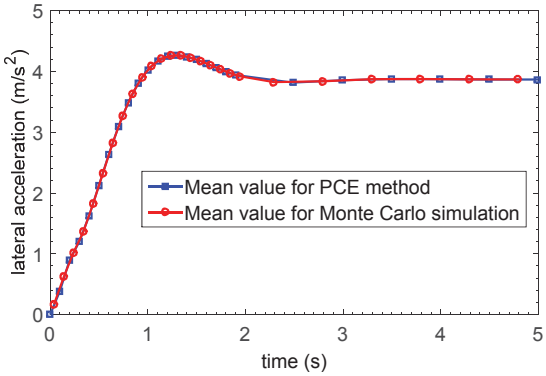

Figure 4-4 Mean value for lateral acceleration

Figure 4-5 and 4-6 present the standard deviations of yaw velocity and lateral acceleration for PC expansion method results and Monte Carlo simulation, respectively. The standard deviations of the yaw velocity and lateral acceleration for PC expansion method are consistent with the result of Monte Carlo simulation before 0.5s, but it is smaller than that of Monte Carlo simulation after 0.5s. The main reason is that only the second order of PC

expansion is used, which produces large truncated error. If higher order PC expansion is employed, they will be well consistent.

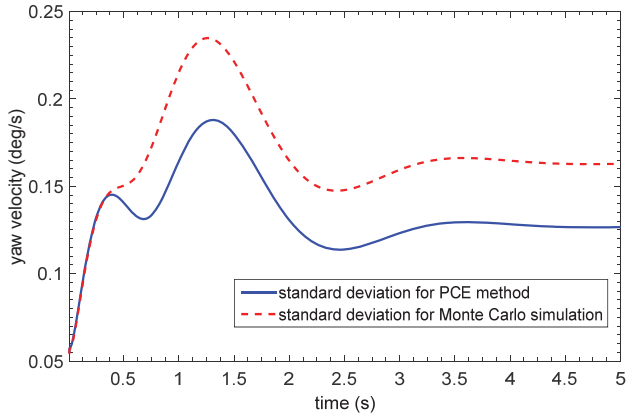

Figure 4-5 Standard deviation for yaw velocity

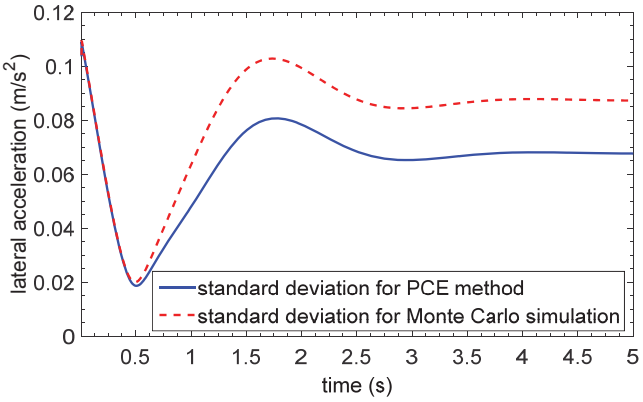

Figure 4-6 Standard deviation for lateral acceleration

4.2 The hybrid uncertain analysis method

4.2.1 The Chebyshev interval analysis using LSM

Chapter 4 has proposed the Chebyshev inclusion function, in which the coefficients of Chebyshev series are computed by using the Gaussian-Chebyshev integral formula. This section will use the least square method (LSM) to compute the coefficients. For simplicity

without losing the generality, here we consider the 1-dimensional problem. Based on the Eq. (3-39), the Chebyshev series expansion is expressed by

$$f(x) \approx \frac{1}{2} f_0 + \sum_{i=1}^{k} f_i C_i(x) = \sum_{i=0}^{k} \gamma_i C_i(x) \tag{3-39}$$

The coefficients are computed by Eq. (3-45)

$$f_i = \frac{2}{\pi} \int_{-1}^{1} \frac{f(x) C_i(x)}{\sqrt{1-x^2}} dx \approx \frac{2}{\pi} \frac{\pi}{p} \sum_{j=1}^{p} f\left(x^{(j)}\right) C_i\left(x^{(j)}\right) \tag{3-45}$$

Consider use the LSM to compute the coefficients γ_i in Eq. (3-39), i.e.

$$\boldsymbol{\gamma} = \left(\mathbf{C}^{\mathrm{T}}\mathbf{C}\right)^{-1} \mathbf{C}^{\mathrm{T}}\mathbf{f} \tag{4-15}$$

$\boldsymbol{\gamma} = [\gamma_0 \quad \gamma_1 \quad \cdots \quad \gamma_k]^{\mathrm{T}}$ is the coefficient vector, $\mathbf{f} = [f(x^{(1)}) \quad \cdots \quad f(x^{(p)})]^{\mathrm{T}}$ denotes the function value vector at the sampling points $x^{(i)}$, i=1, …p, and $\mathbf{C}$ is the $p\times(k+1)$ transform matrix (or design matrix), which can be expressed by

$$\mathbf{C} = \begin{bmatrix} C_0\left(x^{(1)}\right) & C_1\left(x^{(1)}\right) & \cdots & C_n\left(x^{(1)}\right) \\ \vdots & \vdots & \ddots & \vdots \\ C_0\left(x^{(p)}\right) & C_1\left(x^{(p)}\right) & \cdots & C_n\left(x^{(p)}\right) \end{bmatrix} \tag{4-16}$$

When the sampling points are selected as the zeros of Chebyshev polynomial with the order p, the coefficients obtained by Eq. (4-15) will be equal to the coefficients obtained by Eq. (3-45).

Theorem 4.1: *The coefficients of Chebyshev series can be obtained by using the least square method when the zeros of Chebyshev polynomial are used as the sampling points, which will provide the same result as the Gauss-Chebyshev quadrature formula.*

Proof: Considering the Eq. (4-16) and Eq. (4-15), we have

$$\overline{\mathbf{C}}_{(k+1)\times(k+1)}=\mathbf{C}^{\mathrm{T}}\mathbf{C}=\begin{bmatrix}\sum_{j=1}^{p}C_0\left(x^{(j)}\right)C_0\left(x^{(j)}\right) & \cdots & \sum_{j=1}^{p}C_0\left(x^{(j)}\right)C_k\left(x^{(j)}\right)\\ \vdots & \ddots & \vdots\\ \sum_{j=1}^{p}C_k\left(x^{(j)}\right)C_0\left(x^{(j)}\right) & \cdots & \sum_{j=1}^{p}C_k\left(x^{(j)}\right)C_k\left(x^{(j)}\right)\end{bmatrix} \tag{4-17}$$

Since the sampling points are the zeros of Chebyshev polynomial with the order *m*, based on the discrete orthogonality of Chebyshev polynomial (Eq. (3-37)), the matrix $\overline{\mathbf{C}}$ can be transformed to a diagonal matrix

$$\overline{\mathbf{C}}=\begin{bmatrix}K_0 & & 0\\ & K_1 & \\ & \ddots & \\ 0 & & K_p\end{bmatrix}=\begin{bmatrix}p & & 0\\ & p/2 & \\ & \ddots & \\ 0 & & p/2\end{bmatrix} \tag{4-18}$$

Substituting Eq. (4-18) into Eq. (4-15), the coefficient vector can be calculated by

$$\boldsymbol{\gamma}=\begin{bmatrix}\gamma_0\\ \gamma_1\\ \vdots\\ \gamma_k\end{bmatrix}=\overline{\mathbf{C}}^{-1}\mathbf{C}^{\mathrm{T}}\mathbf{f}=\begin{bmatrix}\frac{1}{p}\sum_{j=1}^{p}f(\cos\theta^{(j)})\cos 0\theta^{(j)}\\ \frac{2}{p}\sum_{j=1}^{p}f(\cos\theta^{(j)})\cos 1\theta^{(j)}\\ \vdots\\ \frac{2}{p}\sum_{j=1}^{p}f(\cos\theta^{(j)})\cos k\theta^{(j)}\end{bmatrix}=\begin{bmatrix}\frac{1}{2}f_0\\ f_1\\ \vdots\\ f_k\end{bmatrix} \tag{4-19}$$

Therefore, the LSM produces the same coefficients as Gaussian-Chebyshev quadrature formula.

For the multi-dimensional problems, introducing the *m*-dimensional interval variable $[\boldsymbol{\eta}]=[-1, 1]^m$, the *k*-th order Chebyshev series expansion (Eq. (3-49)) can be expressed as

$$f\left([\boldsymbol{\eta}]\right)=\sum_{i_1=0}^{k}\cdots\sum_{i_m=0}^{k}\left(\frac{1}{2}\right)^{l}f_{i_1,\ldots,i_m}C_{i_1,\ldots,i_m}\left([\boldsymbol{\eta}]\right) \tag{4-20}$$

where l denotes the total number of *zero*(s) to be occurred in the subscripts $i_1,...,i_m$, and $C_{i_1,...,i_m}(\boldsymbol{\eta})$ are the m-dimensional Chebyshev series, which are defined as the tensor product of each dimensional Chebyshev series (Eq. (3-48)).

The interpolation points are the tensor product of each dimensional interpolation points, so the total number of interpolation points is $(k+1)^m$, which also equals to the number of coefficients $f_{i_1,...,i_m}$. The total number of interpolation points will be very large for the high dimensional problems, which will be computationally prohibited. Therefore, we change the format of Chebyshev series expansion as

$$f([\boldsymbol{\eta}]) \approx \sum_{0\le i_1+...+i_m\le k} \left(\frac{1}{2}\right)^l f_{i_1,...,i_m} C_{i_1,...,i_m}([\boldsymbol{\eta}]) = \sum_{i=0}^{p-1} \gamma_i \psi_i([\boldsymbol{\eta}]) \tag{4-21}$$

Here, the coefficients $(1/2)^l f_{i_1,...,i_m}$ are corresponded to γ_i one by one, and $C_{i_1,...,i_m}([\boldsymbol{\eta}])$ are corresponded to $\psi_i([\boldsymbol{\eta}])$ one by one, i.e.

$$\begin{cases} \gamma_0 = (1/2)^m f_{0,...,0}, & \psi_0([\boldsymbol{\eta}]) = C_{0,...,0}([\boldsymbol{\eta}]); \\ \gamma_1 = (1/2)^{m-1} f_{1,0,...,0}, & \psi_1([\boldsymbol{\eta}]) = C_{1,0,...,0}([\boldsymbol{\eta}]); \\ \vdots & \\ \gamma_{p-1} = (1/2)^{m-1} f_{0,...,0,k}, & \psi_{p-1}([\boldsymbol{\eta}]) = C_{0,...,0,k}([\boldsymbol{\eta}]) \end{cases} \tag{4-22}$$

In Eq. (4-21), the terms higher than order k are deleted, and the number of remained terms equals to $p = (m+k)!/(m!k!)$. After the change, we do not need to evaluate all the interpolation points. Similar to the SRSM, some interpolation points are chosen to build the Chebyshev series. Use the LSM to compute the coefficients, i.e.

$$\boldsymbol{\gamma} = \left(\mathbf{X}(\boldsymbol{\eta})^T \mathbf{X}(\boldsymbol{\eta})\right)^{-1} \mathbf{X}(\boldsymbol{\eta})^{\mathrm{T}} \mathbf{f}, \text{ where } \mathbf{X}(\boldsymbol{\eta}) = \begin{bmatrix} \psi_0(\boldsymbol{\eta}_1) & \cdots & \psi_{k-1}(\boldsymbol{\eta}_1) \\ \vdots & \ddots & \vdots \\ \psi_0(\boldsymbol{\eta}_M) & \cdots & \psi_{k-1}(\boldsymbol{\eta}_M) \end{bmatrix} \tag{4-23}$$

where M=2p denotes the number of interpolation points, $\mathbf{f}=[f(\boldsymbol{\eta}_1)...f(\boldsymbol{\eta}_M)]^{\mathrm{T}}$ denotes the model output vector at the m-dimensional interpolation points $\boldsymbol{\eta}_i$, $\boldsymbol{\gamma}=[\gamma_0,\gamma_1...\gamma_{p-1}]^{\mathrm{T}}$ is the coefficients vector of Chebyshev polynomials. Since $\psi_0([\boldsymbol{\eta}])=1$, and $\psi_i([\boldsymbol{\eta}])=[-1,1]$, $i\geq 1$, based on the interval arithmetic, we can calculate the bounds of the interval function as follows:

$$[f]([\boldsymbol{\eta}])=\gamma_0+\left(\sum_{i=1}^{p-1}|\gamma_i|\right)[-1,1] \tag{4-24}$$

It should be noted that Eq. (4-24) cannot eliminate the overestimation induced by the wrapping effect [160], although it can reduce the overestimation. Therefore, some optimization algorithms may be incorporated to avoid the wrapping effect in interval computation.

4.2.2 The statistical evaluation based on interval variables

In this section, both the random and interval variables are contained in a function $F(\boldsymbol{\xi},[\boldsymbol{\eta}])$, which is assumed to be a computationally expensive model. Particurlarily, we consider the n-dimensional random variable $\boldsymbol{\xi}\in U(-1,\ 1)^n$ and the m-dimensional interval variable $[\boldsymbol{\eta}]=[-1,\ 1]^m$. Hence, the output of the function will have the characteristics of both random and interval variables.

Consider the random variable $\boldsymbol{\xi}$ only, and use Eq. (4-2) to expand the function $F(\boldsymbol{\xi},[\boldsymbol{\eta}])$

$$F(\boldsymbol{\xi},[\boldsymbol{\eta}])=\sum_{j=0}^{s-1}\beta_j\phi_j(\boldsymbol{\xi}) \tag{4-25}$$

Here we use β_j denotes the PC coefficients. Since the left side of Eq. (4-25) contains both the interval variable $[\boldsymbol{\eta}]$ and the random variable $\boldsymbol{\xi}$, while $\phi_j(\boldsymbol{\xi})$ at the right side is the Legendre polynomials which is only the function of $\boldsymbol{\xi}$, the coefficients β_j will be a

function with respect to $[\boldsymbol{\eta}]$, namely $\beta_j([\boldsymbol{\eta}])$. Use the Chebyshev expansion Eq. (4-21) to the coefficients $\beta_j([\boldsymbol{\eta}])$, obtaining its Chebyshev inclusion function

$$[\beta_j]([\boldsymbol{\eta}])=\sum_{i=0}^{p-1}\beta_{i,j}\psi_i([\boldsymbol{\eta}]) \tag{4-26}$$

Here $\beta_{i,j}$ denotes the element in the coefficient matrix $\boldsymbol{\beta}$ with p rows and s columns. Substitute Eq. (4-26) into Eq. (4-10), the mean and variance will be obtained as follows:

$$\begin{aligned}\mu([\boldsymbol{\eta}]) &= \beta_0([\boldsymbol{\eta}])=\sum_{i=0}^{p-1}\beta_{i,0}\psi_i([\boldsymbol{\eta}])\\ \sigma^2([\boldsymbol{\eta}]) &= \sum_{j=1}^{s-1}\beta_j^2([\boldsymbol{\eta}])\left\langle\phi_j^2\right\rangle=\sum_{j=1}^{s-1}\left(\sum_{i=0}^{p-1}\beta_{i,j}\psi_i([\boldsymbol{\eta}])\right)^2\left\langle\phi_j^2\right\rangle\end{aligned} \tag{4-27}$$

Since the expression of the mean and variance contains interval variables, the two statistics will also be interval numbers: interval mean (IM) $[\mu]$ and interval variance (IV) $[\sigma^2]$, respectively. Based on the Chebyshev inclusion function, the IM $[\mu]$ can be expressed as

$$[\mu]([\boldsymbol{\eta}])=[\beta_0]([\boldsymbol{\eta}])=\sum_{i=0}^{p-1}\beta_{i,0}\psi_i([\boldsymbol{\eta}])=\beta_{0,0}+\left(\sum_{i=1}^{p-1}\left|\beta_{i,0}\right|\right)[-1,1] \tag{4-28}$$

Similarly, the IV $[\sigma^2]$ may be expressed by

$$[\sigma^2]([\boldsymbol{\eta}])=\sum_{j=1}^{s-1}\left(\left(\sum_{i=0}^{p-1}\beta_{j,i}\psi_i([\boldsymbol{\eta}])\right)^2\left\langle\phi_j^2\right\rangle\right)=\sum_{j=1}^{s-1}\left(\left(\beta_{j,0}+\left(\sum_{i=1}^{p-1}\left|\beta_{j,i}\right|\right)[-1,1]\right)^2\left\langle\phi_j^2\right\rangle\right) \tag{4-29}$$

Since $[\mu]$ and $[\sigma^2]$ are the functions with respect to the interval numbers $[-1,1]$, the above equations (4-28) and (4-29) still involve the overestimation [36] according to the interval arithmetic, particularly, when the evaluated functions are multimodal. Here, the bounds of IM and IV can be calculated respectively as

$$\begin{aligned}
[\mu] &= \left[\underline{\mu}, \overline{\mu}\right] = \left[\min_{-\mathbf{1}\le\boldsymbol{\eta}\le\mathbf{1}} \sum_{i=0}^{p-1} \beta_{i,0}\psi_i(\boldsymbol{\eta}),\ \max_{-\mathbf{1}\le\boldsymbol{\eta}\le\mathbf{1}} \sum_{i=0}^{p-1} \beta_{i,0}\psi_i(\boldsymbol{\eta})\right] \\
\left[\sigma^2\right] &= \left[\underline{\sigma}^2, \overline{\sigma}^2\right] = \left[\min_{-\mathbf{1}\le\boldsymbol{\eta}\le\mathbf{1}} \sum_{j=1}^{s-1}\left(\left(\sum_{i=0}^{p-1} \beta_{i,j}\psi_i(\boldsymbol{\eta})\right)^2 \left\langle \phi_j^2 \right\rangle\right),\ \max_{-\mathbf{1}\le\boldsymbol{\eta}\le\mathbf{1}} \sum_{j=1}^{s-1}\left(\left(\sum_{i=0}^{p-1} \beta_{i,j}\psi_i(\boldsymbol{\eta})\right)^2 \left\langle \phi_j^2 \right\rangle\right)\right]
\end{aligned} \tag{4-30}$$

In interval analysis, the scanning method or global optimization algorithms are often applied to the above equations, in order to solve the "min" and "max" problems to obtain the bounds. In this case, the overestimation of the interval computation can be well controlled. Based on the explicit expressions of IM and IV, both the scanning method and the global optimization algorithm can efficiently find the bounds for IM and IV. If the dimension of the interval variables is less than 3 (m<3), the scanning method [162]can directly produce accurate bounds. However, for the high dimensional problems, some global optimization algorithms, such as the genetic algorithm, particle swarm algorithm, and simulated annealing algorithm, may be more effective.

In the numerical implementation of Eq. (4-30), the coefficient matrix $\boldsymbol{\beta}$ is required to be solved. Firstly, $\beta_j([\boldsymbol{\eta}])$ is considered as an interval function with respect to $[\boldsymbol{\eta}]$, so its Chebyshev coefficient vector can be calculated by using Eq. (4-23), i.e.

$$\begin{bmatrix} \beta_{0,j} \\ \vdots \\ \beta_{p-1,j} \end{bmatrix} = \left(\mathbf{X}_1(\boldsymbol{\eta})^T \mathbf{X}_1(\boldsymbol{\eta})\right)^{-1} \mathbf{X}_1(\boldsymbol{\eta})^{\mathrm{T}} \begin{bmatrix} \beta_j(\boldsymbol{\eta}_1) \\ \vdots \\ \beta_j(\boldsymbol{\eta}_M) \end{bmatrix},\ \mathbf{X}_1(\boldsymbol{\eta}) = \begin{bmatrix} \psi_0(\boldsymbol{\eta}_1) & \cdots & \psi_{p\text{-}1}(\boldsymbol{\eta}_1) \\ \vdots & \ddots & \vdots \\ \psi_0(\boldsymbol{\eta}_M) & \cdots & \psi_{p\text{-}1}(\boldsymbol{\eta}_M) \end{bmatrix} \tag{4-31}$$

where $\beta_j(\boldsymbol{\eta}_i)$ denotes the function value of $\beta_j([\boldsymbol{\eta}])$ at the interpolation points $\boldsymbol{\eta}_i$. Repeating Eq. (4-31) from j=0 to j=s-1 leads to

$$\boldsymbol{\beta} = \begin{bmatrix} \beta_{0,0} & \cdots & \beta_{0,s-1} \\ \vdots & \ddots & \vdots \\ \beta_{p-1,0} & \cdots & \beta_{p-1,s-1} \end{bmatrix} = \left(\mathbf{X}_1(\boldsymbol{\eta})^T \mathbf{X}_1(\boldsymbol{\eta})\right)^{-1} \mathbf{X}_1(\boldsymbol{\eta})^{\mathrm{T}} \begin{bmatrix} \beta_0(\boldsymbol{\eta}_1) & \cdots & \beta_{s-1}(\boldsymbol{\eta}_1) \\ \vdots & \ddots & \vdots \\ \beta_0(\boldsymbol{\eta}_M) & \cdots & \beta_{s-1}(\boldsymbol{\eta}_M) \end{bmatrix} \tag{4-32}$$

Then consider Eq. (4-11) and (4-12), the function value vector $\left[\beta_0(\boldsymbol{\eta}_i),...,\beta_{s-1}(\boldsymbol{\eta}_i)\right]^{\mathrm{T}}$ can be calculated as

$$\begin{bmatrix}\beta_0(\boldsymbol{\eta}_i)\\ \vdots \\ \beta_{s-1}(\boldsymbol{\eta}_i)\end{bmatrix}=\left(\mathbf{X}_2(\boldsymbol{\xi})^{\mathrm{T}}\mathbf{X}_2(\boldsymbol{\xi})\right)^{-1}\mathbf{X}_2(\boldsymbol{\xi})^{\mathrm{T}}\begin{bmatrix}F(\boldsymbol{\xi}_1,\boldsymbol{\eta}_i)\\ \vdots \\ F(\boldsymbol{\xi}_N,\boldsymbol{\eta}_i)\end{bmatrix},\mathbf{X}_2(\boldsymbol{\xi})=\begin{bmatrix}\phi_0(\boldsymbol{\xi}_1) & \cdots & \phi_{s\text{-}1}(\boldsymbol{\xi}_1)\\ \vdots & \ddots & \vdots \\ \phi_0(\boldsymbol{\xi}_N) & \cdots & \phi_{s\text{-}1}(\boldsymbol{\xi}_N)\end{bmatrix} \quad (4\text{-}33)$$

Apply Eq. (4-33) to all interpolation points from $\boldsymbol{\eta}_1$ to $\boldsymbol{\eta}_M$, the function value matrix $\beta(\boldsymbol{\eta})$ will be

$$\begin{bmatrix}\beta_0(\boldsymbol{\eta}_1) & \cdots & \beta_0(\boldsymbol{\eta}_M)\\ \vdots & \ddots & \vdots \\ \beta_{s-1}(\boldsymbol{\eta}_1) & \cdots & \beta_{s-1}(\boldsymbol{\eta}_M)\end{bmatrix}=\left(\mathbf{X}_2(\boldsymbol{\xi})^{\mathrm{T}}\mathbf{X}_2(\boldsymbol{\xi})\right)^{-1}\mathbf{X}_2(\boldsymbol{\xi})^{\mathrm{T}}\begin{bmatrix}F(\boldsymbol{\xi}_1,\boldsymbol{\eta}_1) & \cdots & F(\boldsymbol{\xi}_1,\boldsymbol{\eta}_M)\\ \vdots & \ddots & \vdots \\ F(\boldsymbol{\xi}_N,\boldsymbol{\eta}_1) & \cdots & F(\boldsymbol{\xi}_N,\boldsymbol{\eta}_M)\end{bmatrix} \quad (4\text{-}34)$$

Substitute Eq. (4-34) into Eq. (4-32), we have the following equation.

$$\begin{aligned}\boldsymbol{\beta}&=\left(\mathbf{X}_1(\boldsymbol{\eta})^{\mathrm{T}}\mathbf{X}_1(\boldsymbol{\eta})\right)^{-1}\mathbf{X}_1(\boldsymbol{\eta})^{\mathrm{T}}\left(\left(\mathbf{X}_2(\boldsymbol{\xi})^{\mathrm{T}}\mathbf{X}_2(\boldsymbol{\xi})\right)^{-1}\mathbf{X}_2(\boldsymbol{\xi})^{\mathrm{T}}\mathbf{F}\right)^{\mathrm{T}}\\ &=\left(\mathbf{X}_1(\boldsymbol{\eta})^{\mathrm{T}}\mathbf{X}_1(\boldsymbol{\eta})\right)^{-1}\mathbf{X}_1(\boldsymbol{\eta})^{\mathrm{T}}\mathbf{F}^{\mathrm{T}}\mathbf{X}_2(\boldsymbol{\xi})\left(\mathbf{X}_2(\boldsymbol{\xi})\mathbf{X}_2(\boldsymbol{\xi})^{\mathrm{T}}\right)^{-1}\end{aligned} \quad (4\text{-}35)$$

where **F** is the function value matrix at the collocation points and interpolation points.

$$\mathbf{F}=\begin{bmatrix}F(\boldsymbol{\xi}_1,\boldsymbol{\eta}_1) & \cdots & F(\boldsymbol{\xi}_1,\boldsymbol{\eta}_M)\\ \vdots & \ddots & \vdots \\ F(\boldsymbol{\xi}_N,\boldsymbol{\eta}_1) & \cdots & F(\boldsymbol{\xi}_N,\boldsymbol{\eta}_M)\end{bmatrix} \quad (4\text{-}36)$$

After obtaining the coefficient matrix **β** via Eqs. (4-35) and (4-36), as aforementioned, the scanning method or the global optimization algorithms can be applied to evaluate the bounds of the IM and IV.

4.2.3 The bounds evaluation based on random variables

Substituting Eq. (4-26) into Eq. (4-25), the function can be expressed as

$$F\left(\xi,[\boldsymbol{\eta}]\right)=\sum_{j=0}^{s-1}\left(\sum_{i=0}^{p-1}\beta_{j,i}\psi_i\left([\boldsymbol{\eta}]\right)\right)\phi_j\left(\xi\right) \tag{4-37}$$

Since $\psi_0\left([\boldsymbol{\eta}]\right)=1$ and $\psi_i\left([\boldsymbol{\eta}]\right)=[-1,1]$ for any $i\geq 1$, the lower bound and upper bound of $F\left(\xi,[\boldsymbol{\eta}]\right)$ can be directly estimated using interval arithmetic. Due to the wrapping effect in interval arithmetic, the global optimization algorithms or scanning method are often used to find the bounds of $F\left(\xi,[\boldsymbol{\eta}]\right)$. The lower bound and upper bound are defined as

$$\begin{cases}\underline{F}\left(\xi,[\boldsymbol{\eta}]\right)=\min\limits_{-\mathbf{1}\leq\boldsymbol{\eta}\leq\mathbf{1}}\sum\limits_{j=0}^{s-1}\left(\sum\limits_{i=0}^{p-1}\beta_{j,i}\psi_i\left(\boldsymbol{\eta}\right)\right)\phi_j\left(\xi\right)\\ \overline{F}\left(\xi,[\boldsymbol{\eta}]\right)=\max\limits_{-\mathbf{1}\leq\boldsymbol{\eta}\leq\mathbf{1}}\sum\limits_{j=0}^{s-1}\left(\sum\limits_{i=0}^{p-1}\beta_{j,i}\psi_i\left(\boldsymbol{\eta}\right)\right)\phi_j\left(\xi\right)\end{cases} \tag{4-38}$$

Since the above bounds contains the random variable ξ, the bounds are not an exact number but a random number satisfying probability characteristics. In order to evaluate the bounds more precisely, we need to calculate the mean value and variance. These indexes are termed as mean of lower bound (MLB) and mean of upper bound (MUB), as well as variance of lower bound (VLB) and variance of upper bound (VUB), respectively.

The PC expansion theory can still be used to calculate the mean and variance, but the Eq. (4-38) is not the standard form of the PC expansion because the min and max operations are included in the expression. Thus, the PC expansion procedure has to be used to expand the lower bound and upper bound again. Based on Eq. (4-2), the bounds of $F(\xi,[\boldsymbol{\eta}])$ can be expanded as

$$\underline{F}\left(\xi,[\boldsymbol{\eta}]\right)=\sum_{j=0}^{s'-1}\underline{\beta}_j\phi_j\left(\xi\right),\ \overline{F}\left(\xi,[\boldsymbol{\eta}]\right)=\sum_{j=0}^{s'-1}\overline{\beta}_j\phi_j\left(\xi\right) \tag{4-39}$$

where $s'=\left(n+k'\right)!/\left(n!k'!\right)$ denotes the number of the coefficients, and k' denotes the order of Legendre polynomial. Using Eqs. (4-11) and (4-12), the coefficients can be calculated by

$$\begin{aligned}\begin{bmatrix}\underline{\beta}_0\\ \vdots\\ \underline{\beta}_{s'\text{-}1}\end{bmatrix}&=\left(\mathbf{X}_3\left(\boldsymbol{\xi}\right)^T\mathbf{X}_3\left(\boldsymbol{\xi}\right)\right)^{-1}\mathbf{X}_3\left(\boldsymbol{\xi}\right)^{\mathrm{T}}\begin{bmatrix}\underline{F}\left(\xi_1\right)\\ \vdots\\ \underline{F}\left(\xi_{N'}\right)\end{bmatrix}\\ \begin{bmatrix}\overline{\beta}_0\\ \vdots\\ \overline{\beta}_{s'\text{-}1}\end{bmatrix}&=\left(\mathbf{X}_3\left(\boldsymbol{\xi}\right)^T\mathbf{X}_3\left(\boldsymbol{\xi}\right)\right)^{-1}\mathbf{X}_3\left(\boldsymbol{\xi}\right)^{\mathrm{T}}\begin{bmatrix}\overline{F}\left(\xi_1\right)\\ \vdots\\ \overline{F}\left(\xi_{N'}\right)\end{bmatrix}\end{aligned}\tag{4-40}$$

where the number of collocation points $N'=2s'$, and $\mathbf{X}_3\left(\boldsymbol{\xi}\right)$ is the transform matrix expressed as

$$\mathbf{X}_3\left(\boldsymbol{\xi}\right)=\begin{bmatrix}\phi_0\left(\xi_1\right) & \cdots & \phi_{s'\text{-}1}\left(\xi_1\right)\\ \vdots & \ddots & \vdots\\ \phi_0\left(\xi_{N'}\right) & \cdots & \phi_{s'\text{-}1}\left(\xi_{N'}\right)\end{bmatrix}\tag{4-41}$$

Due to the min and max operations involved in Eq. (4-38), we use higher order of polynomials to expand it ($k'>k$). Utilizing Eq. (10), the MLB, VLB, MUB, and VUB can be calculated as

$$\mu_{\underline{F}}=\underline{\beta}_0,\ \sigma_{\underline{F}}^2=\sum_{i=1}^{s'\text{-}1}\underline{\beta}_i^2\left\langle\phi_i^2\right\rangle,\ \mu_{\overline{F}}=\overline{\beta}_0,\ \sigma_{\overline{F}}^2=\sum_{i=1}^{s'\text{-}1}\overline{\beta}_i^2\left\langle\phi_i^2\right\rangle\tag{4-42}$$

According to the previous description, the proposed method includes two regression processes, the first of which is to obtain the coefficient matrix $\boldsymbol{\beta}\in R^{p\times s}$, and the second of which is to get the coefficient vectors $\underline{\boldsymbol{\beta}}\in R^{s'\times 1}$ and $\overline{\boldsymbol{\beta}}\in R^{s'\times 1}$. The flowchart for the proposed uncertain method is given in Fig. 4-7.

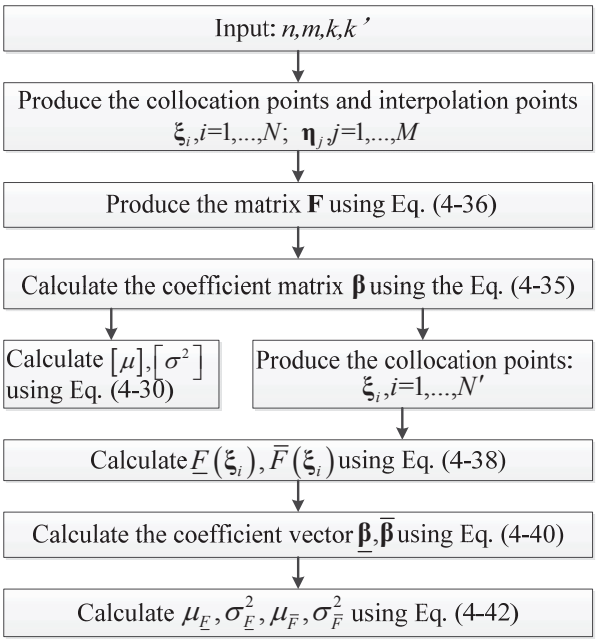

Figure 4-7 The flowchart of the PCCI method

There are three steps involved in each regression process: the first step is to produce the collocation points or interpolation points, and then compute the function values at these collocation points or interpolation points, and finally use the least square method to calculate the coefficients. Since the original function $F(\boldsymbol{\xi},[\boldsymbol{\eta}])$ is computationally expensive, the proposed method is highly efficient, as it only computes the function values $N\times M$ times, which is much less than the Monte Carlo method and scanning method. It is noted that $F(\boldsymbol{\xi},[\boldsymbol{\eta}])$ can be any formats, e.g. ODEs, DAEs, and even for complex black-box models in engineering. As a result, the proposed method can be applied to vehicle dynamics including uncertainty.

From the previous illustration, we can find that the proposed method is the combination of PC expansion method and Chebyshev interval method, so we call this method as Polynomial-Chaos-Chebyshev-Interval (PCCI) method. To validate the result given by the PCCI method, the Monte Carlo method is used as the reference in the probability

analysis and the scanning method is utilized to validate the bounds of interval analysis. Both methods are combined to obtain the reference solution, which is termed as Monte-Carlo-Scanning test.

Considering the function $F(\boldsymbol{\xi},[\boldsymbol{\eta}]),\boldsymbol{\xi}\in U(-1,\ 1)^n,[\boldsymbol{\eta}]=[-1,\ 1]^m$, if the number of Monte Carlo sampling points is N_0, choosing the q asymmetry scanning points in each dimension of interval variables, then the total number of experiment points is $N_0\times q^m$. Let $M_0= q^m$, we can write these experiment points in the format of matrix

$$\mathbf{C}\left(\boldsymbol{\xi},\boldsymbol{\eta}\right)=\begin{bmatrix}\left(\boldsymbol{\xi}_1,\boldsymbol{\eta}_1\right) & \cdots & \left(\boldsymbol{\xi}_1,\boldsymbol{\eta}_{M_0}\right)\\ \vdots & \ddots & \vdots\\ \left(\boldsymbol{\xi}_{N_0},\boldsymbol{\eta}_1\right) & \cdots & \left(\boldsymbol{\xi}_{N_0},\boldsymbol{\eta}_{M_0}\right)\end{bmatrix} \tag{4-43}$$

The output of the function at these experiment points can also be noted as a matrix $\mathbf{F}\in R^{N_0\times M_0}$

$$\mathbf{F}=\mathbf{F}(\mathbf{C}(\boldsymbol{\xi},\boldsymbol{\eta}))=\begin{bmatrix}F\left(\boldsymbol{\xi}_1,\boldsymbol{\eta}_1\right) & \cdots & F\left(\boldsymbol{\xi}_1,\boldsymbol{\eta}_{M_0}\right)\\ \vdots & \ddots & \vdots\\ F\left(\boldsymbol{\xi}_{N_0},\boldsymbol{\eta}_1\right) & \cdots & F\left(\boldsymbol{\xi}_{N_0},\boldsymbol{\eta}_{M_0}\right)\end{bmatrix} \tag{4-44}$$

The unbiased estimator of the mean value and variance of $F(\boldsymbol{\xi},[\boldsymbol{\eta}])$ at the scanning point $\boldsymbol{\eta}_i$ will be

$$\mu_i=\frac{1}{N_0}\sum_{j=1}^{N_0}F\left(\boldsymbol{\xi}_j,\boldsymbol{\eta}_i\right),\ \sigma_i^2=\frac{1}{N_0-1}\sum_{j=1}^{N_0}\left(F\left(\boldsymbol{\xi}_j,\boldsymbol{\eta}_i\right)-\mu_i\right)^2 \tag{4-45}$$

After calculating the mean and variance at each scanning points, we can find the minimum value (lower bounds) the maximum value (upper bounds) to obtain the IM and IV

$$\left[\mu\right]=\left[\min_i\mu_i,\ \max_i\mu_i\right],\ \left[\sigma^2\right]=\left[\min_i\sigma_i^2,\ \max_i\sigma_i^2\right] \tag{4-46}$$

The bounds of function $F(\boldsymbol{\xi},[\boldsymbol{\eta}])$ at each Monte Carlo sampling point $\boldsymbol{\xi}_j$ can be calculated as

$$\left[F_j\right]=\left[\underline{F}_j,\overline{F}_j\right],\ \underline{F}_j=\min_i F\left(\boldsymbol{\xi}_j,\boldsymbol{\eta}_i\right),\ \overline{F}_j=\max_i F\left(\boldsymbol{\xi}_j,\boldsymbol{\eta}_i\right) \tag{4-47}$$

The MLB, VLB, MUB, and VUB are calculated as follows:

$$\mu_{\underline{F}}=\frac{1}{N_0}\sum_{j=1}^{N_0}\underline{F}_j,\ \sigma_{\underline{F}}^2=\frac{1}{N_0-1}\sum_{j=1}^{N_0}\left(\underline{F}_j-\mu_{\underline{F}}\right)^2,\ \mu_{\overline{F}}=\frac{1}{N_0}\sum_{j=1}^{N_0}\overline{F}_j,\ \sigma_{\overline{F}}^2=\frac{1}{N_0-1}\sum_{j=1}^{N_0}\left(\overline{F}_j-\mu_{\underline{F}}\right)^2 \tag{4-48}$$

4.3 Application of hybrid uncertain analysis in vehicle dynamics

4.3.1 Model description

To demonstrate the effectiveness of the proposed PCCI method in engineering, the 4-DOF roll plan model of vehicles [163] is studied in this section. The roll plan model is shown in Fig. 4-8.

There is an added mass M on the roll bar, which denotes the driver, the passenger, and other object in the vehicle. The d denotes the distance from the added mass position to the left end of the roll bar. The vehicle body is presented by a roll bar with mass m, length l, and inertia I. The mass of left tyre and right tyre is m_{t1} and m_{t2}, respectively, and the tyre stiffness is k_{t1} for the left side and k_{t2} for the right side. Considering the nonlinear stiffness of suspension, the linear stiffness is denoted by k_i and the nonlinear stiffness is represented by k_i', where i=1for the left suspension and i=2 for the right suspension. The damping ratio for the left suspension and right suspension is noted as c_1 and c_2, respectively.

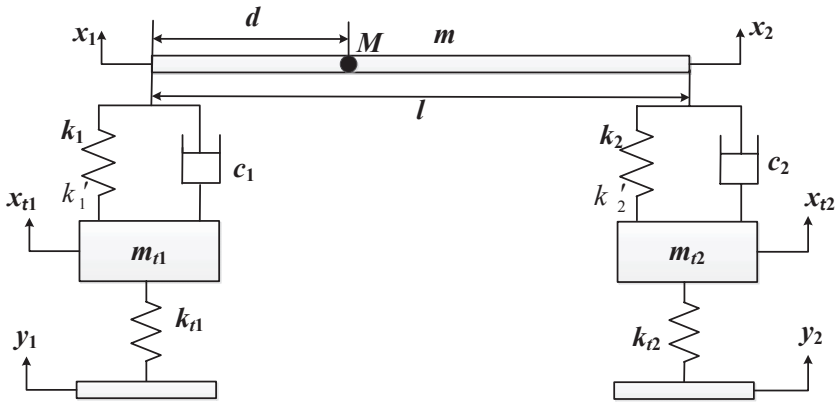

Figure 4-8 The roll plan model of a vehicle

When the roll angle is small, i.e. $(x_2\text{-}x_1)/l$ is small, the dynamics equations of the system are

$$\begin{cases} \left((m+M)(\ddot{x}_2+\ddot{x}_1)+M(\ddot{x}_2\text{-}\ddot{x}_1)(2d/l\text{-}1)\right)/l+F_{k1}+F_{k2}+F_{C1}+F_{C2}=0 \\ \cos\left((x_2\text{-}x_1+x_{2s}\text{-}x_{1s})/l\right)\left(D(F_{k1}+F_{C1})\text{-}(l\text{-}D)(F_{k2}+F_{C2})+g(M(D\text{-}d)\text{-}m(l/2\text{-}D))\right) \\ +\left(I+m(l/2\text{-}D)^2+M(D-d)^2\right)(\ddot{x}_2+\ddot{x}_1)/l=0 \\ m_{t1}\ddot{x}_{t1}+F_{k1}+F_{C1}+k_{t1}(x_{t1}\text{-}y_1)=0 \\ m_{t2}\ddot{x}_{t2}+F_{k2}+F_{C2}+k_{t2}(x_{t2}\text{-}y_2)=0 \end{cases} \quad (4\text{-}49)$$

where $D=\dfrac{Md+ml/2}{M+m}$, y_1 and y_2 denote the road input for each wheel, and F_{k1} and F_{k2} denote the spring forces of the suspension. The nonlinear stiffness is expressed by

$$F_{k1}=k_1(x_1\text{-}x_{t1})+k_1'(x_1\text{-}x_{t1})^3,\ F_{k2}=k_2(x_2\text{-}x_{t2})+k_2'(x_2\text{-}x_{t2})^3 \quad (4\text{-}50)$$

F_{C1} and F_{C2} are the damping force of the suspension, defined as

$$F_{C1}=0.2c_1\tanh(\dot{x}_1\text{-}\dot{x}_{t1}),\ F_{C2}=0.2c_2\tanh(\dot{x}_2\text{-}\dot{x}_{t2}) \quad (4\text{-}51)$$

x_{1s} and x_{2s} represent the static position of the vehicle body relative to the ground, which may be estimated by numerical methods in solving the following nonlinear system

$$\begin{cases} k_1\left(x_{1s}\text{-}x_{t1s}\right)+k_1'\left(x_{1s}\text{-}x_{t1s}\right)^3+\dfrac{mg}{2}+M\mathrm{g}\dfrac{l\text{-}d}{l}=0 \\ k_2\left(x_{2s}\text{-}x_{t2s}\right)+k_2'\left(x_{2s}\text{-}x_{t2s}\right)^3+\dfrac{mg}{2}+M\mathrm{g}\dfrac{d}{l}=0 \\ k_{t1}x_{t1s}+\dfrac{mg}{2}+M\mathrm{g}\dfrac{l\text{-}d}{l}+m_{t1}g=0 \\ k_{t2}x_{t2s}+\dfrac{mg}{2}+M\mathrm{g}\dfrac{d}{l}+m_{t2}g=0 \end{cases} \tag{4-52}$$

Table 4-2 Parameters of the roll plan model

Parameters	m (kg)	m_{t1},m_{t2} (kg)	c_1,c_2 (N/(m/s))	k_1, k_2 (N/m)	k_1', k_2' (N/m^3)
values	580	36.26	710.7	U(19000,20000)	U(95000,105000)
Parameters	l (m)	I (kg.m^2)	k_{t1},k_{t2} (N/m)	M (kg)	d (m)
values	1.524	63.3316	96319.76	[150, 250]	[0.5, 1]

Assume that there are some uncertain parameters in this system, including the stiffness of the suspension k_1, k_2, k_1', k_2', the added mass M, and the position of added mass d. The stiffness parameters are considered as random variables, assuming that they satisfy the uniform distribution. For the added mass and its position, it is practically hard to obtain their probability distribution, but their variation ranges are limited inside some intervals. Therefore, the added mass M and its position d are described as interval parameters. The uncertain and other parameters are shown in Table 4-2.

4.3.2 Hybrid uncertain analysis of vehicle model

From Tab 4-2, there are 4 random and 2 interval parameters, which can be expressed by standard format as:

$$\begin{aligned} &k_1=19500+500\xi_1;k_2=19500+500\xi_2;k_1'=100000+5000\xi_3;k_2'=100000+5000\xi_4 \\ &M=200+50\left[\eta_1\right];d=0.75+0.25\left[\eta_2\right] \end{aligned} \tag{4-53}$$

where $\boldsymbol{\xi} \sim U(-1,\ 1)^4$ and $[\boldsymbol{\eta}] = [-1,\ 1]^2$.

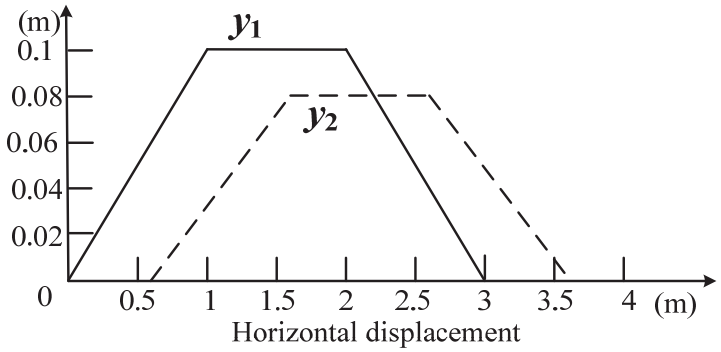

Figure 4-9 The road input

The road input is given in Fig. 4-9, and the vehicle velocity is 16 km/h. The left tyre moves upgrade from 0m, and reaches the highest position 0.1m where the horizontal displacement is 1m. Keeping the height 0.1m unchanged until the left tyre goes downgrade, which is asymmetrical to the upward slope. The right tyre moves along a similar track to the left one, but its upgrade starts from 0.6m of the horizontal displacement, and its maximum height is 0.08m. The output of the roll plan model are defined as the deformation of the suspension, i.e. $z_1 = x_1 - x_{t1}$ and $z_2 = x_2 - x_{t2}$.

Due to the uncertainty of suspension stiffness, the added mass, and its position, the output should also be uncertain. The PCCI method is used to solve this problem. Replacing the function $F(\boldsymbol{\xi},[\boldsymbol{\eta}])$ in the flowchart Fig. 4-7 by the output of this roll plan model, we can obtain the IM, IV, MLB, VLB, MUB, and VUB of the output. In this thesis, we choose the order of PC expansion and Chebyshev series expansion as 4 (k=4), and the scanning method with 20 symmetrical scanning points in each dimension of interval parameters is used to compute Eq. (4-30) and (4-38), which provides accurate bounds information. To validate the proposed method, the Monte-Carlo-Scanning test is also performed, in which the number of Monte Carlo sampling points is 1000, and 20 scanning points are used in

each dimension of interval parameters, so the total number of the simulation running is 1000×20^2=400,000. The PCCI method takes about 180.4s to obtain the results, while the Monte-Carlo-Scanning test takes 9915.3s, which is more than 50 times than that of the PCCI method.

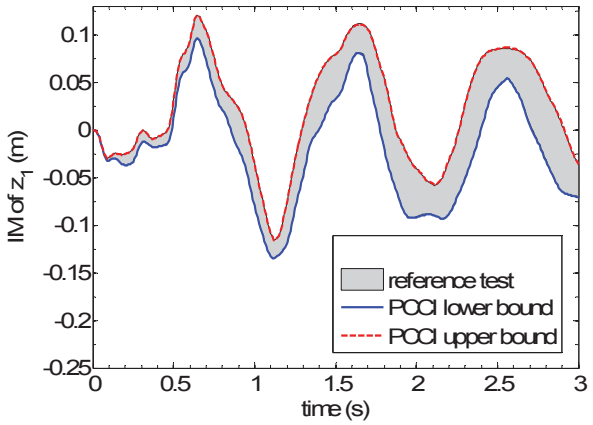

Figure 4-10 IM of z_1

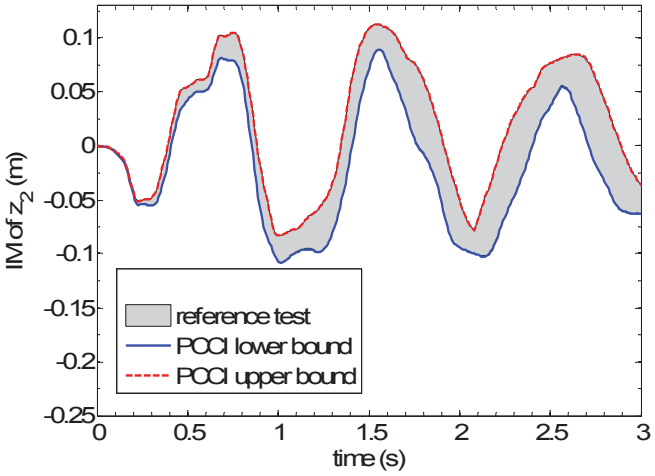

Figure 4-11 IM of z_2

The IM and IV of the output are shown in Fig. 4-10 to 4-13. The results show that the IM of the PCCI method are close to the IM of the Monte-Carlo-Scanning test, and the test results of IM are contained in that of PCCI tightly. So the PCCI method can provide

sufficient accuracy to the interval mean. For the IV, the intervals of the PCCI method do not contain all the intervals obtained by the reference test, but there is only small difference between them. Thus, the PCCI method can also provide good estimation for interval variance.

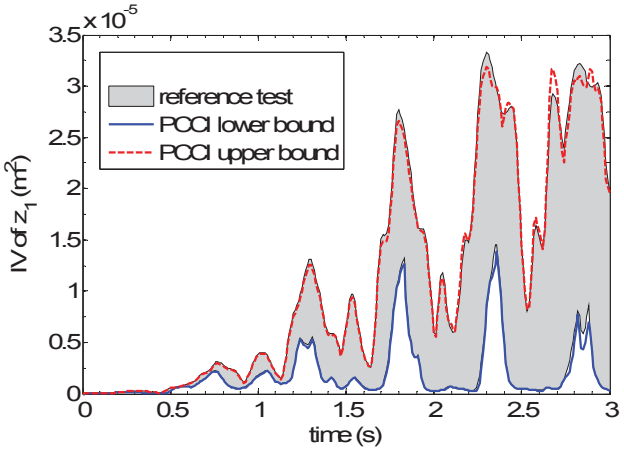

Figure 4-12 IV of z_1

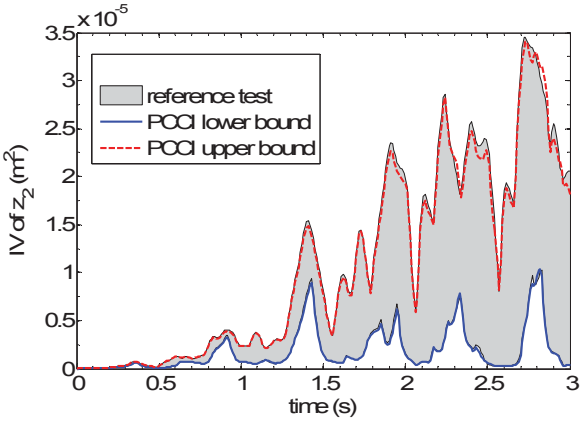

Figure 4-13 IV of z_2

Figures 4-14 and 4-15 show the MLB and MUB of output. The results indicate that the PCCI method can provide similar results relative to the reference test in MLB and MUB. The MLB and MUB of the proposed method are in line with the Monte-Carlo-Scanning test, which is similar to that of the IM.

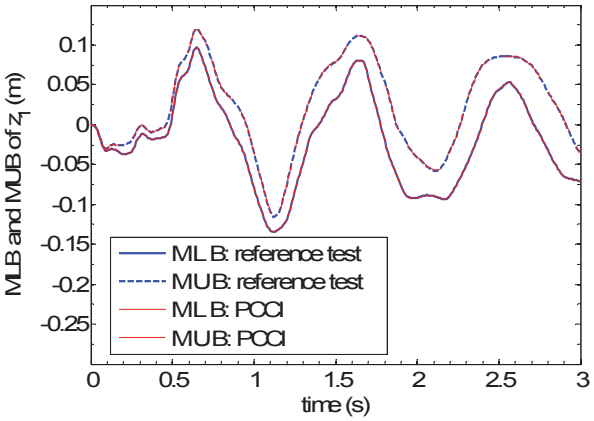

Figure 4-14 MLB and MUB of z_1

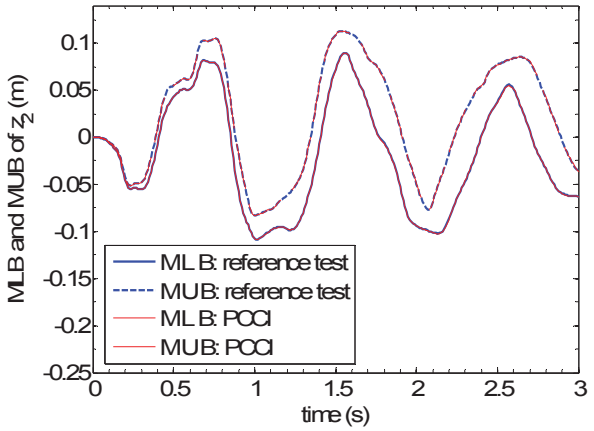

Figure 4-15 MLB and MUB of z_2

The VLB and VUB of the output are shown in Fig. 4-16 to 4-19. It can be seen that the overall shapes of the VLB and VUB of the two methods match well, and the small difference only happened at local regions with sharp fluctuations.

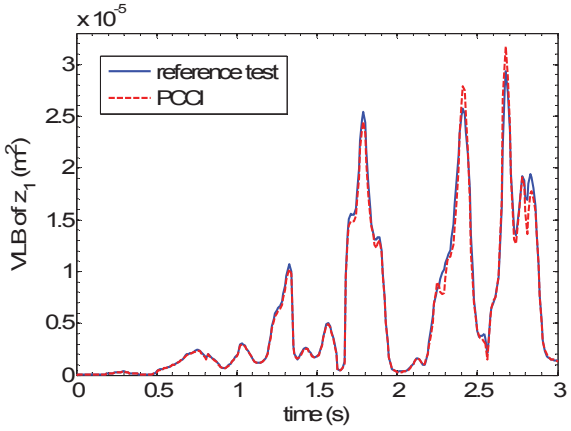

Figure 4-16 VLB of z_1

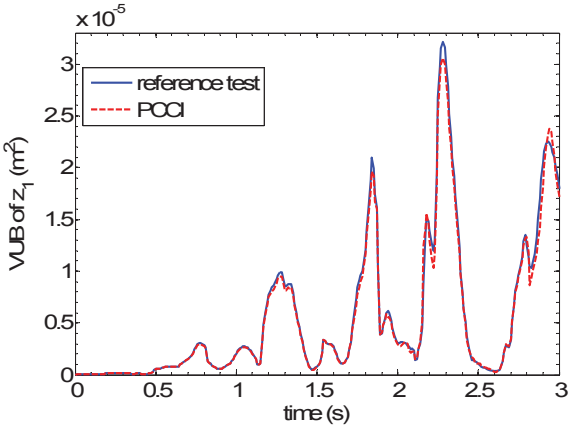

Figure 4-17 VUB of z_1

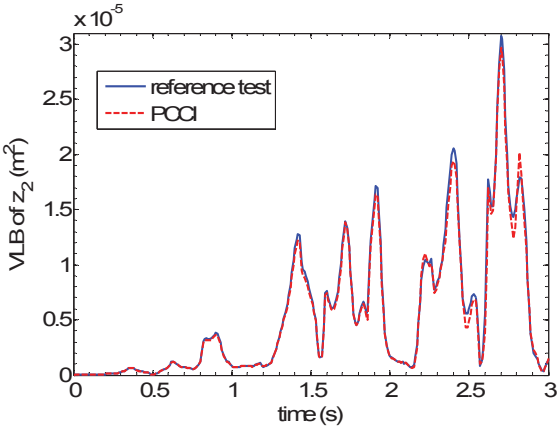

Figure 4-18 VLB of z_2

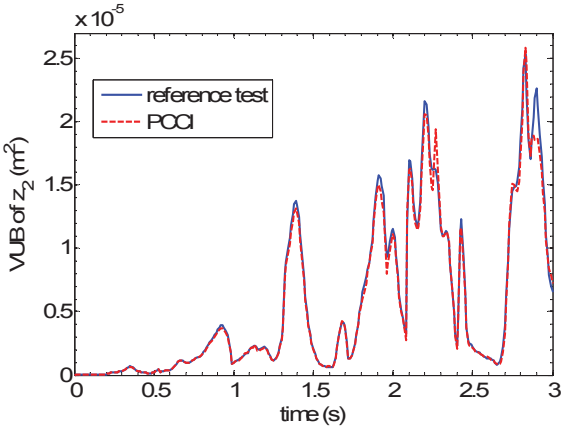

Figure 4-19 VUB of z_2

4.4 Summary

This chapter proposes an uncertain analysis method, termed as PCCI method, for systems involving hybrid uncertain parameters, namely the random parameters and interval variables. In this method, the PC expansion is applied to deal with the random uncertainty and the Chebyshev inclusion function is used to handle the interval uncertainty. It is proved that the least square method can be used to build the Chebyshev inclusion function directly, which provides the same result computed by the integral formula shown in Chapter 3. Two types of evaluation indexes are proposed, the first of which include the interval mean (IM) and interval variance (IV), considering the random parameters firstly and then the interval parameters, and the second of which are the mean of lower bound (MLB), variance of lower bound (VLB), mean of upper bound (MUB), and variance of upper bound (VUB), considering interval parameters firstly and then the random parameters. To validate the accuracy of the PCCI method, a Monte-Carlo-Scanning test scheme that combines the Monte Carlo method and the scanning method to calculate the two types of evaluation indexes is proposed.

A 4-DOF vehicle roll plan model is used to demonstrate the effectiveness of the proposed PCCI method, in which the stiffness of the suspension are regarded as random parameters while the added mass and its position are considered as interval parameters. The numerical results show that the PCCI method can provide accurate numerical results for both types of the evaluation indexes. Furthermore, the PCCI method only takes 180.4s, but the Monte-Carlo-Scanning test takes 9915.3s. Also, the PCCI method is a kind of non-intrusive method, so it can be used to solve the uncertainty of black box problems.

Chapter 5 Optimization under interval uncertainty

Design of optimization has experienced considerable development over the past two decades with a wide range of engineering applications. However, the majority of these works are focused on the investigation of the deterministic problems. This chapter proposes a new interval uncertain optimization methodology for engineering. The uncertain design problem is often formulated as a double-loop optimization. To improve the optimization efficiency, the interval arithmetic is introduced to directly evaluate the bounds of interval functions and eliminate the inner loop optimization. The high-order Taylor inclusion function is employed to compress the overestimation of interval arithmetic. A Chebyshev surrogate model is proposed to compute the high-order coefficients of the Taylor inclusion function.

5.1 The interval uncertain optimization model

This section will propose a new uncertainty optimization model, in which the design variables are considered as interval numbers. In engineering problems, there are many cases that the design variables are also uncertain variables. For example, the stiffness in vehicle suspensions can be both the design variable and the uncertain parameters due to the material property variations. The cross section areas of a truss structure can be design variables, and at the same time uncertain parameters due to manufacturing tolerance. Therefore, the proposed uncertainty optimization model will be more suitable for practical problems. As mentioned above, the information of interval variables can be easily obtained compared to the precise probabilistic distributions of random variables, so the interval uncertain optimization is investigated in this chapter.

A general deterministic optimization model is given by

$$\begin{cases} \min\limits_{\mathbf{x}} & f(\mathbf{x}) \\ \text{s.t.} & g_i(\mathbf{x}) \le 0, \quad i = 1,2,...,n \\ & \mathbf{x}^l \le \mathbf{x} \le \mathbf{x}^u \end{cases} \tag{5-1}$$

The above mathematical model is used to minimize the objective f subject to constraints g_i . $\mathbf{x} \in R^k$ is the vector including deterministic design variables. To describe uncertainties in the design, interval numbers are introduced to express the variations induced by the uncertainty, so the deterministic optimization model (5-1) can be re-defined as follows:

$$\begin{cases} \min\limits_{[\mathbf{x}]} & f([\mathbf{x}]) \\ \text{s.t.} & g_i([\mathbf{x}]) \le 0, \; i = 1,2,...,n \\ & \mathbf{x}^l \le [\mathbf{x}] \le \mathbf{x}^u \end{cases} \tag{5-2}$$

Since the width of an interval design variable [**x**] is pre-given as **η**, any interval design variable can be expressed as

$$[\mathbf{x}]=\mathbf{x}_c+[-\boldsymbol{\eta}, \boldsymbol{\eta}] \tag{5-3}$$

The objective and constraints will also be interval numbers, denoted by [*f*] and [*g*], respectively, because the design variables are interval numbers.

To ensure the "robustness" of the design, the above minimization problem is to minimize both the average value and the width of the uncertain objective function. The minimization of the width will lead to the decrease of the variance of the objective function, to make the uncertain objective function insensitive to the variation due to the uncertainty. It is noted that the midpoint value and width are functionally similar to the probabilistic counterparts in the conventional robust design optimization [114], which is a standard technique to minimize both the mean value and the standard deviation of the objective function.

To optimize the objective, both the midpoint and width of the objective should be minimized, which can actually be regarded as a type of robust designs. Thus, the new objective f_{obj} can be specified as

$$f_{obj}=\alpha_1 f_c+\alpha_2 w([f]) \tag{5-4}$$

where α_1 and α_2 denotes the weighting coefficients, and we set both α_1 and α_2 as 1 in this study. Then the objective can be re-defined as follows:

$$f_{obj}=f_c+w([f])=\overline{f} \tag{5-5}$$

Then the objective would be the upper bound of interval $[f]$, which is the maximum value of f under the uncertainty, as shown in Fig. 5-1.

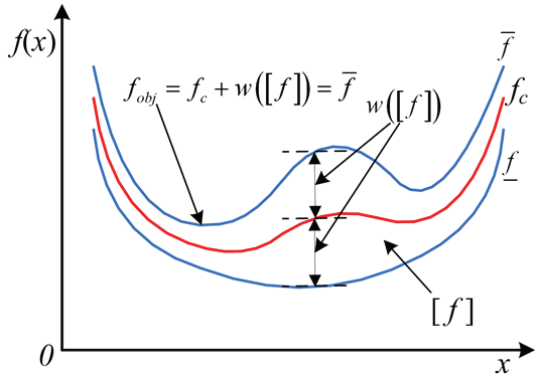

Figure 5-1 Interval objective function

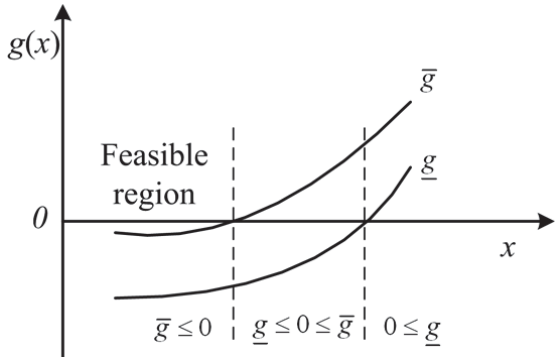

Figure 5-2 Interval constraints

For the interval constraints, there are three cases in the design space: $0 \le \underline{g}$, $\underline{g} \le 0 \le \overline{g}$ and $\overline{g} \le 0$, as shown in Fig. 5-2. The first case violates the constraint, and the second case contains the possibility of violating the constraint. Only the last case can guarantee the design points in the feasible region, which denotes a 100% reliability index. So the upper bounds should be used to meet the constraints

$$\overline{g}_i\left([\mathbf{x}]\right) \le 0, \ \ i = 1, 2, ..., n \tag{5-6}$$

The upper bounds of the objective and constraints can be calculated through maximizing the value in the range of uncertainty. Consider Eqs. (5-3), (5-5) and (5-6), the optimization model can be finally expressed as

$$\begin{cases} \min\limits_{\mathbf{x}_c} & \max\limits_{\mathbf{x}\in[\mathbf{x}]} f(\mathbf{x}) \\ \text{s.t.} & \max\limits_{\mathbf{x}\in[\mathbf{x}]} g_i(\mathbf{x}) \le 0, \ i = 1, 2, ..., n \\ & [\mathbf{x}]=\mathbf{x}_c+[-\boldsymbol{\eta}, \boldsymbol{\eta}] \\ & \mathbf{x}^l+\boldsymbol{\eta} \le \mathbf{x}_c \le \mathbf{x}^u-\boldsymbol{\eta} \end{cases} \tag{5-7}$$

It should be noted that the optimization result of the uncertain optimization model (5-7) is different from that of the deterministic optimization model (5-1). The difference between the two optimization models can be demonstrated by a simple one-dimensional function, considering the function in Eq. (5-8).

$$f(x) = -251x^5 + 771x^4 - 889x^3 + 479x^2 - 116x + 10, \ 0 \le x \le 1 \tag{5-8}$$

If the width of the interval variable $[x]$ is set to η=0.1, the objective under deterministic and uncertain conditions is shown in Fig. 5-3, respectively. It can be found that the deterministic optimal result is about 0.25, and the upper bound of $f([x])$ around this point is about 0.75. However, the actual uncertain optimal result would be near to 0.27, where the upper bound is about 0.36.

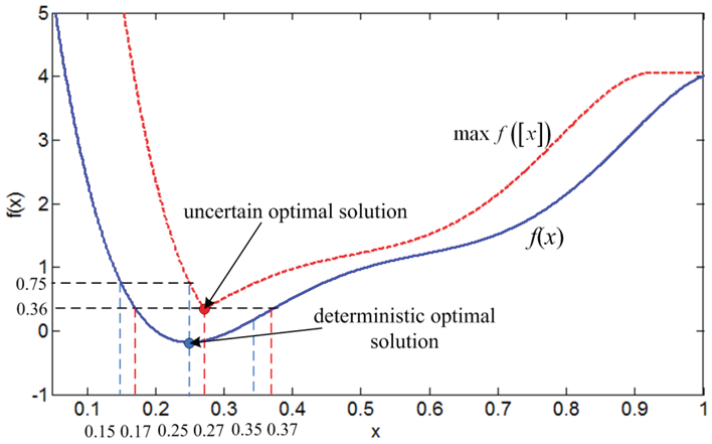

Figure 5-3 Difference of the deterministic optimization and uncertain optimization

5.2 Nested optimization method

The optimization model in Eq. (5-7) is typically a nested double-loop optimization problem. The outer loop optimization searches the optimal midpoint of interval design variables to minimize the objective, while the inner loop finds the maximum values (or minimum values) of the objective and constraints within the ranges of interval parameters. Different optimization algorithms are usually employed at the two loops in order to balance the numerical accuracy and computational efficiency, considering the different characteristics of the two loops.

Outer loop optimization

To seek the global optimal solution and avoid multiple local minima, many heuristic techniques with strong global searching ability can be used. This study employs the Multi-Island Genetic Algorithm (MIGA) [164, 165] to solve the outer loop optimization problem. The flowchart of MIGA is shown in Fig. 5-4. MIGA divides each population of individuals into several sub-populations called “islands”. In the evolution, some individuals are selected from each island and migrated to different islands periodically,

which may make the solution converge to the global optimal solution faster than conventional genetic algorithms.

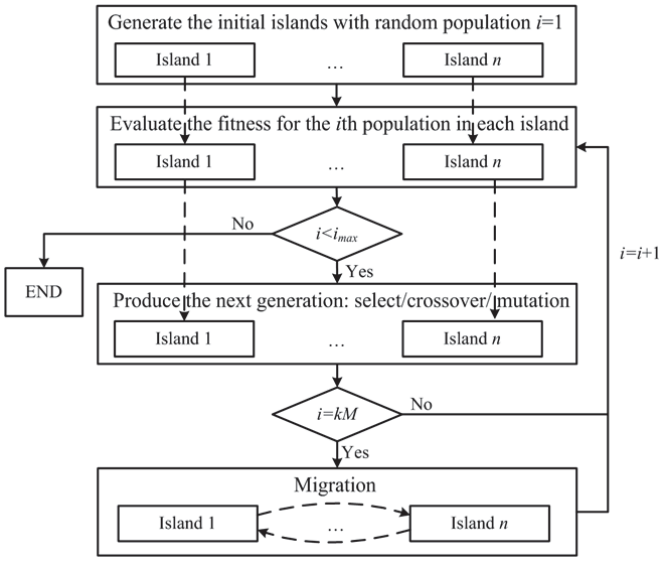

Figure 5-4 Flowchart of MIGA

The MIGA is similar to the general GA, which consists of two processes: the first process is the selection of individuals for the production of the next generation, and the second process is the manipulation of the selected individuals to produce the next generation by crossover and mutation techniques. However, in MIGA, the population is divided into several sub-populations and the migration operation is added. Each sub-population evolves independently for optimizing the same objective function. The migration occurs every M generation, and copies of the individuals which are the best N% of the island populations are allowed to migrate. M is called the interval of the migration and N% is called the rate of the migration. In the migration, the top N% strings in the sub-population A may be copied to another sub-population B, and the least N% strings of the sub-population B will be eliminated. Similarly, the sub-population A will receive the top

strings from other sub-population and eliminates its least strings. This operation repeats until each sub-population achieves top strings from another sub-population.

Although MIGA has the ability to search the global optimum, its convergence ratio is normally slower than the conventional gradient-based algorithms, especially within the neighborhood of the optimal solution. To improve the efficiency, the Sequential Quadratic Programming (SQP) [166] will be combined with the MIGA to search the optimum, which means the optimal point of MIGA will be used as the initial point of SQP. In this case, the number of generations in MIGA can be reduced, because only a limited number of points near the global optimal solution are required, which will greatly reduce the calculation time of MIGA.

Inner loop optimization

The design space of the inner loop optimization is relatively narrow, and the inner loop optimization can be searched by using many optimization algorithms. This chapter employs the Active Set Optimization (ASO) method in MATLAB. The idea of ASO is to define a working set as the active set in terms of a set of constraints at each step. The working set is chosen to be a subset of the constraints that are actually active at the current point, and hence the current point is feasible for the working set. The algorithm then proceeds to move on the surface defined by the working set of constraints to an improved point. At this new point the working set may be changed. An ASO consists of the following components: (1) determination of a current working set that is a subset of the current active constraints, and (2) movement on the surface defined by the working set to an improved point.

In the nested double loop optimization, the computational efficiency of the design problem is a key issue to be considered. The computational cost of the inner optimization

is not very high, but the total cost for the entire double loop optimization will be computationally prohibitive. For instance, if MIGA-SQP in the outer loop requires 1000 iterations and the inner ASO algorithm requires 100 iterations, the total number of iterations will be $1000\times100=10^5$. To improve the computational efficiency, the linearization method has been widely applied to the inner loop [e.g. [120]]. That is, the objective can be expressed with respect to the design variables and parameters at the midpoints via the first-order Taylor series

$$f(\mathbf{x})=f(\mathbf{x}_c)+\left.\frac{\partial f}{\partial \mathbf{x}}\right|_{\mathbf{x}_c}(\mathbf{x}-\mathbf{x}_c)+\mathrm{O}(2) \tag{5-9}$$

If the higher order terms are ignored, the maximum value can be determined as

$$f_{\max}(\mathbf{x})\approx f(\mathbf{x}_c)+\left|\left.\frac{\partial f}{\partial \mathbf{x}}\right|_{\mathbf{x}_c}\right| w([\mathbf{x}]) \tag{5-10}$$

where $w([\mathbf{x}])$ denotes the width of interval variables $[\mathbf{x}]$. Similarly, the maximum value of constraint functions g_i can also be calculated via the linearization model as

$$g_{\max}(\mathbf{x})\approx g(\mathbf{x}_c)+\left|\left.\frac{\partial g}{\partial \mathbf{x}}\right|_{\mathbf{x}_c}\right| w([\mathbf{x}]) \tag{5-11}$$

The truncated errors exit in this linearization model, due to the neglect of the higher-order terms in Eq. (5-9). For highly nonlinear problems, the truncation error cannot be ignored. The linearization model can improve computational efficiency of the nested optimization. However, it may result in a poor numerical accuracy due to the truncated error. To reduce the computational time without sacrificing numerical accuracy, a new optimization strategy will be proposed in next section based on the interval arithmetic.

The flowcharts for the nested optimization (Fig. 5-5(a)) and the linearization optimization using the first-order Taylor series (Fig. 5-5(b)) are shown in Fig. 5-5, respectively. In Fig.

5-5(a), the outer optimization is implemented by a combination of MIGA and SQP. The midpoints of the interval variables are updated in each step of the outer loop, and the bounds of the interval design functions are calculated by the inner optimization using the ASO algorithm. In Fig. 5-5(b), the first-order Taylor series expansion is used to replace the inner loop optimization, to avoid the computationally expensive double-loop process. This study will employ an alternative method to balance the efficiency and numerical accuracy in the numerical implementation.

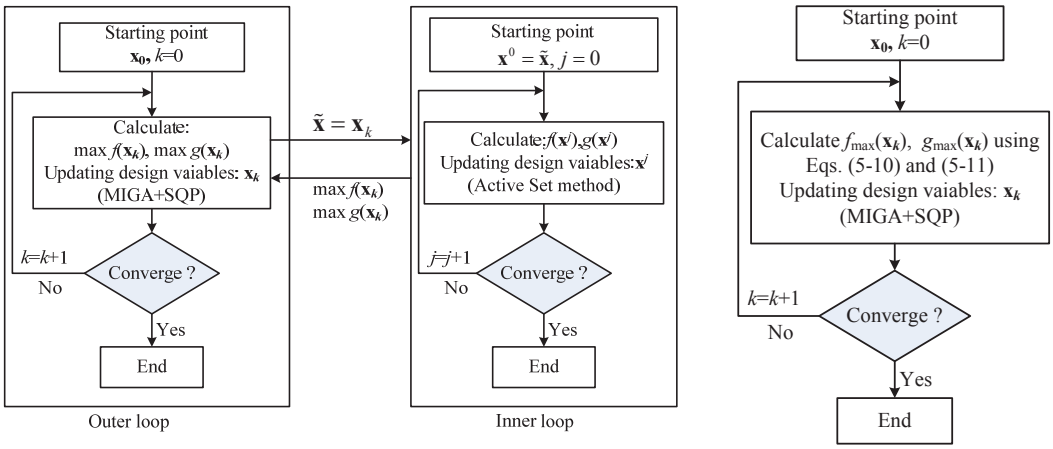

(a) Double loop process (b) Linearization process

Figure 5-5 Flowchart of optimization under interval uncertainty

5.3 The interval optimization method

5.3.1 Chebyshev surrogate model

The double loop optimization process is very expensive, so the interval arithmetic can be used to replace the inner optimization directly to improve the optimization efficiency. The Chebyshev inclusion function proposed in Chapter 3 has better performance for large uncertain range, but the uncertain extent in design optimization is usually small. As a

result, the Taylor inclusion function will be used to evaluate the bounds of objective and constraints.

However, there is a problem for using the Taylor inclusion function, which is the high-order derivatives of the evaluated functions (objective and constraints) should be computed firstly. For most of the evaluated functions (objective and constraints), we do not know their analytical expression, so the derivatives cannot be accurately obtained. If the numerical differential method is used to compute the derivatives, the computational cost will be high while the accuracy may still be low. To use the Taylor inclusion function, a polynomial approximation model (or surrogate model, meta-model) should be constructed. As aforementioned in Chapter 3, the Chebyshev series has higher accuracy than the Taylor series, so the Chebyshev series will be used to construct the surrogate model.

Using the *k*-th order Chebyshev series as the polynomial surrogate model of the surrogate model can be expressed by

$$f(\mathbf{x}) \approx \sum_{0 \le i_1 + \ldots + i_n \le k} \left(\frac{1}{2}\right)^l f_{i_1 \ldots i_n} C_{i_1 \ldots i_n}(\mathbf{x}) = \boldsymbol{\gamma}^{\mathrm{T}} \mathbf{c} =: \hat{f}(\mathbf{x}) \tag{5-12}$$

Here $\hat{f}(\mathbf{x})$ denotes the polynomial surrogate model. The coefficient vector $\boldsymbol{\gamma}=[\gamma_1,\ldots,\gamma_s]^{\mathrm{T}}$ $=[1/2^k f_{0,\ldots,0},\ldots,1/2^l f_{i_1 \ldots i_n}]^{\mathrm{T}}$, and $\mathbf{c}=[c_1,\ldots,c_s]^{\mathrm{T}}=[C_{0,\ldots,0}(\mathbf{x}),\ldots,C_{i_1 \ldots i_n}(\mathbf{x})]^{\mathrm{T}}$ is the polynomial basis vector with $s=(n+k)!/n!k!$. The coefficient vector can be calculated by the LSM as the Chapter 4 has proved.

$$\boldsymbol{\gamma} = \left(\mathbf{C}^{\mathrm{T}}\mathbf{C}\right)^{-1} \mathbf{C}^{\mathrm{T}}\mathbf{Y} \tag{5-13}$$

where $\mathbf{Y}=\left[f\left(\mathbf{x}_1\right) \quad \cdots \quad f\left(\mathbf{x}_s\right)\right]^{\mathrm{T}}$ is the vector of function value at the sampling points, and the matrix $\mathbf{C} \in R^{s\times s}$ is composed by the value of polynomial basis vector at the sampling points

$$\mathbf{C}=\begin{bmatrix} c_1\left(\mathbf{x}_1\right) & \cdots & c_s\left(\mathbf{x}_1\right) \\ \vdots & \ddots & \vdots \\ c_1\left(\mathbf{x}_s\right) & \cdots & c_s\left(\mathbf{x}_s\right) \end{bmatrix} \tag{5-14}$$

where $\mathbf{x}_1 \ldots \mathbf{x}_s$ denote the sampling points, which are the zeros of Chebyshev polynomials. The expression of Eq. (5-12) is respect to the Chebyshev series, and it can also be expressed with respect to Taylor series

$$\tilde{f}\left(\mathbf{x}\right)=\boldsymbol{\gamma}'^{\mathrm{T}}\mathbf{b} \tag{5-15}$$

where the polynomial basis vector $\mathbf{b}=[b_1 \quad \cdots \quad b_s]^{\mathrm{T}}=[\prod_{i=1}^{n} x_i^0 \quad \cdots \quad \prod_{\substack{i=1 \\ k_1+\ldots+k_n=k}}^{n} x_i^{k_i}]^{\mathrm{T}}$, and the coefficient vector $\boldsymbol{\gamma}'=[\gamma_1' \quad \cdots \quad \gamma_s']^{\mathrm{T}}$ may be calculated by

$$\boldsymbol{\gamma}'=\left(\mathbf{B}^{\mathrm{T}}\mathbf{B}\right)^{-1}\mathbf{B}^{\mathrm{T}}\mathbf{Y} \tag{5-16}$$

where the matrix $\mathbf{B} \in R^{s\times s}$ is determined by

$$\mathbf{B}=\begin{bmatrix} b_1\left(\mathbf{x}_1\right) & \cdots & b_s\left(\mathbf{x}_1\right) \\ \vdots & \ddots & \vdots \\ b_1\left(\mathbf{x}_s\right) & \cdots & b_s\left(\mathbf{x}_s\right) \end{bmatrix} \tag{5-17}$$

If the sampling points $\mathbf{x}_1 \ldots \mathbf{x}_s$ used in Eq. (5-14) and (5-17) are the same, Eq. (5-12) and (5-15) will provide the same approximation model. This will lead to the following theorem:

Theorem 5.1: *When the least square method is used to build an approximation polynomial model with predefined order n, the accuracy of this polynomial is*

determined by the sampling points rather than the basis vector of the polynomial model.

Proof: If we can prove that the two approximation polynomial models (5-12) and (5-15) are equivalent, this theorem can be proved. From Eq. (3-35), we know that the polynomial basis vector **c** can be obtained through a linear transformation from vector **b**, such as

$$\mathbf{b} = \mathbf{A}\mathbf{c} \tag{5-18}$$

where $\mathbf{A} \in R^{s\times s}$ is the linear transformation matrix between the two vectors **c** and **b**. Substituting Eq. (5-18) to Eq. (5-14) and (5-17), we can obtain

$$\mathbf{B} = \mathbf{C}\mathbf{A}^{\mathrm{T}} \tag{5-19}$$

Substitute Eq. (5-13) to Eq. (5-12)

$$\hat{f}(\mathbf{x}) = \boldsymbol{\gamma}^{\mathrm{T}}\mathbf{c} = \left(\left(\mathbf{C}^{\mathrm{T}}\mathbf{C}\right)^{-1}\mathbf{C}^{\mathrm{T}}\mathbf{Y}\right)^{\mathrm{T}}\mathbf{c} = \mathbf{Y}^{\mathrm{T}}\mathbf{C}\left(\mathbf{C}^{\mathrm{T}}\mathbf{C}\right)^{-1}\mathbf{c} \tag{5-20}$$

Substitute Eq. (5-16) to Eq. (5-15)

$$\tilde{f}(\mathbf{x}) = \boldsymbol{\gamma}'^{\mathrm{T}}\mathbf{b} = \left(\left(\mathbf{B}^{\mathrm{T}}\mathbf{B}\right)^{-1}\mathbf{B}^{\mathrm{T}}\mathbf{Y}\right)^{\mathrm{T}}\mathbf{b} = \mathbf{Y}^{\mathrm{T}}\mathbf{B}\left(\mathbf{B}^{\mathrm{T}}\mathbf{B}\right)^{-1}\mathbf{b} \tag{5-21}$$

Substituting Eq. (5-18) and (5-19) to Eq. (5-21), we will finally find the following equation

$$\begin{aligned}\tilde{f}(\mathbf{x}) &= \mathbf{Y}^{\mathrm{T}}\mathbf{B}\left(\mathbf{B}^{\mathrm{T}}\mathbf{B}\right)^{-1}\mathbf{b} \\ &= \mathbf{Y}^{\mathrm{T}}\mathbf{C}\mathbf{A}^{\mathrm{T}}\left(\left(\mathbf{C}\mathbf{A}^{\mathrm{T}}\right)^{\mathrm{T}}\mathbf{C}\mathbf{A}^{\mathrm{T}}\right)^{-1}\mathbf{A}\mathbf{c} \\ &= \mathbf{Y}^{\mathrm{T}}\mathbf{C}\mathbf{A}^{\mathrm{T}}\left(\mathbf{A}^{\mathrm{T}}\right)^{-1}\left(\mathbf{C}^{\mathrm{T}}\mathbf{C}\right)^{-1}\mathbf{A}^{-1}\mathbf{A}\mathbf{c} = \mathbf{Y}^{\mathrm{T}}\mathbf{C}\left(\mathbf{C}^{\mathrm{T}}\mathbf{C}\right)^{-1}\mathbf{c} = \hat{f}(\mathbf{x})\end{aligned} \tag{5-22}$$

Therefore, the two approximation models shown in Eq. (5-12) and (5-15) are absolutely equivalent, which means the sampling points determine the polynomial model rather than

the basis vector for the polynomial model. Since the zeros of Chebyshev polynomials are used as the sampling points, we called this polynomial approximation model as Chebyshev surrogate model. It should be noted that the Chebyshev surrogate model may be expressed as many different types corresponding to the basis vector, and we choose the Taylor series-based expression shown in Eq. (5-15) to be conveniently used in Taylor inclusion function.

The number of interpolation points for constructing Chebyshev surrogate model equals to $(k+1)^n$, which is computationally expensive, especially for the high dimensional problems. To save the computational cost, only a part of the interpolation points are used to build the Chebyshev surrogate model. The number of coefficients in Eq. (5-15) is $s=(n+k)!/n!k!$, so the number of sampling points from the interpolation should not be less than s. Therefore, the number of sampling points can be chosen in the interval $[(n+k)!/n!k!,\ (k+1)^n]$. The larger number of sampling points, the smaller error of the approximation, but lower efficiency. Similar to the collocation method in Chapter 4, the number of the sampling points is set as twice of the number of the evaluated coefficients, to make the numerical method stable. Thus, when $(k+1)^n > 2(n+k)!/n!k!$, $2(n+k)!/n!k!$ interpolation points will be chosen as the sampling points randomly. Otherwise, all the interpolation points will be chosen as the sampling points. After the set of sampling data is obtained, the LSM is used to calculate the coefficients and establish the surrogate model.

The flowchart of constructing Chebyshev surrogate model is shown in Fig. 5-6. The process of constructing Chebyshev surrogate model contains two main steps: to obtain the sampling data and to calculate the coefficients. The sampling points are the zeros of the Chebyshev polynomial, and their sizes are determined by the dimension of interval

variables and the order of polynomials. When the sampling data is obtained, the least square method can be used to calculate the coefficients, and then calculate the bounds of the function based on the interval arithmetic.

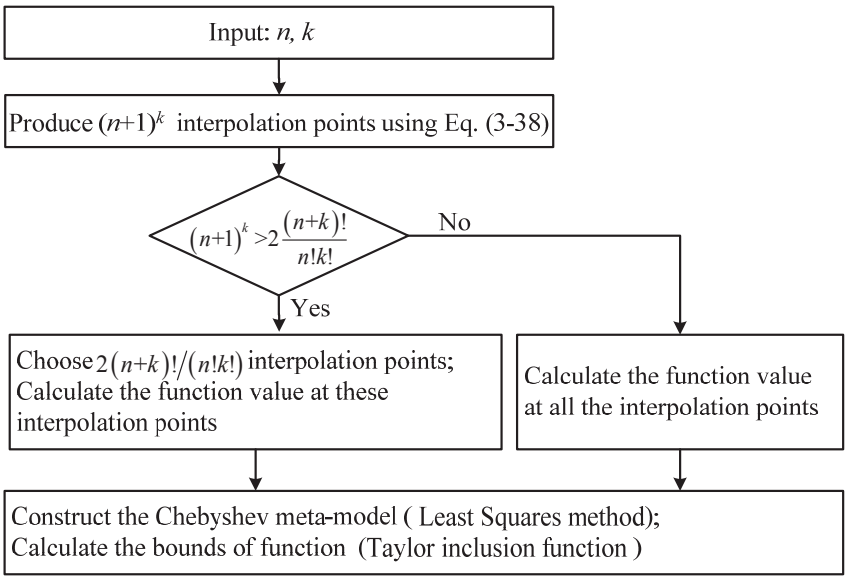

Figure 5-6 Flowchart of Chebyshev surrogate model

5.3.2 Optimization algorithm using interval arithmetic

The Chebyshev surrogate model can then be combined with the outer loop optimization (MIGA+SQP) to implement the uncertain optimization. The major advantage of the interval arithmetic is that the maximum and minimum values of a function are contained in the interval results, which provide rigorous constraints for the outer loop to guarantee the outer loop optimal solution is in the feasible region. The optimal design of the interval arithmetic may be more conservative than that of the nested optimization, but it is more reliable than the nested optimization or linearization optimization.

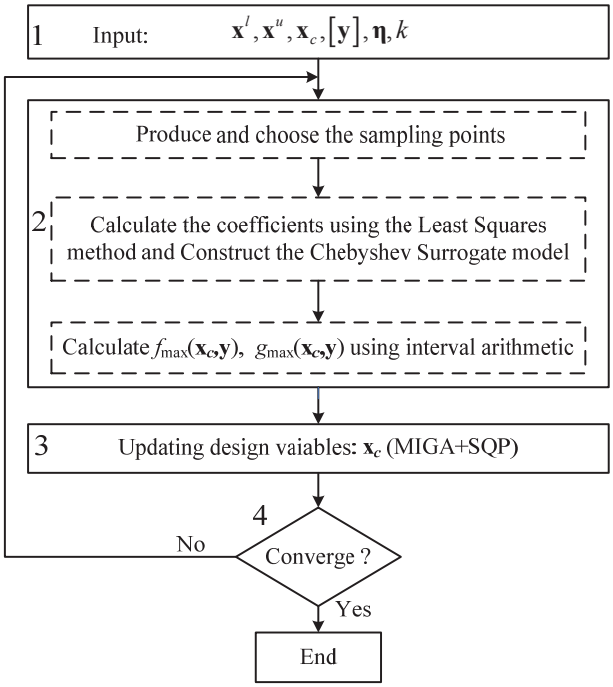

Figure 5-7 The flowchart of interval optimization

The flowchart in Fig. 5-7 illustrates the numerical process of the proposed interval optimization strategy. The first step is to define some initialization parameters, where $\mathbf{x}_c$ denotes the mid value of design variables, and k denotes the order of the Chebyshev surrogate model. The second step is to calculate the objective $f_{max}(\mathbf{x}_c)$, and constraints $g_{max}(\mathbf{x}_c)$ in the outer loop using the interval arithmetic. The high-order Taylor inclusion function is used to reduce the overestimation in the interval arithmetic. However, the high-order derivatives in the inclusion function are hard to obtain. As a result, the Chebyshev surrogate model is constructed to approximate the Taylor inclusion function. The second step contains several sub-steps to build the Chebyshev surrogate model. In this stage, we produce several interpolation points which are the zeros of Chebyshev polynomials, and then choose some interpolation points as the sampling points based on the strategy described in Fig. 5-7 to calculate the values of the evaluation function at these sampling points. Then, the Least Square method is used to calculate the coefficients of the

Chebyshev surrogate model and then construct the Chebyshev approximation model. Lastly, the interval arithmetic is used to evaluate the objective $f_{\max}(\mathbf{x}_c)$ and constraints $g_{\max}(\mathbf{x}_c)$. Hence, the third step is to update the nominal values of design variables based on the outer loop optimization algorithm (MIGA+SQP). If the result satisfies the convergence condition, the algorithm will be end; otherwise the algorithm will go to the step 2.

5.4 Application of interval optimization

5.4.1 The 18-bar planar truss optimization

Figure 5-8 shows the 18-bar cantilever planar truss. The objective is to minimize the total weight of the truss subject to the stress limitations of ±20000lb/in^2 and Euler buckling compressive stress limitation [167]

$$b^{\sigma_i} = -\frac{KEA_i}{L_i^2} \tag{5-23}$$

where K=4 denotes a constant determined by the cross-sectional geometry, E=10^7 lb/in2 is the modulus of elasticity, L_i is the ith member length, and A_i denotes the cross-sectional area of the ith member. The minimum cross-sectional area of members is 0.1 in^2, and the maximum value is 50 in^2.

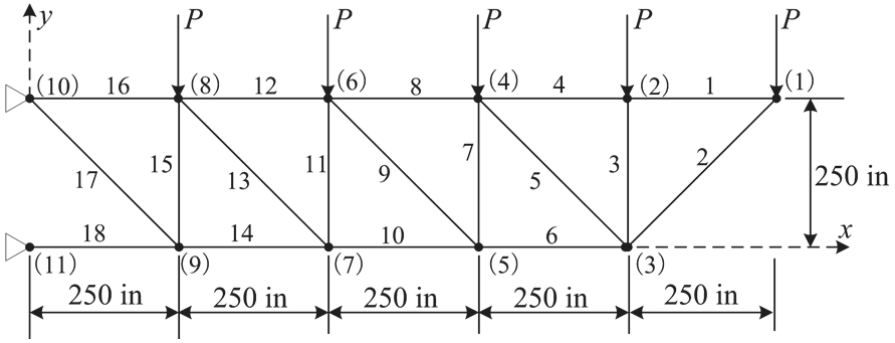

Figure 5-8 18-bar planar truss structure

The members can be categorized into different groups, according to the cross-sectional areas (design variables): $x_1=A_1=A_4=A_8=A_{12}=A_{16}$, $x_2=A_2=A_6=A_{10}=A_{14}=A_{18}$, $x_3=A_3=A_7=A_{11}=A_{15}$, and $x_4=A_5=A_9=A_{13}=A_{17}$. Here the design variables are considered as interval variables that has the interval width of 0.2in^2. The material density is $\rho = 0.1\,\text{lb/in}^3$. The vertical loads P=20000lb is applied at the upper side of the truss.

The uncertain optimization model can be defined as follows:

$$\begin{aligned}
\min_{\mathbf{x}_c} \quad & \max_{\mathbf{x}\in[\mathbf{x}]} \; w = \sum_{i=1}^{18} A_i L_i \rho \\
\text{s.t.} \quad & g_1 = \max_{i=1,\ldots,18}\left(\max_{\mathbf{x}\in[\mathbf{x}]} \left(|\sigma_i| \right) \right) \le 20000 \\
& g_2 = \max_{i=1,\ldots,18}\left(\max_{\mathbf{x}\in[\mathbf{x}]} \left(\sigma_i / b^{\sigma_i} \right) \right) \le 1 \\
& [\mathbf{x}] = \mathbf{x}_c + [-\boldsymbol{\eta}, \boldsymbol{\eta}] \quad \boldsymbol{\xi} = [0.2 \quad \ldots \quad 0.2]^{\mathrm{T}}_{1\times 4} \\
& [0.1 \quad \ldots \quad 0.1]^{\mathrm{T}}_{1\times 4} + \boldsymbol{\eta} \le \mathbf{x}_c \le [50 \quad \ldots \quad 50]^{\mathrm{T}}_{1\times 4} - \boldsymbol{\eta}
\end{aligned} \tag{5-24}$$

where σ_i denotes the stress of ith member, c_1 and c_2 denotes the stress constraints and Euler buckling compressive stress limitation, respectively. The results, obtained with the three different methods: the nested optimization, linearization model, and the proposed interval strategy, are shown in Table 5-1.

The objective and constraint shown in the bracket denotes the validated value, which is obtained through the scanning method in the uncertain range around the design point. The results show that the linearization model gives the lightest design solution 6622.74lb, and then the nested optimization method is 6623.95lb and the interval solution is 6650.27lb. However, the linearization optimization method violates both of the two constraints shown with underlines, and the second constraint is violated for the nested optimization solution. The interval method can ensure the satisfaction of both constraints, and so we can say that the interval method is able to provide more reliable optimization results. For

the calculation cost, the interval method takes 139s, which is close to the linearization method and much less than the nested optimization method.

Table 5-1 The optimization results of 18-bar planar truss

	Nested optimization	Linearization optimization	Interval optimization
$x_1(\text{in}^2)$	10.2024	10.1962	10.2000
$x_2(\text{in}^2)$	21.8514	21.8480	21.8517
$x_3(\text{in}^2)$	12.6160	12.6310	12.8889
$x_4(\text{in}^2)$	7.2761	7.2657	7.2711
$g_1(\text{lb/in}^2)$	19995(19995)	20000(20015)	20000(20000)
g_2	1.000(1.014)	1.000(1.011)	1.000(1.000)
w(lb)	6623.95	6622.74	6650.27
Time(s)	288	103	139

5.4.2 Vehicle suspension optimization

The characteristics of wishbone suspension can be mathematically divided into two groups, namely, kinematic performance and dynamic performance [168]. The kinematic performance of suspension has large influence on the vehicles' handling, while the dynamic performance influences the ride comfort. Since the positions of hardpoints obviously influence the kinematic performance rather than dynamic performance, only the kinematic characteristics of the suspension will be optimized in this section. Compared to the Macpherson suspension [169], the double wishbone suspension has better kinematic performance but relatively a more complicate structure, making the optimization of structure more difficult.

Figure 5-9 shows the model of a double wishbone suspension system, mainly including tie rod, knuckle, absorber, upper control arm, and lower control arm. In this study, the kinematic analysis model is developed using the commercial software ADAMS/Car. The simulation condition for the wheel stroke is a bump of 50 mm and a rebound of -50 mm.

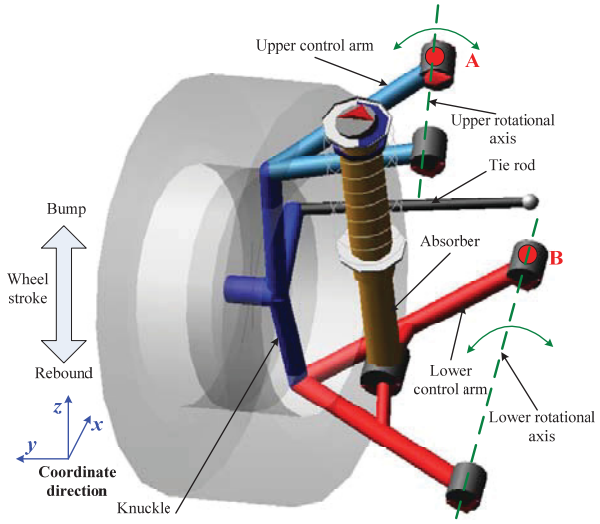

Figure 5-9 The model of double wishbone suspension

With the suspension model, the kinematic characteristics which are described with the camber angle, caster angle, kingpin inclination angle, and toe angle, shown as Fig. 5-10.

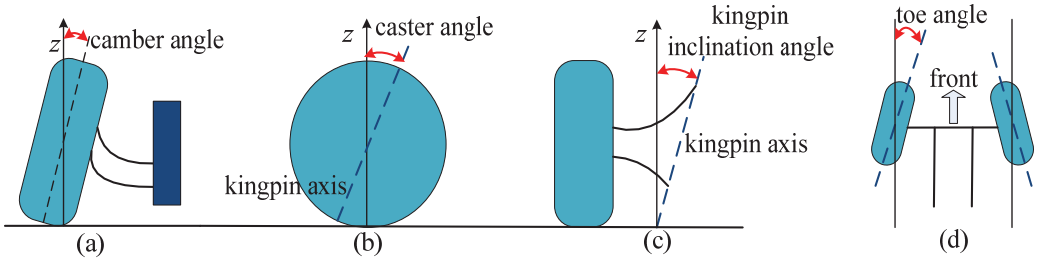

Figure 5-10 Camber angle, caster angle, kingpin inclination angle, and toe angle

The camber angle is the angle between the vertical axis of the wheels used for steering and the vehicle *z*-axis (Fig. 5-10(a)). If the top of the wheel is farther out than the bottom,

the camber angle would be positive, otherwise it will be negative. Caster is the angle to which the kingpin axis is tilted forward or rearward from vertical, as viewed from the side (Fig. 5-10(b)). If the kingpin axis is tilted backward (that is, the top pivot is positioned farther rearward than the bottom pivot), then the caster is positive; if it's tilted forward, then the caster is negative. Kingpin inclination angle is measured in degrees from the center line kingpin to vertical, as viewed from the front or rear (Fig. 5-10(c)). The angle of the two front wheels or two rear wheels relative to each other and the car as seen from above is the toe angle (Fig. 5-10(d)).

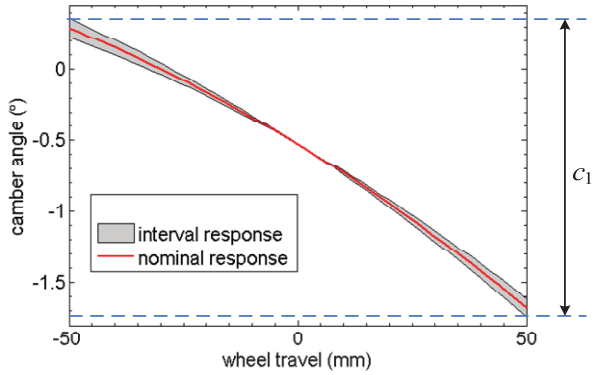

Figure 5-11 Camber angle

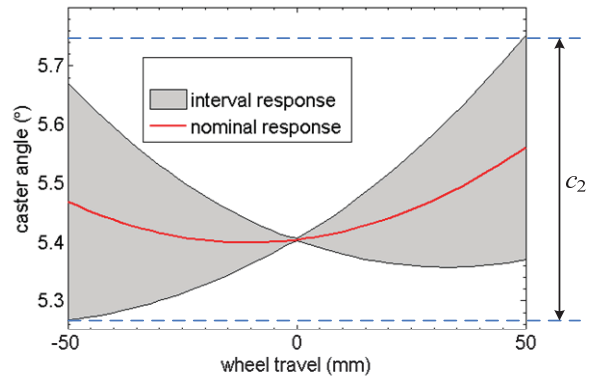

Figure 5-12 Caster angle

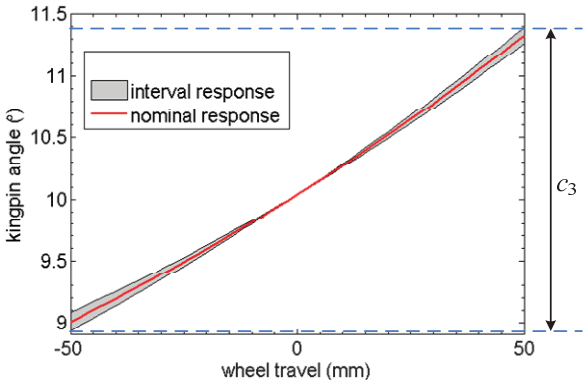

Figure 5-13 Kingpin inclination angle

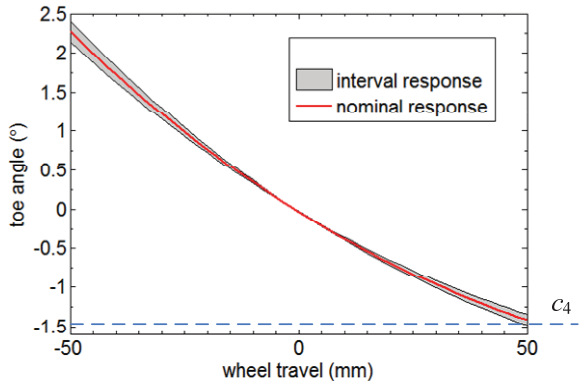

Figure 5-14 Toe angle

These angles are changed with the wheel stroke, and they can be obtained through the numerical simulation. The plots of these characteristic indexes with respect to the wheel travel are shown from Fig. 5-11 to Fig. 5-14, respectively.

The axis direction of inner revolution joint of upper control arm and lower control arm (Fig. 5-9) influences the kinematic performance of the suspension, so the coordinates of rear inner hardpoint of upper control arm (point *A*) and rear inner hardpoint of lower control arm (point *B*) are chosen as design variables. As the *x*-directional coordinates of the two hardpoints have little influence on the axis direction of revolution joint, only the *y*- and *z*-directional coordinates are considered as design variables. The relevant design

vector is denoted as $\mathbf{u}=[u_1 \quad u_2 \quad u_3 \quad u_4]^{\mathrm{T}}=[y_A \quad z_A \quad y_B \quad z_B]^{\mathrm{T}}$. The initial values of the design variables are set as $\mathbf{u}=[490 \quad 560 \quad 450 \quad 185]^{\mathrm{T}}$ *mm*, and the range of design variables are set as ±60 *mm* in terms of the initial values.

As described in above, the design variables contain uncertainties, which lead the actual values to fluctuate at their nominal values. It is assumed that the uncertain range of each design variable is ±3 *mm* from its nominal value, and then the design vector can be expressed as interval vector as:

$$[\mathbf{u}]=\mathbf{u}+[\mathbf{\Delta u}],\ [\mathbf{\Delta u}]=\left[[-3,3] \quad [-3,3] \quad [-3,3] \quad [-3,3]\right]^{\mathrm{T}} \tag{5-25}$$

If the design variables are considered as interval variables, the response of kinematic performance will not be a curve but an interval belt, as shown in Fig. 5-11 to 5-14 To improve the kinematic performance, the maximum variation in the transient responses over the wheel travel is required to be minimized. In details, the maximum variation of camber angle, caster angle, and kingpin inclination angle is required to be no more than 2°, 1°, and 3° over the wheel travel, respectively, and the toe angle is no less than -0.5° when the wheel travel is set to 50 *mm*. To minimize the variation of camber angle and kingpin inclination angle, the optimization problem is defined as follows:

$$\begin{aligned}
&\text{Find} && \mathbf{u}=[u_1 \quad u_2 \quad u_3 \quad u_4]^{\mathrm{T}}\\
&\text{minimize} && \alpha_1 c_1(\mathbf{u})+\alpha_3 c_3(\mathbf{u})\\
&\text{subject to} && c_1(\mathbf{u})=\max_{\mathbf{u}\in[\mathbf{u}],t} f^1(\mathbf{u},t)-\min_{\mathbf{u}\in[\mathbf{u}],t} f^1(\mathbf{u},t)\le 2^\circ\\
& && c_2(\mathbf{u})=\max_{\mathbf{u}\in[\mathbf{u}],t} f^2(\mathbf{u},t)-\min_{\mathbf{u}\in[\mathbf{u}],t} f^2(\mathbf{u},t)\le 1^\circ\\
& && c_3(\mathbf{u})=\max_{\mathbf{u}\in[\mathbf{u}],t} f^3(\mathbf{u},t)-\min_{\mathbf{u}\in[\mathbf{u}],t} f^3(\mathbf{u},t)\le 3^\circ\\
& && c_4(\mathbf{u})=\min_{\mathbf{u}\in[\mathbf{u}]} f^4(\mathbf{u},t)\big|_{t=50}\ge -0.5^\circ\\
& && \mathbf{lb}\le[\mathbf{u}]=\mathbf{u}+[\mathbf{\Delta u}]\le\mathbf{ub},\ -50\le t\le 50\\
& && \mathbf{lb}=\left[430 \quad 500 \quad 390 \quad 125\right]^{\mathrm{T}},\ \mathbf{ub}=\left[550 \quad 620 \quad 510 \quad 245\right]^{\mathrm{T}}
\end{aligned} \tag{5-26}$$

where the t denotes the wheel travel from -50 *mm* to 50 *mm*, **lb** and **ub** denotes the lower bound and upper bound of design vector, $f^1(\mathbf{u},t)$, $f^2(\mathbf{u},t)$, $f^3(\mathbf{u},t)$, and $f^4(\mathbf{u},t)$ respectively denotes the camber angle, caster angle, kingpin inclination angle, and toe angle, which are the functions with respect to design variables and wheel travel. $c_1(\mathbf{u})$, $c_2(\mathbf{u})$, $c_3(\mathbf{u})$, and $c_4(\mathbf{u})$ respectively denotes the variation of camber angle, caster angle, kingpin inclination angle, and the minimum value of toe angle when the wheel stroke equals to 50*mm*, shown from Fig. 5-11 to 5-14. α_1 and α_3 are the weighting coefficients which are both set to 0.5 in this paper, indicating two equally weighted individual objectives in the design. Since the suspension model is built in software, we may not obtain the explicit expression of the four indexes (camber, caster, kingpin inclination and toe), and the simulation of the complex model is very time-consuming. To reduce the computational cost, the Chebyshev surrogate model will be used to approximate the four indexes.

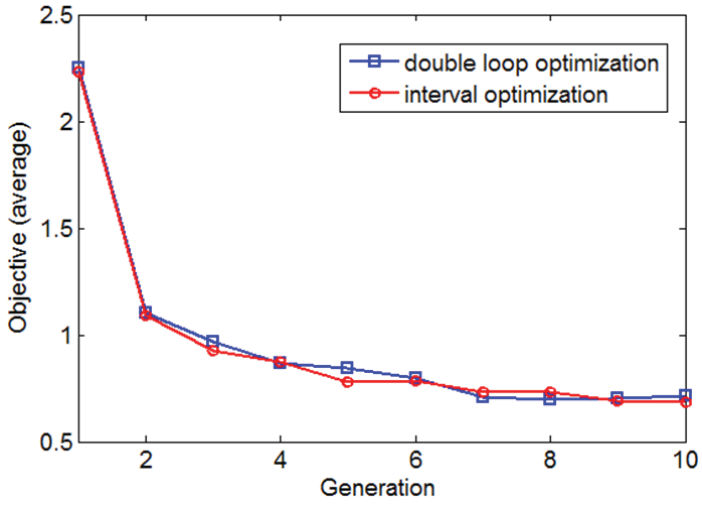

Figure 5-15 The average objective

The kinematic performance of the double wishbone suspension is evaluated with the conventional nested double-loop optimization approach and the proposed interval

arithmetic-based approach, respectively. The parameters of MIGA are set as: 100 populations in each island, 10 islands and 10 generations, so there are 1000 populations in each generation. The objective in average value and best value changing with the generation are shown in Figs. 5-15 and 5-16, respectively.

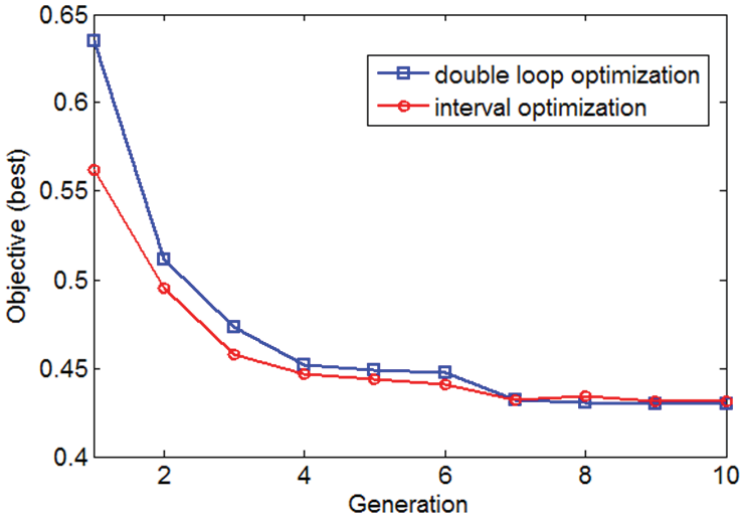

Figure 5-16 The best objective

The final optimization results are shown in Table 5-2. The bold number in Table 5-2 indicates that the constraint is violated. The optimization results show that the optimized suspension satisfies the constraints by minimizing the objective function relative to the initial condition. The objective function evaluated using the interval arithmetic-based method is equal to that calculated by the double-loop approach, but the constraints are some different. The difference is because the interval arithmetic-based method produces a wrap of original function, which means the maximal value produced by interval arithmetic is slightly larger than that obtained by optimization. Correspondingly, the minimal value of the interval arithmetic is slightly smaller than the minimum of optimization. Thus, the interval arithmetic-based optimization method more rigorously satisfies the constraints.

Table 5-2 Optimization results of vehicle suspension

	u_1	u_2	u_3	u_4	c_1	c_2	c_3	c_4	obj	time(')
Initial	490.0	560.0	450.0	185.0	**2.10**	0.49	2.46	**-1.48**	2.28	-
Double-loop	518.9	525.7	394.2	128.0	0.40	0.94	0.47	-0.44	0.43	265
Interval	541.9	524.4	393.0	128.0	0.38	1.00	0.48	-0.44	0.43	81

The computational time indicates that the interval method is more efficient, because it only requires less than one third of time compared to the double-loop method. Fig. 5-17 to 5-20 show the variations of the camber angle, caster angle, kingpin inclination angle, and toe angle respectively with respect to the wheel travel, considering the initial conditions, double-loop optimization solutions and interval arithmetic based optimization solutions. The figures are plotted through the scanning method using the kinematic model of double wishbone suspension. The plots show a great improvement of the suspension kinematic performance. The two different optimization approaches can provide very close optimization results.

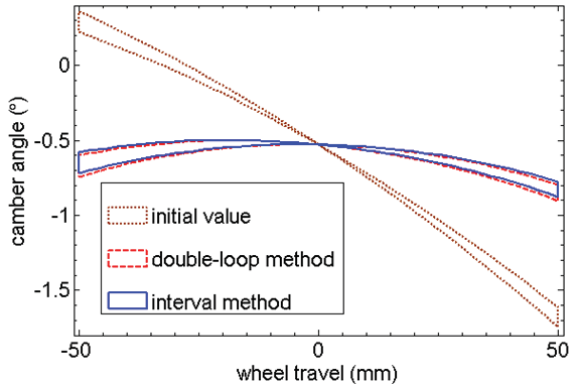

Figure 5-17 Comparison of camber angle

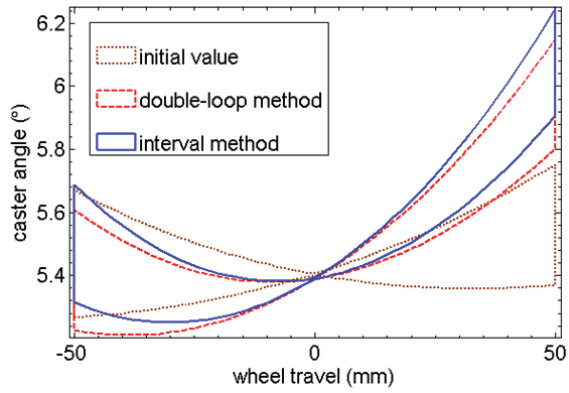

Figure 5-18 Comparison of caster angle

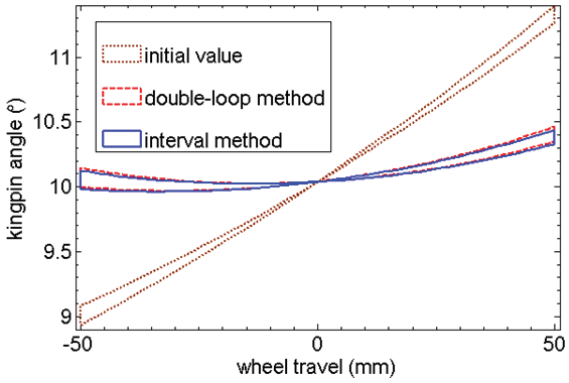

Figure 5-19 Comparison of kingpin inclination angle

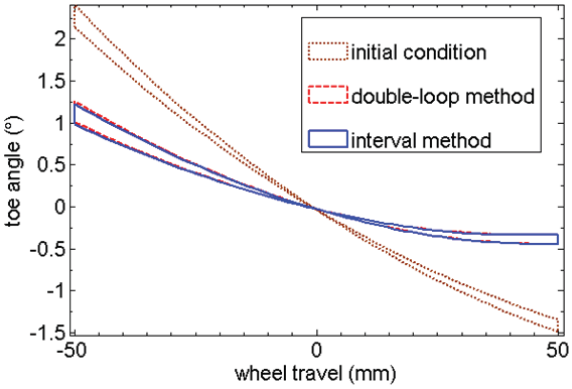

Figure 5-20 Comparison of toe angle

The maximum variation of camber angle over the wheel travel reduces to 0.40° and 0.38° from 2.10° with the same initial conditions after optimized by the double-loop method and the interval method, respectively. The maximum variation of caster angle over the wheel travel increases to 0.94° and 1.00° from the same initial value 0.49° after optimized by the double-loop method and the interval method. However, both the optimization results satisfy the constraints. At the same time, the maximum variation of kingpin inclination angle over the wheel travel is reduced to 0.47° and 0.48° from the initial value 2.46° optimized by the double-loop method and the interval method, respectively. The toe angle when wheel travel equals to 50 *mm* increase to -0.44° for both the optimization methods, while the initial value is -1.48° violated the constraint.

5.5 Robust topology optimization under interval uncertainty

In the field of structural optimization, topology optimization has experienced considerable development over the past two decades with a wide range of engineering applications [170]. Topology optimization is essentially a numerical iterative process to optimize a prescribed objective function under specific constraints by distributing a given amount of material, until the best layout of the material is achieved within the design domain. The topology optimization is different from general parameter optimization problem. The number of design variables in topology optimization is usually quite large, so the gradient-based optimization algorithms have to be used, in order to save the computational cost. Several typical methods have been developed for topology optimization of structures, such as the homogenization method [171], the SIMP based methods [172, 173], and the level set-based methods [174-176].

However, the majority of current studies about the topology optimization are based on the deterministic assumption, which may result in a design that cannot satisfy the expected

goal or even unfeasible design, as most problems in engineering inevitably involve various uncertainties, including the manufacturing tolerance, load variation, inhomogeneity of material property, and so on [177]. For a structure, the topological design may be quite different when uncertain factors are considered. As a result, the performance of a structure, such as robustness and reliability, is unavoidably subject to variations in practice due to various uncertainties [125, 178]. Hence, it is necessary to incorporate uncertainties into structural topology optimization problems quantitatively, in order to enhance structural safety and avoid failure in extreme working conditions.

The Robust Design Optimization (RDO) aims to reduce the sensitivity of the objective function with respect to uncertain parameters, so it can minimize both the mean and variation of the objective function. The application of RDO to structural topology optimization refers to the robust topology optimization, termed as RTO which is the major focus of this section. There have been some studies which investigate RTO under the uncertainties of load conditions, material properties, and geometry. For instance, Sigmund [179] presented a topology optimization method by using the concept of density filtering to include uncertainties during the fabrication of micro and nano structures, which was further applied to RTO problems by [180]. Guest et al. [181] presented a perturbation-based topology optimization method for solving optimization problems with small uncertainty in the magnitude and location of the applied loads. Asadpoure and et al. [177] combined deterministic topology optimization techniques with a perturbation method for quantification of uncertainties associated with structural stiffness. For the continuous problems with uncertainty, the stochastic spectrum-based method is usually used to discretize the random field. Tootkaboni et al. [182] combined the PC expansion with topology optimization, to design continuum structures to achieve robustness in presence of random uncertainties. Zhao et al. [183] considered loading uncertainty of

random field by using the K-L expansion to characterize the random field as a reduced set of random variables. The K-L expansion was also used to develop robust topology optimization method [184] with random field uncertainty, in which the univariate dimension-reduction method was combined with the Gauss type quadrature sampling to calculate statistical moments of the objective function. Jansen et al. [185] discretised the random field by using the expansion optimal linear estimation method, which particularly suits for discretizing random fields with a relatively large correlation length. Zhao et al. [186] proposed an efficient approach by completely separating the Monte Carlo sampling with topology optimization to solve the RTO problem of structures under loading uncertainty, which obtained the accurate calculation of the objective function.

Most of the aforementioned RTO methods are based on the theory of random field or random variables, using a combination of the first and second order statistical moments (mean and variance) of the design response as the objective function of the RTO problems. However, in engineering, how to accurately describe probability distribution functions for random variables is a challenging task, especially for variables with limited uncertainty information. In some cases, for the uncertain variables the lower and upper bounds can be more easily obtained than the evaluation of accurate probability distributions [187]. Hence, the uncertain-but-bounded parameters may be more suitable for describing uncertainties under some situations. When non-probabilistic parameters are used to describe the uncertainty, the performance under the worst condition can be used to define the objective function of RTO problems.

In this section, the Chebyshev inclusion function will be applied to solve the RTO problems of continuum structures under interval uncertainty. The interval objective function of the RTO will be calculated by using the interval arithmetic to improve the computational efficiency. In particular, a new numerical method will be developed to

compute the derivatives of the interval functions, which makes the RTO problems be solved by using the traditional gradient-based optimization algorithms.

5.5.1 Material Density based approach for topology optimization

A typical topology optimization problem is the one where we try to find the best possible layout of material within a given design domain, to minimize an objective function while satisfying a set of constraints. The well-known design problem of minimizing structural mean compliance will be discussed in this paper, as a typical case. A limited volume of material is given, and the goal of the optimization is to identify structural topologies that store the minimum amount of strain energy under a set of applied loads. Using the SIMP method [188], the optimization model is defined as follows:

$$\begin{aligned} \min_{\boldsymbol{\rho}} \quad & C(\boldsymbol{\rho}) = \mathbf{U}^{\mathrm{T}}\mathbf{K}\mathbf{U} = \sum_{e=1}^{N} (\rho_e)^p \, \mathbf{u}_e^{\mathrm{T}}\mathbf{k}_0\mathbf{u}_e \\ \text{s.t.} \quad & \mathrm{g}(\boldsymbol{\rho}) = \frac{\sum_{e=1}^{N} \rho_e v_e}{\sum_{e=1}^{N} v_e} - V \le 0, \\ & 0 < \rho_{\min} \le \rho_e \le 1. \end{aligned} \tag{5-27}$$

where $C(\boldsymbol{\rho})$ is the compliance, $\boldsymbol{\rho}$ is the vector including all elemental design variables, $\mathbf{k}_0$ denotes the element stiffness matrix, ρ_e is an entry in $\boldsymbol{\rho}$ corresponding to element e, v_e is a quantity that gives the volume of the element e when multiplied by the design variable ρ_e, and V is the upper bound for the amount of material that are allowable for usage. $\rho_{\min}$ is a vector of minimal densities, N is the number of elements used to discretise the design domain, and p is the penalization power. $\mathbf{U}$ and $\mathbf{F}$ denotes the global displacement vector and forcing vector, respectively, and they satisfy the following equation

$$\mathbf{K}\mathbf{U} = \mathbf{F} \tag{5-28}$$

where $\mathbf{K}$ denotes the global stiffness matrix.

The above optimization model can often be solved by several types of optimization algorithms, such as the Optimality Criteria (OC) method [189], the Method of Moving Asymptotes (MMA) [190], and so on. If the MMA is used, the sensitivity of the objective function with respect to the design variables should be derived firstly, as follows [188]:

$$h(\boldsymbol{\rho}) = \frac{\partial C(\boldsymbol{\rho})}{\partial \rho_e} = -p(\rho_e)^{p-1} \mathbf{u}_e^{\mathrm{T}} \mathbf{k}_0 \mathbf{u}_e \tag{5-29}$$

To avoid numerical instability of the relaxed topology optimization, the filter technique [191, 192] will be used. Therefore, the element sensitivity is normally modified as

$$\frac{\partial \hat{C}(\boldsymbol{\rho})}{\partial \rho_e} = \frac{1}{\rho_e \sum_{i \in N_e} w_i} \sum_{i \in N_e} w_i \rho_i \frac{\partial C(\boldsymbol{\rho})}{\partial \rho_e} \tag{5-30}$$

where *Ne* is the set of elements whose center-center distance to element *e* is no larger than the filter radius *R,* and w_i is the weight factor, determined by the following equation

$$w_i = R - dist(\rho_i, \rho_e) \tag{5-31}$$

Using Eq. (5-30) to compute the derivatives of the objective function, the optimization given in Eq. (5-27) can be solved by the gradient-based optimization algorithms, e.g. the MMA.

5.5.2 Robust topology optimization under interval uncertainty

When interval uncertain parameters (e.g. loads and material properties) involved in topology optimization model, the formulation (5-27) will be rewritten as follows:

$$\begin{aligned} \min_{\boldsymbol{\rho}} \quad & C(\boldsymbol{\rho}, [\mathbf{x}]) = \sum_{e=1}^{N} (\rho_e)^p \, \mathbf{u}_e^{\mathrm{T}}([\mathbf{x}]) \mathbf{k}_0([\mathbf{x}]) \mathbf{u}_e([\mathbf{x}]) \\ \text{s.t.} \quad & \mathrm{g}(\boldsymbol{\rho}) \le 0, \\ & 0 < \rho_{\min} \le \rho_e \le 1. \end{aligned} \tag{5-32}$$

Here, $[\mathbf{x}] \in \mathbf{IR}^n$ denotes a n-dimensional vector of interval parameters. Since the constraint is the volume fraction, the interval parameters are not involved in it. In this case, the original compliance (float function) has become an interval function of mean compliance, so it will be expressed by its lower bound $\underline{C}\left(\boldsymbol{\rho},[\mathbf{x}]\right)$ and upper bound $\overline{C}\left(\boldsymbol{\rho},[\mathbf{x}]\right)$. Considering the worst case of the objective under uncertainty, the upper bound of the interval objective function will be used as the new objective to define the RTO model.

$$\begin{aligned} \min_{\boldsymbol{\rho}} \quad & \overline{C}\left(\boldsymbol{\rho},[\mathbf{x}]\right) \\ \text{s.t.} \quad & \mathrm{g}\left(\boldsymbol{\rho}\right) \le 0, \\ & 0 < \rho_{\min} \le \rho_e \le 1. \end{aligned} \tag{5-33}$$

If we know the explicit expression of the objective with respect to interval parameters [**x**], the interval arithmetic can be used directly to produce the upper bound of the interval objective function. However, it is hard to obtain its explicit expression, so we have to solve the following interval linear system to obtain the interval displacement, and then calculate the interval function of the mean compliance.

$$\mathbf{K}\left([\mathbf{x}]\right)\mathbf{U} = \mathbf{f}\left([\mathbf{x}]\right) \tag{5-34}$$

The Eq. (5-34) is difficult to solve by using interval arithmetic directly, especially for the large dimensional case in the finite element analysis. On the other hand, each node displacement occurs several times in the expression of compliance, which may produce large overestimation if the interval arithmetic is used directly. To overcome these problems, the non-intrusive Chebyshev inclusion function will be employed to calculate the interval compliance.

Let $C^e(\boldsymbol{\rho},[\mathbf{x}])$ denote the interval element compliance under the interval parameters, i.e.

$$C^e\left(\boldsymbol{\rho},[\mathbf{x}]\right) = \left(\rho_e\right)^p \mathbf{u}_e^{\mathrm{T}}\left([\mathbf{x}]\right)\mathbf{k}_0\left([\mathbf{x}]\right)\mathbf{u}_e\left([\mathbf{x}]\right) \tag{5-35}$$

Based on the Chebyshev inclusion function proposed in Chapter 3, the interval element compliance $C^e(\boldsymbol{\rho},[\mathbf{x}])$ can be approximated by the following k-th order truncated Chebyshev series:

$$C^e\left(\boldsymbol{\rho},[\mathbf{x}]\right)=\sum_{j_1=0}^{n}\cdots\sum_{j_k=0}^{n}\frac{1}{2^l}c^e_{j_1\cdots j_k}\left(\boldsymbol{\rho}\right)\prod_{i=1}^{k}\cos\left(j_i\left[\theta_i\right]\right) \tag{5-36}$$

It should be noted that the coefficients $c^e_{j_1\cdots j_k}$ will be changed with the design variables $\boldsymbol{\rho}$, noted as $c^e_{j_1\cdots j_k}\left(\boldsymbol{\rho}\right)$. Considering Eq. (5-32), the interval compliance can be expressed as

$$C\left(\boldsymbol{\rho},[\mathbf{x}]\right)=\sum_{e=1}^{N}C^e\left(\boldsymbol{\rho},[\mathbf{x}]\right)=\sum_{e=1}^{N}\sum_{j_1=0}^{n}\cdots\sum_{j_k=0}^{n}\frac{1}{2^l}c^e_{j_1\cdots j_k}\left(\boldsymbol{\rho}\right)\prod_{i=1}^{k}\cos\left(j_i\left[\theta_i\right]\right) \tag{5-37}$$

Based on the Chebyshev inclusion function, the objective function of the RTO problem can finally be expressed as follows:

$$\overline{C}\left(\boldsymbol{\rho},[\mathbf{x}]\right)=\sum_{e=1}^{N}\left(\frac{1}{2^k}c^e_{0\cdots0}\left(\boldsymbol{\rho}\right)+\sum_{\substack{0\le j_1,\ldots,j_k\le n\\ j_1+\ldots+j_k>0}}\frac{1}{2^l}\left|c^e_{j_1\cdots j_k}\left(\boldsymbol{\rho}\right)\right|\right) \tag{5-38}$$

The Eq. (5-38) assumes that all the interval element compliance gets their upper bound simultaneously, so it usually makes $\overline{C}(\boldsymbol{\rho},[\mathbf{x}])$ be larger than its exactly upper bound. However, the $\overline{C}(\boldsymbol{\rho},[\mathbf{x}])$ has the same trend of the exactly upper bound, so it can be used as the objective to replace the exactly upper bound.

5.5.3 Numerical implementation of RTO using interval arithmetic

To use the MMA to solve the RTO, the derivatives of the objective with respect to the design variables have to be produced. The objective shown in Eq. (5-36) contains the operation of computing the absolute value, which is difficult to calculate the derivative, so we reform the Eq. (5-38) as the Eq. (5-39).

$$\overline{C}\left(\boldsymbol{\rho},[\mathbf{x}]\right)=\sum_{e=1}^{N}\left(\frac{1}{2^k}c^e_{0\cdots0}\left(\boldsymbol{\rho}\right)+\sum_{\substack{0\le j_1,\ldots,j_k\le n\\ j_1+\ldots+j_k>0}}\frac{1}{2^l}c^e_{j_1\cdots j_k}\left(\boldsymbol{\rho}\right)\operatorname{sign}\left(c^e_{j_1\cdots j_k}\left(\boldsymbol{\rho}\right)\right)\right) \tag{5-39}$$

where the sign function is defined as

$$\operatorname{sign}(x)=\begin{cases}-1, & x<0\\ 0, & x=0\\ 1, & x>0\end{cases} \tag{5-40}$$

Differentiating Eq. (5-39) with respect to design variables ρ_e, we have the sensitivity

$$\frac{\partial \bar{C}(\boldsymbol{\rho},[\mathbf{x}])}{\partial \rho_e}=\sum_{e=1}^{N}\left(\frac{\partial c_{0\ldots0}^{e}(\boldsymbol{\rho})}{2^k\partial\rho_e}+\sum_{\substack{0\le j_1,\ldots,j_k\le n\\ j_1+\ldots+j_k>0}}\frac{\partial c_{j_1\ldots j_k}^{e}(\boldsymbol{\rho})}{2^l\partial\rho_e}\left(\operatorname{sign}\left(c_{j_1\ldots j_k}^{e}(\boldsymbol{\rho})\right)+\frac{\partial\operatorname{sign}\left(c_{j_1\ldots j_k}^{e}(\boldsymbol{\rho})\right)}{\partial c_{j_1\ldots j_k}^{e}(\boldsymbol{\rho})}c_{j_1\ldots j_k}^{e}(\boldsymbol{\rho})\right)\right) \tag{5-41}$$

The sign function sign(x) is not continuous, so it cannot be derivative at the point x=0. To make the stability of optimization, the Heaviside projection method is used to smooth the sign function, as

$$s(x)=\tanh(\beta x) \tag{5-42}$$

where the parameter β is a positive real number. The $s(x)$ and the sign(x) are plot in Fig. 5-21, which indicates that the $s(x)$ will be equal to sign(x) when the parameter β tends to be infinite.

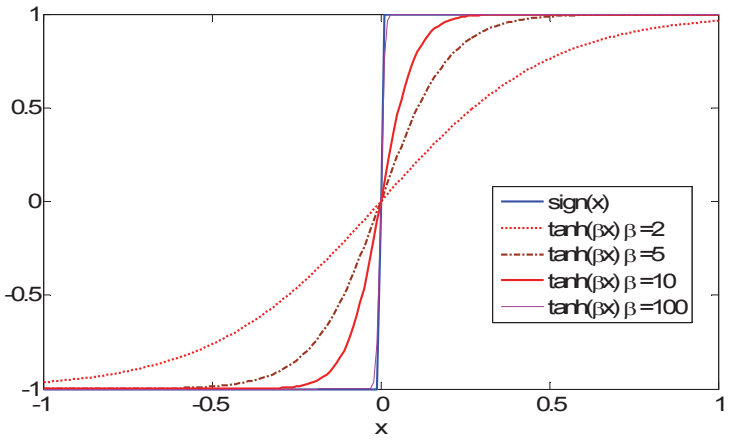

Figure 5-21 The plot of sign(x) and tanh(βx)

Replacing sign(x) by $s(x)$ in Eq. (5-41), we can obtain the following equation

$$\frac{\partial \bar{C}\left(\boldsymbol{\rho},[\mathbf{x}]\right)}{\partial \rho_e}=\sum_{e=1}^{N}\left(\frac{\partial c_{0\ldots0}^{e}\left(\boldsymbol{\rho}\right)}{2^k\partial \rho_e}+\sum_{\substack{0\le j_1,\ldots,j_k\le n\\ j_1+\ldots+j_k>0}}\frac{\partial c_{j_1\ldots j_k}^{e}\left(\boldsymbol{\rho}\right)}{2^l\partial \rho_e}\left(\tanh\left(\beta c_{j_1\ldots j_k}^{e}\left(\boldsymbol{\rho}\right)\right)+\beta\,\mathrm{sech}^2\left(\beta c_{j_1\ldots j_k}^{e}\left(\boldsymbol{\rho}\right)\right)c_{j_1\ldots j_k}^{e}\left(\boldsymbol{\rho}\right)\right)\right) \tag{5-43}$$

Since the first-order derivatives of the coefficients $c_{j_1\ldots j_n}$ with respect to ρ_e (sensitivities) cannot be explicitly obtained, we will consider the following expansion, to approximate these first-order derivatives. Considering the interval parameters, the derivative of compliance in Eq. (5-29) should be rewritten as

$$h\left(\boldsymbol{\rho},[\mathbf{x}]\right)=\frac{\partial C\left(\boldsymbol{\rho},[\mathbf{x}]\right)}{\partial \rho_e}=-p\left(\rho_e\right)^{p-1}\mathbf{u}_e^{\mathrm{T}}\left([\mathbf{x}]\right)\mathbf{k}_0\left([\mathbf{x}]\right)\mathbf{u}_e\left([\mathbf{x}]\right) \tag{5-44}$$

Similar to the procedure shown in previous section, the derivative can also be expanded by the truncated Chebyshev series, as follows:

$$h\left(\boldsymbol{\rho},[\mathbf{x}]\right)=\sum_{j_1=0}^{k}\cdots\sum_{j_n=0}^{k}\frac{1}{2^l}h_{j_1\ldots j_n}\left(\boldsymbol{\rho}\right)\prod_{i=1}^{n}\cos\left(j_i\left[\theta_i\right]\right) \tag{5-45}$$

It is noted that the above equation involves the coefficients $h_{j_1\ldots j_k}(\boldsymbol{\rho})$, which actually can be directly calculated by using the same quadrature formula shown in Chapter 3 or by the LSM shown in Chapter 4.

Differentiating Eq. (5-37) with respect to ρ_e, we have

$$\frac{\partial C\left(\boldsymbol{\rho},[\mathbf{x}]\right)}{\partial \rho_e}=\sum_{e=1}^{N}\sum_{j_1=0}^{n}\cdots\sum_{j_k=0}^{n}\frac{\partial c_{j_1\ldots j_k}^{e}\left(\boldsymbol{\rho}\right)}{2^l\partial \rho_e}\prod_{i=1}^{k}\cos\left(j_i\left[\theta_i\right]\right) \tag{5-46}$$

Comparing the Eq. (5-45) and Eq. (5-46), we will have

$$\sum_{e=1}^{N}\frac{\partial c_{j_1\ldots j_k}^{e}\left(\boldsymbol{\rho}\right)}{\partial \rho_e}=h_{j_1\ldots j_k}\left(\boldsymbol{\rho}\right) \tag{5-47}$$

In this case, we can get the first-order derivatives of the coefficients $\sum_{e=1}^{N} c_{j_1\cdots j_k}^{e}(\boldsymbol{\rho})$ with respect to ρ_e in the right-hand side of Eq. (5-43). Hence, substituting Eq. (5-47) into Eq. (5-43), we can finally find the design sensitivity of the objective function as

$$\frac{\partial \bar{C}(\boldsymbol{\rho},[\mathbf{x}])}{\partial \rho_e} = \frac{1}{2^k} h_{0\ldots 0}(\boldsymbol{\rho}) + \sum_{\substack{0\le j_1,\ldots,j_k\le n \\ j_1+\ldots+j_k>0}} \frac{1}{2^l} h_{j_1\cdots j_k}(\boldsymbol{\rho}) \left(\tanh\left(\beta c_{j_1\cdots j_k}^{e}(\boldsymbol{\rho})\right) + \beta \operatorname{sech}^2\left(\beta c_{j_1\cdots j_k}^{e}(\boldsymbol{\rho})\right) c_{j_1\cdots j_k}^{e}(\boldsymbol{\rho}) \right) \quad (5\text{-}48)$$

After the Eq. (5-48) is obtained, it can be substituted in the filter Eq. (5-30) to produce the modified element sensitivity which will be finally used by the MMA solver. Therefore, the process of robust topology optimization under interval uncertainties can be summarized as follows:

1) Initialize the design variables $\boldsymbol{\rho}$ and produce the interpolation points of the interval parameters θ_i by using Eq. (3-42);

2) Setting the interval parameters to be the values at the interpolation points produced in step (1), solve the displacements by finite element method and then evaluate the compliance $C(\boldsymbol{\rho},\cos(\theta_{i_1}),\ldots,\cos(\theta_{i_n}))$ and sensitivity $h(\boldsymbol{\rho},\cos(\theta_{i_1}),\ldots,\cos(\theta_{i_n}))$ at these interpolation points;

3) Calculate the coefficients $c_{j_1\cdots j_k}^{e}$ and $h_{j_1\cdots j_n}$ using the quadratic formula or LSM;

4) Calculate the upper bound of interval compliance $\bar{C}(\boldsymbol{\rho},[\mathbf{x}])$ using Eq. (5-38);

5) Calculate the sensitivity of objective $\frac{\partial \bar{C}(\boldsymbol{\rho},[\mathbf{x}])}{\partial \rho_e}$ using Eq. (5-48) and then substituting it into filter Eq. (5-30) to produce the final sensitivity used in MMA;

6) Use the MMA to update the design variables, and go back to step 2) until convergence.

5.5.4 Numerical example

This section the Mitchell-type structure will be used as the numerical example, the boundary conditions and loads of which are shown in Fig. 5-22. The volume fraction is set as 0.3, and the magnitude of the three forces are F_1=1, F_2=2, and F_3=1. The force direction is assumed to be $\theta_1=\theta_2=\theta_3=$-90° in the deterministic condition. For the uncertain conditions, the force direction is assumed to be: 1) $\boldsymbol{\theta}$=[-95°, -85°]^3 ; 2) $\boldsymbol{\theta}$=[-100°, -80°]^3; 3) $\boldsymbol{\theta}$=[-110°, -70°]^3.

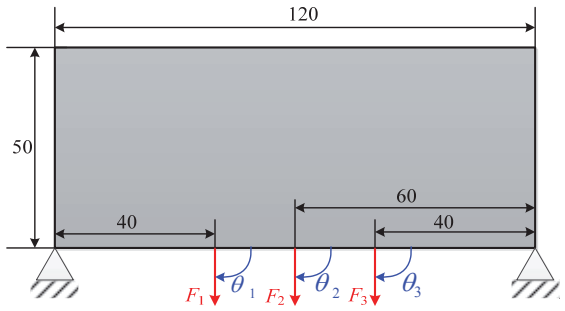

Figure 5-22 Mitchell-type structure design

Figures. 5-23 and 5-24 show the deterministic topology optimization result and RTO results, respectively. The detailed objective values are provided in Table 5-3. For the deterministic topology optimization, there are no materials between the two end points and the locations of F_1 and F_3.

Figure 5-23 Deterministic topology optimization

(a) $\boldsymbol{\theta}=[-95^\circ, -85^\circ]^3$ (b) $\boldsymbol{\theta}=[-100^\circ, -80^\circ]^3$ (c) $\boldsymbol{\theta}=[-110^\circ, -70^\circ]^3$

Figure 5-24 The RTO of Mitchell-type structure

When the uncertainty extent is 5°, two crossing structures are happened in the left bottom and right bottom domain, which may bear some lateral force induced by the force direction perturbation. When the uncertainty extent gets 10°, we can find that the two crossing structures move downward. When the uncertainty extent gets 20°, the crossing structures have moved to the bottom of the design domain, and they have degenerated to the direct linked bar. It can be found that there are more materials distributed in the bottom area when the uncertainty extent increases, which can improve the lateral stiffness, so as to keep the stability of the structure.

The compliance shown in Table 5-3 demonstrates that the RTO produces quite smaller worst-case compliance than the deterministic topology optimization.

Table 5-3 The compliance of Mitchell-type under the worst condition

	$\boldsymbol{\theta}=[-95^\circ, -85^\circ]^3$	$\boldsymbol{\theta}=[-100^\circ, -80^\circ]^3$	$\boldsymbol{\theta}=[-110^\circ, -70^\circ]^3$
Deterministic	310	556	1503
RTO	257	276	266

Figure 5-25 shows the iteration history of the RTO under different uncertainty extent. After 40 iterations, the variation of worst-compliance is not very large.

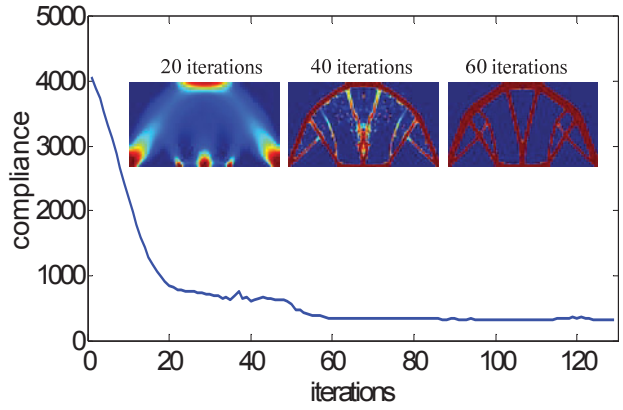

(a) $\boldsymbol{\theta}=[-95^{\circ}, -85^{\circ}]^3$

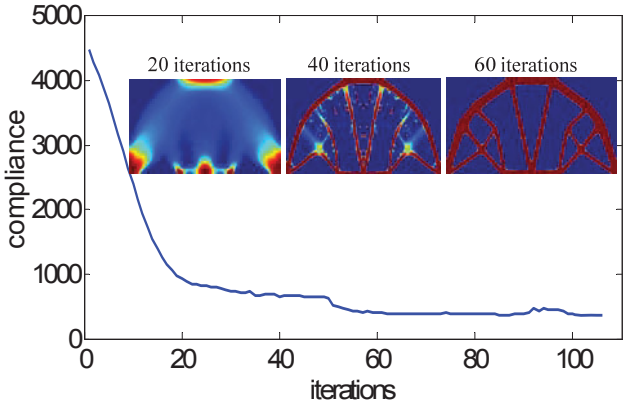

(b) $\boldsymbol{\theta}=[-100^{\circ}, -80^{\circ}]^3$

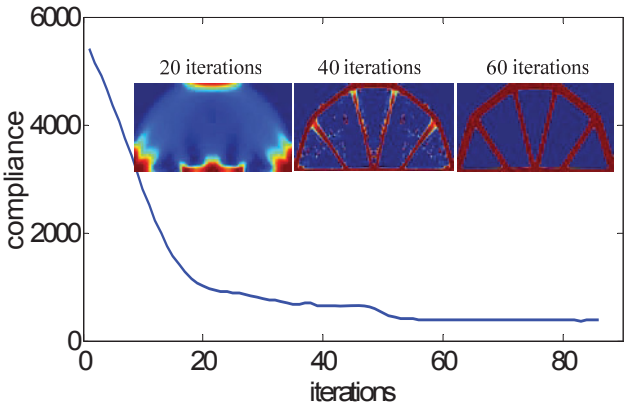

(c) $\boldsymbol{\theta}=[-110^{\circ}, -70^{\circ}]^3$

Figure 5-25 The iteration history of the RTO for Mitchell beam

5.6 Summary

This Chapter is focused on the design of optimization under interval uncertainty, which is based on the interval uncertainty analysis in Chapter 3. The interval uncertainty optimization model is proposed, which integrates the RBDO and RDO into one framework. The worst case scenario is used as the constraints to guarantee the reliability of the design solution.

The interval arithmetic based optimization method is proposed to improve the optimization efficiency and feasibility of solution. The Taylor inclusion function is employed to compute the bounds of objective and constraints directly. The Chebyshev surrogate model is proposed to derive a polynomial approximation model, which is used by the Taylor inclusion function. This chapter also proves that the accuracy of polynomials surrogate model is only determined by the sampling points rather than the basis vector, so the selection of sampling points is very important. Two numerical examples, which are truss structure and vehicle suspension optimization problem, show that the proposed interval arithmetic based optimization method has higher efficiency and provides a more feasible solution.

The topology optimization under interval uncertainty (Robust Topology Optimization with interval uncertainty) is also researched. The upper bound of mean compliance is used as the objective of RTO, and the sensitivity of the objective is derived. The numerical example indicates that the RTO gives better design solution than the deterministic optimization when the load uncertainty is considered.

Chapter 6 Optimization under hybrid uncertainty

Chapter 5 investigates the design of optimization under interval uncertainty. There have also been many studies investigating the probabilistic uncertainty optimization. However, there is only a little research about the optimization under hybrid uncertainty (containing both the interval uncertainty and probabilistic uncertainty). In fact, many engineering problems involve both types of uncertainties simultaneously.

In this chapter, we will systematically combine the interval arithmetic, the Monte Carlo simulation and the PC expansion to quantify the hybrid uncertainty, so as to deliver a new hybrid uncertainty analysis-based optimization method for structures including design sensitivity analysis for interval mean and interval standard deviation. In the proposed method, the role of the PCCI method proposed in Chapter 4 is to firstly expand the evaluation functions via a series of orthogonal polynomials with respect to both the random and interval variables, and then the interval mean and variance of evaluation functions are calculated conveniently and effectively by using the characteristic of orthogonal polynomials. At the same time, the derivatives of the interval objective function and constraints can be evaluated, to enable the application of gradient-based optimization algorithms to the uncertainty design optimization. Finally, the Monte Carlo simulation will be applied to estimate the probability density function and cumulative distribution function of the two bounds of the evaluation functions. It is noted that the Monte Carlo simulation is not computationally expensive in this case, because the PCCI has built a relatively cheaper surrogate model for the original complicated evaluation functions. The optimization under hybrid uncertainty is formulated with the feasible robustness under the random uncertainty and the reliability of the worst-case scenario

under the interval uncertainty. A typical numerical example will be used to demonstrate the effectiveness of the proposed method.

6.1 The hybrid uncertain optimization model

The conventional deterministic optimization model can be expressed as follows:

$$\begin{cases} \min\limits_{\mathbf{x}} & f(\mathbf{x}) \\ \text{s.t.} & \mathbf{g}(\mathbf{x}) \le \mathbf{0} \\ & \mathbf{x}^l \le \mathbf{x} \le \mathbf{x}^u \end{cases} \tag{6-1}$$

where $\mathbf{x} \in R^n$ are the n-dimensional design variables, $f(\mathbf{x})$ is the objective function, and $\mathbf{g}(\mathbf{x}) = [g_1(\mathbf{x}) \quad \cdots \quad g_p(\mathbf{x})]^{\mathrm{T}}$ is the p-dimensional constraints. All the design variables in the vector $\mathbf{x}$ and other parameters are deterministic in the above equation.

As aforementioned, we will extend the deterministic optimization problem as an uncertain optimization problem. If the design variables and parameters are supposed to involve uncertainty, there may be some uncertain variables contained in both objective and constraint functions. Thus, the optimization formulation will be changed to the following

$$\begin{cases} \min\limits_{\mathbf{x}} & f(\mathbf{x}+\boldsymbol{\eta}, \boldsymbol{\xi}) \\ \text{s.t.} & \mathbf{g}(\mathbf{x}+\boldsymbol{\eta}, \boldsymbol{\xi}) \le \mathbf{0} \\ & \mathbf{x}^l \le \mathbf{x} \le \mathbf{x}^u \end{cases} \tag{6-2}$$

where $\boldsymbol{\eta} = [\eta_1 \quad \cdots \quad \eta_m]^{\mathrm{T}}$ are the uncertain part of the design variables, $\boldsymbol{\xi} = [\xi_1 \quad \cdots \quad \xi_n]^{\mathrm{T}}$ denotes the uncertain parameters. It is noted that the $\boldsymbol{\eta}$ and $\boldsymbol{\xi}$ can be either random variables or interval variables, or the mixture of random and interval variables. However, for simplicity but without losing any generality, this study will only consider parameters $\boldsymbol{\xi}$ as the n-dimensional independent random variables, and $\boldsymbol{\eta}$ as the m-dimensional

independent interval variables, to be noted by $[\boldsymbol{\eta}] = [\underline{\boldsymbol{\eta}}, \overline{\boldsymbol{\eta}}]$, in which $\underline{\boldsymbol{\eta}}$ and $\overline{\boldsymbol{\eta}}$ are the lower bounds and upper bounds of the interval variables, respectively.

Since both the objective function f and constraints $\mathbf{g}$ contain the uncertain variables, the objective and constraints should be re-formulated to reflect the influence of the uncertainty. Firstly, if only the random variables are included in f and $\mathbf{g}$, the mean μ_f and $\boldsymbol{\mu}_\mathbf{g}$, as well as the variance σ_f^2 and $\boldsymbol{\sigma}_\mathbf{g}^2$ are usually used as uncertainty evaluation indexes. For the feasible robustness approach, the objective and constraints will be the weighted summation of the mean value and standard deviation, so the uncertain optimization model can be transformed to the following expression [115, 193]

$$\begin{cases} \min\limits_{\mathbf{x}} & \mathrm{w}_1\mu_f\left(\mathbf{x}+[\boldsymbol{\eta}],\boldsymbol{\xi}\right)+\mathrm{w}_2\sigma_f\left(\mathbf{x}+[\boldsymbol{\eta}],\boldsymbol{\xi}\right) \\ \text{s.t.} & \boldsymbol{\mu}_\mathbf{g}\left(\mathbf{x}+[\boldsymbol{\eta}],\boldsymbol{\xi}\right)+\mathrm{w}_3\boldsymbol{\sigma}_\mathbf{g}\left(\mathbf{x}+[\boldsymbol{\eta}],\boldsymbol{\xi}\right)\le\mathbf{0} \\ & \mathbf{x}^l\le\mathbf{x}\le\mathbf{x}^u \end{cases} \tag{6-3}$$

where w_1 and w_2 is the weighting coefficients of the mean value and standard deviation in objective, respectively. w_3 is the weighting coefficient of constraints, usually considered to be 3, which indicates the probability of constraints satisfaction will be $\Phi(3)=0.9987$ [193].

Secondly, considering the additional interval uncertainty $[\boldsymbol{\eta}]$ included in the equation (6-3), the value of the mean and standard deviation would also be an interval number rather than the float number. Therefore, the interval mean and interval deviation vary between their lower bounds and upper bounds. To guarantee the reliability, the worst case scenario will be considered in the optimization formulation, which uses the maximum value (or the upper bounds) of the original objective function and constraints as the new objective function and constraints. Hence, the optimization model can be expressed as follows:

$$\begin{cases} \min\limits_{\mathbf{x}} & \mathrm{w}_1\bar{\mu}_f\left(\mathbf{x}+[\boldsymbol{\eta}],\boldsymbol{\xi}\right)+\mathrm{w}_2\bar{\sigma}_f\left(\mathbf{x}+[\boldsymbol{\eta}],\boldsymbol{\xi}\right) \\ \text{s.t.} & \bar{\boldsymbol{\mu}}_{\mathbf{g}}\left(\mathbf{x}+[\boldsymbol{\eta}],\boldsymbol{\xi}\right)+\mathrm{w}_3\bar{\boldsymbol{\sigma}}_{\mathbf{g}}\left(\mathbf{x}+[\boldsymbol{\eta}],\boldsymbol{\xi}\right)\le\mathbf{0} \\ & \mathbf{x}^l\le\mathbf{x}\le\mathbf{x}^u \end{cases} \tag{6-4}$$

The above optimization problem can be solved by many traditional optimization methods. Here the discussion of the optimization algorithm is out of the major scope of this study. The key procedure in the optimization is the evaluation of the objective function and constraints. Both the objective function and constraints are composed of the bounds of interval mean and interval deviation, so how to obtain the two measure metrics efficiently is an important issue, which will be discussed in the next section.

6.2 The realization of hybrid uncertain optimization

6.2.1 Hybrid uncertainty analysis model

Chapter 4 has proposed the hybrid uncertainty analysis method (PCCI), which will also be used in this chapter, but the format of the polynomial will be adjusted. Still consider the function $F(\boldsymbol{\xi}, [\boldsymbol{\eta}])$ which includes both the random variables $\boldsymbol{\xi}$ and interval variables $[\boldsymbol{\eta}]$. Here the n-dimensional random variables are assumed to be in the form of standard Gaussian distribution $\boldsymbol{\xi}\in N(0,\ 1)^n$ and the m-dimensional interval variables are defined as $[\boldsymbol{\eta}]=[-1,\ 1]^m$.

To evaluate the interval mean and interval variance of $F(\boldsymbol{\xi}, [\boldsymbol{\eta}])$, which will be expanded by using the truncated Hermit series (PC expansion) with respect to the random variables $\boldsymbol{\xi}$ as

$$F(\boldsymbol{\xi},[\boldsymbol{\eta}])=\sum_{j=0}^{s-1}\beta_j([\boldsymbol{\eta}])\phi_j(\boldsymbol{\xi}) \tag{6-5}$$

where the $\beta_j([\boldsymbol{\eta}])$ denotes the coefficients of Hermit polynomials, and ϕ_j denotes the Hermit polynomials which are the basis of the expansion. The Hermit polynomials correspond to the Gaussian distribution of the random variables. If the random variables satisfy another type of distribution, the corresponding orthogonal polynomials will be used as the basis [127]. The coefficients $\beta_j([\boldsymbol{\eta}])$ have a relationship with interval variables $[\boldsymbol{\eta}]$, so they can be expanded by the Chebyshev polynomials [111].

Expanding the coefficients $\beta_j([\boldsymbol{\eta}])$ with respect to $[\boldsymbol{\eta}]$ using the *k*-terms truncated Chebyshev series, we can obtain its Chebyshev inclusion function as follows:

$$[\beta_j]([\boldsymbol{\eta}])=\sum_{i=0}^{k-1}\beta_{i,j}\psi_i([\boldsymbol{\eta}]) \tag{6-6}$$

Here $\beta_{i,j}$ denotes the elements in the coefficient matrix $\boldsymbol{\beta}$ with *k* rows and *s* columns, ψ_i denotes the Chebyshev polynomials. The coefficient matrix $\boldsymbol{\beta}$ can be obtained by using the least square method twice, i.e. Eq. (4-35).

The Chebyshev series may be transformed to the power series, so the Eq. (6-6) can be expressed by the following power series

$$[\beta_j]([\boldsymbol{\eta}])=\sum_{i=0}^{k-1}\beta_{i,j}\psi_i([\boldsymbol{\eta}])=\sum_{i=0}^{k-1}\alpha_{i,j}P_i([\boldsymbol{\eta}]) \tag{6-7}$$

where $\alpha_{i,j}$ are the elements of coefficient matrix $\boldsymbol{\alpha}$ of the power function P_i, and the *m*-dimensional power function $P_i(\boldsymbol{\eta})$ are defined as follows:

$$
\begin{aligned}
&P_0(\boldsymbol{\eta}) = \prod_{i=1}^{m} \eta_i^0 = 1, \\
&P_1(\boldsymbol{\eta}) = \eta_1 \prod_{i=2}^{m} \eta_i^0 = \eta_1, \ \cdots, P_m(\boldsymbol{\eta}) = \eta_m \prod_{i=1}^{m-1} \eta_i^0 = \eta_m, \\
&P_{m+1}(\boldsymbol{\eta}) = \eta_1^2 \prod_{i=2}^{m} \eta_i^0 = \eta_1^2, P_{m+2}(\boldsymbol{\eta}) = \prod_{i=1}^{2} \eta_i \prod_{i=3}^{m} \eta_i^0 = \eta_1\eta_2, \ \cdots, P_{\frac{(m+2)!}{2!m!}-1}(\boldsymbol{\eta}) = \eta_m^2 \prod_{i=1}^{m-1} \eta_i^0 = \eta_m^2, \\
&\cdots
\end{aligned}
\tag{6-8}
$$

The coefficient matrix $\boldsymbol{\alpha}$ can be calculated by using a linear transformation from the coefficient matrix $\boldsymbol{\beta}$, or evaluated by the least square method by

$$
\boldsymbol{\alpha} = \left(\mathbf{X}_3(\boldsymbol{\eta})^{\mathrm{T}} \mathbf{X}_3(\boldsymbol{\eta})\right)^{-1} \mathbf{X}_3(\boldsymbol{\eta})^{\mathrm{T}} \mathbf{F}^{\mathrm{T}} \mathbf{X}_2(\boldsymbol{\xi}) \left(\mathbf{X}_2(\boldsymbol{\xi}) \mathbf{X}_2(\boldsymbol{\xi})^{\mathrm{T}}\right)^{-1} \tag{6-9}
$$

where the $\mathbf{F}$ and $\mathbf{X}_2$ are as the same shown in Eq. (4-33) and (4-36), and the transform matrix $\mathbf{X}_3$ is expressed by

$$
\mathbf{X}_3(\boldsymbol{\eta}) = \left[\mathbf{P}(\boldsymbol{\eta}^{(1)}) \quad \cdots \quad \mathbf{P}(\boldsymbol{\eta}^{(M)})\right]^{\mathrm{T}} \tag{6-10}
$$

Here $\mathbf{P} = [P_0, \ \cdots, P_{k-1}]^{\mathrm{T}}$ denotes the vector of the power function.

Using $\boldsymbol{\Phi} = [\phi_0, \ \cdots, \phi_{s-1}]^{\mathrm{T}}$ and $\boldsymbol{\Psi} = [\psi_0, \ \cdots, \psi_{k-1}]^{\mathrm{T}}$ to denote the vectors of Hermit polynomials and Chebyshev polynomials, respectively, the two transform matrix will be expressed by

$$
\mathbf{X}_1(\boldsymbol{\eta}) = \left[\boldsymbol{\Psi}(\boldsymbol{\eta}^{(1)}) \quad \cdots \quad \boldsymbol{\Psi}(\boldsymbol{\eta}^{(M)})\right]^{\mathrm{T}}, \ \mathbf{X}_2(\boldsymbol{\xi}) = \left[\boldsymbol{\Phi}(\boldsymbol{\xi}^{(1)}) \quad \cdots \quad \boldsymbol{\Phi}(\boldsymbol{\xi}^{(N)})\right]^{\mathrm{T}} \tag{6-11}
$$

where the $\boldsymbol{\xi}^{(i)} (i = 1,...,N)$ denotes the collocation points of the random variables which are the zeros of Hermit polynomials, and $\boldsymbol{\eta}^{(i)}$ $(i = 1,...,M)$ are the collocation points of interval variables which are the zeros of Chebyshev polynomials. To enhance the numerical stability, the number of collocation points and interpolation points are usually selected by the following criteria: $N \geq 2s$ and $M \geq 2k$.

Once the coefficients are obtained, the interval mean $[\mu_F]$ and interval variance $[\sigma_F^2]$ of the evaluation functions can be calculated based on the PC expansion theory [11, 127] and interval arithmetic, as follows

$$[\mu_F] = [\beta_0]([\boldsymbol{\eta}]) = \sum_{i=0}^{k-1} \alpha_{i,0} P_i([\boldsymbol{\eta}]) \tag{6-12}$$

$$[\sigma_F^2] = \sum_{j=1}^{s-1} [\beta_j]^2 \left\langle \phi_j^2 \right\rangle = \sum_{j=1}^{s-1} \left(\sum_{i=0}^{k-1} \alpha_{i,j} P_i([\boldsymbol{\eta}]) \right)^2 \left\langle \phi_j^2 \right\rangle \tag{6-13}$$

where $\left\langle \phi_j^2 \right\rangle$ represents the inner product of ϕ_j^2.

Using Eq. (6-12) and (6-13) to calculate the interval mean and interval variance of function *f* and **g** given in Eq. (6-4), the uncertainty optimization can be implemented. It can be found that the proposed method analyses the random uncertainty and interval uncertainty in one integrated framework, and can be implemented easily. After obtain the function value matrix **F** at the collocation points and interpolation points (Eq. (4-36)), the coefficients can be produced by the least square method, and then the interval mean and variance can be calculated according to the above two equations.

6.2.2 Quantification of hybrid uncertainty

We can obtain the interval mean and interval variance of evaluation functions based on the derivation in the previous section, but these two evaluation indexes may not provide the comprehensive information of the hybrid uncertainty. Besides the interval mean and interval variance, the hybrid uncertainty can be more comprehensively assessed by the p-box, the measures of belief and plausibility in the evidence theory [194, 195]. Here the probability density function (PDF) and cumulative distribution function (CDF) of the lower and upper bounds of evaluation functions will be applied to express the comprehensive information. The CDF of lower bound may be equivalent to the measure

of belief, while the CDF of the upper bound may be equivalent to the measure of plausibility.

Substituting Eq. (6-6) into Eq. (6-5), the evaluation function can be expressed by

$$F\left(\boldsymbol{\xi},[\boldsymbol{\eta}]\right)=\sum_{j=0}^{s-1}\left(\sum_{i=0}^{k-1}\beta_{i,j}\psi_i\left([\boldsymbol{\eta}]\right)\right)\phi_j\left(\boldsymbol{\xi}\right)=\sum_{i=0}^{k-1}\left(\sum_{j=0}^{s-1}\beta_{i,j}\phi_j\left(\boldsymbol{\xi}\right)\right)\psi_i\left([\boldsymbol{\eta}]\right) \tag{6-14}$$

Therefore, the two bounds of the evaluation functions will be defined as

$$\underline{F}\left(\boldsymbol{\xi},[\boldsymbol{\eta}]\right)=\min_{\boldsymbol{\eta}}\sum_{i=0}^{k-1}\left(\sum_{j=0}^{s-1}\beta_{i,j}\phi_j\left(\boldsymbol{\xi}\right)\right)\psi_i\left(\boldsymbol{\eta}\right),\ \overline{F}\left(\boldsymbol{\xi},[\boldsymbol{\eta}]\right)=\max_{\boldsymbol{\eta}}\sum_{i=0}^{k-1}\left(\sum_{j=0}^{s-1}\beta_{i,j}\phi_j\left(\boldsymbol{\xi}\right)\right)\psi_i\left(\boldsymbol{\eta}\right) \tag{6-15}$$

The optimization algorithms or scanning method can be used to calculate the two bounds with respect to interval variables. On the other hand, the bounds of evaluation functions contain the random variables $\boldsymbol{\xi}$, so we can obtain the PDF and CDF of the bounds through the Monte Carlo simulation. It should be noted that both the optimization process and Monte Carlo simulation are not computationally expensive in this case, because the analytical expression (Eq. (6-15)) has been obtained.

To validate the proposed method, we consider the following test example. For simplicity, the $F(\xi,[\eta])$ is a scalar function containing 1-dimenisonal random variable $\xi \in N(0,\ 1)$ and 1-dimensional interval variable $[\eta]=[-1,\ 1]$, which can be defined as

$$F(\xi,[\eta])=\xi^2\sin\left(\frac{[\eta]}{2}\right) \tag{6-16}$$

The PCCI method is used to expand Eq. (6-32), in which the number of collocation points and interpolation points are set as N=M=3. Hence, the total number of computing points for the original function is $N\times M$=9. After obtaining the coefficients, the Monte Carlo simulation and optimization algorithm can be used to obtain the sampling data of the

bounds (Eq. (6-15)). Based on a large amount of sampling data, we can plot the PDF and CDF of the two bounds for the function *F*, shown in Fig.6-1.

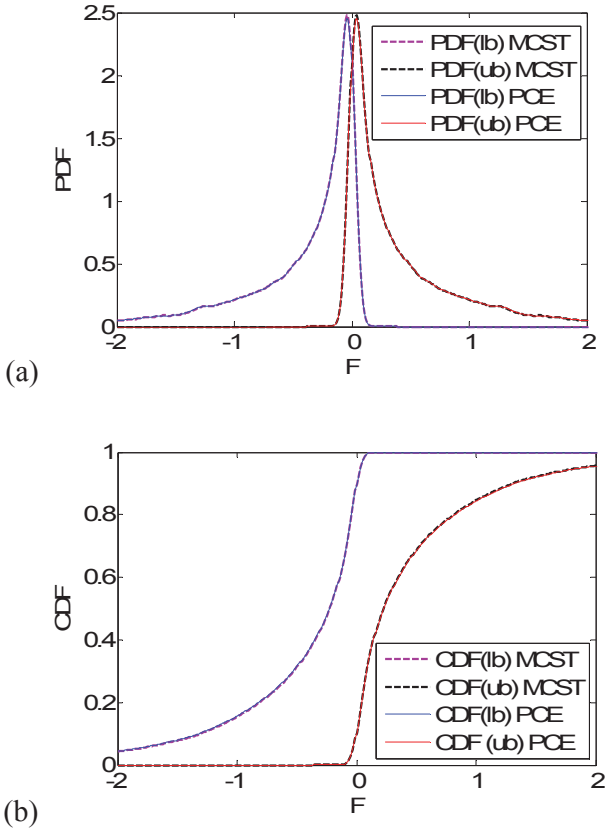

Figure 6-1 (a) The PDF of two bounds; (b) The CDF of two bounds

The reference result of the PDF and CDF of the two bounds can be obtained by the combination of Monte Carlo simulation and the scanning test for the original function, termed as Monte-Carlo-Scanning-Test (MCST). The MCST uses the Monte Carlo simulation collect the sampling points in the space of random variables and employs the scanning test that is a symmetrical dense grid to sample the space of interval variables. The scanning test will find the bounds of the evaluation function, and the Monte Carlo simulation will find the corresponding PDF and CDF. The results of MCST are also given in Fig. 6-1, which shows that the PDF and CDF of two bounds obtained by the PCCI method is very close to that of MCST. In practical applications, the cost of evaluating the

original function is very expensive usually, so we use the number of evaluating the original function as the index of efficiency. For this numerical testing example, the 10000 samples are used in the Monte Carlo simulation and 10 symmetrical samples are used in the scanning test, so the total number of computing the original function is 10000×10, which is much larger than the 9 samples for the PCCI method. Hence, the PCCI method has higher efficiency than the MCST.

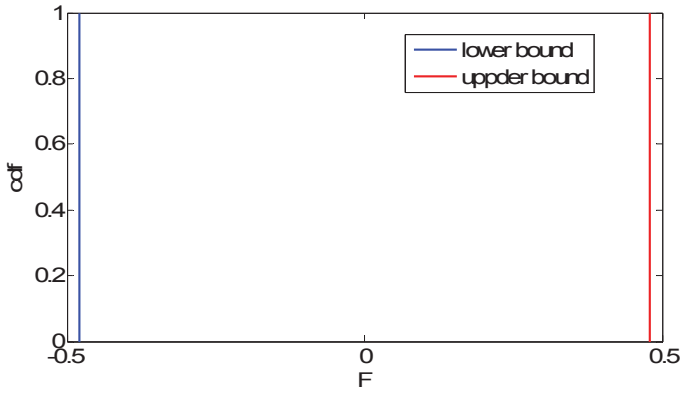

Figure 6-2 The CDF of two bounds for pure interval function

If the random variable is considered as constant, e.g. ξ=1, then CDF of the two bounds will be degenerated into two vertical lines (pure interval), as shown in Fig. 6-2. In this case, the PDF will be infinite, so we do not plot it. On the other hand, if there is no interval variable in the function, the CDF of the two bounds will be one traditional CDF.

Some researchers just consider the uncertain-but-bounded variables as uniformly distributed random variables, which may produce some large deviations. For example, if the uncertain variable η in Eq. (6-16) is assumed to satisfy the uniform distribution, i.e. $\eta \sim U(-1,1)$, we can draw its PDF and CDF of $F(\xi, \eta)$ by using the Monte Carlo method, shown in Fig. 6-3. However, if the actual probability distribution is $\eta \sim$ Beta(2,4) or $\eta \sim$ Beta(4,2), the corresponding PDF and CDF of function $F(\xi, \eta)$ will be quite different,

shown as Fig. 6-3. Since we do not know the actual distribution of η, the unfit assumption will make large error. In this case, if we just use the bounds information, the envelope of the possible actual CDF can be obtained, i.e. the various CDF under different probability distribution are contained in the CDF belt constructed by the bounds of hybrid uncertainty (Fig. 6-3).

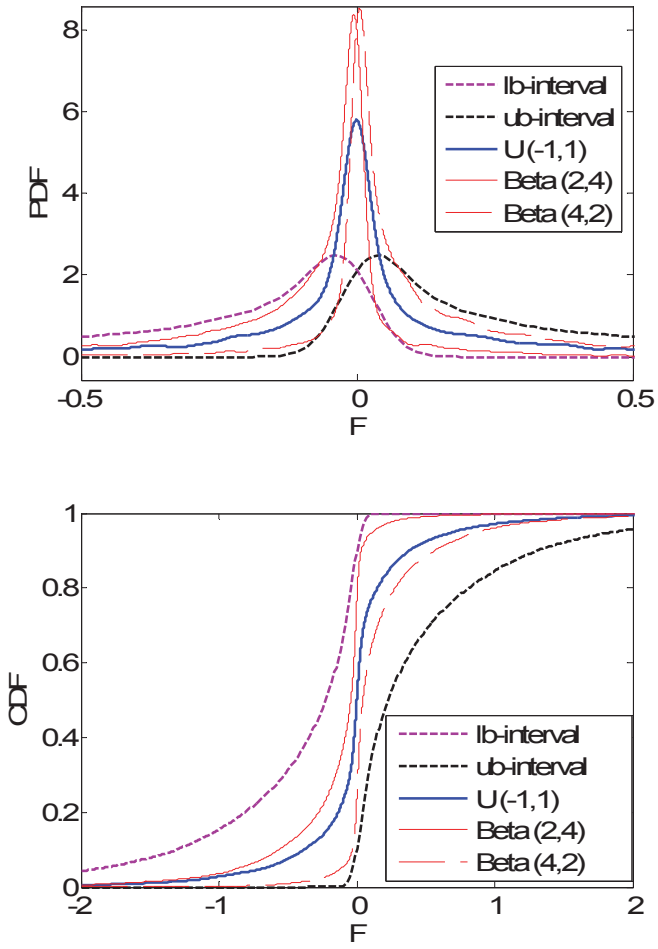

Figure 6-3 The PDF and CDF of $F(\xi, \eta)$ for different types of random variable

6.3 The sensitivity of hybrid uncertain optimization model

When the mathematic programming methods are used as the optimization algorithm, the derivatives of objective and constraints with respect to the design variables are required.

Although the finite difference method can be used to approximate the derivatives, the computational cost will be expensive and the numerical accuracy will be low for large-scale optimization problems. In this section, we will derive the first-order derivatives of the interval mean and interval standard deviation.

Based on Eq. (6-4), it can be found that the derivatives of the evaluation functions (both the objective function and the constraint functions) with respect to **x** is equal to the derivatives with respect to **η**, Considering the 1-dimensional case, the coefficients of Hermit polynomials in Eq. (6-7) can be regarded as a standard power series with respect to $[\eta]$

$$[\beta_j]([\eta]) = \sum_{i=0}^{k-1} \alpha_{i,j} P_i([\eta]) = \alpha_{0,j} + \sum_{i=1}^{k-1} \alpha_{i,j} [\eta]^i \tag{6-17}$$

If there is a small increment $\Delta\eta$, the coefficient can also be expressed as another standard power series

$$[\beta_j]([\eta]+\Delta\eta) = \alpha_{0,j} + \sum_{i=1}^{k-1} \alpha_{i,j} ([\eta]+\Delta\eta)^i = b_{0,j} + \sum_{i=1}^{k-1} b_{i,j} [\eta]^i \tag{6-18}$$

where the coefficients b_i will be determined by

$$b_{i,j} = a_{i,j} + (i+1) a_{i+1,j} \Delta\eta + \mathrm{O}(\Delta\eta^2) \tag{6-19}$$

Using the interval arithmetic, the upper and lower bound of the coefficients can be calculated by

$$\overline{\beta}_j = \alpha_{0,j} + \sum_{i=2p-1} \alpha_{i,j} \mathrm{sign}(\alpha_{i,j}) + \sum_{i=2p} \alpha_{i,j} \mathrm{sign1}(\alpha_{i,j}) \tag{6-20}$$

$$\underline{\beta}_j = \alpha_{0,j} + \sum_{i=2p-1} \alpha_{i,j} \mathrm{sign}(-\alpha_{i,j}) + \sum_{i=2p} \alpha_{i,j} \mathrm{sign1}(-\alpha_{i,j}) \tag{6-21}$$

where p denotes the positive integer, and the function sign and sign1 are defined as

$$\mathrm{sign}(x)=\begin{cases}1, & x>0\\ -1, & x\le 0\end{cases},\quad \mathrm{sign1}(x)=\begin{cases}1, & x>0\\ 0, & x\le 0\end{cases} \tag{6-22}$$

Combining the Eq. (6-17) to Eq. (6-21), the derivative of the two bounds of the coefficients can be expressed by

$$\begin{aligned}\frac{\partial \overline{\beta}_j}{\partial \eta} &= \lim_{\Delta\eta\to 0}\frac{\overline{\beta}_j([\eta]+\Delta\eta)-\overline{\beta}_j([\eta])}{\Delta\eta}\\ &= \alpha_{1,j}+\sum_{i=2p-1}(i+1)\alpha_{i+1,j}\mathrm{sign}\left(\alpha_{i,j}\right)+\sum_{i=2p}(i+1)\alpha_{i+1,j}\mathrm{sign1}\left(\alpha_{i,j}\right)\end{aligned} \tag{6-23}$$

$$\begin{aligned}\frac{\partial \underline{\beta}_j}{\partial \eta} &= \lim_{\Delta\eta\to 0}\frac{\underline{\beta}_j([\eta]+\Delta\eta)-\underline{\beta}_j([\eta])}{\Delta\eta}\\ &= \alpha_{1,j}+\sum_{i=2p-1}(i+1)\alpha_{i+1,j}\mathrm{sign}\left(-\alpha_{i,j}\right)+\sum_{i=2p}(i+1)\alpha_{i+1,j}\mathrm{sign1}\left(-\alpha_{i,j}\right)\end{aligned} \tag{6-24}$$

The Eq. (6-23) and (6-24) contain the sign function, which will make the derivatives discontinuous. The discontinuous derivatives may make the optimization process unstable, so the Heaviside projection method is used to smooth the sign function, shown as follows

$$\mathrm{sign}(x)\approx\tanh(\gamma x),\quad \mathrm{sign1}(x)\approx\frac{1}{2}+\frac{1}{2}\tanh(\gamma x) \tag{6-25}$$

where the coefficient γ is a positive real number. The function $\tanh(\gamma x)$ will be equal to $\mathrm{sign}(x)$ when the parameter γ tends to be infinite. Therefore, the derivatives of the two bounds will be transformed to

$$\frac{\partial \overline{\beta}_j}{\partial \eta}=\alpha_{1,j}+\sum_{i=2p-1}(i+1)\alpha_{i+1,j}\tanh\left(\gamma\alpha_{i,j}\right)+\sum_{i=2p}\frac{i+1}{2}\alpha_{i+1,j}\left(1+\tanh\left(\gamma\alpha_{i,j}\right)\right) \tag{6-26}$$

$$\frac{\partial \underline{\beta}_j}{\partial \eta}=\alpha_{1,j}+\sum_{i=2p-1}(i+1)\alpha_{i+1,j}\tanh\left(-\gamma\alpha_{i,j}\right)+\sum_{i=2p}\frac{i+1}{2}\alpha_{i+1,j}\left(1+\tanh\left(-\gamma\alpha_{i,j}\right)\right) \tag{6-27}$$

Combining Eq. (6-14) and (6-26), the derivative of the upper bound of the interval mean will be

$$\frac{\partial \bar{\mu}_F}{\partial \eta} = \frac{\partial \bar{\beta}_0}{\partial \eta} = \alpha_{1,0} + \sum_{i=2p-1} (i+1)\alpha_{i+1,0}\tanh\left(\gamma\alpha_{i,0}\right) + \sum_{i=2p} \frac{i+1}{2}\alpha_{i+1,0}\left(1+\tanh\left(\gamma\alpha_{i,0}\right)\right) \quad (6\text{-}28)$$

Using the interval arithmetic in Eq. (6-15), the upper bound of the interval variance can be calculated by

$$\bar{\sigma}_F^2 = \sum_{j=1}^{s-1} \max\left(\underline{\beta}_j^2, \bar{\beta}_j^2\right)\left\langle \phi_j^2 \right\rangle \quad (6\text{-}29)$$

Therefore, the derivative of the upper bound of the standard deviation is given as

$$\frac{\partial \bar{\sigma}_F}{\partial \eta} = \frac{1}{2\bar{\sigma}_F^2}\sum_{j=1}^{s-1} \frac{\partial\left(\max\left(\underline{\beta}_j^2, \bar{\beta}_j^2\right)\right)}{\partial \eta}\left\langle \phi_j^2 \right\rangle, \frac{\partial\left(\max\left(\underline{\beta}_j^2, \bar{\beta}_j^2\right)\right)}{\partial \eta} = \begin{cases} 2\bar{\beta}_j \dfrac{\partial \bar{\beta}_j}{\partial \eta}, & \left|\bar{\beta}_j\right| \geq \left|\underline{\beta}_j\right| \\ 2\underline{\beta}_j \dfrac{\partial \underline{\beta}_j}{\partial \eta}, & \left|\bar{\beta}_j\right| < \left|\underline{\beta}_j\right| \end{cases} \quad (6\text{-}30)$$

Based on the sensitivity information given by Eq. (6-28) and (6-30), the hybrid uncertainty optimization defined in Eq. (6-4) can be implemented by conventional gradient-based optimization algorithms.

6.4 Numerical examples

6.4.1 Planar truss structure

Consider the same 18-bar planar truss structure in Section 5.4.1, shown as Fig. 5-8. The members are still classified into four groups when the cross-sectional areas are regarded as the design variables: x_1 (A_1, A_4, A_8, A_{12}, A_{16}), x_2 (A_2, A_6, A_{10}, A_{14}, A_{18}), x_3 (A_3, A_7, A_{11}, A_{15}), and x_4 (A_5, A_9, A_{13}, A_{17}). Considering the design variables as interval variables, the interval width is 0.1in^2. The nominal value of the material density ρ=0.1lb/in^3, and the vertical loads is P=20000lb acting on the upper nodes of the planar truss. However, the E and ρ are considered as random parameters here, satisfying the Gaussian distribution where the mean value is the nominal value and the standard deviation is 2% of the

nominal value, that is $E \sim N(10^7,\ (2\times10^5)^2)$ and $\rho \sim N(0.1,\ 0.002^2)$. For this problem, the deterministic optimization formulation can be defined as follows:

$$\begin{cases} \min\limits_{\mathbf{x}} & f = \sum\limits_{i=1}^{18} A_i(\mathbf{x}) L_i \rho \\ \text{s.t.} & g_1 = \max\limits_{i=1,\ldots,18} (\sigma_i(\mathbf{x}) / b^{\sigma_i}(\mathbf{x}, E)) \le 1,\ g_2 = \max\limits_{i=1,\ldots,18} |\sigma_i(\mathbf{x})| \le 20000 \\ & [0.1 \quad \ldots \quad 0.1]^{\mathrm{T}}_{1\times4} \le \mathbf{x} \le [50 \quad \ldots \quad 50]^{\mathrm{T}}_{1\times4} \end{cases} \tag{6-31}$$

where f is the total mass of the truss, σ_i denotes the stress of the ith member, g_1 and g_2 are the stress constraints and Euler buckling compressive stress limitation, respectively. Three cases of the optimization will be considered:

(1) the deterministic optimization without considering uncertain parameters and variables (defined as problem (6-31));

(2) the uncertain optimization with considering the random parameters (E and ρ)

$$\begin{cases} \min\limits_{\mathbf{x}} & f(\mathbf{x}, \boldsymbol{\xi}) \\ \text{s.t.} & g_1(\mathbf{x}, \boldsymbol{\xi}) \le 1,\ g_2(\mathbf{x}) \le 20000 \\ & [0.1 \quad \ldots \quad 0.1]^{\mathrm{T}}_{1\times4} \le \mathbf{x} \le [50 \quad \ldots \quad 50]^{\mathrm{T}}_{1\times4} \end{cases} \tag{6-32}$$

where $\boldsymbol{\xi}$ denotes the random parameters E and ρ.

(3) the uncertain optimization with considering the hybrid uncertainties for both the interval variables and random parameters

$$\begin{cases} \min\limits_{\mathbf{x}} & f(\mathbf{x} + [\boldsymbol{\eta}], \boldsymbol{\xi}) \\ \text{s.t.} & g_1(\mathbf{x} + [\boldsymbol{\eta}], \boldsymbol{\xi}) \le 1,\ g_2(\mathbf{x} + [\boldsymbol{\eta}]) \le 20000 \\ & [0.1 \quad \ldots \quad 0.1]^{\mathrm{T}}_{1\times4} \le \mathbf{x} \le [50 \quad \ldots \quad 50]^{\mathrm{T}}_{1\times4} \end{cases} \tag{6-33}$$

where the interval variables $[\boldsymbol{\eta}] = [-0.05, 0.05]^4$.

Use the active-set algorithm in MATLAB to implement the optimization, and the initial values of design variables are set as $\mathbf{x}_0$=[10 10 10 10]$^{\mathrm{T}}$. The 2nd order orthogonal

polynomials (Hermite and Chebyshev polynomials) are used to expand the objective function and constraint function of the hybrid uncertain optimization model. Therefore, the collocation points will be chosen from the zeros of the 3rd order Hermite polynomial and Chebyshev polynomials. Since there are 2 random variables and 4 interval variables, the number of coefficients for Hermite polynomials expansion and Chebyshev polynomials expansion will be 6 and 15, respectively. To make the numerical stability, we will use all the 9 zeros of the 3rd order Hermite polynomial (2 dimension) as the collocation points of random variables, and randomly choose 30 zeros of the 3rd order Chebyshev polynomial (4 dimension) as the collocation points of interval variables. The optimization results are shown in Table 6-1.

Table 6-1 Optimization results of planar truss structure

	$x_1(\text{in}^2)$	$x_2(\text{in}^2)$	$x_3(\text{in}^2)$	$x_4(\text{in}^2)$
Deterministic	10.00	21.65	12.50	7.07
Random	10.00	22.30	12.87	7.07
Hybrid	10.10	22.44	12.97	7.18

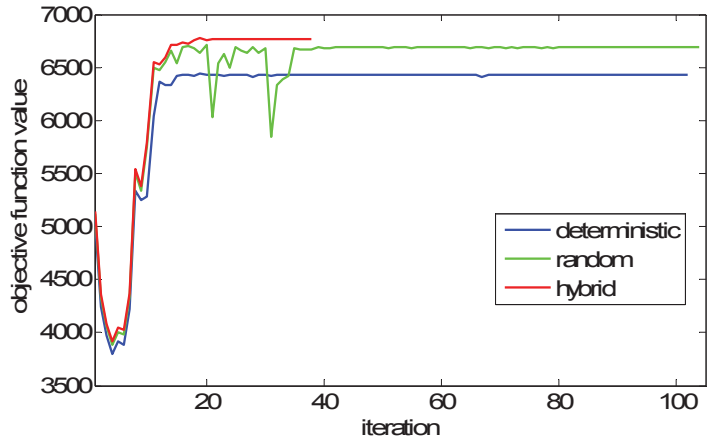

Figure 6-4 The iteration history of the objective function

The iteration history of the objective function of the three optimization models is shown as Fig. 6-4. It can be found that the hybrid uncertain optimization process (Chebyshev polynomials) converges after 20 iterations, so this hybrid uncertain optimization model is stable. To compare the optimization results comprehensively, the PDF and CDF of the two bounds of the objective function and constraints are shown in Fig. 6-5 to Fig. 6-9.

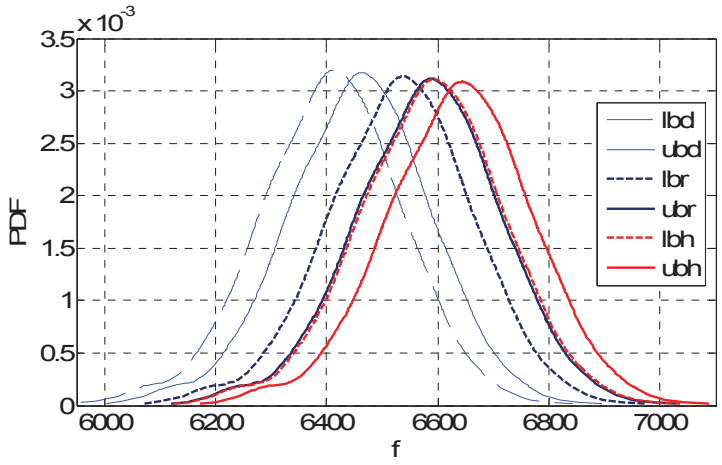

Figure 6-5 PDF of f

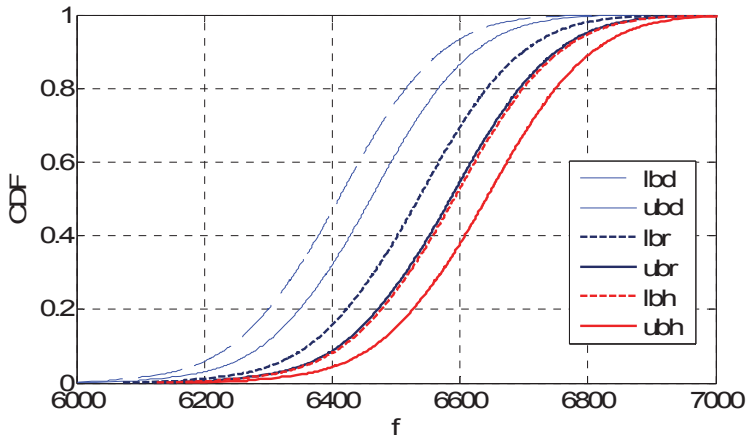

Figure 6-6 CDF of f

The legend ‘lbh’ and ‘ubh’ denote the lower bound and upper bound of the hybrid optimization using Chebyshev polynomials, respectively; the ‘lbr’ and ‘ubr’ show the lower bound and upper bound of the random uncertainty-based optimization; the ‘lbd’ and

'ubd' are the lower bound and upper bound of the deterministic optimization. The constraint g_2 is only related to the interval variables, so only its CDF is plot.

It can be found that the objective functions of the random uncertainty optimization and the hybrid uncertainty optimization are more conservative than that of the deterministic optimization. However, for the upper bound of constraint g_1, there are more than 60% probabilities to be violated for the deterministic optimization, while the failure probability for both the random uncertainty optimization and the hybrid uncertainty optimization is very small (close to zero).

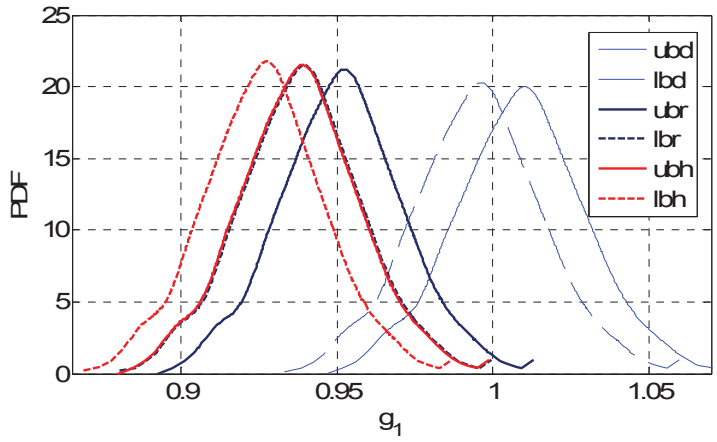

Figure 6-7 PDF of constraint g1

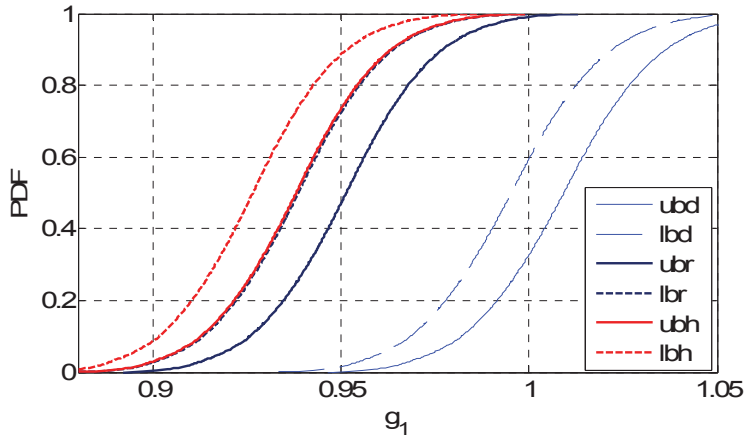

Figure 6-8 CDF of constraint g1

For the bounds of constraint g_2, the deterministic optimization and random uncertainty optimization give the same results, because both of them do not consider the interval uncertainty. Therefore, the upper bounds of the deterministic optimization and random uncertainty optimization are larger than the given condition (20000lb/in^2), which means that the two optimization results have possibility to be located in the unfeasible region. The hybrid uncertainty optimization makes the upper bound of g_2 smaller than 20000lb/in^2, which makes the optimal solution located inside the feasible region.

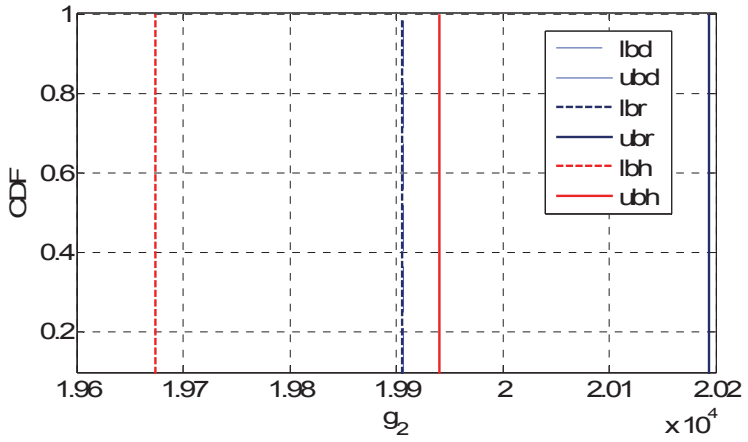

Figure 6-9 CDF of constraint g2

6.4.2 Space truss structure

Consider the 25-bar space truss structure for transmission towers as the numerical example, shown as Fig. 6-4. The cross-sectional areas of truss members are regarded as interval design variables, and the interval width is 0.1in^2. The nominal value of the material density and the elasticity modulus is ρ=0.1lb/in^3 and E=10^7 lb/in^2, respectively, which satisfy the Gaussian distribution $E \sim N(10^7,\ (2\times10^5)^2)$ and $\rho \sim N(0.1,\ 0.002^2)$. The optimization problem is to minimize the total weight of the space truss.

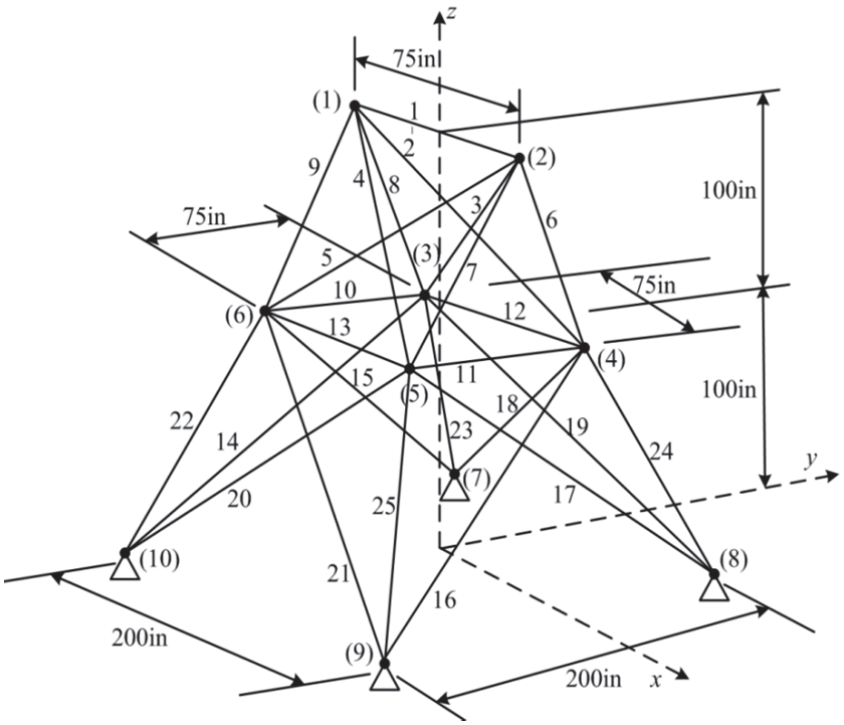

Figure 6-10 25-bar space truss structure

This space truss is subjected to two loading conditions, which are shown in Table 6-2. The structure is required to be symmetric, so the truss members can be grouped in Table 6-3, which also shows the stress limitations of each group. At the same time, the maximum displacements of nodes in each direction are limited to ±0.35in. The cross-sectional areas of all members vary in the range 0.1-10 in^2.

Table 6-2 Loading conditions

Node	Condition 1			Condition 2		
	P_x (lb)	P_y (lb)	P_z (lb)	P_x (lb)	P_y (lb)	P_z (lb)
1	0	20000	5000	1000	10000	-5000
2	0	-20000	-5000	0	10000	-5000
3	0	0	0	500	0	0
6	0	0	0	500	0	0

Table 6-3 Member stress limitations

Variables	x_1	x_2	x_3	x_4	x_5	x_6	x_7
	A_1	$A_2 \sim A_5$	$A_6 \sim A_9$	$A_{10} \sim A_{13}$	$A_{14} \sim A_{17}$	$A_{18} \sim A_{21}$	$A_{22} \sim A_{25}$
Compressive stress limitations (lb/in^2)	-35000	-11000	-17000	-35000	-6000	-6000	-11000
Tensile stress limitations (lb/in^2)	40000	40000	40000	40000	40000	40000	40000

The deterministic optimization formulation can be given as

$$\begin{cases} \min\limits_{\mathbf{x}} & f=\sum\limits_{i=1}^{25} A_i(\mathbf{x})L_i\rho \\ \text{s.t.} & g_1=\max\limits_{i=1,\ldots,25}\sigma_i(\mathbf{x})\le 40000; g_2=\min\limits_{i=1,10,\ldots,13}\sigma_i(\mathbf{x})\ge -35000; g_3=\min\limits_{i=2,\ldots,5}\sigma_i(\mathbf{x})\ge -11000; \\ & g_4=\min\limits_{i=6,\ldots,9}\sigma_i(\mathbf{x})\ge -17000; g_5=\min\limits_{i=14,\ldots,17}\sigma_i(\mathbf{x})\ge -6000; g_6=\min\limits_{i=18,\ldots,21}\sigma_i(\mathbf{x})\ge -6000; \\ & g_7=\min\limits_{i=22,\ldots,25}\sigma_i(\mathbf{x})\ge -11000; g_8=\max\limits_{i=1,\ldots,30}\left|d_i(\mathbf{x},E)\right|\le 0.35; \\ & \left[0.01 \quad \ldots \quad 0.01\right]_{1\times 7}^{\mathrm{T}}\le \mathbf{x}\le \left[10 \quad \ldots \quad 10\right]_{1\times 7}^{\mathrm{T}} \end{cases} \tag{6-34}$$

where L_i is the length of the ith bar, σ_i is the stress of the ith member, and d_i represents the displacement of each node in each direction. The random optimization model and hybrid optimization model are given as follows

$$\begin{cases} \min\limits_{\mathbf{x}} & f\left(\mathbf{x},\boldsymbol{\xi}\right) \\ \text{s.t.} & g_1\left(\mathbf{x}\right)\le 40000;\ g_2\left(\mathbf{x}\right)\ge -35000; g_3\left(\mathbf{x}\right)\ge -11000;\ g_4\left(\mathbf{x}\right)\ge -17000; \\ & g_5\left(\mathbf{x}\right)\ge -6000;\ g_6\left(\mathbf{x}\right)\ge -6000; g_7\left(\mathbf{x}\right)\ge -11000;\ g_8\left(\mathbf{x},\boldsymbol{\xi}\right)\le 0.35; \\ & \left[0.01 \quad \ldots \quad 0.01\right]_{1\times 7}^{\mathrm{T}}\le \mathbf{x}\le \left[10 \quad \ldots \quad 10\right]_{1\times 7}^{\mathrm{T}} \end{cases} \tag{6-35}$$

$$\begin{cases} \min\limits_{\mathbf{x}} & f\left(\mathbf{x}+[\boldsymbol{\eta}],\boldsymbol{\xi}\right) \\ \text{s.t.} & g_1\left(\mathbf{x}+[\boldsymbol{\eta}]\right)\le 40000;\ g_2\left(\mathbf{x}+[\boldsymbol{\eta}]\right)\ge -35000; g_3\left(\mathbf{x}+[\boldsymbol{\eta}]\right)\ge -11000; \\ & g_4\left(\mathbf{x}+[\boldsymbol{\eta}]\right)\ge -17000; g_5\left(\mathbf{x}+[\boldsymbol{\eta}]\right)\ge -6000;\ g_6\left(\mathbf{x}+[\boldsymbol{\eta}]\right)\ge -6000; \\ & g_7\left(\mathbf{x}+[\boldsymbol{\eta}]\right)\ge -11000;\ g_8\left(\mathbf{x}+[\boldsymbol{\eta}],\boldsymbol{\xi}\right)\le 0.35; \\ & \left[0.1 \quad ... \quad 0.1\right]_{1\times 7}^{\mathrm{T}} \le \mathbf{x} \le \left[10 \quad ... \quad 10\right]_{1\times 7}^{\mathrm{T}} \end{cases} \tag{6-36}$$

where $\boldsymbol{\xi}$ denotes the random parameters E and ρ , and the interval variables $[\boldsymbol{\eta}]=[-0.05,0.05]^7$.

The active-set optimization algorithm in MATLAB is used to solve the optimization problem, and the initial values of the design variables are set as $\mathbf{x}_0=[1 \ \dots \ 1]^{\mathrm{T}}{}_{1x7}$. The 2nd order orthogonal polynomials (Hermit and Chebyshev polynomials) are used in PCCI method to expand the objective function and constraint function of the hybrid uncertain optimization model. Therefore, the collocation points will be chosen from the zeros of the 3rd order Hermit polynomial and Chebyshev polynomials. Since there are 2 random variables and 7 interval variables, the number of coefficients for Hermit polynomials expansion and Chebyshev polynomials expansion will be 6 and 36, respectively. To make the numerical stability, we will use all the 9 zeros of the 3rd order Hermit polynomial (2 dimension) as the collocation points of random variables, and randomly choose 72 zeros of the 3rd order Chebyshev polynomial (7 dimension) as the collocation points of interval variables.

Table 6-4 Optimization results

	$x_1(\text{in}^2)$	$x_2(\text{in}^2)$	$x_3(\text{in}^2)$	$x_4(\text{in}^2)$	$x_5(\text{in}^2)$	$x_6(\text{in}^2)$	$x_7(\text{in}^2)$
Deterministic	0.10	1.77	2.95	0.10	0.69	1.95	2.61
Random	0.10	1.97	3.15	0.10	0.73	1.93	2.80
Hybrid	0.10	2.13	3.24	0.10	0.75	2.00	2.95

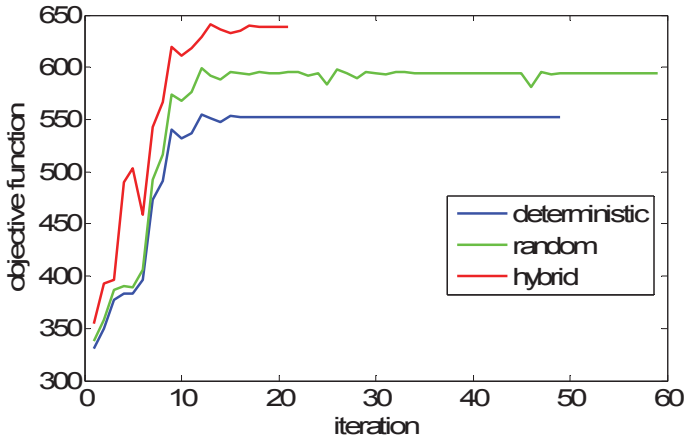

Figure 6-11 The iteration history of objective function

The optimization results are shown in Table 6-3, and the iteration history of the objective function is provided in Fig. 6-11.

The PDF and CDF of the bounds for the objective function and active constraints are shown in Fig.6-12 to Fig. 6-16, respectively. The weight of the truss by using the uncertainty design optimization is larger than that of the deterministic optimization, because the constraints of the uncertainty optimization are more rigorous.

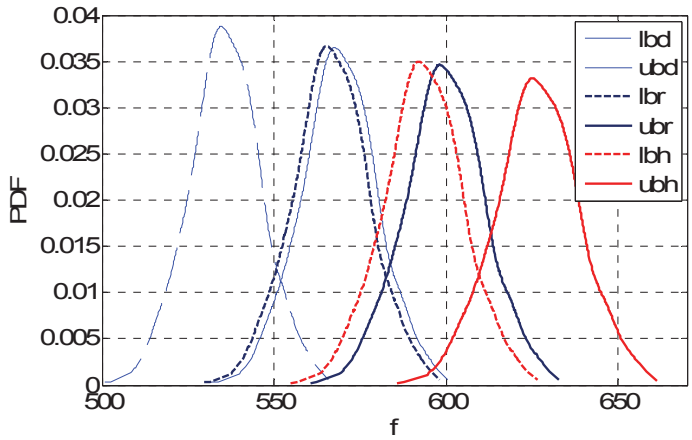

Figure 6-12 PDF of objective *f*

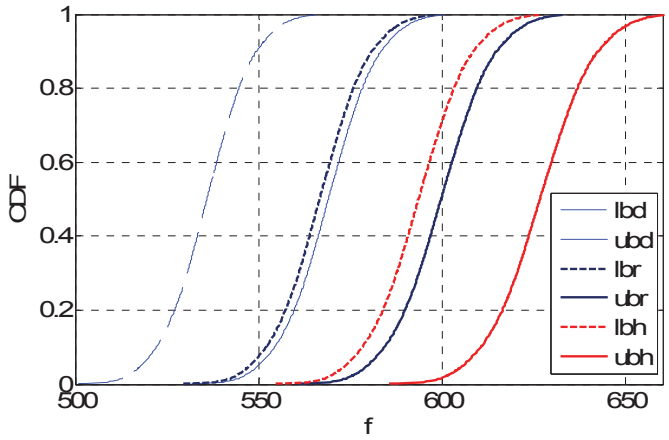

Figure 6-13 CDF of objective *f*

One of the active constraints g_6 is only related to the interval variables, so only the CDF is plotted, as shown in Fig.6-14. Since g_6 is only related to the interval variables, the random uncertainty optimization and the deterministic optimization almost lead to the same results (Here, the lbr and lbd are coincidence, and the ubr and ubd are coincidence), and the lower bound of g_6 is smaller than -6000lb/in^2, which indicates that the constraint is not satisfied. However, for the hybrid uncertainty design optimization, its lower bound is larger than -6000lb/in^2, so it satisfies the constraint even in the worst case of scenario.

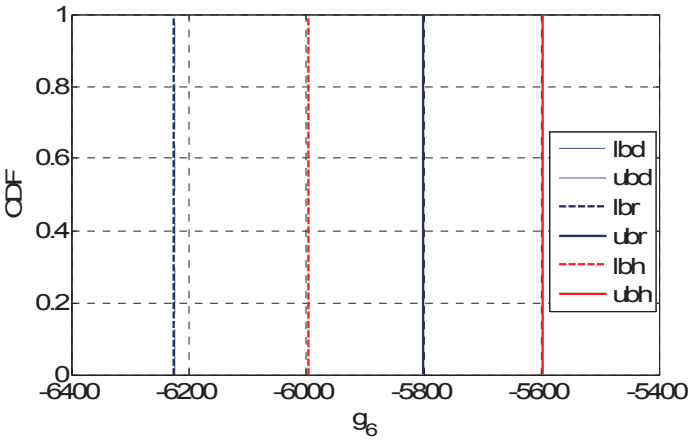

Figure 6-14 CDF of constraint g_6

The PDF and CDF of the other active constraint g_8 ($\leq$0.35) are given in Fig. 6-15 and Fig. 6-16. It can be seen that the failure probability of the deterministic optimization is around 90% for the worst case of scenario. The failure probability of the random uncertainty optimization is much smaller, but it is still has about 10% failure probability under the worst condition. However, the failure probability of the hybrid uncertainty optimization tends to zero under the worst-case scenario.

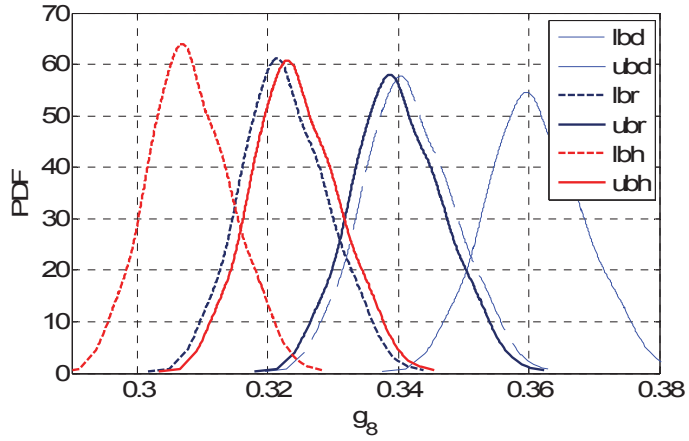

Figure 6-15 PDF of constraint g_8

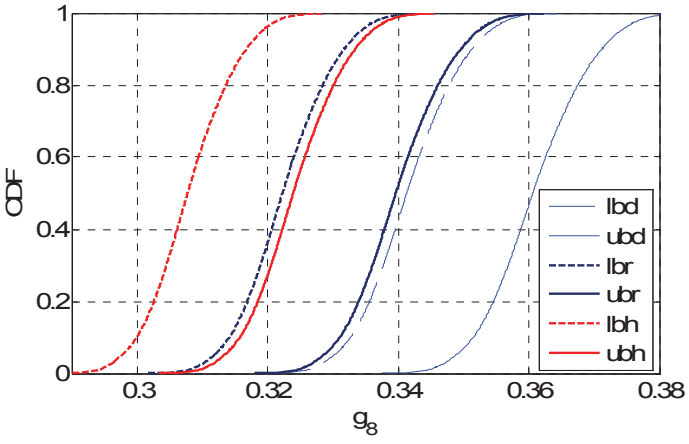

Figure 6-16 CDF of objective g_8

6.5 Summary

A new uncertain design optimization method is proposed in this chapter, in which both random uncertainty and interval uncertainty are considered. In the optimization model, the objective and constraints trade off the mean value and standard deviation produced by random parameters, under the worst case of scenario with interval variables. The numerical analysis of hybrid uncertainty is implemented by using the PCCI method proposed in Chapter 4. The design sensitivity of the bounds of the interval mean and interval standard deviation are explicitly developed, which greatly facilitate the direct application of many more efficient gradient-based optimization algorithms. The interval arithmetic is applied to estimate the interval mean and interval variance of the evaluation functions based on the characteristic of orthogonal polynomials. Besides the interval mean and variance, the probabilistic density function and cumulative distribution function of the lower bound and upper bound of the evaluation functions are also employed to characterize the hybrid uncertainty. Two truss structures are utilized to showcase the effectiveness of the proposed method for the design of structural problems under hybrid uncertainty. The numerical results indicate that the proposed optimization method has a larger possibility to produce feasible solution than the deterministic and pure random uncertainty optimization methods.

Chapter 7 Summary and prospect

7.1 Summary

This thesis is mainly focused on the uncertainty analysis and optimization, including the interval uncertainty analysis, hybrid uncertainty analysis, design of optimization under interval uncertainty and hybrid uncertainty. Since there are many uncertain factors in engineering, this topic is valuable for both theory research and practical application.

Chapter 2 provides a comprehensive review of the research of uncertainty, including the probabilistic uncertainty analysis, interval uncertainty analysis, and the design of optimization under uncertainty. The review indicates that there are some problems have not been solved yet, e.g. interval uncertainty analysis in dynamic problems, hybrid uncertainty analysis, the low efficiency and accuracy of optimization under uncertainty.

The interval uncertainty analysis for the dynamic problem is investigated in Chapter 3. A new Chebyshev inclusion function is proposed to control the overestimation induced by interval arithmetic. The Chebyshev inclusion function uses the Chebyshev series to expand the original function and then employs the interval arithmetic to compute the bounds of original function. Using Chebyshev inclusion function to solve the dynamic problems (governed by ODEs and DAEs) is researched, and it is applied in mechanical dynamics. The numerical examples for dynamic problems indicate that Chebyshev inclusion function has better performance than traditional Taylor inclusion function. On the other hand, since the Chebyshev inclusion function does not need the derivatives information of original function, so it is easier to implement than the Taylor inclusion function that has to utilize the derivatives of original function.

For solving the hybrid uncertainty problems that contain both random uncertainty and interval uncertainty simultaneously, a new PCCI method is proposed in Chapter 4. The PCCI incorporates the PC expansion method used in probabilistic uncertainty analysis with the Chebyshev interval method, since both the two types of methods are based on the orthogonal series expansion. Two types of evaluation index of hybrid uncertainty are also proposed, i.e. 1) the interval mean and interval variance; 2) bounds of mean and bounds of variance. A 4-DOF roll plan model of automotive is employed as the numerical example to validate the PCCI method, and the results indicate it has high accuracy and efficiency. The most important novelty of PCCI method is that two types of uncertainties are solved in one framework. At the same time, the PCCI method is a non-intrusive method, so it can be easily implemented for solving the complicated engineering model (even in black box model).

Chapter 5 investigates the design of optimization under interval uncertainty. An interval optimization model is proposed, which considers both robustness of objective and reliability of constraints. For general parameter optimization problems, the interval arithmetic is used to replace the inner optimization process of the traditional double-loop optimization method, which improves the efficiency significantly. A new Chebyshev polynomials-based surrogate model is proposed, which demonstrates that the accuracy of a polynomial surrogate model is only determined by the sampling points rather than the basis vector. The combination of Chebyshev surrogate model and Taylor inclusion function controls the overestimation effectively. The application in truss structural and vehicle suspension design shows the high accuracy and efficiency of the interval arithmetic based optimization algorithm. The robust topology optimization (RTO) under interval uncertainty is also presented. Chebyshev inclusion function is used in RTO, as

well as the sensitivity of interval objective function is derived, to use the gradient-based optimization algorithms.

The design of optimization under hybrid uncertainty is proposed in Chapter 6. In the hybrid uncertainty optimization model, the objective and constraints trade off the mean value and standard deviation produced by random parameters, under the worst case of scenario with interval variables. The hybrid uncertain evaluation indexes are computed by using the PCCI method. The sensitivity of the bounds of the interval mean and interval standard deviation are explicitly developed, which greatly facilitate the direct application of many more efficient gradient-based optimization algorithms. Besides the interval mean and variance, the probabilistic density function and cumulative distribution function of the lower bound and upper bound of the evaluation functions are also employed to characterize the hybrid uncertainty. The numerical results indicate that the proposed optimization method has larger possibility to produce feasible solution than the deterministic and random uncertainty optimization methods.

7.2 Perspective for future work

The future work can be deeply developed in theory research and widely extended in engineering application.

Firstly, the efficiency of uncertainty analysis and optimization for high-dimensional problems is still a quite challenging problem. The uncertainty analysis method proposed in this thesis is based on the orthogonal series, in which the selection of interpolation points is extremely important. The higher dimensional problems, the more interpolation points required, which means the more computational cost is spent. Therefore, how to choose fewer interpolation points to get higher accuracy will be an important issue for future work.

Secondly, the hybrid uncertainty of random field and interval parameters is another issue. The random uncertainty in this thesis only considers the discrete parameter. For many problems, the random uncertainty is a continuous parameter, such as the Young's modulus and Poisson's ratio in structure analysis and flexible multibody systems. Researching the hybrid of continuous random uncertainty and interval uncertainty should solve more difficult problems.

Thirdly, the uncertain analysis method proposed in the thesis is a kind of non-intrusive method, so the procedure can be thought as constructing a polynomials surrogate model (or model reduction). The polynomials surrogate model has many advantages than other complicated surrogate model, especially in efficiency, conceptual simplicity, and transparency. The accuracy of the polynomials surrogate model is a weakness should be improved. As the theory 5.1 proved in Chapter 5, the accuracy of polynomials surrogate model is only determined by the sampling points, so how to choose the sampling set to improve the accuracy of polynomials surrogate model should be a key issue. The surrogate model can be used in many different areas, besides the engineering, the information technology area can also use it, such as the machine learning, artificial intelligence, and so on. Therefore, the application of surrogate modeling will also be another research direction.

References

[1] J. C. Helton, *et al.*, "A sampling-based computational strategy for the representation of epistemic uncertainty in model predictions with evidence theory," *Computer Methods in Applied Mechanics and Engineering,* vol. 196, pp. 3980-3998, 2007.

[2] J. Y. Dantan, *et al.*, "Tolerance Analysis Approach based on the Classification of Uncertainty (Aleatory/Epistemic)," *Procedia CIRP,* vol. 10, pp. 287-293, 2013.

[3] Y. Ben-Haim and I. Elishakoff, *Convex Models of Uncertainty in Applied Mechanics*. Amsterdam: Elsevier Science, 1990.

[4] S. S. Isukapalli, "Uncertainty analysis of transport-transformation models," Doctor of Philosophy, The State University of New Jersey, New Brunswick, New Jersey, 1999.

[5] A. Papoulis, *Probabilisty, Random Variables, and Stochastic Processes.* New York: McGraw-Hill, 1991.

[6] P. H. Huber, *Robust statistical procedures*. Philadelphia: SIAM, 1996.

[7] G. S. Fishman, *Monte Carlo: Concepts, Algorithms, and Applications.* New York: Springer-Verlag, 1996.

[8] I. M. Sobol, *A Primer for the Monte Carlo Method*. Boca Raton CRC Press, 1994.

[9] F. A. C. Viana, *et al.*, "An algorithm for fast optimal Latin hypercube design of experiments," *International Journal for Numerical Methods in Engineering,* vol. 82, pp. 135-156, 2009.

[10] T. W. Simpson, *et al.*, "Sampling Strategies for Computer Experiments Design and Analysis," *International Journal of Reliability and Applications,* vol. 2, pp. 209-240, 2001.

[11] D. Xiu and G. E. Karniadakis, "Modeling uncertainty in steady state diffusion problems via generalized polynomial chaos," *Computer Methods in Applied Mechanics and Engineering,* vol. 191, pp. 4927-4948, 2002.

[12] M. Kleiber and T. D. Hien, "The stochastic finite element method," ed: Wiley, 1992.

[13] W. K. Liu, *et al.*, "Applications of probabilistic finite element methods in elastic/plastic dynamics," *Journal of Engineering for Industry, ASME,* vol. 109, pp. 2-8, 1987.

[14] R. G. Ghanem and P. D. Spanos, *Stochastic Finite Elements: A Spectral Approach*. New York: Springer-Verlag, 1991.

[15] F. Wang, *et al.*, "On projection methods, convergence and robust formulations in topology optimization," *Structural and Multidisciplinary Optimization,* vol. 43, pp. 767-784, 2010.

[16] B. S. Lazarov, *et al.*, "Topology optimization with geometric uncertainties by perturbation techniques," *International Journal for Numerical Methods in Engineering,* vol. 90, pp. 1321-1336, 2012.

[17] B. Bourdin, "Filters in topology optimization," *International Journal for Numerical Methods in Engineering,* vol. 50, pp. 2143 - 2158, 2001.

[18] D. Xiu and G. E. Karniadakis, "Modeling uncertainty in flow simulations via generalized polynomial chaos," *Journal of Computational Physics,* vol. 187, pp. 137-167, 2003.

[19] R. Field Jr, V. and M. Grigoriu, "On the accuracy of the polynomial chaos approximation," *Probablistic Engineering Mechanics,* vol. 19, pp. 65-80, 2004.

[20] X. Wan and G. E. Karniadakis, "An adaptive multi-element generalized polynomial chaos method for stochastic differential equations," *Journal of Computational Physics,* vol. 209, pp. 617-642, 2005.

[21] R. Ghanem*, et al.*, "Identification and prediction of stochastic dynamical systems in a polynomial chaos basis," *Computer Methods in Applied Mechanics and Engineering,* vol. 194, pp. 1641-1654, 2005.

[22] M. Williams, "Polynomial chaos functions and stochastic differential equations," *Annals of Nuclear Energy,* vol. 33, pp. 774-785, 2006.

[23] L. Li and C. Sandu, "On the impact of cargo weight, vehicle parameters, and terrain characteristics on the prediction of traction for off-road vehicles," *Journal of Terramechanics,* vol. 44, pp. 221-238, 2007.

[24] S. S. Isukapalli*, et al.*, "Stochastic Response Surface Methods (SRSMs) for uncertainity propagation application to environmental and biological systems," *Risk Analysis,* vol. 18, pp. 351-363, 1998.

[25] G. E. P. Box and N. R. Draper, *Empirical Model-Building and Response Surfaces*. New York: John Wiley & Sons, 1987.

[26] G. E. P. Box*, et al.*, *Statistics for Experimenters: An Introduction to Design, Data Analysis and Model Building*. New York: John Wiley & Sons, 1978.

[27] A. I. Khuri and J. A. Cornell, *Response Surfaces: Design and Analyses*. New York: Marcel Dekker, 1987.

[28] A. Sandu*, et al.*, "Modeling Multibody Systems with Uncertainties. Part I: Theoretical and Computational Aspects," *Multibody System Dynamics,* vol. 15, pp. 369-391, 2006.

[29] H. Elman*, et al.*, "Efficient iterative algorithms for the stochastic finite element method with application to acoustic scattering," *Computer Methods in Applied Mechanics and Engineering,* vol. 194, pp. 1037-1055, 2005.

[30] C. Soize, "Identification of high-dimension polynomial chaos expansions with random coefficients for non-Gaussian tensor-valued random fields using partial and limited experimental data," *Computer Methods in Applied Mechanics and Engineering,* vol. 199, pp. 2150-2164, 2010.

[31] A. Sarkar and R. Ghanem, "Mid-frequency structural dynamics with parameter uncertainty," *Computer Methods in Applied Mechanics and Engineering,* vol. 191, pp. 5499-5513, 2002.

[32] X. Xu, "A multiscale stochastic finite element method on elliptic problems involving uncertainties," *Computer Methods in Applied Mechanics and Engineering,* vol. 196, pp. 2723-2736, 2007.

[33] D. Lucor*, et al.*, "Stochastic design optimization: Application to reacting flows," *Computer Methods in Applied Mechanics and Engineering,* vol. 196, pp. 5047-5062, 2007.

[34] G. Alefeld and G. Mayer, "Interval analysis: theory and applications," *Journal of Computational and Applied Mathmatics,* vol. 121, pp. 421-464, 2000.

[35] H. Grell*, et al.*, *Enzyklopadie der Elementarmathematik, Band I Arithmetik, Dritte Auage*. Berlin: VEB Deutscher Verlag der Wissenschaften, 1966.

[36] R. E. Moore, *Interval analysis*. Englewood Cliffs, New Jersey: Prentice-Hall, 1966.

[37] P. S. Dwyer, *Linear Computations*. New York: Wiley, 1951.

[38] T. Sunaga, "Theory of an interval algebra and its application to numerical analysis," *RAAG Memoirs,* vol. 2, 1958.

[39] L. Jaulin, *Applied Interval Analysis: with Examples in Parameter and State Estimation, Robust Control and Robotics*. New York: Springer, 2001.
[40] R. E. Moore, "Interval Arithmetic and Automatic Error Analysis in Digital Computing," PhD thesis, Department of Mathematics, Stanford University, Stanford, California, 1962.
[41] R. E. Moore, *Methods and application of interval analysis*. Philadelphia, PA.: SIAM, 1979.
[42] G. Hargreaves, I, "Interval analysis in MATLAB," Manchester2002.
[43] C. Bliek, "Computer methods for design automation," PhD thesis, Massachusetts Institute of Technology, 1992.
[44] E. R. Hansen, "Bounding the solution of interval linear equations," *SIAM Journal on Numerical Analysis,* vol. 29, pp. 1493-1503, 1992.
[45] A. Numaier, "A simple derivation of the Hansen-Bliek-Rohn-Ning-Kearfott enclosure for linear interval equations " *Reliable Computing,* vol. 5, pp. 131-136, 1999.
[46] S. Ning and R. B. Kearfott, "A comparison of some methods for solving linear interval equations," *SIAM Journal on Numerical Analysis,* vol. 34, pp. 1289-1305, 1997.
[47] J. Rohn, "Cheap and tight bounds: The recent result by E. Hansen can be made more efficient," *Interval Computations,* pp. 13-21, 1993.
[48] R. Krawczyk, "Newton-Algorithmen zur Bestimmung von Nullstellen mit Fehlerschranken," *Computing,* vol. 4, pp. 187-201, 1969.
[49] A. Neumaier, *Interval Methods for Systems of Equations*. Cambridge, UK: Cambridge University Press, 1990.
[50] F. Behamous*, et al.*, "Revising hull and box consistency," in *Proceeding of the International Conference on Logic Programming*, Las Cruces, NM., 1999, pp. 230-244.
[51] E. R. Hansen and S. Sengupta, "Bounding solutions of systems of equations using interval analysis," *BIT,* vol. 21, pp. 203-211, 1981.
[52] J. C. Cleary, "Logic arithmetic," *Future Computing Systems,* vol. 2, pp. 125-149, 1987.
[53] E. Davis, "Constraint propagation with interval labels," *Artificial Intelligence,* vol. 32, pp. 281-331, 1987.
[54] D. Waltz, "Generating semantic descriptions from drawings of scenes with shadows," ed. New York: McGraw-Hill, 1975.
[55] J. Rohn, "Eigenvalues of a sysmmetric interval matrix," *Freobirger Intervall-Berichte,* vol. 87, pp. 67-72, 1987.
[56] C. V. Hallot and A. C. Bartlett, "On the eigenvalues of interval matrices," in *Proceedings of the IEEE Conference on Descision and Control Including the Symposium on Adaptive Processes 26th*, Los Angeles, 1987, pp. 794-799.
[57] A. Dief, *Advance Matrix theory for Scientists and Engineers*. Tunbridge Wells, UK: Abaqus Press, 1991.
[58] Z. P. Qiu*, et al.*, "Natural frequencies of structures with uncertain-but-non-random parameters," *Journal of Optimization Theory and Applications,* vol. 6, pp. 669-683, 1995.
[59] Z. P. Qiu*, et al.*, "Bounds of eigenvalues for structures with an interval descrption of uncertain-but-non-random parameters," *Chaos, Solitons & Fractals,* vol. 7, pp. 425-434, 1996.

[60] Z. P. Qiu*, et al.*, "The Rayleigh Quotient method for computing eigenvalue bounds of vibrational systems with interval parameters," *Acta Mechanics Solid Sinica,* vol. 6, pp. 309-318, 1993.

[61] S. Chen*, et al.*, "Interval static displacement analysis for structures with interval parameters," *International Journal for Numerical Methods in Engineering,* vol. 53, pp. 393-407, 2002.

[62] S. Chen*, et al.*, "Robustness analysis of responses of vibration control structures with uncertain parameters using interval algorithm," *Structural Safety,* vol. 29, pp. 94-111, 2007.

[63] Z. Qiu, "Comparison of static response of structures using convex models and interval analysis method," *International Journal for Numerical Methods in Engineering,* vol. 56, pp. 1735-1753, 2003.

[64] Z. Qiu, "Convex models and interval analysis method to predict the effect of uncertain-but-bounded parameters on the buckling of composite structures," *Computer Methods in Applied Mechanics and Engineering,* vol. 194, pp. 2175-2189, 2005.

[65] D. Moens and D. Vandepitte, "Interval sensitivity theory and its application to frequency response envelope analysis of uncertain structures," *Computer Methods in Applied Mechanics and Engineering,* vol. 196, pp. 2486-2496, 2007.

[66] W. Gao, "Interval Finite Element Analysis using Interval Factor Method," *Computational Mechanics,* vol. 39, pp. 709-717, 2006.

[67] M. Li*, et al.*, "Interval Uncertainty Reduction and Single-Disciplinary Sensitivity Analysis With Multi-Objective Optimization," *Journal of Mechanical Design,* vol. 131, p. 031007, 2009.

[68] R. L. Muhanna*, et al.*, "Combined axial and bending stiffness in interval finite-element methods," *Journal of Structural Engineering,* vol. 133, pp. 1700-1709, 2007.

[69] S. S. Rao and L. Cao, "Optimum Design of Mechanical Systems Involving Interval Parameters," *Journal of Mechanical Design,* vol. 124, p. 465, 2002.

[70] S. Shary, P, "A New Technique in Systems Analysis under Interval Uncertain and Ambiguidy," *Reliable Computing,* vol. 8, pp. 321-418, 2002.

[71] N. S. Nedialkov, "Computing rigorous bounds on the solution of an initial value problem for an ordinary differential equation," phd, University of Toronto, Toronto, 1999.

[72] N. S. Nedialkov*, et al.*, "Validated solutions of initial value problems for odinary differential equations.," *Applied Mathematics and Computation,* vol. 105, pp. 21-68, 1999.

[73] K. R. Jackson and N. S. Nedialkov, "Some recent advances in validated methods for IVPs for ODEs," *Applied Mathematics and Computation,* vol. 42, pp. 269-284, 2002.

[74] M. Berz and K. Makino, "Verified integration of ODEs and flows using differential algebraic methods on high-order Taylor models," *Reliable Computing,* vol. 4, pp. 361-369, 1998.

[75] K. Makino and M. Berz, "Efficient Control of the Dependency Problem Based on Taylor Model Methods," *Reliable Computing,* vol. 5, pp. 3-12, 1999.

[76] J. Hoefkens, "Rigorous numerical analysis with high-order taylor models," phd, Michigan State University, 2001.

[77] K. Makino and M. Berz, "Taylor models and other validated functional inclusion methods," *International Journal of Pure and Applied Mathematics,* vol. 4, pp. 379-456, 2003.

[78] R. J. Lohner, "Step size and order control in the verified solution of IVP with ODE's," presented at the SciCADE'95 International Conference on Scienfific Computation and Differential Equations, Standford University, Calif., 1995.

[79] G. F. Corliss and R. Rihm, "Validating an a priori enclosure using high-order Taylor series," *Scientific Computing, Computer Arithmetic, and Validated Numerics,* pp. 228-238, 1996.

[80] R. E. Moore, *Automatic local coordinate transformations to reduce the growth of error bounds in interval computation of solutions of ordinary differential equations*. New York: Wiley, 1965.

[81] F. Kruckeberg, *Ordinary differential equations, in: E. Hansen (Ed.), Topics in Interval Analysis*. Oxford: Clarendon Press, 1969.

[82] R. J. Lohner, *Enclosing the solutions of ordinary initial and boundary value problems, in: E.W. Kaucher, U.W. Kulisch, C. Ullrich (Eds.), Computer Arithmetic: Scientific Computation and Programming Languages*. Stuttgart: Wiley-Teubner Series in Computer Science, 1987.

[83] R. Rihm, "On a Class of Enclosure Methods for Initial Value Problems," *Computing,* vol. 53, pp. 369-377, 1994.

[84] N. S. Nedialkov and K. R. Jackson, "Interval Hermite-Obreschkoff Method for Computing Rigorous Bound on the Solution of Initial Value Problem for an Ordinary Differential Equation," *Reliable Computing,* vol. 5, pp. 289-310, 1999.

[85] K. Makino and M. Berz, "Supression of the wrapping effect by Taylor model-based verified integratiors: long-term stabilization by preconditioning," *International Journal of Differential Equations and Applications,* vol. 10, pp. 353-384, 2005.

[86] K. Makino and M. Berz, "Suppression of the wrapping effect by Taylor model-based verified integrators: long-term stabilization by Shrink wrapping," *International Journal of Differential Equations and Applications,* vol. 10, pp. 385-403, 2005.

[87] K. Makino and M. Berz, "Suppression of the wrapping effect by taylor model-based verified integrators: the single step," *International Journal of Pure and Applied Mathematics,* vol. 36, pp. 175-197, 2006.

[88] R. Armellin*, et al.*, "Apophis Encounter 2029 Differential Algebra and Taylor Model Approaches," presented at the IAA Planetary Defense Conference: Protecting Earth from Asteroids, Granada, Spain, 2009.

[89] M. Berz and K. Makino, "Rigorous Global Search using Taylor Models," in *Proceedings of the 2009 conference on Symbolic numeric computation*, Kyoto, Japan, 2009, pp. 11-20.

[90] K. Makino and M. Berz, "Rigorous Integration of Flows and ODEs using Taylor models," *Symbolic Numeric Computation* pp. 79-84, 2009.

[91] N. Revol*, et al.*, "Taylor models and floating-point arithmetic: proof that arithmetic operations are validated in COSY," *Journal of Logic and Algebraic Programming,* vol. 64, pp. 135-154, 2005.

[92] Y. Lin and M. A. Stadtherr, "Validated solutions of initial value problems for parametric ODEs," *Applied Numerical Mathematics,* vol. 57, pp. 1145-1162, 2007.

[93] Z. Qiu and X. Wang, "Comparison of dynamic response of structures with uncertain-but-bounded parameters using non-probabilistic interval analysis method and probabilistic approach," *International Journal of Solids and Structures,* vol. 40, pp. 5423-5439, 2003.

[94] Z. Qiu and X. Wang, "Parameter perturbation method for dynamic responses of structures with uncertain-but-bounded parameters based on interval analysis," *International Journal of Solids and Structures,* vol. 42, pp. 4958-4970, 2005.

[95] J. Wu*, et al.*, "An improved interval analysis method for uncertain structures," *Structural Engineering and Mechanics,* vol. 20, pp. 713-726, 2005.

[96] X. Zhang*, et al.*, "Interval finite element method for dynamic response of closed-loop system with uncertain parameters," *International Journal for Numerical Methods in Engineering,* vol. 70, pp. 543-562, 2007.

[97] X. Han*, et al.*, "Transient waves in composite - laminated plates with uncertain load and material property," *International Journal for Numerical Methods in Engineering,* vol. 75, pp. 253-274, 2008.

[98] Z. Qiu*, et al.*, "Non-probabilistic interval analysis method for dynamic response analysis of nonlinear systems with uncertainty," *Journal of Sound and Vibration,* vol. 319, pp. 531-540, 2009.

[99] M. Modarreszadeh, "Dynamic analysis of structures with interval uncertainty " phd, Case Western Reserve University, 2005.

[100] H. Degersem*, et al.*, "Interval and fuzzy dynamic analysis of finite element models with superelements," *Computers & Structures,* vol. 85, pp. 304-319, 2007.

[101] X. Wang*, et al.*, "Comparisons of Probabilistic and Two Nonprobabilistic Methods for Uncertain Imperfection Sensitivity of a Column on a Nonlinear Mixed Quadratic-Cubic Foundation," *Journal of Applied Mechanics,* vol. 76, p. 011007, 2009.

[102] J. Wu and Y. Zhang, "The Dynamic Analysis of Multibody Systems with Uncertain Parameters Using Interval Method," *Applied Mechanics and Materials,* vol. 152-154, pp. 1555-1561, 2012.

[103] M. Plum, "Inclusion methods for ellptic boundary value problems,," in *J. Herzberger*, ed Amsterdam: Elsevier, 1994, pp. 322-379.

[104] M. Koeber, "Losungseinschlieung bei Anfangswertproblemen fur quasilineare hyperbolische Dierentialgleichungen," Univeristat Karlsruhe, Karlsruhe, 1997.

[105] H.-J. Dobner, "Einschlieungsalgorithmen fur hyperbolische Dierentialgleichungen," Universitat Karlsruhe, Karlsruhe, 1986.

[106] N. S. Nedialkov and J. D. Pryce, "Solving Differential-Algebraic Equations by Taylor Series (I) Computing Taylor Coefficients," *BIT,* pp. 001-030, 2005.

[107] N. S. Nedialkov and J. D. Pryce, "Solving differential-algebraic equations by Taylor series (II): Computing the System Jacobian," *BIT Numerical Mathematics,* vol. 47, pp. 121-135, 2006.

[108] N. S. Nedialkov and J. D. Pryce, "Solving Differential-Algebraic Equations by Taylor Series (III) the DAETS Code," *Journal of Numerical Analysis, Industrial and Applied Mathmatics,* vol. 1, pp. 1-30, 2007.

[109] J. D. Pryce, "Solving high-index DAEs by Taylor series," *Numerical Algorithms,* vol. 19, pp. 195-211, 1998.

[110] R. Barrio, "Performance of the Taylor series method for ODEs/DAEs," *Applied Mathematics and Computation,* vol. 163, pp. 525-545, 2005.

[111] J. Wu*, et al.*, "Interval uncertain method for multibody mechanical systems using Chebyshev inclusion functions," *International Journal for Numerical Methods in Engineering,* vol. 95, pp. 608-630, 2013.

[112] M. A. Valdebenito and G. I. Schuëller, "A survey on approaches for reliability-based optimization," *Structural and Multidisciplinary Optimization* vol. 42, pp. 645-663, 2010.

[113] S. B. Lazarus*, et al.*, "Vehicle localization using sensors data fusion via integration of covariance intersection and interval analysis," *IEEE Sensors Journal,* vol. 7, pp. 1302-1314, Sep-Oct 2007.
[114] I. Doltsinis and Z. Kang, "Robust design of structures using optimization methods," *Computer Methods in Applied Mechanics and Engineering,* vol. 193, pp. 2221-2237, 2004.
[115] H.-G. Beyer and B. Sendhoff, "Robust optimization – A comprehensive survey," *Computer Methods in Applied Mechanics and Engineering,* vol. 196, pp. 3190-3218, 2007.
[116] X. Du*, et al.*, "An integrated framework for optimization under uncertainty using inverse reliability strategy," *Journal of Mechanical Design,* vol. 126, p. 562, 2004.
[117] A. Chiralaksanakul and S. Mahadevan, "First-Order Approximation Methods in Reliability-Based Design Optimization," *Journal of Mechanical Design,* vol. 127, p. 851, 2005.
[118] F. Li*, et al.*, "Interval multi-objective optimisation of strucutres using adaptive Kriging approximations," *Computers and Structures,* vol. 119, pp. 68-84, 2013.
[119] X. Du and W. Chen, "Sequential Optimization and Reliability Assessment Method for Efficient Probabilistic Design," *Journal of Mechanical Design,* vol. 126, pp. 225-233, 2004.
[120] Z. Kang and Y. Luo, "Reliability-based structural optimization with probability and convex set hybrid models," *Structural and Multidisciplinary Optimization,* vol. 42, pp. 89-102, 2009.
[121] S. Chakraborty and B. K. Roy, "Reliability based optimum design of Tuned Mass Damper in seismic vibration control of structures with bounded uncertain parameters," *Probabilistic Engineering Mechanics,* vol. 26, pp. 215-221, 2011.
[122] T. H. Nguyen*, et al.*, "Single-Loop System Reliability-Based Design Optimization Using Matrix-Based System Reliability Method: Theory and Applications," *Journal of Mechanical Design,* vol. 132, p. 011005, 2010.
[123] J. Liang*, et al.*, "A Single-Loop Approach for System Reliability-Based Design Optimization," *Journal of Mechanical Design,* vol. 129, p. 1215, 2007.
[124] J. Liang*, et al.*, "A single-loop method for reliability-based design optimisation," *Int. J. Product Development,* vol. 5, pp. 76-92, 2008.
[125] M. A. Valdebenito and G. I. Schuëller, "A survey on approaches for reliability-based optimization," *Structural and Multidisciplinary Optimization,* vol. 42, pp. 645-663, 2010.
[126] S. K. Au*, et al.*, "Compartment fire risk analysis by advanced Monte Carlo simulation," *Engineering Structures,* vol. 29, pp. 2381-2390, 2007.
[127] D. Xiu and G. E. Karniadakis, "The Wiener-Askey polynomial chaos for stochastic differential equations," *SIAM Journal on Scientific Computing,* vol. 24, pp. 619-644, 2002.
[128] A. Gallina, "Response surface methodology as a tool for analysis of uncertainty in structural dynamics," Ph. D. Thesis, AGH - University of Science and Technology, 2009.
[129] B. D. Youn and K. K. Choi, "A new response surface methodology for reliability-based design optimization," *Computers & Structures,* vol. 82, pp. 241-256, 2004.
[130] C. Hu and B. D. Youn, "Adaptive-sparse polynomial chaos expansion for reliability analysis and design of complex engineering systems," *Structural and Multidisciplinary Optimization,* vol. 43, pp. 419-442, 2010.
[131] J. Li and D. Xiu, "Evaluation of failure probability via surrogate models," *Journal of Computational Physics,* vol. 229, pp. 8966-8980, 2010.

[132] R. Filomeno Coelho*, et al.*, "Hierarchical stochastic metamodels based on moving least squares and polynomial chaos expansion," *Structural and Multidisciplinary Optimization,* vol. 43, pp. 707-729, 2010.
[133] F. Xiong*, et al.*, "Weighted stochastic response surface method considering sample weights," *Structural and Multidisciplinary Optimization,* vol. 43, pp. 837-849, 2011.
[134] C. Jiang*, et al.*, "A sequential nonlinear interval number programming method for uncertain structures," *Computer Methods in Applied Mechanics and Engineering,* vol. 197, pp. 4250-4265, 2008.
[135] S. Tangaramvong*, et al.*, "Mathematical programming approaches for obtaining sharp collapse load bounds in interval limit analysis," *Computers & Structures,* vol. 125, pp. 114-126, 2013.
[136] J. Wu*, et al.*, "Uncertain analysis of vehicle handling using interval method," *International Journal of Vehicle Design,* vol. 56, pp. 81-105, 2011.
[137] J. Wu*, et al.*, "An interval uncertain optimization method for vehicle suspensions using Chebyshev metamodels," *Applied Mathematical Modelling,* vol. 38, pp. 3706-3723, 2014.
[138] J. Wu*, et al.*, "A new interval uncertain optimization method for structures using Chebyshev surrogate models," *Computers & Structures,* vol. 146, pp. 185-196, 2015.
[139] J. Wang and Z. Qiu, "The reliability analysis of probabilistic and interval hybrid structural system," *Applied Mathematical Modelling,* vol. 34, pp. 3648-3658, 2010.
[140] W. Gao*, et al.*, "Hybrid probabilistic interval analysis of bar structures with uncertainty using a mixed perturbation Monte-Carlo method," *Finite Elements in Analysis and Design,* vol. 47, pp. 643-652, 2011.
[141] X. Du, "Unified Uncertainty Analysis by the First Order Reliability Method," *Journal of Mechanical Design,* vol. 130, p. 091401, 2008.
[142] C. Jiang*, et al.*, "Structural reliability analysis based on random distributions with interval parameters," *Computers & Structures,* vol. 89, pp. 2292-2302, 2011.
[143] X. Du*, et al.*, "Reliability-Based Design With the Mixture of Random and Interval Variables," *Journal of Mechanical Design,* vol. 127, p. 1068, 2005.
[144] R. Ge*, et al.*, "Reliability-based design of composites under the mixed uncertainties and the optimization algorithm," *Acta Mechanica Solida Sinica,* vol. 21, pp. 19-27, 2008.
[145] M. S. Eldred*, et al.*, "Mixed aleatory-epistemic uncertainty quantification with stochastic expansions and optimization-based interval estimation," *Reliability Engineering & System Safety,* vol. 96, pp. 1092-1113, 2011.
[146] J. Wu*, et al.*, "A new uncertain analysis method and its application in vehicle dynamics," *Mechanical Systems and Signal Processing,* vol. 50-51, pp. 659-675, 2015.
[147] B. Erret, "A Generalization of the Stone-Weierstrass theorem," *Pacific Journal of Mathematics* vol. 11, pp. 777-783, 1961.
[148] Q. Li, et al., Numerical Analysis, 3rd ed. Wuhan: Huazhong University of Science and Technology Press, 2003.
[149] R. Wang, Numerical Approximation. Beijing: Higher Education Press, 2000.
[150] T. J. Rivlin, *An Introduction to the Approximation of Functions*. New York: Dover, 1981.
[151] A. Gil*, et al.*, *Numerical Methods for Special Functions*: SIAM, 2007.

[152] E. Jiang, *et al.*, *Numerical Approximation*. Shanghai: Fudan University Press, 2008.
[153] M. Abramowitz and I. A. Stegun, *Handbook of Mathematical Functions with Formulas, Graphs, and Mathematical Tables*. New York: Dover, 1972.
[154] N. S. Nedialkov, *et al.*, "An Effective High-Order Interval Method for Validating Existence and Uniqueness of the Solution of IVP for an ODE," *Reliable Computing,* vol. 7, pp. 446-465, 2001.
[155] D. Negrut, *et al.*, "A Discussion of Low-Order Numerical Integration Formulas for Rigid and Flexible Multibody Dynamics," *Journal of Computational and Nonlinear Dynamics,* vol. 4, p. 021008, 2009.
[156] A. Laulusa and O. A. Bauchau, "Review of Classical Approaches for Constraint Enforcement in Multibody Systems," *Journal of Computational and Nonlinear Dynamics,* vol. 3, p. 011004, 2008.
[157] O. A. Bauchau and A. Laulusa, "Review of Contemporary Approaches for Constraint Enforcement in Multibody Systems," *Journal of Computational and Nonlinear Dynamics,* vol. 3, p. 011005, 2008.
[158] N. M. Newmark, "A method of computation for structural dynamics," *Journal of Engineering Mechanics Division,* pp. 67-94, 1959.
[159] D. Negrut, *et al.*, "On an implementation of the Hilber–Hughes–Taylor method in the context of index 3 differential-algebraic equations of multibody dynamics," *Journal of Computational and Nonlinear Dynamics,* vol. 2, pp. 73-85, 2007.
[160] J. Chung and G. Hulbert, "A time integration algorithm for structural dynamics with improved numerical dissipation: The generalized-a method," *Journal of Applied Mechanics,* vol. 60, pp. 371-375, 1993.
[161] C. Barbarosie, "Reducing the wrapping effect," *Computing,* vol. 54, 1995.
[162] A. J. Buras, *et al.*, "A 1996 Analysis of the CP. Violating Ratio ε'/ε," *Physics Letters B,* vol. 389, pp. 749-756, 1996.
[163] E. Blanchard, *et al.*, "Comparison between a polynomial-chaos-based Bayesian approach and a polynomial-chaos-based EKF approach for parameter estimation with application to vehicle dynamics " in *the ASME 2009 International Design Engineering Technical Conferences & Computers and Inforamtion in Engineering Conference*, San Diego, California, 2009, pp. DETC2009-86402.
[164] D. Whitley, *et al.*, "The island model genetic algorithm: on separability, population size and convergence," *Journal of Computing and Information Technology,* vol. 7, pp. 33-47, 1998.
[165] M. Miki, *et al.*, "A parallel genetic algorithm with distributed enviroment scheme," presented at the IEEE International Conference on Systems, Man, and Cybernetics, 1999.
[166] P. T. Boggs and J. W. Tolle, "Sequential quadratic programming," *Acta Numerica,* vol. 4, pp. 1-52, 1995.
[167] W. Gao, "Natural frequency and mode shape analysis of structres with uncertainty," *Mechanical Systems and Signal Processing,* vol. 21, pp. 24-39, 2007.
[168] M. S. Kim, *et al.*, "Robust design optimization of the McPherson suspension system with consideration of a bush compliance uncertainty," *Proceedings of the Institution of Mechanical Engineers, Part D: Journal of Automobile Engineering,* vol. 224, pp. 705-716, 2010.
[169] X. Wang, *Automotive Chassis Dsign*. Beijing: TsingHua Univeristy Press, 2010.
[170] M. P. Bendsoe and O. Sigmund, *Topology Optimization: Theory, Methods, and Applications*. Berlin, Heidelberg: Springer, 2003.

[171] M. P. Bendsøe and N. Kikuchi, "Generating optimal topology in structural design using a homogenization method," *Computer Methods in Applied Mechanics and Engineering,* vol. 71, pp. 197-224, 1988.
[172] M. Zhou and G. I. Z. Rozvany, "The COC algorithm, Part II: topological, geometry and generalized shape optimization," *Computer Methods in Applied Mechanics and Engineering,* vol. 89, pp. 197-224, 1991.
[173] M. P. Bendsoe and O. Sigmund, "Material interpolation schemes in topology optimization," *Archive of Applied Mechanics,* vol. 69, pp. 635-654, 1999.
[174] J. A. Sethian and A. Wiegmann, "Structural boundary design via level set and immersed interface methods," *Journal of Computational Physics,* vol. 163, pp. 227-246, 2000.
[175] M. Y. Wang*, et al.*, "A level set method for structural topology optimization," *Computer Methods in Applied Mechanics and Engineering,* vol. 192, pp. 227-246, 2003.
[176] G. Allaire and F. Jouve, "Structural optimization using sensitivity analysis and a level-set method," *Journal of Computational Physics,* vol. 194, pp. 363-393, 2004.
[177] A. Asadpoure*, et al.*, "Robust topology optimization of structures with uncertainties in stiffness – Application to truss structures," *Computer & Structures,* vol. 89, pp. 1131-1141, 2011.
[178] G. I. Schuëller and H. A. Jensen, "Computational methods in optimization considering uncertainties - an overview," *Computer Methods in Applied Mechanics and Engineering* vol. 198, pp. 2-13, 2008.
[179] O. Sigmund, "Manufacturing tolerant topology optimization," *Acta Mechanica Solida Sinica,* vol. 25, 2009.
[180] F. Wang*, et al.*, "Robust topology optimization of photonic crystal waveguides with tailored dispersion properties," *Journal of Optical Socity of America B,* vol. 28, pp. 387-397, 2011.
[181] J. K. Guest and T. Igusa, "Structural optimization under uncertain loads and nodal locations," *Computer Methods in Applied Mechanics and Engineering,* vol. 198, pp. 116-124, 2008.
[182] M. Tootkaboni*, et al.*, "Topology optimization of continuum structures under uncertainty – A Polynomial Chaos approach," *Computer Methods in Applied Mechanics and Engineering,* vol. 201-204, pp. 263-275, 2012.
[183] J. Zhao and C. Wang, "Robust structural topology optimization under random field loading uncertainty," *Structural and Multidisciplinary Optimization,* vol. 50, pp. 517-522, 2014.
[184] S. Chen*, et al.*, "Level set based robust shape and topology optimization under random field uncertainties," *Structural and Multidisciplinary Optimization,* vol. 41, pp. 507-524, 2010.
[185] M. Jansen*, et al.*, "Robust topology optimization accounting for misplacement of material," *Structural and Multidisciplinary Optimization,* vol. 47, pp. 317-333, 2013.
[186] J. Zhao and C. Wang, "Robust topology optimization under loading uncertainty based on linear elastic theory and orthogonal diagonalization of symmetric matrices," *Computer Methods in Applied Mechanics and Engineering,* vol. 273, pp. 204-218, 2014.
[187] N. F. Wang and Y. W. Yang, "Structural design optimization subjected to uncertainty using fat Bezier curve," *Computer Methods in Applied Mechanics and Engineering,* vol. 199, pp. 210-219, 2009.

[188] O. Sigmund, "A 99 line topology optimization code written in matlab," *Structural and Multidisciplinary Optimization,* vol. 21, pp. 120-127, 2001.
[189] M. P. Bendsoe, "Optimization of structureal topology, shape and material," ed Berlin, Heidelberg: New York: Springer, 1995.
[190] K. Svanberg, "The method of moving asymptotes - a new method for structural optimization," *International Journal for Numerical Methods in Engineering,* vol. 24, pp. 359-373, 1987.
[191] O. Sigmund, "Design of material structures using topology optimization," Ph. D., Department of Solid Mechanics, Technical University of Denmark, 1994.
[192] O. Sigmund, "On the design of compliant mechanisms using topology optimization," *Mechanics of Structures and Machines,* vol. 25, pp. 495-526, 1997.
[193] X. Du*, et al.*, "Robust mechanism synthesis with random and interval variables," *Mechanism and Machine Theory,* vol. 44, pp. 1321-1337, 2009.
[194] S. Ferson*, et al.*, "Constructing probability boxes and Dempster–Shafer structure," Sandia National Laboratories, Albuquerque, New Mexico2003.
[195] J. C. Helton*, et al.*, "A sampling-based computational strategy for the representation of epistemic uncertainty in model predictions with evidence theory," *Computer Methods in Applied Mechanics and Engineering,* vol. 196, pp. 3980-3998, 2007.